Investigating the function of microtubule-associated protein tau (MAPT) and its genetic association with Parkinson's using human iPSC-derived dopamine neurons

Thesis submitted to the Department of Physiology, Anatomy and Genetics towards the degree of Doctor of Philosophy

by

Joel Edward Beevers

St Peter's College Oxford

Trinity Term 2016

Abstract

Parkinson's disease (PD) primarily manifests as loss of motor control through the degeneration of nigrostriatal dopaminergic neurons. The microtubule-associated protein tau (*MAPT*) locus is highly genetically associated with PD, wherein the H1 haplotype confers disease risk and the H2 haplotype is protective. As this haplotype variation does not alter the amino acid sequence, disease risk may be conferred by altered gene expression, either of total *MAPT* or of specific isoforms, of which there are six in adult human brain. To investigate haplotype-specific control of *MAPT* expression in the neurons that die in PD, induced pluripotent stem cells (iPSCs) from H1/H2 heterozygous individuals were differentiated into dopaminergic neuronal cultures that expressed all six mature isoforms of *MAPT* after six months' maturation. A reporter construct using the human tyrosine hydroxylase locus was also generated to identify human dopaminergic neurons in mixed cultures. Haplotype-specific differences in the inclusion of exon 3 and total *MAPT* were observed in iPSC-derived dopaminergic neuronal cultures and a novel variant in *MAPT* intron 10 increased the inclusion of exon 10 by two-fold. RNA interference tools were generated to knockdown total *MAPT* or specific isoforms, wherein knockdown of the 4-repeat isoform of tau protein increased the velocity of axonal transport in iPSC-derived neurons. *MAPT* knockdown also reduced p62 levels, suggesting an impact of tau on macroautophagy, likely through altered axonal transport. These results demonstrate how variation at a disease susceptibility locus can alter gene expression, thereby impacting on neuronal function.

Acknowledgements

First, I would like to thank my supervisors Professor Richard Wade-Martins and Dr Tara Caffrey for their training and guidance throughout my DPhil. Their encouragement and support have been invaluable. I am particularly grateful for the sacrifices they have made to provide support on occasion from home on evenings and weekends or on maternity leave.

Second, a huge thank you to my wonderful colleagues in the Wade-Martins laboratory. You have provided so much friendship and support (and cake) over these four years. Special mention goes to the iPSC team, particularly Heather Booth and Federico Zambon for establishing the protocols, helping with cell feeding and making things fun in the office. Also to Mang-Ching Lai as we have worked on studying *MAPT* together and for his assistance with the allele-specific expression assays, and Dr Óscar Cordero Llana for his support with lentiviruses and helping me to be a better scientist through his example. Thank you to Dr Hugo Fernandes for assistance with all of the GBA work and to Dr Brent Ryan for guidance with Western blots and useful discussions. I also wish to thank Paul Robertson, who we all dearly miss, for his tremendous work generating a FACS immunostaining protocol.

I would like to thank Laura Parkkinen for providing midbrain tissue for analysis and allowing me to use the bioanalyzer. Also Samuel Evetts for providing DNA from the OPDC cohort and Jane Vowles and Sally Cowley for the invaluable supply of stem cells.

Finally, I cannot thank enough my wife and children for their support over these years of my DPhil. They have had to endure my absence for long days in the laboratory and weekend feedings, as well my long hours locked away writing this summer, and I am grateful for their love and support. Also thank you to the rest of my family who have been tremendously supportive.

I have been supported in my DPhil by a PhD studentship from Parkinson's UK, the Gustav Born Scholarship in Biomedical Science from St Peter's College and a Goodger Scholarship from the Medical Sciences Division, without which I could not have undertaken or completed these studies.

Table of Contents

Abbreviations

0N	0 N-terminal segments (tau), i.e. exon 2-/3-
1N	1 N-terminal segment (tau), i.e. exon 2+/3-
2N	2 N-terminal segments (tau), i.e. exon 2+/3+
3R	three-repeat (tau)
4-MUGlc	4 methylumbelliferyl β-D-glucopyranoside
4R	four-repeat (tau)
AD	Alzheimer's disease
ANOVA	analysis of variance
APP	amyloid precursor protein
Aβ	amyloid-beta
BAC	bacterial artificial chromosome
BDNF	brain-derived neurotrophic factor
BiP/GRP78	binding immunoglobulin protein / 78 kDa glucose-regulated protein
BMP	bone morphogenetic protein
bp	base pairs
BSA	bovine serum albumin
CBD	corticobasal degeneration
CBE	conduritol B epoxide
cDNA	complementary DNA
CHO	chinese hamster ovary (cells)
CNS	central nervous system
CT	threshold cycle
DAPI	4',6-diamidino-2-phenylindole
DAPT	*N*-[*N*-(3,5-difluorophenacetyl-L-alanyl)]-(*S*)-phenylglycine *t*-butyl ester
dibutyryl-cAMP	N^6,2'-*O*-dibutyryladenosine 3',5'-cyclic monophosphate
DIV	days *in vitro* (from protocol start)
DLB	dementia with Lewy bodies
DMEM	Dulbecco's modified Eagle's medium
DNA	deoxyribonucleic acid
DNase	deoxyribonuclease
dNTPs	deoxynucleotide triphosphates
DPBS	Dulbecco's PBS
DTT	dithiothreitol
E. coli	*Escherichia coli*
EBFP2	enhanced blue fluorescent protein 2
EDTA	ethylenediaminetetraacetic acid
EGFP	enhanced green fluorescent protein
ER	endoplasmic reticulum
ESC	embryonic stem cell
FACS	fluorescence-activated cell sorting
FBS	foetal bovine serum
FGF8a	fibroblast growth factor 8a
FOXA2	hepatocyte nuclear factor 3-beta
FRET	Förster resonance energy transfer
FTDP-17	frontotemporal dementia with parkinsonism linked to chromosome 17
FTLD	frontotemporal lobar degeneration
GBA	beta-glucocerebrosidase
GDNF	glial cell line-derived neurotrophic factor
GFAP	glial fibrillary acidic protein
GFP	green fluorescent protein
GSK3β	glycogen synthase kinase 3 beta
GWAS	genome-wide association study
HEPES	4-(2-hydroxyethyl)-1-piperazineethanesulfonic acid
HGPS	Hutchinson-Gilford progeria syndrome
hnRNP	heterogeneous ribonucleoprotein particle
HRP	horseradish peroxidase
HSV-1	Herpes simplex virus 1

iPSC	induced pluripotent stem cell
kb	kilobase(s)
L-DOPA	levodopa, L-3,4-dihydroxyphenylalanine
lacZ	lac operon gene Z, encoding beta-galactosidase
LAMP1	lysosome-associated membrane protein 1
LAMP2A	lysosome-associated membrane protein 2A
LB	lysogeny broth
LC3B	microtubule-associated proteins 1A/1B light chain 3B
LD	linkage disequilibrium
LRRK2	leucine-rich repeat kinase 2
LTR	long terminal repeat
MAPT	microtubule-associated protein tau
MOI	multiplicity of infection
mRNA	messenger RNA
MSA	multiple system atrophy
n.s.	not significant
NCAM	neural cell adhesion molecule
NMDA	*N*-methyl-D-aspartate
nt	nucleotide(s)
NT	non-targeting (shRNA)
OD	optical density
p62 / SQSTM1	ubiquitin-binding protein p62 / sequestosome-1
PAC	P1-derived artificial chromosome
PBS	phosphate buffered saline
PBST	phosphate buffered saline with Triton X-100
PCR	polymerase chain reaction
PD	Parkinson's disease
PINK1	PTEN-induced putative kinase 1
PITX3	pituitary homeobox 3
polyA	polyadenylation (signal sequence)
PSC	pluripotent stem cell
PSEN1	presenilin-1
PSEN2	presenilin-2
PSP	progressive supranuclear palsy
PTBP1	polypyrimidine tract-binding protein 1
qRT-PCR	quantitative reverse transcription real-time PCR
RBM4	RNA-binding protein 4
RCF	relative centrifugal force
RIPA	radioimmunoprecipitation assay
RNA	ribonucleic acid
RNase	ribonuclease
ROCKi	Rho kinase (ROCK) inhibitor, Y-27632
RPM	revolutions per minute
RT	reverse transcriptase
RT-PCR	reverse transcription PCR
SDS	sodium dodecyl sulphate
SHH	sonic hedgehog
shRNA	short hairpin RNA
siRNA	short interfering RNA
SNCA	alpha-synuclein
SNP	single nucleotide polymorphism
SNpc	*substantia nigra pars compacta*
SOC	super optimal broth
STH	saitohin
TBS	tris buffered saline
TBST	tris buffered saline with Tween 20
TE	tris-EDTA
TGF-β	transforming growth factor beta
TH	tyrosine hydroxylase
Tuj1	neuron-specific beta-III tubulin
UTR	untranslated region
VTA	ventral tegmental area

List of Figures

List of Tables

Chapter 1: Introduction

1.1 Parkinson's disease

1.1.1 General features of Parkinson's disease

Parkinson's disease (PD) is foremost considered as a movement disorder by the appearance of the classical triad of cardinal motor symptoms: bradykinesia, or slowness of movement, resting tremor and rigidity, in addition to postural instability and gait problems in a selection of sufferers (Zetusky et al. 1985). Several other disorders exhibit the motor symptoms of PD as part of a different disease presentation and ultimately with different post-mortem neuropathology. These are known as parkinsonism disorders, and include progressive supranuclear palsy (PSP), multiple system atrophy (MSA), corticobasal degeneration (CBD) and dementia with Lewy bodies (DLB).

The triad of motor symptoms in PD is principally due to the progressive neurodegenerative loss of dopaminergic neurons with cell bodies in the *substantia nigra pars compacta* (SNpc), a structure of the midbrain (Hirsch et al. 1988). Along with neighbouring ventral tegmental area (VTA) dopaminergic neurons, SNpc neurons are involved in reward-motivated learning and action, wherein neuronal firing correlates with reward prediction and unexpected rewards but decreases with prediction failure (Schultz et al. 1997). SNpc dopaminergic neurons form the nigrostriatal pathway projecting to the striatum; striatal release of dopamine can be evoked by goal-directed movement, as first detected by positron emission tomography (PET) while human subjects were playing a video game (Koepp et al. 1998). The axonal arbour of SNpc dopaminergic neurons forms extra-synaptic inhibitory connections with the medium spiny neurons of the striatum at the sites of incoming synapses with excitatory glutamatergic corticostriatal interneurons. Although the release of dopamine in

the striatum bathes excitatory synapses to modulate their transmission, SNpc neurons do so by specific rhythmic patterns that correlate with periods of movement (Dodson et al. 2016). Additionally, SNpc dopaminergic neurons can co-release the inhibitory neurotransmitter γ-aminobutyric acid (GABA) (Tritsch et al. 2012). Thus SNpc neurons are important not just as static producers of dopamine but form meaningful components of the network of motor co-ordination (Dodson et al. 2016). Dysfunction and then loss of dopaminergic terminals disrupts the motor network, leading to SNpc dopaminergic neuronal death, and, after adjusting for age-related loss, stereological analyses estimate that ~30% of SNpc dopaminergic neurons are lost by the first presentation of motor systems (Fearnley and Lees 1991; Ma et al. 1997; Cheng et al. 2010).

Surviving neurons in the SNpc contain proteinaceous inclusions called Lewy bodies and Lewy neurites, both of which are composed of fibrillar α-synuclein compacted with other proteins (Spillantini et al. 1997). As such, PD is neuropathologically classified as an 'α-synucleinopathy' along with the related diseases MSA and DLB (Spillantini et al. 1998b). Alpha-synuclein is a small protein of 140 amino acids (14 kDa) that localises to synaptic vesicles (Kahle et al. 2000) and has roles in synaptic transmission by regulating vesicle exocytosis (Abeliovich et al. 2000). Most studies agree that the α-synuclein protein is natively unfolded and exists as monomers (Lashuel et al. 2013). However, the prevailing theory for the role of α-synuclein in the disease state is that there exists one or more toxic oligomeric forms that have a toxic gain of function (Winner et al. 2011). Further, following observations that α-synuclein pathology in the brains of PD patients appears to follow stages of progression through from the brainstem upwards via the midbrain to the cortex (Braak et al. 2003), and reports of α-synuclein pathology in neurons grafted into individuals with PD (Kordower et al. 2008; Li et al. 2008), oligomeric α-synuclein has been thought to undergo prion-like transmission. It is unclear to what degree the insoluble Lewy bodies and Lewy

neurites are themselves pathogenic or merely an attempt to protect remaining neurons by sequestering the otherwise toxic oligomers (Soto and Estrada 2008).

Life with PD is further disrupted by a host of non-motor symptoms that are heterogeneous and some of which pre-empt motor manifestations. Non-motor symptoms include: cognitive impairment and dementia after exhibition of motor symptoms in a portion of sufferers (Aarsland et al. 2003); sleep deficits including rapid eye movement (REM) sleep behaviour disorder, which is a significant risk factor for PD (Schenck et al. 1996; Boeve et al. 1998; Schenck et al. 2013); gastrointestinal dysfunction and constipation (Edwards et al. 1991); and loss of smell (hyposmia/anosmia) (Doty et al. 1988). In addition to the presence of α-synuclein pathology outside of the nigrostriatal pathway, these non-motor symptoms demonstrate how PD is more than a movement disorder.

Treatment for PD is limited to symptomatic treatment only. Pharmacological intervention primarily seeks to increase dopamine signalling to counteract its loss in the striatum. The most common of these is levodopa (L-DOPA) replacement; this bypasses tyrosine hydroxylase, the rate-limiting enzyme in the synthesis of dopamine, so that aromatic L-amino acid decarboxylase can convert the L-DOPA to dopamine. Monoamine oxidase inhibitors, such as selegiline, block the catabolism of dopamine, allowing increased persistence in the synapse, whereas dopamine agonists, such as pramiprexole, directly target and activate dopamine receptors; additionally, dopamine reuptake inhibitors that block the dopamine transporter (DAT) are under consideration (Huot et al. 2016). However, all of these treatments are non-specific to the nigrostriatal pathway and so exhibit off-target effects. Additionally, L-DOPA-induced dyskinesia can appear after several years of treatment and is understood to be an effect of the non-continuous pharmacological stimulation of dopamine receptors, whereas animal models treated continuously are spared (Bibbiani et al. 2005). Striatal neurons in both dyskinetic and non-dyskinetic rats treated with L-DOPA were

shown to be capable of establishing long-term potentiation, i.e. strengthening of the synaptic connection following rapid cortical stimulation, but neurons of dyskinetic rats were unable to reverse this, so that the neurons once potentiated remained so (Picconi et al. 2003); further, this inability to depotentiate could be induced by activation of dopamine D1 receptors suggesting that overactivation of striatal D1 receptors by L-DOPA underlies dyskinesia (Picconi et al. 2003). Additionally, factors that alter the regulation of long-term potentiation or D1 receptor signalling may modulate dyskinesia, including a polymorphism in brain-derived neurotrophic factor (BDNF) that alters the length of time before dyskinesia begins to manifest (Foltynie et al. 2009).

A successful alternative to pharmacological treatment is deep brain stimulation surgery, consisting of the implantation of a stimulating electrode in either the globus pallidus or subthalamic nucleus to disrupt the pathogenic network activity that underlies the cardinal motor symptoms. Deep brain stimulation has additionally been shown to reduce dyskinesia (Oyama et al. 2012) and improve some non-motor symptoms (Borgohain et al. 2012). Crucially however, no treatment is currently available that can slow down or halt disease progression, particularly as the disease aetiology is not sufficiently well understood to determine cellular targets for therapy.

1.1.2 Familial genetic aetiology of Parkinson's disease

While PD can be successfully diagnosed, it is still unclear what the underlying causes are so that most cases are considered idiopathic. Genetic studies aim to identify components in the pathways of disease initiation and progression. Even if the specific effects of a mutation are not pertinent to idiopathic PD, it is hoped that the affected pathways discovered in cases of genetic PD may be relevant, so that therapies could be designed that would apply to both

genetic and idiopathic PD. Traditional genetic linkage analysis showing segregation of high-risk mutations (including gene multiplication) within disease-affected individuals in pedigrees has revealed many loci (see Table 1.1 for confirmed loci) but a monogenic cause has been identified for fewer than 10% of cases (Trinh and Farrer 2013).

Table 1.1: Genes confirmed to be associated with monogenic Parkinson's disease.

Locus	Gene	Inheritance	Onset	OMIM Reference
PARK1/4	*SNCA*	Dominant	Early/Late	168601, 605543
PARK2	*PARK2 (parkin)*	Recessive	Early	600116
PARK6	*PINK1*	Recessive	Early	605909
PARK7	*DJ1*	Recessive	Early	606324
PARK8	*LRRK2*	Dominant	Late	607060
PARK9	*ATP13A2*	Recessive	Juvenile	606693
PARK14	*PLA2G6*	Recessive	Early	612953
PARK15	*FBXO7*	Recessive	Early	260300
PARK17	*VPS35*	Dominant	Late	614203

(i) SNCA

The *SNCA* gene on chromosome 4q22.1 encodes α-synuclein, noted for its role in the characteristic aggregates seen in PD and other α-synucleinopathies. Rare high-risk mutations A30P, E46K, A53T, H50Q and G51D have been detected in a small number of families (Polymeropoulos et al. 1997; Krüger et al. 1998; Zarranz et al. 2004; Lesage et al. 2013; Proukakis et al. 2013); all are present in the N-terminal amphipathic region and increase the propensity for α-synuclein to aggregate. The E46K mutation was first discovered in a family with DLB (Zarranz et al. 2004) and the G51D mutation in a family with additional pyramidal signs (Lesage et al. 2013); it is not established whether these clinical differences are due to the mutations themselves, although fibrils made with G51D mutant α-synuclein were shown to be more toxic than wild-type fibrils (Lesage et al. 2013). In addition to point mutations, several kindreds have been identified with duplication (Chartier-Harlin et al. 2004; Ibáñez et al. 2004) and triplication (Singleton et al. 2003) of *SNCA*, showing that higher expression of

this gene alone is sufficient to cause PD. More will be discussed about the roles of α-synuclein and its connection with tau in section 1.3.3 and later chapters.

(ii) LRRK2

The *LRRK2* gene on chromosome 12q12 encodes leucine-rich repeat kinase 2. LRRK2 is a large multi-domain protein in the ROCO family of proteins, so identified because it has a Roc GTPase domain, neighbouring C-terminus of ROC (COR) domain, and a kinase domain, as well as protein-protein interaction domains such as the leucine-rich repeats (Marín et al. 2008). Most mutations have been found in the Roc-COR-kinase triad (Zimprich et al. 2004; Paisán-Ruíz et al. 2004) and the most common mutation, p.G2019S (Kachergus et al. 2005), has been consistently shown to increase the activity of the kinase domain (West et al. 2005; Cookson 2010). It is thought that there is regulatory cross-talk between kinase and GTPase functions (Deng et al. 2008), especially as kinase-dead mutants prevent or diminish the pathogenesis of other *LRRK2* mutations whether in the kinase or GTPase domain (Greggio et al. 2006; Cookson 2010); however, the ultimate output of LRRK2 is unclear. Many cellular pathways have been implicated in *LRRK2* PD, including autophagy (Alegre-Abarrategui et al. 2009; Manzoni, Mamais, Dihanich, McGoldrick, et al. 2013; Manzoni, Mamais, Dihanich, Abeti, et al. 2013), cytoskeletal dynamics and neurite outgrowth (MacLeod et al. 2006; Parisiadou et al. 2009; Dächsel et al. 2010).

(iii) Early-onset recessive PD

Several genes with rare recessive mutations have been found to cause early-onset PD, including *PINK1*, *PARK2* encoding parkin and *DJ1*. As these mutations are sufficiently rare that few post-mortem brains have been donated for examination, it is not yet clear whether

they cause a similar or distinct neuropathological form of PD to that of typical idiopathic PD. Notably, *PINK1* and *PARK2* interact in the same pathway, wherein PINK1 recruits the ubiquitin E3 ligase parkin to the mitochondrial membrane to target it for degradation by the process of mitophagy (Narendra et al. 2008; Narendra et al. 2010). Impairment of this process leads to the persistence of damaged mitochondria in the cell, one consequence of which is the increased production of damaging reactive oxygen species (ROS) (Piccoli et al. 2008).

(iv) GBA

Although not a *PARK* locus, dominant mutations in or chromosomal recombination around *GBA* on chromosome 1q22 are connected with PD. Homozygous mutations in the *GBA* gene that encodes β-glucocerebrosidase cause the lysosomal storage disorder Gaucher's disease (Brady et al. 1966) while individuals bearing a heterozygous carrier state have a higher prevalence of PD (Sidransky et al. 2009), insomuch that low penetrance heterozygous *GBA* mutations may contribute to 7% of PD cases (Sidransky et al. 2009). I will discuss more of the role of *GBA* mutations in PD in chapter 6.

1.1.3 Idiopathic Parkinson's disease non-genetic risk factors

As the majority of PD cases are considered idiopathic with no familial connections that would suggest high-risk mutations that predispose to disease, epidemiological investigations have elucidated some environmental factors that enhance disease risk. The largest of these is age, as advancing age reduces the efficiency of many cellular processes, thus increasing the chance of pathogenic events (Reeve et al. 2014). Age is also an important modifier of monogenic PD, as not all high-risk mutations are fully penetrant for this late-onset disease.

Although there is a degree of cell loss in the SNpc during healthy ageing, a different pattern of cell loss is seen in PD patients (Fearnley and Lees 1991). In addition to age, exposure to certain pesticides, known to be mitochondrial toxins, increases disease risk (Tanner et al. 2011), whereas long-term smoking provides a degree of protection against disease (Chen et al. 2010); interestingly, nicotine can inhibit monoamine oxidase, acting as a drug to increase dopamine levels by reducing its metabolism (Fowler et al. 1996), so could reduce the likelihood of dysfunction at dopamine synapses and thus protect dopaminergic neurons from degeneration.

1.2 Genetic association studies for sporadic Parkinson's disease

1.2.1 Association of chromosome 17q21.31 with Parkinson's disease

Genetic association studies examine the association of genetic architecture, such as single nucleotide polymorphisms (SNPs), with given traits, such as disease. For disease risk, these determine the statistical comparison of allele presence in cohorts of patients vs. controls. Prior to the advent of SNP arrays, studies were limited to hypothesis-driven studies using a manageable number of SNPs that could be examined by PCR or sequencing, according to time and resources. SNP arrays now allow genome-wide association studies (GWAS) by unbiased screening of a large number of SNPs across the whole genome in patients and controls (see section 1.2.2).

One such genetic locus that has been examined is *MAPT*, encoding microtubule-associated protein tau, being the focus of this thesis. *MAPT* has been of interest because tau protein forms aggregates in some neurodegenerative diseases including Alzheimer's disease, giving this family of diseases the name tauopathies (see section 1.3.2). *MAPT* and the surrounding

region of chromosome 17q21.31 are highly polymorphic, containing hundreds of single nucleotide polymorphisms (SNPs).

(i) Initial associations of the a0 allele

In an effort to locate mutations in *MAPT* that may account for tauopathy risk, a polymorphism in intron 9 was detected consisting of a dinucleotide repeat ranging from allele a0 with 11 repeats sequentially to allele a4 with 15 repeats (Conrad et al. 1997). That study found that the a0/a0 genotype was positively associated with PSP. Although Parkinson's disease (PD) is an α-synucleinopathy rather than a tauopathy, initial studies found an association, albeit weaker than for PSP, of the a0 allele and a0/a0 genotype with PD that remained after correction for potential misdiagnosis of PSP (Lazzarini et al. 1997). Many studies have been reported over the subsequent 19 years since the first association of the *MAPT* polymorphism and PD. Early on, the a0 association with PD was tested, producing a mix of studies reporting either little or no association (Morris et al. 1999; Hoenicka et al. 1999) or positive association (i.e. overrepresentation of the allele/genotype in PD cases vs. controls) (Pastor et al. 2000). A meta-analysis of these early studies confirmed the association of a0 with PD, despite the group's own data failing to reach significance when considered alone (Golbe et al. 2001).

The association of a0 with neurodegenerative disease was subsequently extended to reveal a more complex genetic architecture in the *MAPT* region of 17q21.31.

(ii) Two haplotypes and linkage disequilibrium

Baker *et al.* first described two non-recombining haplotypes that encompass a large region of linkage disequilibrium (LD) and named them H1 and H2 (Baker et al. 1999). These two haplotypes can be distinguished from each other by many SNPs within the region of LD, so that the determination of the identity of virtually any one of them would reveal which haplotype it is. However, a 238 bp indel in intron 9 that is deleted in the H2 haplotype (Baker et al. 1999) is commonly used to identify the haplotypes as this indel is more stable than individual SNPs. As the H1 haplotype is the most common, its SNP identities constitute the major allele for each SNP in LD, whereas the less common H2 haplotype contributes the minor allele for each SNP in LD (Baker et al. 1999). Importantly, the dinucleotide polymorphism identified previously was confirmed to be haplotype-specific: a0 was found on H1 only, with a1 and a2 found as less common variants also on the H1 background, while H2 contained the a3 or the more rare a4 allele (Baker et al. 1999). The H1 haplotype was initially associated with PSP (Baker et al. 1999) and later with the related tauopathy CBD (Di Maria et al. 2000; Houlden et al. 2001); generally the H1/H1 genotype proffered the most significant association, but some reports showed association with the H1 haplotype even when found in the heterozygous state. The known region of LD containing *MAPT* was also extended to include much wider regions flanking the gene (Pastor et al. 2002; Pittman et al. 2004; Pastor et al. 2004); the nature of LD means that any functional SNP or masked pathogenic mutation present in only one haplotype would show similar association with disease as the other polymorphisms that surround it, so that individual functional SNPs within regions of LD cannot easily be identified by association studies. The region of LD is now understood to be somewhere between 1.3 Mb and 1.8 Mb within 17q21.31 (Cruts et al. 2005; Pittman et al. 2005).

(iii) Chromosome inversion

The lack of recombination between H1 and H2 haplotypes prompted the explanation by Skipper *et al.* of a chromosomal inversion (Skipper et al. 2004) that would remove the homology needed for crossing over. Evidence came months later with the discovery of a ~900 kb inversion (Stefansson et al. 2005), now extended to ~970 kb (Zody et al. 2008) (Fig. 1.1). Despite evidence that the H2 haplotype is the original orientation found in older primates (Zody et al. 2008), H2 is virtually absent from Asian populations (Conrad et al. 1998; Kobayashi et al. 2006) and has a frequency of only ~20 % in European populations (Stefansson et al. 2005). Further, the H2 haplotype appears to be under positive selection (Stefansson et al. 2005), suggesting that it is favourable.

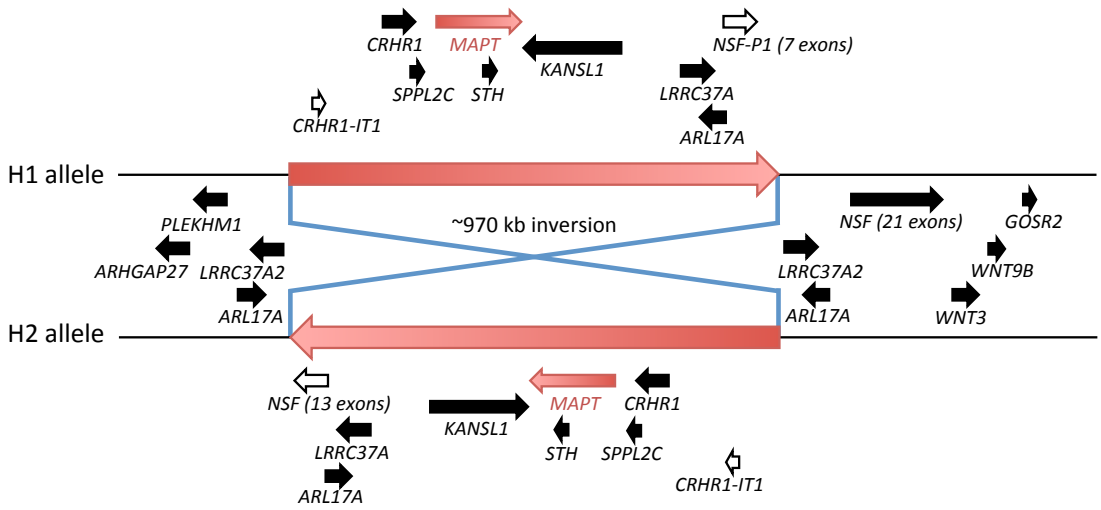

Figure 1.1: The 17q21.31 region of chromosome 17 includes an inversion that creates a region of extended linkage disequilibrium.
Schematic of the ~1.8 Mb of extended LD created by a ~970 kb chromosomal inversion with the inability of non-homologous sequence to recombine during chromosomal crossing over in meiosis. The ends of the inversion additionally include a small degree of duplication or alteration.

(iv) Haplotype association with PD by small-scale studies

Further case-control studies replicated the early association of a0 and a0/a0 (now as the haplotype H1 and the H1/H1 genotype) with risk for PD (Martin et al. 2001; Farrer et al. 2002; Kwok et al. 2004; Healy et al. 2004; Skipper et al. 2004; Mamah et al. 2005; Fidani et al. 2006; Goris et al. 2007; Winkler et al. 2007; Vandrovcova et al. 2009; Tobin et al. 2008; Wider et al. 2010; Ezquerra et al. 2011; Elbaz et al. 2011). A smaller number of studies found no evidence for association (sometimes only in individual populations) (DeStefano et al. 2001; de Silva et al. 2002; Fung, Xiromerisiou, et al. 2006; Winkler et al. 2007) and one claimed association of H2 with disease instead (Zappia et al. 2003). In one study significance was only achieved when patients with signs of dementia were excluded (Maraganore et al. 2001). Subsequent meta-analyses confirmed that the association is indeed real (Healy et al. 2004; Zhang et al. 2005b; Zabetian et al. 2007; Goris et al. 2007).

Intron 9 of *MAPT* contains saitohin (*STH*), a single-exon gene. This gene has a coding polymorphism (Q7R, rs62063857) that is in LD with the *MAPT* haplotype. However, like for *MAPT*, association studies have again showed a mix of positive disease association for the H1-resident Q allele (Levecque et al. 2004) or no significant difference between genotype of cases and controls (Clark et al. 2003; Pepłońska et al. 2003; Johansson et al. 2005). Further studies are ongoing regarding a functional role for saitohin (Andreadis 2012).

(v) Sub-haplotypes within the MAPT *locus*

Although the inverted region of 17q21.31 prevents recombination between the H1 and H2 haplotypes, recombination is common between copies of H1, giving rise to multiple *MAPT* sub-haplotypes that differ in a number of haplotype-tagging SNPs (htSNPs) (Oliveira et al. 2004; Skipper et al. 2004). *MAPT* sub-haplotypes have been investigated for their association

with PD in an aim to narrow down the functional SNPs responsible for disease risk, or to narrow down the area that may contain a currently unknown mutation. Several sets of SNPs have been used for determination of sub-haplotypes within H1, and Oliveira et al. (2004), Skipper et al. (2004) and Tobin et al. (2008) all claimed to have found separate specific sub-haplotypes associated with PD. Of note, the sub-haplotype H1c described by Pittman et al. (2005) is particularly defined by SNPs rs242557 (A vs. G) in the intron between exons 0 and 1 and rs2471738 (T vs. C) in the intron between exons 9 and 10 and on the H1 background. H1c was first associated with PSP (Pittman et al. 2005), which association still holds, later with AD (Myers et al. 2005) and then further tested by others for any association with PD. However, no group has completely replicated any of the above sub-haplotype associations for PD (Zabetian et al. 2007; Vandrovcova et al. 2009; Fung, Xiromerisiou, et al. 2006; Ezquerra et al. 2011; Fidani et al. 2006; Winkler et al. 2007; Goris et al. 2007), though some individual SNPs have been associated in some but not all studies or populations. The closest replication has been by Das et al. (2009) who found that 4 out of 5 of the htSNPs in the H1c sub-haplotype were associated with late onset PD. Overall it is clear that the H1 haplotype, particularly when homozygous, is associated with risk for PD, but there is insufficient evidence for the role played by specific sub-haplotypes or individual SNPs.

1.2.2 Genome-wide association studies of Parkinson's disease

Large-scale GWASs employ a large number of cases and controls in order to provide the necessary statistical power to assess association of genetic risk for disease, overcoming the loss of power from multiple testing correction for thousands of SNPs. Initial genomic screens with only 300-400 markers gave mixed results for evidence of 17q linkage with PD (DeStefano et al. 2001; Scott et al. 2001). Since then many large-scale studies have consistently replicated the association of the *MAPT* region and H1 haplotype SNPs with PD

Table 1.2: Top genes associated with Parkinson's disease through large-scale meta-analysis of GWAS.
Data from PDGene.org (http://pdgene.org/top_results), accessed 31 October 2014.

Polymorphism	Location	Gene	# Samples	Meta OR (95% CI)	Meta P-value
rs356182	chr4	*SNCA* [-19139 bp]	120,238	1.34 (1.30-1.38)	1.85E-82
rs17649553	**chr17**	***MAPT***	**114,483**	**0.77 (0.75-0.80)**	**6.11E-49**
rs34311866	chr4	*TMEM175*	120,238	1.26 (1.22-1.31)	6.00E-41
rs71628662	chr1	*ASH1L*	110,323	0.52 (0.46-0.58)	6.86E-28
rs12637471	chr3	*MCCC1*	120,238	0.84 (0.81-0.87)	5.38E-22
rs1955337	chr2	*STK39* [+24494 bp]	120,238	1.21 (1.16-1.26)	1.67E-20
rs6430538	chr2	intergenic	120,238	0.88 (0.85-0.90)	3.35E-19
rs11724635	chr4	*BST1*	120,238	0.89 (0.87-0.91)	4.26E-17
rs823118	chr1	*NUCKS1* [+4168 bp]	120,238	0.89 (0.87-0.92)	1.96E-16
rs1555399	chr14	*TMEM229B*	108,990	1.15 (1.11-1.19)	5.70E-16
rs76904798	chr12	*LRRK2*	120,238	1.16 (1.11-1.20)	4.86E-14
rs199347	chr7	*GPNMB*	120,238	0.90 (0.87-0.92)	5.62E-14
rs9275326	chr6	*HLA-DQB1* [+30500 bp]	99,286	0.80 (0.75-0.85)	5.81E-13

risk (Pankratz et al. 2009; Simón-Sánchez et al. 2009; Edwards et al. 2010; Hamza et al. 2010; UKPDC and WTCCC2 2011; Saad et al. 2011; IPDGC and WTCCC2 2011; Charlesworth et al. 2012), with only a few exceptions (Maraganore et al. 2005; Fung, Scholz, et al. 2006), including in a Japanese population with little representation of H2 (Satake et al. 2009). Meta-analyses have further confirmed the positive association (IPDGC et al. 2011; Pankratz et al. 2012), with the most recent large-scale meta analysis of 20 studies confirming *MAPT* as the second most highly associated locus after *SNCA* (Table 1.2) (Nalls et al. 2014). Specifically, the SNP in *MAPT* with the strongest association was SNP rs17649553 in intron 1, yielding a minor allele odds ratio of 0.77 (i.e. H2 is protective) with *p*-value 6.11×10^{-49} using 19,012 cases and 95,471 controls (Table 1.2) (Nalls et al. 2014). It is interesting that other *MAPT* SNPs in linkage disequilibrium do not exhibit the same strength of association. Nevertheless, given the large number of SNPs present in this genomic region and the high degree of linkage disequilibrium it is unlikely that a method like GWAS that uses only a subset of known SNPs could identify any one SNP as being a functional variant. As such, rather than pursuing functional studies of particular highly-associated GWAS SNPs in *MAPT*, functional studies of the effects of the entire haplotypes are warranted.

Interestingly, the top GWAS hits (Table 1.2) also include genes that are already associated with PD via high-risk mutations (*SNCA* and *LRRK2*) or gene multiplication (*SNCA*), evidence suggesting that either the expression of their encoded proteins is important in disease or that there are common coding variants that influence protein function.

1.3 *MAPT* and neurodegeneration

1.3.1 MAPT *gene architecture and splicing*

The human microtubule-associated protein tau (*MAPT*) locus is located on chromosome 17q21.31 and comprises 16 exons (Fig. 1.2A). As the nomenclature of the exons derives from the bovine tau locus, the numbering is not straightforward; further, the intron between the final exons 13 and 14 is retained in human transcripts (Andreadis et al. 1992). *MAPT* transcripts are alternatively spliced to produce six major isoforms in the adult human central nervous system (CNS) through the variable inclusion of exons 2, 3 and 10, while omitting exons 4A, 6 and 8 (Fig. 1.2B) (Andreadis 2005). Exons 2 and 3 are cassette exons each encoding 29 amino acid segments near the N-terminus of the protein, but exon 3 is only included following exon 2 inclusion (Goedert et al. 1989b). Protein isoforms with/without these additional N-terminal segments are referred to as 0N, 1N and 2N, being translated from exon 2-3-, 2+3- and 2+3+ transcripts respectively. In the C-terminal half of the protein are a set of four imperfect repeats separated by more variable spacers, encoded by exons 9-12; the cassette exon 10, encoding 31 amino acids, is the second of these (Goedert et al. 1989a; Goedert et al. 1989b). Tau isoforms lacking exon 10 thus have three repeats (3R tau) and the inclusion of exon 10 generates four-repeat tau (4R tau). The full complement of six possibilities of exons 2, 3, and 10 are represented in adult human CNS, whereas human foetal brain expresses only 0N3R tau (Goedert et al. 1989a; Goedert et al. 1989b).

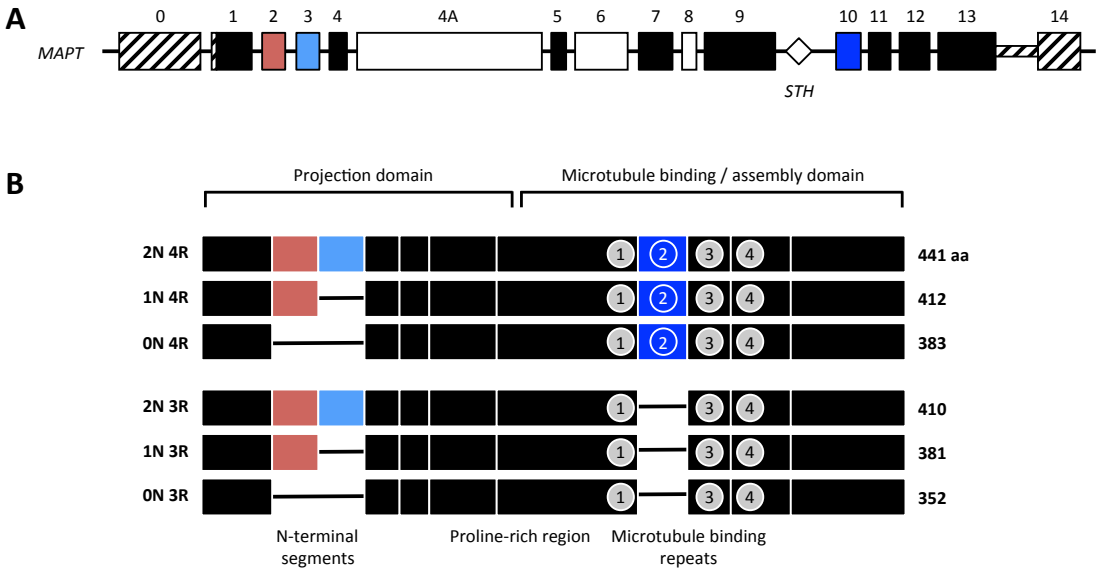

Figure 1.2: Structure of the *MAPT* gene.
(A) Schematic of the *MAPT* locus showing the numbering of 16 exons. Exons 0-13 are shown to scale but not intervening introns. Constitutive exons are shown in black; exons that are alternatively spliced in adult human brain are shown in colour; non-coding mRNA sequences are shown in stripes; exons in white have expression in the peripheral nervous system (exon 4A) or a more complex arrangement (exons 6, 8). The gene *STH* is located within intron 9. The colour coding of alternatively spliced exons 3 and 10 is used consistently throughout this work.
(B) Schematic of the six major isoforms of *MAPT* mRNA transcripts in adult human brain with colour coding as in part (A). Repeats in the microtubule binding domain are shown as numbered circles.

1.3.2 Tauopathies

Deposits of hyperphosphorylated aggregated tau are the neuropathological hallmark that gives name to the tauopathy family of neurodegenerative diseases (Table 1.3). The separate tauopathies differ in the locations of pathology so that some have predominant effect on movement as part of the parkinsonism spectrum (PSP, CBD, sometimes FTDP-17) while others are more associated with dementia (AD, PiD, AGD), although most of them include both elements at least by later stages (Williams 2006). As noted in Table 1.3, the neuropathological presentation of the tauopathies also differs in the nature of the tau pathology itself, not simply in its location. The composition of the various tau aggregates can be predominantly 3R tau or 4R tau.

Table 1.3: Characteristics of several tauopathies.
Sources: Williams (2006), Togo et al. (2002).

Disease	Characteristic neuropathology	Aggregated Tau isoforms	Aggregation type
Alzheimer's disease (AD)	beta-amyloid plaques and tau neurofibrillary tangles	equal 3R/4R	paired helical filaments, some straight filaments
Progressive supranuclear palsy (PSP)	tau neurofibrillary tangles and tufted astrocytes	mainly 4R	straight filaments
Corticobasal degeneration (CBD)	ballooned neurons and diffuse cortical tau	mainly 4R	straight filaments
Frontotemporal dementia and parkinsonism linked to chromosome 17 (FTDP-17)	variable neuronal tau deposits [defined by *MAPT* mutation]	variable: some mainly 3R, some equal, some mainly 4R	variable
Argyrophilic grain disease (AGD)	tau grains in neuropil, glial coiled bodies and ballooned neurons	mainly 4R	straight filaments
Pick's disease (PiD)	cytoplasmic Pick bodies	mainly 3R	paired helical filaments

(i) Alzheimer's disease

Alzheimer's disease (AD) is the most common and thus archetypal form of dementia as well as the most common of all neurodegenerative diseases. Its neuropathology is characterised by deposition of two insoluble aggregates: plaques of β-amyloid (Aβ) within the neuropil between neurons and neurofibrillary tangles composed of hyperphosphorylated tau filaments. The amyloid cascade hypothesis proposes that Aβ (alone or in combination with other truncated forms of APP) is the principal causative agent of AD, and thus that the involvement of tau is secondary and results from Aβ deposition itself (Hardy and Higgins 1992).

The β-amyloid component of AD pathology has a clear link to the known genetic factors for early onset familial AD. Mutations in the amyloid precursor protein (APP) (Goate et al. 1991) or in components involved in the proteolytic processing of APP to Aβ peptides, namely presenilin-1 (PSEN1) (Sherrington et al. 1995) and presenilin-2 (PSEN2) (Levy-Lahad et al. 1995) that contribute to the γ-secretase complex, are responsible for many cases of early-onset familial AD. APP mutations are found either within the Aβ peptide sequence to enhance amyloid aggregation or else flanking the Aβ peptide sequence so as to enhance

cleavage by β and γ-secretases, leading to increased Aβ peptide formation or alteration of the ratio of Aβ peptide isoforms (Weggen and Beher 2012). Additionally, increased expression of APP can cause AD, as evidenced by the existence of AD-like pathology and neuron loss in Down's Syndrome (Ball and Nuttall 1980) due to trisomy chromosome 21, resulting in an extra copy of the *APP* locus.

Given the involvement of tau protein as the second component of AD pathology, it is surprising that there is little evidence of *MAPT* involvement in the genetics of AD. Only a single mutation in *MAPT* (R406W) has been reported for AD, found in three kindreds with clinical presentations more similar to AD than to frontotemporal dementia (Reed et al. 1997; van Swieten et al. 1999; Rademakers et al. 2003). In recognition of the general acceptance of the amyloid cascade hypothesis, AD has been categorised as a *secondary* tauopathy, where tau pathology, though present, is not the primary causative factor of disease. Strong evidence for the directional effect of Aβ or APP on tau pathology has come from murine studies. Mouse models of tauopathy were created with the *MAPT* P301L mutation that causes FTDP-17 (but not AD) and results in neurofibrillary tangle formation; the combination of these mice with either the delivery of $A\beta_{42}$ fibrils (Götz et al. 2001) or the expression of mutant APP by crossing with Tg2576 mice (Lewis et al. 2001) resulted in enhanced neurofibrillary tangle formation, strongly suggesting a directionality of effect from Aβ to tau.

With little evidence that mutations in *MAPT* contribute to AD in humans, genetic association studies have tried to identify association of *MAPT* and its expression with AD to evaluate whether the level of tau expression could be causative in AD. One recent study has claimed association of the *MAPT* H1 haplotype with AD, including showing that the protective H2 haplotype had lower expression of *MAPT* in post-mortem AD brain (Allen et al. 2014). Another group discovered and replicated an association between AD and the H1c sub-haplotype alone (Myers et al. 2005; Myers et al. 2007a), including further analysis showing

that the H1c allele expresses more *MAPT* transcripts, with a higher proportion of those transcripts containing exon 10 to encode 4R tau (Myers et al. 2007a). However, this genetic association has failed to be satisfactorily replicated in independent cohorts (Mukherjee et al. 2007; Abraham et al. 2009; Allen et al. 2014). Further, an Affymetrix-based expression study showed that the H1c allele had no effect on the expression of *MAPT* transcripts (Trabzuni et al. 2012). Despite the above claims, no GWAS has replicated the association of *MAPT* haplotype with AD, evidenced by meta-analysis of GWAS data (Bertram et al. 2007; Bertram and Tanzi 2009; Lambert et al. 2013). Indeed, the closest to a positive result for *MAPT* was by combining SNPs within 20 kb of *APP*, *PSEN1*, *PSEN2* and *MAPT*, wherein it was found that *MAPT* showed gene-wide significance (Gerrish et al. 2012); however, this method only employed multiple testing correction for four genes, rather than performing gene-wide studies with the inclusion of all known genes. If an association does indeed exist between polymorphisms in *MAPT* and AD it is likely to be of small effect or based on the presence of variants that are not covered by GWAS.

In studies of susceptibility for late-onset AD, the ε4 allele of *APOE* is highly associated (Farrer et al. 1997) and has been consistently replicated in genome-wide association studies (Bertram et al. 2007). As this strong association could mask the effect of any effect of polymorphisms in *MAPT*, a recent study examined association only within *APOE* ε4- individuals and discovered 17 SNPs in a region close to *MAPT* between *KANSL1* and *LRRC37A* (Fig. 1.1) that associated with AD (Jun et al. 2016). Expression differences driven by the SNP with the highest association were implied using a related SNP in high LD, which showed an effect on the expression of *MAPT* exon 3 (Jun et al. 2016). Replication is required to confirm this, but there is the possibility that *MAPT* expression could still play a role in AD risk. Nevertheless, any possible association of *MAPT* with AD is not as strong as the associations with PD and PSP. Thus the genetic basis for AD continues to support the amyloid cascade hypothesis with Aβ/APP being the primary causative agent for disease.

Nevertheless, although the amyloid cascade hypothesis judges tau to play a secondary role in AD by its formation of aggregates stimulated by Aβ-dependent processes, tau has also been shown to be required for toxicity mediated by delivery of Aβ. Delivery of tau by transfection to a monkey cell line that does not express tau made the microtubules vulnerable to disassembly when treated with Aβ preparations (King et al. 2006). Tau knockout mice expressing various forms of human APP were protected from the following results of Aβ toxicity: behavioural deficits and excitotoxicity, notably without altering the amount of Aβ pathology (Roberson et al. 2007; Roberson et al. 2011); NMDA receptor-mediated excitotoxicity (Ittner et al. 2010); neuronal DNA double-strand breaks (Suberbielle et al. 2013). Additionally, *ex vivo* cultures from non-transgenic tau knockout mice were protected from the following results of exogenous Aβ delivery: neuronal degeneration (Rapoport et al. 2002); reduction in motility of cargo during axonal transport in primary hippocampal neurons (Vossel et al. 2010; Vossel et al. 2015); impairment of long-term potentiation in hippocampal slices (Shipton et al. 2011; Roberson et al. 2011); aberrant neuronal cell cycle re-entry in primary cortical cultures (Seward et al. 2013). Intermediates for the connection between tau protein and Aβ toxicity include Fyn, which is localised by tau to dendrites where it can phosphorylate NMDA receptors (Ittner et al. 2010), NMDA receptors even in the absence of tau-Fyn interactions (Vossel et al. 2015), and glycogen synthase kinase 3β (GSK-3β) (Shipton et al. 2011), which required tau for its activation by Aβ (Vossel et al. 2015).

(ii) Progressive supranuclear palsy

PSP is commonly misdiagnosed as PD as it shares many clinical features; however, notably PSP patients show impaired voluntary vertical eye movements, axial rigidity rather than a stooped posture and a lack of tremor (Lubarsky and Juncos 2008). By neuropathology, PSP is

a 4R-predominant tauopathy, also displaying unusual tau inclusions in astrocytes (Litvan et al. 1996). The initial association of the H1 haplotype with PSP has already been described in section 1.2 as it formed an important part of the history of the discovery and later association of the *MAPT* haplotype with PD. This was later refined to be a negative association of the H2 haplotype and a positive association solely of the H1c sub-haplotype (Pittman et al. 2005) and/or one of its individual SNPs rs242557 (Rademakers et al. 2005). A subsequent GWAS confirmed association of both the H1 haplotype and rs242557 that forms part of H1c, with the H1 haplotype showing an odds ratio of 5.50 (Höglinger et al. 2011).

(iii) Corticobasal degeneration

As its name suggests, CBD is an atypical parkinsonism involving atrophy of parietal and frontal regions of the cortex and of the basal ganglia, the latter including SNpc dopaminergic neurons (Litvan et al. 1996). This atrophy leads to clinical symptoms of parkinsonism in addition to cortical dysfunction, such as dementia, language impairment, sensory loss and in some cases an alien limb (Williams 2006). Like PSP, CBD is a 4R tauopathy but shows unusual ballooned neurons. Genetic association of the *MAPT* H1 haplotype with CBD was identified in 2000 (Di Maria et al. 2000; Houlden et al. 2001) and later with individual SNPs of the H1c haplotype (Pittman et al. 2005). In a recent GWAS, CBD was found to share the genetic associations previously found for PSP, namely confirmation of the existing association of the *MAPT* H1 haplotype (p=1.42x10^{-12}) and a new association of rs242557 within the H1c sub-haplotype (p=7.91x10^{-6}), although the H1c association did not persist after the number of H1 alleles was accounted for (Kouri et al. 2015). Additionally both diseases shared an association with myelin-associated oligodendrocyte basic protein (*MOBP*) (Kouri et al. 2015).

(iv) Frontotemporal dementia and parkinsonism linked to chromosome 17

FTDP-17 was named following the discovery of kindreds with atypical dementia where the disease segregated with markers on chromosome 17 (Foster et al. 1997). Neuropathologically they present with atrophy within the frontal and temporal lobes, resulting in distinct changes in personality, and often effects on the basal ganglia thus affecting movement (Foster et al. 1997). There is also significant deposition of aggregated tau (Foster et al. 1997). The genetic association was subsequently narrowed down to the *MAPT* gene when several mutations were identified in FTDP-17 patients (Poorkaj et al 1998; Hutton et al. 1998); incidentally, other frontotemporal dementia kindreds with chromosome 17 association showed ubiquitin-positive inclusions instead of tau pathology and were later identified with mutations in *PRGN* (Baker et al. 2006; Cruts et al. 2006). Mutations in *MAPT* seen in FTDP-17 can be divided into those that alter the interaction of tau with microtubules or otherwise form aggregates and those that affect the splicing of exon 10 (Spillantini and Goedert 2013).

Many of the FTDP-17 mutations in and around *MAPT* exon 10 alter conserved splice sites and splice factor binding sites, leading to the increased inclusion of exon 10 and thus more 4R tau (Hutton et al. 1998; Hasegawa et al. 1999). However, some lead to the exclusion of exon 10, such as the +19 and +29 mutations in intron 10 (Stanford et al. 2003); although these mutations lead to an increase in 3R tau, they do not show formation of insoluble tau aggregates (Stanford et al. 2003). The presence of mutations that alter the splicing of tau show that imbalance of *MAPT* exon inclusion can lead to tau aggregation, in the case of increased 4R tau, and neurodegeneration.

1.3.3 Tau and alpha-synuclein

The possible genetic interaction between *MAPT* and *SNCA* has been investigated with regards to modulation of PD risk. Although one study found that the combination of two *SNCA* SNPs with *MAPT* H1/H1 was significant for PD risk (Goris et al. 2007), several other studies detailed below found no genetic association. *SNCA* contains the REP1 promoter polymorphism consisting of common allele lengths 259, 261 and 263 bp (Maraganore et al. 2006) and one study claimed that the REP1 261/261 and *MAPT* H1/H1 genotypes had "separate and equal effects" on risk for PD rather than interacting (Mamah et al. 2005). Further, meta-analysis of four *SNCA* SNPs, *MAPT* H1/H2 and *MAPT* H1c rs242557 found that although the *SNCA* SNPs and *MAPT* H1 haplotype associated with PD, there was no interaction between them (Elbaz et al. 2011). No interaction was seen in Spanish (Botta-Orfila et al. 2011) or Italian populations (Trotta et al. 2012) or in six further populations (Simón-Sánchez et al. 2009; Wider et al. 2011). Finally, analysis of 256 pairings of 26 variants in *MAPT*, *SNCA* and *LRRK2* for association with PD in a large American cohort also found no interaction between any gene that survived multiple correction (Biernacka et al. 2011). Therefore the majority of evidence shows that there is no genetic interaction between *MAPT* and *SNCA* regarding risk for PD.

There is, however, more evidence that tau and α-synuclein interact at the protein level in a manner that may contribute to neurodegeneration. Biochemical studies showed that α-synuclein directly binds to the microtubule-binding domain of tau in competition with tubulin and can facilitate its phosphorylation (Jensen et al. 1999); in line with this, A30P α-synuclein mice show increased phosphorylation of tau (Frasier et al. 2005). Further, the two proteins may mutually stimulate fibrillisation *in vitro* (Giasson et al. 2003), but interestingly also *in vivo* in mice with both P301L tau and α-synuclein transgenes (Giasson et al. 2003). As the P301L tau mutation and A30P α-synuclein mutation each reduced binding

to their wild-type partners shown by luciferase two-hybrid assay and FRET respectively (Benussi et al. 2005; Esposito et al. 2007), this suggests that the mechanisms of co-fibrillisation and phosphorylation might not require the direct binding first described above. Oligomers of both α-synuclein and tau have been detected in PD brains and found to co-localise (Sengupta et al. 2015). Importantly however, unlike for AD models where tau knockout prevented Aβ-mediated toxicity (see section 1.3.2*i*) tau knockout mice were not protected from the effects of human α-synuclein overexpression, suggesting that tau is not a downstream mediator of α-synuclein toxicity, at least not when there is sufficient additional cause for pathogenesis (Morris et al. 2011). Contrariwise, α-synuclein knockout prevented an increase in tau phosphorylation in the striatum of MPTP-treated mice (Duka et al. 2006).

1.4 Functional outcomes of *MAPT* haplotype

1.4.1 Hypotheses

PD is not a tauopathy, so what role does *MAPT* play in PD? So far I have detailed how the genetic association between *MAPT* and PD is mediated by the H1 haplotype; to understand the functional basis of the association of *MAPT* haplotypes with risk for PD therefore requires study of the differences between the haplotypes. Although it is possible that the risk haplotype, H1, harbours rare mutations, the fact that the haplotype-specific association has been found even in small cohorts strongly suggests otherwise. The same argument holds against as-yet unknown variants within a sub-haplotype of H1 such as H1c. Rather, the association is highly likely to be the result of differences inherent in the set of SNPs in LD that form the haplotype, or in the identified SNPs that form any associated sub-haplotype.

SNPs present in the two overarching *MAPT* haplotypes, H1 and H2, do not alter the amino acid sequence of the tau proteins. Thus the association with PD is almost certainly driven by

non-coding variation that alters one or more aspects of gene expression. Two remaining hypotheses may explain the association of disease risk (Caffrey and Wade-Martins 2012): (1) haplotype affects overall expression of tau through variants in the promoter sequence or microRNA (miRNA) sites in the 3' untranslated region (3'UTR); (2) haplotype affects alternative splicing to produce altered ratios of protein isoforms. However, these two mechanisms are not mutually exclusive and may both contribute to susceptibility to PD.

1.4.2 Haplotype-specific expression studies of total MAPT

The first hypothesis is that the H1 and H2 haplotypes express different levels of total tau, and thus that the total amount of tau present in neurons would impact on risk for PD. In an effort to understand whether the H1 and H2 haplotypes differ in the strength of their promoter for *MAPT*, one group cloned fragments of H1 or H2 containing 5' promoter sequence (~720 bp) plus exon 0 and cloned them upstream of luciferase, where the H1 construct showed 10-20% increased luciferase expression compared to the H2 construct in two cell lines (Kwok et al. 2004). Related studies by another group yielded a similar trend to 20% increase from H1 although this was not statistically significant in their report (Myers et al. 2007a).

Quantitative trait locus (QTL) studies combine phenotypic data with genotype to examine association; this has been performed for transcript data from expression chips. However, for a highly polymorphic locus like *MAPT*, some probes overlap with common SNPs, so that any other allele would be detected more weakly by technical error, confounding the true QTL data (Ramasamy et al. 2013). Three studies claimed association of *MAPT* haplotype with gene-level expression of *MAPT* transcripts using array data for human brain regions (Myers et al. 2007b; Gibbs et al. 2010; IPDGC et al. 2011), one of which specifically removed known

polymorphic probe sets from the analysis (Myers et al. 2007b); however, later reports disputed those studies on the basis of newly discovered common polymorphisms (Trabzuni et al. 2012; Ramasamy et al. 2013), and found no haplotype association of *MAPT* gene level expression across several brain regions using a more refined array (Trabzuni et al. 2012). The same lack of association was confirmed in another study (Latourelle et al. 2012). However, a new study performing RNA-seq on post-mortem human brain showed reduced expression of total *MAPT* in H2/H2 individuals (Valenca et al. 2016).

Studies have also investigated expression from the H1c haplotype. Expression of total *MAPT* was higher in post-mortem human cortex samples from cases and controls homozygous for the H1c sub-haplotype compared to homozygotes for H2 or other H1 sub-haplotypes (Myers et al. 2007a). The same study used luciferase reporter constructs derived from portions of the H1 and H2 promoters to show that the addition of segments containing H1c-tagging SNPs resulted in 4-fold greater expression with the H1c allele SNPs than the H2 allele SNPs (Myers et al. 2007a). Other luciferase reporter constructs showed differential effect of rs242557 but with the opposite effect (Rademakers et al. 2005); however, this shows that constructs using portions of regulatory sequence out of context and order are unlikely to represent the complete physiological truth (Caffrey and Wade-Martins 2012). Finally, another study found no effect of the H1c haplotype on total expression in post-mortem human brain from healthy controls, but rather an effect of age on the relative expression from H1 vs. H2 (Hayesmoore et al. 2009).

1.4.3 Haplotype-specific expression studies of splice isoforms

The second hypothesis is that the H1 and H2 haplotypes express different ratios of the six tau isoforms found in the adult CNS, and thus that individual tau isoforms or the ratio of

those isoforms present in neurons would impact on risk for PD. Evidence that altered splicing of *MAPT* can produce neurodegeneration is shown by the high-risk mutations affecting exon 10 splicing leading to frontotemporal dementia with parkinsonism linked to chromosome 17 (FTDP-17) (Hutton et al. 1998; Spillantini et al. 1998a; Hasegawa et al. 1999) (see section 1.3.2 *iv*). Our laboratory has previously shown haplotype-specific control of exon inclusion in post-mortem brain samples from healthy H1/H2 heterozygous individuals (Caffrey et al. 2006; Caffrey et al. 2008). Using allele-specific quantitation of expression, the H1 allele expressed up to 40% more exon 10+ transcripts and the H2 allele expressed two-fold more exon 2+3+ transcripts (Caffrey et al. 2006; Caffrey et al. 2008). The increased relative expression of exon 10+ transcripts from the H1 haplotype was corroborated by another study using an alternative allele-specific quantitation technique (Majounie et al. 2013) and also by the new RNA-seq study, which used paired-end sequencing to find that the H2 haplotype expresses fewer 1N/4R (exon 2+/exon10+) *MAPT* transcripts (Valenca et al. 2016). In support of the haplotype-specific effect on exon 3, the curated QTL analysis discussed in section 1.4.2, although not finding association of haplotype with total *MAPT* expression, did show enhanced expression of exon 3 alone with increasing number of H2 alleles in all brain regions except white matter (Trabzuni et al. 2012).

The H1c sub-haplotype has also been associated with increased expression of exon 10+ transcripts, encoding 4R tau. Expression of exon 10+ transcripts was elevated from H1c compared to H2 and other H1 sub-haplotype alleles, both in homozygotes and by allele-specific PCR in heterozygotes (Myers et al. 2007a); the exon 10+ increase also appeared to be higher than that of total *MAPT* expression, suggesting that H1c contributes to both hypotheses (Myers et al. 2007a). Another study examined 4R/3R ratio in PSP brains but found no effect of haplotype, although they were considerably underpowered to make that analysis (Ezquerra et al. 2007). Finally, a different H1c-related SNP, rs7521, was associated with higher 4R tau expression in two brain regions (Majounie et al. 2013).

In summary, while there are some data supporting the hypothesis that the H1 haplotype increases total *MAPT* expression, there remains some dispute for this hypothesis. In contrast, the data in support of haplotype-specific effects on *MAPT* isoform expression are stronger and suggest that specific tau isoforms or the ratios of those isoforms play a role in susceptibility for PD, as well as for PSP and CBD.

1.5 Tau protein function

1.5.1 Tau protein domain structure

The tau protein is an intrinsically disordered protein with no permanent secondary structure (Mukrasch et al. 2009), but can be divided into three domains both by virtue of its interactions and by the flexibility of the protein structure (Fig. 1.2A) (Gustke et al. 1994; Mukrasch et al. 2009). The projection domain covers approximately the N-terminal half of the protein, encoded by exons 1, 2, 3, 4, 5, 7 and a small part of exon 9, up to amino acid 197 (numbering of 2N4R, 441 amino acid isoform). The microtubule binding or microtubule assembly domain (amino acids 198-400) comprises the three or four microtubule binding repeats encoded by exons 9-12 and part of exon 13. A proline-rich region in the centre of the protein overlaps the projection and microtubule binding domains, and includes seven PXXP motifs where non-receptor tyrosine kinase proteins containing Src-homology 3 (SH3) domains, such as Fyn, can bind (Lee et al. 1998; Lau et al. 2016). Finally the remaining 41 amino acids at the C-terminus form the C-tail.

1.5.2 Microtubule binding domain

Despite being referred to as microtubule binding repeats, the repeats themselves do not bind strongly to microtubules, but rather the regions immediately flanking the region of three or four repeats, giving rise to a description of the flanks as 'jaws' (Gustke et al. 1994; Preuss et al. 1997). In this model, the microtubule binding repeats act as assembly units, as constructs without the repeats can bind to microtubules but not promote their assembly, both *in vitro* and *in vivo* (Gustke et al. 1994; Preuss et al. 1997). Once microtubules are assembled, tau further acts to stabilise them (Drubin and Kirschner 1986). In addition, the microtubule binding domain and proline-rich region are capable of binding to actin (He et al. 2009; Elie et al. 2015), whereby they can induce the formation of actin bundles (He et al. 2009) or assist in their organisation alongside the microtubule network (Elie et al. 2015). For the latter it was determined that the microtubule binding domain alone was sufficient, but that at least two repeats were required so that one could interact with and assemble each kind of cytoskeletal protein in concert (Elie et al. 2015).

The effect of an extra repeat in the microtubule binding domain constituting 4R tau is discussed further in chapters 4 and 5.

1.5.3 Phosphorylation of tau

Phosphorylation is an important controller of protein function and mediator of signal transduction. Full-length tau protein has 80 serine/threonine residues and 5 tyrosine residues that could alter tau function and/or form potential signalling sites; many kinases have been identified that can phosphorylate 74 and 4 of these respectively (Diane Hanger Laboratory, Tau phosphorylation sites, http://cnr.iop.kcl.ac.uk/hangerlab/tautable, accessed September 2016), including GSK-3β (Muñoz-Montaño et al. 1997) and cyclic-AMP-

dependent protein kinase (PKA) (Litersky et al. 1996). Additionally, while tau extracted from the brains of healthy controls shows phosphorylation of 16 serine/threonine residues, hyperphosphorylation of tau in AD brain leads to the formation of paired helical filaments, which show phosphorylation of at least 42 serine/threonine and three tyrosine residues (http://cnr.iop.kcl.ac.uk/hangerlab/tautable). Immunodetection by the tau-1 antibody is blocked by phosphorylation of the epitope; tau-1 immunohistochemistry shows the presence of non-phosphorylated tau along axonal microtubules, but following dephosphorylation, tau can be detected in the soma and dendrites, showing that phosphorylation state regulates cellular localisation, and thus the function, of tau (Papasozomenos and Binder 1987). Phosphorylation of tau at particular residues, notably S262 in the first microtubule binding repeat, can both induce the detachment of tau from microtubules (Biernat et al. 1993) and protect tau from aggregation into paired helical filaments (Schneider et al. 1999).

1.5.4 Projection domain

While the repeats in the C-terminal half of tau bind to microtubules, the N-terminal 'projection domain' of tau, as its name suggests, protrudes from the microtubule surface (Vallee and Borisy 1977; Vallee 1980; Chen et al. 1992). In doing so, the projection domain acts to repel neighbouring microtubules by entropic force, i.e. to maintain maximal entropy and flexibility of possible conformations of tau, thus each tau molecule acts as a single bristle that assists in determining the spacing of brush-like microtubules (Chen et al. 1992; Mukhopadhyay and Hoh 2001; Ciasca et al. 2012). Further, there is evidence that this spacing is adjustable by phosphorylation state (Mukhopadhyay and Hoh 2001; Shahpasand et al. 2012). Recent evidence from cell-free systems also suggests that microtubule spacing

by tau is both repulsive and attractive, with an opportunity for projection domains on neighbouring microtubules to interact via oppositely-charged segments (Chung et al. 2016).

Experiments using FRET have shown that the N-terminus of tau can interact with the C-terminus, which itself simultaneously interacts with a portion of the microtubule binding repeats, the whole protein being proposed to form a paper clip confirmation (Jeganathan et al. 2006). However, truncation experiments suggest that the important portion of the N-terminus that contributes to these interactions is formed by residues 18-42 (within exon 1) and that the absence of the residues encoded by exons 2 and 3 makes no difference (Horowitz et al. 2006), so that it does not appear to be a function that is differentially regulated by 0N, 1N or 2N tau. A separate investigation of the propensity of tau to undergo 'thermal collapse' and form interactions with parts of itself showed that these contacts were predicted to form by a stretch of residues beginning in exon 3 (Ciasca et al. 2012). A short stretch of the segment encoded by exon 3 shows propensity towards beta-sheet structure, whereas the 0N and 1N forms are predicted to lack particular secondary structure in the N-terminal portion (Mukrasch et al. 2009).

The N-terminus of tau interacts with the p150 subunit of dynactin, a complex that associates with the motor protein dynein, directing the attachment of dynactin to microtubules (Magnani et al. 2007); however, the interaction of tau and dynactin is independent of the sequence encoded by exons 2 and 3 (Magnani et al. 2007).

Finally, tau interacts with the plasma membrane (Brandt et al. 1995) via interactions with Fyn in the proline-rich region (Lee et al. 1998; Pooler et al. 2012). This localisation to the plasma membrane is dependent on the dephosphorylation of tau at many serine/threonine residues (Pooler et al. 2012) and results in the phosphorylation of tau at tyrosine residues by Fyn and Lck kinases, notably residue Y18 in the N-terminus (Lee et al. 2004; Scales et al.

2011). These findings suggest that the projection domain of tau plays some role in signal transduction at the plasma membrane (Pooler and Hanger 2010; Scales et al. 2011).

1.5.5 Axonal transport

Tau is predominantly localised to neuronal axons, so much so that it is implicit in establishing axonal identity and outgrowth, evidenced in primary neurons with acute tau depletion (Caceres and Kosik 1990; Liu et al. 1999). As a regulator of microtubule assembly and stability, tau is important in maintaining the microtubule network needed for the axonal transport of cargo, comprising organelles and vesicles. As microtubules have inherent orientation, with axonal microtubules oriented with the plus end at the distal tip and the minus end at the soma (Black and Baas 1989), the direction of movement along them is dependent on the specific motor protein. The kinesin family of motors is predominantly plus-end directed so they perform anterograde transport and dynein is a predominantly minus-end directed motor that transports retrogradely. While tau is important for stabilising and spacing microtubules, it can also hinder movement of motors along microtubules: *in vitro* experiments with tau-decorated microtubules showed that kinesin detached from microtubules with increasing tau concentration, while dynein was less affected and able to reverse (Dixit et al. 2008); overexpression of tau in primary retinal ganglion cells increased the number of stationary mitochondria and severely inhibited kinesin-mediated anterograde transport (Mandelkow et al. 2004; Stamer et al. 2002). These suggest that the balance of tau in the axon is important for correct functioning of axonal transport. However, overexpression of tau in a human neuronal model showed no effect on axonal transport except when a phosphorylated form of tau was expressed (Mertens et al. 2013). I will discuss more regarding the role of tau and its isoforms in axonal transport in chapter 5.

1.6 Human induced pluripotent stem cell-derived dopamine neurons

The clear monogenic forms of PD, such as mutations in *LRRK2*, *SNCA*, *PINK1* and *PARK2*, have been studied using a wealth of animal and cellular models in order to elucidate possible disease mechanisms that could provide a unifying pathway for PD. Generally, cellular models are more amenable to genetic and environmental manipulation and to analysis by detailed imaging and electrophysiology. However, cancer cell lines, even from human neuroblastomas, offer only limited physiological relevance as cellular models of human neurons and neurodegenerative disease.

1.6.1 Dopamine neuron differentiation from pluripotent stem cells

Pluripotent stem cells (PSCs) are capable of continual self-renewal and of differentiation into all three germ layers: endoderm, mesoderm and ectoderm, the latter of which incorporates all neural tissue. Manipulation of PSCs with specific morphogens can direct differentiation to specific cell fates, including neuronal populations. Since the generation of the first embryonic stem cell (ESC) lines from human blastocysts (Thomson et al. 1998), human ESCs have been used to generate many cell types, including midbrain-type dopaminergic neurons with the potential for both study and transplantation with respect to PD (Perrier et al. 2004; Chambers et al. 2009; Kriks et al. 2011; Sánchez-Danés et al. 2012a).

Several protocols have been published for the generation of dopaminergic neurons from PSCs, using a similar selection of morphogens and growth factors as they have built upon previous work. As an overview, stem cells first undergo neural induction by blocking differentiation to endodermal and mesodermal cell fates (Chambers et al. 2009), second undergo patterning to a ventral midbrain fate by sonic hedgehog (SHH) pathway activation and delivery of anterior-posterior patterning factors (Perrier et al. 2004), and third receive

various factors stimulating neuronal maturation (Badger et al. 2014). As I employed two different protocols in the current study I will discuss more about these in chapter 3.

1.6.2 Induced pluripotent stem cells

The differentiation of cells to particular lineages is a terminal commitment through the application of epigenetic markings that control the expression of key genes and transcription factors, although cycles of epigenetic reprogramming do occur at specific times during embryonic development to reset cell fate, such as the reprogramming of parental imprinting in primordial germ cells (Lee et al. 2002). Ten years ago the first report was made that terminal cell fate could be reversed through delivery of a set of exogenous transcription factors that are normally expressed in stem cells, thus creating induced pluripotent stem cells (iPSCs) (Takahashi and Yamanaka 2006). Yamanaka discovered these factors by selecting a bank of genes thought to control pluripotency in ESCs, delivering them to mouse fibroblasts and then selecting for cells that expressed a resistance gene from the *Fbx15* locus, a gene that is normally expressed in ESCs (Takahashi and Yamanaka 2006). Single factors were not sufficient for reprogramming, but the minimal combination of Oct-3/4, Sox2, Klf4 and c-Myc successfully generated iPSCs (Takahashi and Yamanaka 2006). Distinct from their original identity, the new iPSCs, first made from mouse fibroblasts, were able to self-renew, differentiate into all three germ layers and form functional chimeric embryos when injected into blastocysts (Takahashi and Yamanaka 2006). The process was subsequently performed to generate iPSCs from human fibroblasts, which was successful with the same four factors (Takahashi et al. 2007) and the four transcription factors used in this process have since been named 'Yamanaka factors'. After reprogramming, iPSC colonies begin expressing their endogenous pluripotency factors and silence transgene expression (Takahashi and Yamanaka 2006; Takahashi et al. 2007).

The particular advantage of iPSCs over ESCs is the distinct genetic background of iPSCs corresponding to their specific donor, given that ESCs were already capable of generating physiologically relevant human cell types through differentiation. Thus iPSCs are particularly important in the fields of disease modelling for diseases with a genetic component, and in the fledgling field of personalised cell transplantation. However, in addition to the expected biological variation inherent in the identity of the donor, the nature of the reprogramming leads to differences between clones made from the same donor cells. One study found that some lines still show expression of the reprogramming transgenes in a manner that correlated with the ability of those lines to be directed to differentiate (Boulting et al. 2011). Indeed, even after clones are verified to be free of chromosomal abnormalities, the use of integrating retroviruses that can potentially disrupt/enhance endogenous gene expression or continue to express the transgene after reprogramming may be a significant contributor to intra-individual clonal variation (Beevers et al. 2013). Evidence for the worth of "factor-free" reprogramming (Soldner et al. 2009) to generate iPSC clones includes the finding that the expression signature of iPSCs following Cre-mediated excision of the transgene was more similar to ESCs than for iPSCs with transgene integration (Soldner et al. 2009). However, the technique used in that study still left a small 'footprint' in the genomic DNA, and thus techniques involving no integration and no persistence of factors such as CytoTune Sendai virus are highly preferred (Lieu et al. 2013).

Inter-individual variation can be minimised or controlled for in iPSC studies of particular genetic mutations/variants by generating isogenic lines using genome editing techniques, including homologous recombination (Liu et al. 2011), zinc-finger nucleases (ZFNs) (Soldner et al. 2011), transcription activator-like effector nucleases (TALENs) (Hockemeyer et al. 2011) and the clustered regularly interspaced short palindromic repeats (CRISPR)-associated protein-9 nuclease (CRISPR/Cas9) system (Mali et al. 2013). Unless isogenic lines are

available, variability between clones from the same individual and from different individuals requires the use of multiple lines from multiple individuals to confirm findings.

1.6.3 iPSC-derived dopaminergic neuronal cultures as a model to study Parkinson's disease

The natural consequence of being able to reprogramme fibroblasts from any individual into iPSCs is to use the technique to study cells from patients, dubbed "Diseases in a Dish" (Vogel 2010). There are four groups that could be studied in this regard: (1) patients with identified monogenic causes of PD; (2) patients with idiopathic PD; (3) any individual with a genotype of interest including those considered at risk for disease; (4) healthy individuals as controls alongside groups 1-3. Studying these groups can inform about disease processes and susceptibility in order to better understand PD.

(i) Monogenic PD

Group 1 has been the most studied so far, with iPSC lines reported for dominant *LRRK2* mutations (Nguyen et al. 2011; Sánchez-Danés et al. 2012b; Cooper et al. 2012; Reinhardt et al. 2013; Orenstein et al. 2013; Su and Qi 2013; Sanders et al. 2014; Fernández-Santiago et al. 2015; Hsieh et al. 2016), dominant *SNCA* mutations (Soldner et al. 2011), multiplications of *SNCA* (Devine et al. 2011; Byers et al. 2011) and recessive mutations in *PARK2* (Imaizumi et al. 2012; Aboud et al. 2012; Jiang et al. 2012; Shaltouki et al. 2015) and *PINK1* (Seibler et al. 2011; Cooper et al. 2012; Rakovic et al. 2013); yet although these were differentiated into dopaminergic neuronal cultures, not all reports included phenotypic characterisation. Additionally, lines have been made bearing mutations in *GBA*, considered at risk for PD (Woodard et al. 2014; Fernandes et al. 2016).

In the same way that gene-targeted knock-in mice are more physiologically relevant than those overexpressing a transgene, iPSC models from individuals with disease-related mutations are expected to show better physiological expression patterns and cell-type specific functions than other cell models. For example, in one study human fibroblasts overexpressing Parkin demonstrated Parkin-mediated autophagy of mitochondria (mitophagy), but iPSC-derived dopaminergic neuronal cultures did not produce detectable mitophagy even with Parkin overexpression, despite translocation of Parkin to mitochondria (Rakovic et al. 2013), suggesting that the timing and/or downstream process of mitophagy is different in real neurons (Grenier et al. 2013). The use of these physiologically relevant models to understand PD can reduce the discovery of artefactual or irrelevant phenotypes.

What have iPSC-derived dopaminergic neurons from PD patients with disease-causing mutations told us about PD? First, given that the differentiation protocols produce mixed cultures, some phenotypes have been specifically observed in the dopaminergic neurons and not in non-dopaminergic neighbouring cells, which strongly supports the concept of selective vulnerability of SNpc neurons. These include: an enlarged lysosomal compartment in *GBA* N370S dopaminergic neurons (Fernandes et al. 2016); mutant-specific defects in dopaminergic neuronal survival and mitochondrial volume within *PARK2* mutant cultures (Shaltouki et al. 2015); specific sensitivity of *LRRK2* G2019S dopaminergic neurons to apoptosis following oxidative stress induced by hydrogen peroxide or 6-hydroxydopamine (Nguyen et al. 2011) or following inhibition of mitochondrial complex I by rotenone (Reinhardt et al. 2013). Thus iPSC-derived dopaminergic neurons bearing PD-related mutations are selectively more prone to cell death mediated by reactive oxygen species and show selective defects in autophagy and/or protein clearance mechanisms.

Second, phenotypes observed in whole cultures, or in dopaminergic neurons but without non-dopaminergic neuron comparison, centre on three themes: altered mitochondrial

biology including oxidative stress, altered autophagy and/or protein clearance, and accumulation of α-synuclein. Important examples include: fragmented mitochondria in *LRRK2* G2019S cultures with evidence of overactivation of the mitochondrial fission protein DRP1 (Su and Qi 2013); reduced autophagic flux and autophagosome clearance with accompanying α-synuclein accumulation in *LRRK2* G2019S cultures (Sánchez-Danés et al. 2012b); reduced chaperone-mediated autophagy by *LRRK2* G2019S with α-synuclein accumulation (Orenstein et al. 2013); reduced degradation of Miro with accompanying reduction in mitochondrial clearance in *LRRK2* G2019S cultures (Hsieh et al. 2016); increased accumulation (Woodard et al. 2014) or extracellular release (Fernandes et al. 2016) of α-synuclein in *GBA* N370S cultures.

(ii) Idiopathic PD

Group 2, individuals with idiopathic PD, is one of the most interesting potentials for iPSCs, because any robust phenotypes they display compared to controls would be strong candidates for signatures of disease. As such, the first phenotyping study of iPSC-derived dopaminergic neurons from idiopathic PD patients found some overlap with phenotypes of *LRRK2* mutants in autophagy (Sánchez-Danés et al. 2012b), while a recent study found mitophagy to be impaired in *LRRK2* and idiopathic PD lines, linked to reduced degradation of the mitochondrial adaptor protein Miro (Hsieh et al. 2016). Additionally, iPSC-derived dopaminergic neuronal cultures from both *LRRK2* mutant lines and idiopathic PD lines showed an altered DNA methylation signature compared to control lines, and this signature was specific to dopaminergic neuronal differentiation (Fernández-Santiago et al. 2015), suggesting that dopaminergic neurons in PD patients are inherently different in their gene expression profile. Much more can be done to investigate PD using iPSC-derived dopaminergic neurons from patients with idiopathic PD.

(iii) Additional modelling

Group 3, any genotype of interest, is similar to group 1 but need not be about disease modelling but rather about human genetics. In chapter 4 I use lines corresponding to this group to understand more about *MAPT* haplotype-specific expression in healthy controls with the H1/H2 genotype. With the advent of more reliable genome editing, iPSC/ESC lines can be generated to investigate genetic variants through the engineering of isogenic lines; this was described recently for variants in *SNCA* promoter and enhancer sequences engineered into isogenic ESC lines, accompanied by allele-specific expression analysis, which confirmed that an enhancer element regulates *SNCA* expression but the REP1 polymorphism that had previously been thought to alter *SNCA* expression has no discernable effect (Soldner et al. 2016).

1.6.4 Neuronal maturity and modelling ageing

A major challenge for the study of neurodegenerative diseases associated with ageing is to establish models that represent aged human neurons. Neuronal maturity can be measured by global transcriptome signature, epigenetic markings, neuronal functionality (e.g. electrophysiology) and the presence of mature protein isoforms (e.g. those of *MAPT*).

Global transcriptome profiling by RNAseq and microarrays suggests that human PSC-derived dopaminergic neurons are immature compared to human *SNpc* (Xia et al. 2016), in concert with single-cell RNAseq data from human iPSC-derived cortical neurons revealing a foetal rather than adult identity (Handel et al. 2016). Nevertheless, PSC-derived dopaminergic neuronal cultures from PD patients still exhibited expression signatures observed in *SNpc* from PD patients (Xia et al. 2016), suggesting that immature models remain informative.

The epigenetic signature of donor fibroblasts is generally lost through reprogramming with the Yamanaka factors. Cells acquire an age-related epigenetic signature over time (e.g. reduced histone H3 Lysine-9 trimethylation) according to their 'physiological age', but when 'old' fibroblasts are reprogrammed, their age-related markers reset to align with fibroblasts from young donors and are not regained following differentiation (Miller et al. 2013).

iPSC-derived dopaminergic neurons require extended maturation to display mature electrophysiology and dopamine release. iPSC-derived dopaminergic neurons 8-10 weeks post-differentiation exhibited mature trains of evoked action potentials, some spontaneous action potentials and oscillatory calcium activity (Hartfield et al. 2014).

(i) Progerin expression

One strategy for modelling ageing in iPSC-derived neurons used progerin, a short splice variant of lamin A expressed in Hutchinson-Gilford progeria syndrome (HGPS), to induce rapid 'ageing' of cells (Miller et al. 2013). iPSC-derived fibroblasts either expressing progerin or from HGPS patients showed an 'aged' marker profile, while progerin treatment exposed mutant-specific phenotypes in iPSC-derived dopaminergic neurons bearing *PINK1* or *PARK2* mutations, including reduced neuronal arbour *in vitro* and increased dopaminergic cell death *in vivo* post-transplantation (Miller et al. 2013). However, this technique awaits wider use to create 'aged' iPSC-derived neurons to model PD; reticence may be due to its artificial nature, as even HGPS patients display low expression of lamin A/progerin in neurons (Nissan et al. 2012). The technique may only induce a 'progeria-like' state with similarities to aged cells.

(ii) Induced neurons (transdifferentiation)

Another strategy is 'transdifferentiation', which directly converts somatic cells to another cell type by forced expression of key transcription factors without a pluripotent stem cell stage. "Induced neurons" have been generated by delivering *Ascl1*(*Mash1*)/*Brn2*/*Myt1* to mouse fibroblasts (Vierbuchen et al. 2010), delivering *Ascl1*(*Mash1*)/*Brn2*/*Myt1*/*NeuroD1* to human fibroblasts (Pang et al. 2011), or expressing regulatory microRNAs miR-9/9* and miR-124 assisted by *ASCL1*/*MYTL1*/*NEUROD2* in human fibroblasts (Yoo et al. 2011). Transdifferentiated dopaminergic neurons have been generated from human fibroblasts using *Ascl1*(*Mash1*)/*Brn2*/*Myt1* plus dopaminergic factors *Lmx1a* and *FoxA2* (Pfisterer et al. 2011) and from mouse and human fibroblasts using *Ascl1*(*Mash1*)/*Nurr1*/*Lmx1a* (Caiazzo et al. 2011). Further, knockdown of p53 or Tet1 overexpression may aid transdifferentiation to dopaminergic neurons performed by *Ascl1*(*Mash1*)/*Nurr1*/*Lmx1a* with miR-124 (Jiang et al. 2015).

Transdifferentiated neurons reach stages of electrophysiological maturity much earlier than iPSC-derived neurons (non-dopaminergic), with report of spontaneous action potentials 6 days post-induction (Pang et al. 2011) compared to between 40 and 80 days in culture from iPSCs (Shi et al. 2012). The electrophysiological maturity of transdifferentiated dopaminergic neurons differed whether the starting human fibroblasts were foetal or adult; neurons from human adult fibroblasts showed a less mature electrophysiological profile than their foetal counterparts (Caiazzo et al. 2011) and another study found spontaneous action potentials by 28 days post-induction (Pfisterer et al. 2011). These findings could reflect either (i) the activation of the right transcription factors induces expression of genes responsible for mature neuronal physiology, or (ii) that transdifferentiated neurons retain a 'memory' of their physiological age that is not removed by reprogramming to pluripotency.

Dopaminergic neurons transdifferentiated from mouse embryonic fibroblasts exhibited transcriptome profiles closer to adult midbrain dopaminergic neurons than their source fibroblasts, but nevertheless an incomplete overlap (Caiazzo et al. 2011). In a clearer study, FACS-purified transdifferentiated neurons (non-dopaminergic, $NCAM^{+}$) and their originating fibroblasts both showed transcriptome profiles that differed according to donor age, but the age-specific differences were erased after reprogramming fibroblasts to iPSCs (Mertens et al. 2015). Thus transdifferentiation appears to maintain age-related epigenetic markings that control gene expression, ideal for modelling age-related neurodegenerative disease, whereas iPSC reprogramming resets these marks.

Dopaminergic transdifferentiation has focussed on possible transplantation and published studies of PD phenotypes are still awaited; however, transdifferentiated dopaminergic neurons bearing the FTDP-17 mutation *MAPT* K298E have been reported (Iovino et al. 2014). Transdifferentiated neurons may be a safe option for transplantation as transdifferentiation avoids a pluripotent/progenitor stage that could result in tumour growth (Caiazzo et al. 2011). Transdifferentiated dopaminergic neurons are functional have rescued aberrant movement behaviour caused by unilateral 6-hydroxydopamine lesioned rats (Dell'Anno et al. 2014).

Despite their potential advantages as 'aged' models, the supply of transdifferentiated neurons is limited per reprogramming batch, and ultimately restricted by the expansion capacity of the original fibroblasts. Although the technique has been applied to iPSCs as a 'one-step differentiation protocol' (Theka et al. 2013), they would have already lost any age-related markers through reprogramming.

(iii) Maturity of MAPT

iPSC lines have been made with mutations in *MAPT* to study FTDP-17 then differentiated into cortical neuronal cultures (Iovino et al. 2015; Sposito et al. 2015) or dopaminergic neuronal cultures (Ehrlich et al. 2015). These FTDP-17 studies revealed that iPSC-derived neuronal cultures are not mature with respect to *MAPT* expression. As *MAPT* expression is developmentally regulated, initially only foetal 0N3R tau is expressed and may require significant lengths of culture to detect all isoforms; indeed, the Iovino study found that it took 150 days of differentiation to properly detect three additional isoforms of tau (0N4R, 1N3R, 1N4R) in control cortical neuronal cultures, whereas the *MAPT* splicing mutant line N279K showed clear 1N4R expression by day 55 (Iovino et al. 2015). In contrast the Sposito study required a year of maturation to detect all six adult isoforms in control cortical neuronal cultures, but the exon 10+16 mutant showed at least 0N3R and 0N4R isoforms by day 100 (Sposito et al. 2015). iPSC-derived dopaminergic neuronal cultures were only cultured for a short period so that *MAPT* exon 10+ (4R) transcripts were hardly detectable except with the N279K splicing mutant line, and no exon 3+ transcripts were detected (Ehrlich et al. 2015).

Interestingly, other human PSC-derived neurons have been shown to express adult isoforms of tau in a relatively short period of maturation; forebrain neuronal cultures generated from human embryonic and foetal stem cells both showed clear expression of at least five of the adult isoforms by day 56, with the foetal stem cell-derived cultures maturing more quickly than those from ESCs (Iovino et al. 2010). However, it is not clear whether the rapid maturation of these non-iPSC derived neurons is truly the consequence of the cells themselves or differences in the differentiation protocol. In contrast, transdifferentiated dopaminergic neurons from adult fibroblasts expressed both 3R and 4R tau by day 30 post-induction while those transdifferentiated from embryonic fibroblasts expressed only 3R

tau even at 53 days post-induction (Iovino et al. 2014), affirming that transdifferentiation maintains the physiological age of the donor cells.

I will discuss more about the expression of mature isoforms of tau in iPSC-derived neuronal cultures in chapter 4.

1.7 Aims of the thesis

This thesis comprises four results chapters in which I describe work towards understanding the role of *MAPT* and its encoded tau protein isoforms in iPSC-derived dopaminergic neurons in order to identify reasons underlying the association of the H1/H2 haplotypes with risk for PD.

- In chapter 3 I will outline efforts to generate a human dopaminergic neuronal reporter to identify dopaminergic neurons in live culture. I employed a novel strategy of deliverable reporter, using virtually the entire tyrosine hydroxylase (*TH*) locus from a BAC to drive expression of a fluorescent protein, and packaged the final constructs as herpes simplex virus-1 amplicons. The chapter will detail the construction, refinement and testing of the reporter in immortalised human cell lines and iPSC-derived dopaminergic neuronal cultures to determine its specificity for dopamine neurons.
- In chapter 4 I will describe my findings of haplotype-specific control of *MAPT* expression in iPSC-derived dopaminergic neuronal cultures and human post-mortem midbrain. Importantly I will show how my iPSC-derived cultures express all mature isoforms of tau, and how a newly identified variant alters *MAPT* isoform expression. I will also outline efforts to isolate dopaminergic neurons by fluorescence-activated cell sorting for expression analysis.

- In chapter 5 I will describe the generation of RNA interference tools to knockdown *MAPT* and some of its specific isoforms. I will further describe the effects of tau knockdown on the process of axonal transport of mitochondria in iPSC-derived dopaminergic neuronal cultures at both a young time point and following maturation to express adult isoforms.
- Finally in chapter 6 I will describe preliminary findings of the use of the RNA interference tools generated in chapter 5 to assess the effects of tau knockdown on phenotypes seen previously in our laboratory in iPSC-derived dopaminergic neuronal cultures bearing *GBA* N370S mutation.

Chapter 2: General Methods

All reagents were from Sigma unless specified. All shaking incubation had a 5.1 cm orbit.

2.1 Bacterial culture

E. coli were grown as single colonies on plates of autoclaved LB-Miller agar (Fisher Scientific) or with single colony inoculation of autoclaved LB-Miller broth (Fisher Scientific), with addition of one or more antibiotics: 100 µg/ml ampicillin, 15 µg/ml chloramphenicol, 3 µg/ml tetracycline and 15 µg/ml kanamycin. Starter cultures (1.5 ml LB-Miller broth) were incubated for 16 hours (37°C, 225 RPM) for plasmid minipreps or for 8 hours followed by transfer to 250 ml LB-Miller broth for plasmid maxipreps. Plates were incubated for 16 hours (37°C) to observe single colonies.

2.2 Purification of DNA

2.2.1 Plasmid miniprep

Three methods were used: the Wade-Martins method, suitable for BAC/PAC constructs; the QIAprep Miniprep Kit (QIAGEN) for plasmids <10 kb; the PureLink HiPure Plasmid Miniprep Kit (Invitrogen) for the final versions of lentiviral plasmids, producing low endotoxin minipreps suitable for transfection. The three protocols adopt similar principles but the first does not use a DNA-binding column. The column kits were used according to manufacturer's instructions. DNA from all column-based purification methods was quantified by Nanodrop spectrophotometer (ThermoScientific).

(i) Wade-Martins method

Cultured *E. coli* (1.5 ml) were pelleted by microcentrifugation (2400 RCF, 10 min) and resuspended in 70 µl STET buffer (8% sucrose, 5% Triton X-100, 50 mM EDTA, 50 mM tris, pH 8) by pipetting. Lysis was achieved with 200 µl lysis buffer (1% SDS, 0.2 M NaOH), then neutralised with 150 µl 7.5 M ammonium acetate and incubated briefly on ice. Supernatant from microcentrifugation (18000 RCF, 20 min, 4°C) was mixed with 250 µl isopropanol to precipitate DNA and microcentrifuged (9600 RCF, 8 min). The pellet was washed with 70% ethanol, air-dried and resuspended in 50 µl TE buffer (1mM EDTA, 10mM tris, pH 8) with 5 µg/ml RNase A.

(ii) QIAprep Miniprep Kit

Cultured *E. coli* (1.5 ml) were pelleted by microcentrifugation (2400 RCF, 10 min), resuspended in 250 µl Buffer P1, lysed with addition of 250 µl Buffer P2 (5 min) and neutralised by mixing with 350 µl Buffer P3. Supernatant from microcentrifugation (18000 RCF, 20 min, 4°C) was applied to a QIAprep Spin column and microcentrifuged (16250 RCF, 1 min henceforth). The column was washed with 500 µl Buffer PB, microcentrifuged, washed with 750 µl Buffer PE and microcentrifuged twice before elution of DNA with 30-50 µl Buffer EB or water.

(iii) PureLink HiPure Plasmid Miniprep Kit

PureLink HiPure Mini Columns (gravity flow) were equilibrated with 2 ml Equilibration Buffer. Cultured *E. coli* (3 ml) were pelleted by microcentrifugation (2400 RCF, 10 min), resuspended in 400 µl Buffer R3 with RNase A, lysed with addition of 400 µl Buffer L7 (5 min)

and neutralised by mixing with 400 µl Buffer N3. Supernatant from microcentrifugation (16250 RCF, 10 min, ambient temperature) was applied to an equilibrated column, followed by two washes with 2.5 ml Buffer W8. Elution was achieved with 900 µl Buffer E4. DNA in the eluate was precipitated with 630 µl isopropanol, microcentrifuged (18000 RCF, 30 min, 4°C), resuspended in 1 ml 70% ethanol and microcentrifuged (18000 RCF, 5 min, 4°C). The pellet was air-dried and resuspended in 50 µl TE buffer.

2.2.2 Plasmid maxiprep

Three methods were used: QIAGEN Plasmid Maxi Kit (QIAGEN) with modifications by R. Wade-Martins to accommodate BACs/PACs; NucleoBond Xtra Maxi EF Kit (Machery-Nagel) with modifications to accommodate BACs/PACs, used for endotoxin-free preparations prior to nucleofection; PureLink HiPure Plasmid Maxiprep Kit (Invitrogen), used for low endotoxin preparations prior to lentiviral packaging. All centrifugation steps were carried out in an Avanti J-E Centrifuge with JLA 10.500 rotor (pre-column steps) or JA 17 rotor (post-column steps) (Beckman Coulter). The column kits were used according to manufacturer's instructions with modifications for BACs/PACs. DNA was quantified by Nanodrop spectrophotometer (ThermoScientific).

(i) QIAGEN Plasmid Maxi Kit

Cultured *E. coli* (250 ml) were pelleted (5000 RPM, 15 min, 4°C), resuspended in 15 ml Buffer P1, lysed with addition of 15 ml Buffer P2 (5 min), neutralised by mixing with 15 ml Buffer P3 and incubated on ice (20 min). After centrifugation to remove protein precipitate (8000 RPM, 30 min, 4°C), supernatant was applied to a QIAGEN-tip 500 column that was pre-equilibrated with 10 ml Buffer QBT, using a tissue to prevent fouling of the column. The

column was washed twice with 30 ml Buffer QC then DNA was eluted with 15 ml Buffer QF warmed to 55°C, precipitated with addition of 10.5 ml isopropanol and centrifuged (14000 RPM, 30 min, 4°C). DNA was washed with 3.5 ml 70% ethanol, centrifuged again, then air-dried and resuspended in 250 µl TE buffer for 24 hours (4°C).

(ii) NucleoBond Xtra Maxi Kit

Cultured *E. coli* (300 ml) were pelleted (5000 RPM, 15 min, 4°C), resuspended in 15 ml Buffer RES-EF, lysed with addition of 15 ml Buffer LYS-EF (5 min), neutralised by mixing with 15 ml Buffer NEU-EF and incubated on ice (5 min). NucleoBond Maxi columns were equilibrated with 35 ml Buffer EQU-EF. The neutralised lysate was mixed by inversion and applied to a column with attached filter. The filter was washed with 10 ml Buffer FIL-EF, then removed before washing the column successively with 90 ml Buffer ENDO-EF, 45 ml Buffer WASH-EF and eluting DNA with 15 ml Buffer ELU-EF. DNA was precipitated with 10.5 ml isopropanol, centrifuged (14000 RPM, 30 min, 4°C), washed with 5 ml 70% ethanol, centrifuged (14000 RPM, 5 min, ambient temperature), then air-dried and resuspended in 250 µl H_2O-EF for 24 hours (4°C).

(iii) PureLink HiPure Plasmid Maxiprep Kit

PureLink HiPure Maxi Columns (gravity flow) were equilibrated with 30 ml Buffer EQ1. Cultured *E. coli* (250 ml) were pelleted (5000 RPM, 15 min), resuspended in 10 ml Buffer R3 with RNase A, lysed with addition of 10 ml Buffer L7 (5 min) and neutralised by mixing with 15 ml Buffer N3. After centrifugation (8000 RPM, 30 min), supernatant was applied to an equilibrated column, followed by two washes with 30ml Buffer W8. Elution was achieved with 15 ml Buffer E4. DNA in the eluate was precipitated with 10.5 ml isopropanol,

centrifuged (14000 RPM, 30 min, 4°C), washed with 5 ml 70% ethanol and centrifuged (14000 RPM, 5 min, 4°C). The pellet was air-dried and resuspended in 250 µl TE buffer.

2.2.3 Purification of linear DNA

PCR products and single-fragment digested plasmids <10 kb were purified by QIAquick PCR Purification Kit (QIAGEN). Gel extraction of PCR products and digested plasmids was performed by QIAquick Gel Extraction Kit (QIAGEN). In the following manufacturer's instructions, all microcentrifuge steps were at 16250 RCF for 30-60 s. DNA was eluted with 30 µl water by microcentrifugation.

(i) QIAquick PCR Purification Kit

Five volumes of Buffer PB were added to reaction mixtures with 10 µl 3 M sodium acetate, pH 5.0 if required to bring to pH ≤7.5, then the mixture was applied to a QIAquick column, microcentrifuged, washed with 750 µl Buffer PE and microcentrifuged twice.

(ii) QIAquick Gel Extraction Kit

Following gel electrophoresis, the portion of the gel containing the desired band(s) was removed, weighed and dissolved by incubation with Buffer QG (300 µl/100 mg gel, 50°C, 10 min) with intermittent vortexing. The dissolved DNA/gel mixture was mixed with isopropanol (100 µl/100 mg gel), applied to a QIAquick column and microcentrifuged. The column was washed with 500 µl Buffer QG, microcentrifuged, then washed with 750 µl Buffer PE before being microcentrifuged twice.

2.2.4 Genomic DNA extraction

Genomic DNA from cultured cells was extracted using the Illustra tissue and cells genomicPrep Mini Spin Kit (GE Healthcare) according to manufacturer's instructions. Briefly, frozen cell pellets were lysed in 100 µl Lysis buffer 1 plus 200 µg Proteinase K (15 min, 56°C; 2 min, 70°C) then incubated with 100 µg RNase A (15 min). Following incubation with 500 µl Lysis buffer 4 (10 min), lysate was applied to a spin column (1 min, all microcentrifuge steps at 11000 RCF), washed with 500 µl Lysis buffer 4, microcentrifuged (1 min), washed with 500 µl Lysis buffer 6 and microcentrifuged (3 min). Elution was achieved by microcentrifugation with 200 µl pre-warmed Elution buffer 5.

2.3 Plasmid vector enzymatic reactions

2.3.1 Restriction digests

Analytical digests of plasmid preparations (400 ng) were incubated with 2-10 U restriction enzyme (New England Biolabs Inc., hereafter NEB) in a 15-25 µl reaction for 1-3 hours using the manufacturer's recommended buffers and temperatures, prior to gel electrophoresis.

To facilitate the insertion of PCR-amplified sequences (e.g. mCherry) into a vector, restriction digests were set up to cleave 5 µg of vector maxiprep and the PCR-insert generated with primer-introduced restriction sites using manufacturer's recommended buffers and temperatures. When a single restriction enzyme was used, vector ends were dephosphorylated using calf intestinal phosphatase or Antarctic phosphatase (NEB) according to manufacturer's instructions. Overnight digestion with *Dpn*I enzyme was also used to remove template DNA from PCR products if gel extraction was not required. Digested cloning fragments were purified as detailed in section 2.2.3.

2.3.2 Ligation

Ligation was achieved using T4 DNA ligase (NEB) and multiple ratios of insert:vector (3:1, 5:1, 9:1) with 50 ng vector in a 20 µl reaction, incubated for 2 hours (25°C) or overnight (16°C). Reactions were incubated for 2 hours at room temperature then drop-dialysed using 0.025 µm VSWP membrane discs on Milli-Q water for 1 hour before electroporating.

Ligation of PCR products into pGEM-T Easy was performed using the pGEM-T Easy Vector System (Promega) as per manufacturer's instructions with 30 ng vector and molar ratios of insert:vector between 8:1 and 1:8, then incubated etc. as above.

2.4 Electrophoresis of DNA

DNA fragments (<10 kb) were separated using agarose gel electrophoresis in 1% (w/v) agarose gels with 1X tris-borate-EDTA buffer with $5x10^{-5}$ % (w/v) ethidium bromide staining. Large DNA fragments (>10 kb) were separated using pulsed-field gel electrophoresis (PFGE) 1% (w/v) agarose gels with 0.5X tris-borate-EDTA buffer using the CHEF-DR II system (Bio-Rad) for 16 hours at 14°C, 6 V/cm and post-stained with $7.5x10^{-5}$ % (w/v) ethidium bromide before UV-visualisation.

2.5 Polymerase Chain Reaction (PCR)

2.5.1 AmpliTaq Gold PCR

Unless specified, the AmpliTaq Gold PCR System (Applied Biosystems) was used for analytical PCR according to manufacturer's instructions using experimentally optimised annealing temperatures. The general conditions are shown in Table 2.1.

Table 2.1: Conditions for PCR using AmpliTaq Gold.

PCR component	Volume per reaction (µl)	Final concentration
Water	13.4	-
10X Gold Buffer	2.0	1X
$MgCl_2$ (25 mM)	2.0	2.5 mM
dNTPs (2.5mM each, 10 mM total)	0.5	0.25 mM total
Forward Primer (10 µM)	0.5	0.25 µM
Reverse Primer (10 µM)	0.5	0.25 µM
Taq Gold	0.1	0.25 U
DNA (10 ng/µl)	1.0	-
TOTAL	20.0	-
Cycling Conditions		
Temperature	**Time**	**Cycles**
95°C	15 min	1
95°C	30 s	35
x°C (50-70°C)	30 s	
72°C	30-45 s	
72°C	10 min	1
15°C	hold	1

2.5.2 KAPA HiFi PCR Kit

High fidelity cloning of sequences for incorporation into vectors (*TH* reporter construct in Chapter 3 and shRNA lentiviral constructs in Chapter 5) was performed using the KAPA HiFi PCR Kit or KAPA HiFi HotStart ReadyMix PCR Kit (KAPA Biosystems). Primers introduced additional sequence either including restriction sites to allow ligation into the target vector or homologous sequence to enable Gibson Assembly. PCR reactions (5 x 25 µl) were set up according to manufacturer's instructions using experimentally optimised annealing

temperatures, then pooled PCR products were purified as section 2.2.3 *i*. The general conditions for both kits are shown in Table 2.2.

Table 2.2: Conditions for PCR using KAPA HiFi PCR Kits.

PCR component	Volume per reaction (µl)	Final concentration
Water	17.10	-
5X KAPA Hi-Fi Buffer	5.00	1X
KAPA dNTP Mix (10 mM each)	0.75	0.3 mM each
Forward Primer (10 µM)	0.75	0.3 µM
Reverse Primer (10 µM)	0.75	0.3 µM
KAPA HiFi DNA Polymerase	0.50	1 U
DNA (miniprep)	0.15	-
TOTAL	25.00	-

PCR component	Volume per reaction (µl)	Final concentration
Water	10.00	-
2X KAPA Hi-Fi HotStart ReadyMix	12.50	1X
Forward Primer (10 µM)	0.75	0.3 µM
Reverse Primer (10 µM)	0.75	0.3 µM
DNA (10 ng/µl)	1.00	-
TOTAL	25.00	-

Cycling Conditions		
Temperature	**Time**	**Cycles**
95°C	5 min	1
98°C	20 s	35
x°C (55-70°C)	15-30 s	
72°C	20-120 s	
72°C	5 min	1
15°C	hold	1

2.5.3 Expand High Fidelity PCR System

The Expand High Fidelity PCR System (Roche) was used to amplify sequences >2 kb prior to homologous recombination where primers included 80 bp homology arms at the primer 5' end, or as a first stage of sequencing to amplify a target region from BAC/PAC or genomic DNA. PCR reactions (1-5 x 50 µl) were set up according to manufacturer's instructions using experimentally optimised annealing temperatures, with general conditions shown in Table 2.3. For cloning PCR, template DNA was removed from pooled PCR products by *Dpn*I digestion and purified as section 2.2.3 *i*. For pre-sequencing PCR, unused primers and

nucleotides were subsequently removed by incubation (37°C, 30 min; 80°C, 15 min) with 2 µl FastAP (ThermoScientific), 0.1 µl Exonuclease I (NEB) and 0.9 µl water.

Table 2.3: Conditions for PCR using Expand High Fidelity PCR System.

PCR component	Volume per reaction (µl)	Final concentration
MIX1		
Water	18.00	-
dNTPs (2.5mM each, 10 mM total)	4.0	0.2 mM each
Forward Primer (10 µM)	1.0	0.3 µM
Reverse Primer (10 µM)	1.0	0.3 µM
DNA (20 ng/µl)	1.0	-
SUB-TOTAL	25.0	-
MIX 2		
Water	19.25	-
Expand High Fidelity 10X Buffer with 15 mM $MgCl_2$	5.00	1X 1.5 mM $MgCl_2$
Expand High Fidelity Enzyme Mix	0.75	2.6 U
SUB-TOTAL	25.00	-
TOTAL	50.00	
Cycling Conditions		
Temperature	**Time**	**Cycles**
94°C	2 min	1
94°C	15 s	30
x°C (50-60°C)	30 s	
72°C	2 min	
72°C	7 min	1
15°C	hold	1

2.5.4 Sanger Sequencing

For Sanger sequencing of DNA, single primers were designed >70 bp outside the region of interest, with multiple nested pairs to cover the target region. Sequencing reactions (10 µl) with BigDye Terminator v3.1 (Applied Biosystems) were set up in deep 96-well plates as shown in Table 2.4. PCR products were precipitated by adding 2 µl 125 mM EDTA, 2 µl 3 M sodium acetate and 50 µl 100% ethanol to each well followed by centrifugation (3000 RCF, 4°C, 30 min) and a further 70% ethanol wash (1650 RCF, 4°C, 15 min) before air-drying and freezing. Sequencing was analysed on a 3730xl DNA Analyzer (Applied Biosystems) at the Zoology Sequencing Facility.

Table 2.4: Conditions for Sanger Sequencing PCR.

PCR component	Volume per reaction (µl)	Final concentration
Water	5.75	-
BigDye Terminator v3.1 Ready Reaction Mix	0.5	-
5X Sequencing Buffer	1.75	0.875X
Single Primer (10 µM)	1.0	0.3 µM
Plasmid DNA	1.0	-
TOTAL	10.00	
Water	1.75	-
BigDye Terminator v3.1 Ready Reaction Mix	0.5	-
5X Sequencing Buffer	1.75	0.875X
Single Primer (10 µM)	1.0	0.3 µM
Purified pre-sequencing PCR from BAC/PAC or genomic DNA	5.0	-
TOTAL	10.00	
Cycling Conditions		
Temperature	**Time**	**Cycles**
96°C	1 min	1
96°C	10 s	30
50°C	5 s	
60°C	4 min	
60°C	4 min	1
15°C	hold	1

2.6 Transformation of *E. coli*

2.6.1 Electroporation of E. coli

DNA (10-500 ng in 1-10 µl plasmid preparation, ligation reaction or purified PCR products) was added to 20-50 µl electrocompetent cells (NEB 10-beta Electrocompetent *E. coli* (NEB) or as described in section 2.6.2). Electroporation was performed using the GenePulser Xcell Electroporation System (BioRad) with 0.1 cm cuvettes and pre-set protocol for *E. coli* (exponential decay pulse, capacitance 25 µF, resistance 200 Ω, voltage 1800 V). SOC medium (450 µl, Invitrogen) was added for recovery for 60-70 min (37°C, 225 RPM) and subsequently spread on LB-agar plates with antibiotic(s). Plates were incubated overnight (37°C) and colonies analysed by miniprep.

2.6.2 Electrocompetent cell production for homologous recombination

E. coli containing a BAC/PAC were further transformed with pRed/ET with tetracycline selection and maintenance at 30°C due to the temperature sensitive pSC101 origin of replication. Starter cultures (16 hours, 30°C, 225 RPM) were transferred to 100 ml LB broth and incubated (30°C, 225 RPM) until OD_{600} = 0.10-0.13. Addition of L-arabinose (1.5% w/v) induced expression of homologous recombination proteins via the pBAD promoter during incubation (37°C, 225 RPM) until OD_{600} = 0.30-0.35. Chilled cultures (4°C, 40 min) were centrifuged (JLA 10.500 rotor, 6000 RPM, 4°C, 15 min) and pellets were washed three times with 100 ml 10% glycerol with repeated centrifugation at 7000, 7500 and 7500 RPM. The final pellet was resuspended in 150-250 µl 10% glycerol and snap frozen (-80°C) in aliquots.

2.6.3 Chemical transformation of E. coli

One Shot TOP10 and One Shot Stbl3 Chemically Competent *E. coli* (Invitrogen) were transformed by heat shock as per manufacturer's instructions. Briefly, cells were incubated on ice (30 min) with 1-5 µl DNA then heat shocked (42°C, 30 s) before recovery on ice (2 min). Cells were incubated (37°C, 225 RPM, 1 hour) with 250 µl warm SOC medium before selection on LB-agar plates.

2.7 Mammalian Cell Culture

2.7.1 Immortalised cell lines

Immortalised cell lines (detailed in Table 2.5) were grown adherently in filtered tissue culture flasks (Corning) at 37°C, 5% CO_2. Passaging was performed every 3-5 days by incubation (3 min, 37°C) with trypsin-EDTA solution followed by neutralisation with medium, centrifugation (2880 RCF, 5 min) and resuspension in medium.

Table 2.5: Immortalised cell culture lines and media.

Cell Line	Tissue of Origin	Cell Culture Medium contents
BE(2)-M17	Human neuroblastoma	OptiMEM (Gibco) 10% foetal bovine serum (Gibco) 2mM l-glutamine (Gibco) 1X penicillin/streptomycin (Gibco)
		(former medium) DMEM High Glucose (PAA Laboratories) 10% foetal bovine serum (Gibco) 2mM l-glutamine 1% penicillin/streptomycin (Gibco)
MRC-5 SV2	Human foetal lung fibroblasts transformed with SV40 virus	DMEM/F-12 (Gibco) 10% foetal bovine serum (Gibco) 2mM l-glutamine 1% penicillin/streptomycin (Gibco)
HEK293	Human embryonic kidney cells transformed with sheared Ad5 DNA	DMEM High Glucose (PAA Laboratories / Sigma) 10% foetal bovine serum (Gibco Gibco) 2mM l-glutamine 1% penicillin/streptomycin (Invitrogen)
Vero 2-2	African green monkey kidney epithelial cell clone expressing HSV-1 protein ICP27	DMEM High Glucose (PAA Laboratories / Sigma) 10% foetal bovine serum (Gibco) 2mM l-glutamine 1% penicillin/streptomycin (Gibco) 500 µg/ml G418 (Gibco)
G16.9	Gli36 (human glioma) clone expressing HSV-1 protein VP16	DMEM High Glucose (PAA Laboratories / Sigma) 10% foetal bovine serum (Gibco) 2mM l-glutamine 1% penicillin/streptomycin (Gibco) 200 µg/ml Hygromycin B (Gibco)

2.7.2 Induced pluripotent stem cells

iPSC stocks from the James Martin Stem Cell Facility (see Appendix Table F) were thawed rapidly in a water bath (37°C), transferred to 9 ml Dulbecco's PBS without Ca^{2+}/Mg^{2+} (hereafter $DPBS^{-/-}$), centrifuged (500 RCF, 5 min) and resuspended in 1 ml mTeSR1 medium (Stem Cell Technologies), 1X penicillin-streptomycin with 10 μM Y-27632 (hereafter ROCKi, Tocris Bioscience). Cells were plated on 6-well plates coated with hESC-qualified Matrigel (Corning). mTeSR1/pen-strep medium (2 ml/well) was changed daily. Single cell passaging was performed by incubation (5 min, 37°C) with TrypLE Express (Gibco), neutralisation by dilution with 9 ml $DPBS^{-/-}$, centrifugation (500 RCF, 5 min) and resuspension in medium with ROCKi for 24 hours. Single cells were counted by Scepter (Millipore).

2.7.3 Dopaminergic differentiation of induced pluripotent stem cells

(i) Modified method of Hartfield et al.

This protocol was published by Hartfield et al. (2014) with the addition of CHIR-99021 by Dr J.L. Badger. Induced pluripotent stem cells (iPSCs) were provided as embryoid bodies by the James Martin Stem Cell Facility, then plated in 6-well plates coated with Geltrex (Gibco) with 1.5 ml neural induction medium 1 (day 1; for all media see Table 2.6). Medium was changed 50% on day 4 and replaced with neural induction medium 2 on day 5 with further 50% changes every 2-3 days. Culture medium was replaced with BASF medium on day 11 and changed 50% every 3-4 days.

Neural structures were selected by incision with a sterile needle using a dissecting microsope and transferred to Geltrex-coated glass coverslips in 24-well plates with final differentiation medium. Culture medium was changed 50% every 3-4 days.

Table 2.6: Media for dopaminergic differentiation by the Hartfield method.

Name	Cell Culture Medium Contents
Neural induction medium 1	DMEM/F12 (Gibco) 2mM L-glutamine (Gibco) 1x N2 supplement (Gibco) 1 mg/ml bovine serum albumin (Sigma) 10 μM ROCKi (Calbiochem) 10 μM SB431542 (Tocris Bioscience) 200 ng/ml noggin (Gibco) 1% antimycotic/antibiotic (Gibco)
Neural induction medium 2	DMEM/F12 (Gibco) 2mM L-glutamine (Gibco) 1x N2 supplement (Gibco) 1 mg/ml bovine serum albumin (Sigma) 10 μM ROCKi (Calbiochem) 200 ng/ml human sonic hedgehog C24II N-terminus (R&D Systems) 1% antimycotic/antibiotic (Gibco)
BASF medium	DMEM/F12 (Gibco) 2mM L-glutamine (Gibco) 1x N2 supplement (Gibco) 1 mg/ml bovine serum albumin (Sigma) 10 μM ROCKi (Calbiochem) 200 ng/ml recombinant human sonic hedgehog C24II N-terminus (R&D Systems) 20 ng/ml brain-derived neurotrophic factor (BDNF) (Gibco) 100 ng/ml fibroblast growth factor 8a (FGF8a) (R&D Systems) 5 μg/ml heparin (Sigma) 200 μM ascorbic acid (Sigma) 1% antimycotic/antibiotic (Gibco)
Final differentiation medium	DMEM/F12 (Gibco) 2mM L-glutamine (Gibco) 1x N2 supplement (Gibco) 1x B27 supplement (Gibco) 1 mg/ml bovine serum albumin (Sigma) 20 ng/ml brain-derived neurotrophic factor (BDNF) (Gibco) 20 ng/ml glial cell-derived neurotrophic factor (GDNF) (Gibco) 1 mM N6,2′-O-dibutyryladenosine 3′,5′-cyclic monophosphate (Sigma) 1 μg/ml laminin (Gibco) 200 μM ascorbic acid (Sigma) 1% antimycotic/antibiotic (Gibco)) *First medium following dissection only:* 10 μM ROCKi (Calbiochem)

This method was used for Figs. 3.21A and 3.23 only.

(ii) Modified method of Kriks et al.

This protocol was published by Kriks et al. (2011) and implemented in our laboratory by Mrs H.A. Booth with minor modifications. iPSCs (125000 cells/cm^2) were plated in 6-well plates coated with Geltrex (Life Technologies) then grown to confluency before starting the differentiation as day 0. Media are detailed in Table 2.7. From day 1-19, media was changed 100% and 50% on alternating days. On day 20, cells were dissociated (6-20 min) with StemPro Accutase (Gibco), neutralised with NB medium, centrifuged (300 RCF, 5 min) and resuspended in maturation medium with 10 µM ROCKi before counting by Scepter (Millipore). Cells were re-plated onto plates/coverslips coated with Geltrex (Gibco) or poly-L-ornithine, mouse laminin (Gibco) and human fibronectin in the desired format and density per experiment, ranging from spots of $5x10^4$ cells to an even monolayer of $3x10^5$ cells/cm^2. On day 21, cultures were incubated with 1 µg/ml mitomycin C in NB medium (1 hour) to remove proliferating cells and washed with neurobasal medium before returning to fresh maturation medium. Following a 100% medium change on day 24 to remove dead cells, medium was changed 50% every 2-3 days until use/harvest (≤DIV190).

2.7.4 Harvesting of cell pellets

For analysis of protein, RNA or DNA, cultures were washed with $DPBS^{-/-}$, manually detached in $DPBS^{-/-}$, gently pelleted by microcentrifugation (400 RCF, 3-5 min) and snap frozen on dry ice with -80°C storage.

Table 2.7: Media for dopaminergic differentiation by the Kriks method.

Name	Cell Culture Medium Contents
KO DMEM KSR (basal medium)	KnockOut DMEM (Gibco) 15% (v/v) KnockOut Serum Replacement (Gibco) 1X MEM non-essential amino acids (Gibco) 10 µM 2-mercaptoethanol 2 mM L-glutamine
NNB (basal medium)	Neurobasal Medium (Gibco) 0.5X N2 Supplement (Gibco) 0.5X B27 Supplement (Gibco) 2 mM L-glutamine
NB (basal medium)	Neurobasal Medium (Gibco) 1X B27 Supplement (Gibco) 2 mM L-glutamine
Day 0 medium	KO DMEM KSR basal medium 100 nM LDN-193189 (Sigma) 10 µM SB-431542 (Tocris Bioscience)
Day 1-2 medium	KO DMEM KSR basal medium 100 nM LDN-193189 (Sigma) 10 µM SB-431542 (Tocris Bioscience) 100 ng/ml recombinant human sonic hedgehog C24II N-terminus (R&D Systems) 2 µM purmorphamine 100 ng/ml fibroblast growth factor 8a (FGF8a) (R&D Systems)
Day 3-4 medium	As Day 1-2 medium plus: 3 µM CHIR-99021 (Tocris Bioscience)
Day 5-6 medium	0.75X KO DMEM KSR basal medium 0.25X NNB basal medium 100 nM LDN-193189 (Sigma) 10 µM SB-431542 (Tocris Bioscience) 100 ng/ml recombinant human sonic hedgehog C24II N-terminus (R&D Systems) 2 µM purmorphamine 100 ng/ml fibroblast growth factor 8a (FGF8a) (R&D Systems) 3 µM CHIR-99021 (Tocris Bioscience)
Day 7-8 medium	0.5X KO DMEM KSR basal medium 0.5X NNB basal medium 100 nM LDN-193189 (Sigma) 3 µM CHIR-99021 (Tocris Bioscience)
Day 9-10 medium	0.25X KO DMEM KSR basal medium 0.75X NNB basal medium 100 nM LDN-193189 (Sigma) 3 µM CHIR-99021 (Tocris Bioscience)
Day 11-12 medium	NB basal medium 3 µM CHIR-99021 (Tocris Bioscience) 20 ng/ml brain derived neurotrophic factor (BDNF) (PeproTech) 20 ng/ml glial cell line-derived neurotrophic factor (GDNF) (PeproTech) 1 ng/ml transforming growth factor β3 (TGFβ3) (PeproTech) 10 µM DAPT [1] (abcam) 200 µM ascorbic acid (Sigma) 500 µM N^6,2′-*O*-dibutyryladenosine 3′,5′-cyclic monophosphate (Sigma)
Maturation medium (Day 13 onwards)	As Day 11-12, without CHIR-99021

[1] DAPT, *N*-[*N*-(3,5-difluorophenacetyl-L-alanyl)]-(*S*)-phenylglycine *t*-butyl ester.

2.8 Immunodetection

2.8.1 Western blotting

(i) Protein lysates

Cell pellets were sonicated in RIPA buffer (50 mM tris-HCL, pH 7.4, 150 mM NaCl, 1% (v/v) Triton X-100, 1% (w/v) sodium deoxycholate, 0.1% (w/v) SDS) for standard Western blotting, or in TBS (20 mM tris-HCl, pH 7.4, 140 mM NaCl) when protein dephosphorylation would follow; cOmplete mini protease inhibitors (Roche) were added to both. After incubation on ice (30 min), the soluble fraction was isolated by microcentrifugation (1200 RCF, 20 min, 4°C).

(ii) Bicinchoninic acid protein assay

Protein concentrations were determined by BCA assay (Sigma) with a calibration curve of bovine serum albumin (BSA) from 0-1 µg/µl in triplicate wells. Protein lysates were diluted 10X in RIPA/cOmplete buffer before running in triplicate wells. Bicinchoninic acid solution and 4% (w/v) copper(II) sulphate pentahydrate in 50:1 ratio were mixed and 100 µl added to each well before incubation (30 min, 37°C). Complexes were detected at 562 nm using a Synergy HT plate reader (BioTek).

(iii) Western blotting

For protein dephosphorylation to reveal tau isoforms, 15-20 µg protein samples were incubated with lambda phosphatase (NEB) (20 units/µl, 60 min, 30°C) followed by denaturation with Laemmli buffer (Laemmli 1970) (95 °C, 10 min). Standard samples without

dephosphorylation had 2.5-10 µg protein loading in Laemmli buffer. Protein separation was achieved using either 10% (dephosphorylated protein blots) or 4-15% (other blots) Criterion TGX polyacrylamide gels (Bio-Rad) in a tris-glycine running buffer, with transfer to a PVDF membrane using the TransBlot-Turbo Transfer System (Bio-Rad) (2.5 A, 12 min), or previously by wet blotting (100 V, 70 min) to an Immobilon-P PVDF 0.45 µm membrane (Millipore) in 0.048 M tris, 0.04 M glycine, 20% (v/v) methanol.

Blots were blocked with 5% milk (Sigma) in TBS with 0.1% (v/v) Tween 20 (TBST), incubated with primary antibody in 1% milk-TBST (overnight, 4°C), washed three times with TBST, probed with horseradish peroxidase (HRP)-conjugated secondary antibody in 1% milk-TBST for 1 hour at room temperature, and washed four times in TBST. Immobilon Western Chemiluminescent HRP Substrate (Millipore) was added and chemiluminescence detected using the Gel Doc™ XR+ System or ChemiDoc Touch System (Bio-Rad). Bound proteins were removed using Restore Western Blot Stripping Buffer (ThermoScientific, 15 min) and immunodetection was repeated using additional antibodies. Antibodies used in this thesis are detailed in Table 2.8.

Table 2.8: Antibodies used in Western blotting.

Name	Supplier	Product Code	Concentration
α-synuclein	Covance	SIG-39730-200	1:250
β-actin	abcam	ab8227	1:10000
β-actin, HRP-conjugated	abcam	ab49900	1:20000
β3-tubulin (Tuj1)	Covance	MMS-435P	1:1000
BiP/GRP78	abcam	ab21685	1:1000
GBA	abcam	ab128879	1:500
LAMP1	abcam	ab24170	1:250
LAMP2A	abcam	ab18528	1:500
LC3B	Sigma	L7543	1:1000
p62	abcam	ab56416	1:500
Tau-1 clone PC1C6	Millipore	MAB3420	1:1000
Tau-5	NeoMarkers	MS-247-P	1:2500-1:5000
Tau, 2N, clone 71C11	Covance	Sig-39408	1:1000
Tau, 4R, repeat isoform RD4	Millipore	05-804	1:250
Tyrosine hydroxylase	Millipore	ab152	1:1000-1:2000
HRP-conjugated goat anti-mouse	Bio-Rad	170-6516	1:5000

HRP-conjugated goat anti-rabbit	Bio-Rad	170-6515	1:5000

2.8.2 Immunocytochemistry

Cultures grown on glass coverslips were washed with Dulbecco's PBS with Ca^{2+}/Mg^{2+} (hereafter $DPBS^{+/+}$), fixed with 4% (w/v) paraformaldehyde in $DPBS^{+/+}$ for 10-15 min and washed three times with $DPBS^{+/+}$. Cell permeabilisation and protein blocking were performed with 10% serum (goat or donkey, matching secondary antibody species) in PBS 0.1% Triton X-100 (PBST, 2 hours) prior to incubation with primary antibodies in PBST with 1% serum (4°C overnight). Coverslips were washed three times with PBST and incubated with Alexa Fluor-labelled secondary antibodies (1 hour). Coverslips were washed with PBS and incubated with 1 µg/ml DAPI in PBS (5 min) then washed with PBS. Coverslips were mounted on glass slides with FluorSave (Calbiochem) and cells imaged using an EVOS FL Auto Imaging System (Life Technologies) or Nikon Eclipse TE-2000-U fluorescent microscope. Antibodies used in this thesis are detailed in Table 2.9.

Table 2.9: Antibodies used in immunocytochemistry.

Name	Supplier	Product Code	Concentration
β3-tubulin (Tuj1)	Covance	MMS-435P	1:500
FOXA2	R&D Systems	AF2400	1:250
GFAP	abcam	ab4674	1:1000
GFP	Aves Labs	GFP-1020	1:300
mCherry	Clontech	632543	1:2500
Tyrosine hydroxylase	Millipore	ab152	1:250-1:300
Donkey anti-goat 647	Invitrogen	A21447	1:500
Donkey anti-mouse 594	Invitrogen	A21203	1:500
Donkey anti-rabbit 488	Invitrogen	A21206	1:500
Goat anti-chicken 488	Invitrogen	A11039	1:500
Goat anti-chicken 647	Invitrogen	A21449	1:500
Goat anti-mouse 488	Invitrogen	A11001	1:500
Goat anti-mouse 594	Invitrogen	A11005	1:500
Goat anti-mouse 647	Invitrogen	A21236	1:500
Goat anti-rabbit 594	Invitrogen	A11012	1:500
Goat anti-rabbit 647	Invitrogen	A21245	1:500

2.9 Transfection of immortalised cell lines

Cells were seeded in 12-well or 6-well plates to achieve ~50% confluency the following day. Unless otherwise stated, plasmids transfection complexes were formed using Lipofectamine or Lipofectamine LTX and Plus Reagent in OptiMEM (all Invitrogen) according to manufacturer's instructions (Table 2.10). Cells were washed 2x with OptiMEM and left in 1 ml OptiMEM before adding complexes. Transfections were left for 4 hours, washed 3x with OptiMEM and replaced with normal medium. Cells were harvested or imaged by fluorescence microscopy after 24-96 h.

Table 2.10: Standard conditions for plasmid transfection of immortalised cell cultures.

Component	Amount per 6-well well	Procedure
Tube A		
OptiMEM	250 µl	Mix and incubate for 10 min
Plasmid DNA maxiprep	5 µg	
PLUS reagent	5 µl	
Tube B		
OptiMEM	250 µl	Mix then add drop-wise to Tube A.
Lipofectamine or Lipofectamine LTX	16 µl or 12.5 µl	

2.10 Transcriptional analysis

2.10.1 RNA extraction

Three kits were used to extract RNA: RNAqueous Micro kit (Ambion) used in chapter 3; RNeasy Mini and RNeasy Micro Kits (QIAGEN) used in subsequent chapters dependent on cell number. All kits were used according to manufacturer's instructions including DNase I treatment. RNA concentration was determined by Nanodrop (Thermo Scientific).

(i) RNAqueous kit

Pelleted cells were lysed in 100 µl Lysis Solution followed by 50 µl 100% ethanol before applying to the spin cartridge by microcentrifugation, washing with 180 µl Wash Solution 1, two washes with 180 µl Wash Solution 2/3 and a further microcentrifugation (16250 RCF, 1 min). Elution was achieved with 2x10 µl Elution Solution (75°C). Eluate (17 µl) was incubated with 1.7 µl 10X DNase I Buffer and 1 µl DNase I (37°C, 20 min) then with 2 µl DNase Inactivation Reagent (2 min) before microcentrifugation (16250 RCF, 1.5 min) and collection of the supernatant.

(ii) RNeasy Mini Kit

Pelleted cells were lysed in 350 µl Buffer RLT, 1% 2-mercaptoethanol and passed through a QIAshredder spin column (16250 RCF, 2 min). After mixing with 350 µl 100% ethanol the lysate was applied to an RNeasy spin column by microcentrifugation (9600 RCF, 15 s hereafter), washed with 350 µl Buffer RW1 then incubated (15 min) with 10 µl DNase I (27 U), 70 µl Buffer RDD before washing with 350 µl Buffer RW1. Two washes with 500 µl Buffer RPE were followed by microcentrifugation (16250 RCF, 1 min) with a fresh collection tube, and then eluted with 30 µl water into a new tube by microcentrifugation (16250 RCF, 1 min).

(iii) RNeasy Micro Kit

Details match those of section 2.10.1 *ii*, with the exception of RNeasy MinElute spin columns, until after the second Buffer RW1 wash. The column was washed once with 500 µl Buffer RPE then with 500 µl 80% ethanol with longer microcentrifugation (9600 RCF, 2 min),

further microcentrifugation (16250 RCF, 5 min) with a fresh collection tube and elution with 14 µl water by microcentrifugation (16250 RCF, 1 min).

2.10.2 cDNA Synthesis

(i) SuperScript III

First-strand cDNA synthesis was performed using SuperScript III Reverse Transcriptase (Invitrogen) as detailed in Table 2.11. Negative controls were made with water in place of SuperScript enzyme.

Table 2.11: Conditions for SuperScript III First-Strand cDNA Synthesis.

Component	Volume per reaction (µl)	Final concentration
Water	11 µl combined	-
Total RNA (600-1000 ng)		-
dNTPs (10 mM each)	1	0.5 mM
Random primers (150 ng/µl)	1	150 ng
SUB-TOTAL	13	-
→ 65ºC for 5 min, ice for 1 min		
5X First-Strand Buffer	4	1X
0.1 M DTT	1	5 mM
RNaseOUT RNase Inhibitor (40 U/µl)	1	2 U
SuperScript III RT (200 U/µl)	1	10 U
TOTAL	20	-
→ 25ºC for 5 min, 55ºC for 60 min, 70ºC for 15 min		

(ii) SuperScript VILO

First-strand cDNA synthesis was performed using SuperScript VILO MasterMix (Invitrogen). RNA (100-1000 ng) and 4 µl SuperScript VILO MasterMix were made to 20 µl with water and incubated (25°C, 10 min; 42°C, 2 hours; 85°C, 5 min). Negative controls were made by heat inactivating the MasterMix and water (65°C, 10 min) before adding the RNA and incubating as above.

2.10.3 End-point RT-PCR

End-point RT-PCR was performed using AmpliTaq Gold (section 2.5.1) with primers detailed in Appendix Table D.

2.10.4 Quantitative Real-Time PCR

All qRT-PCR assays were run on a StepOnePlus System (Applied Biosystems) using either TaqMan Gene Expression Master Mix or Fast SYBR Green Master Mix (Applied Biosystems) as detailed in Tables 2.12 and 2.13. FAM-labelled TaqMan Gene Expression Assays for *MAPT* were multiplexed with VIC-labelled assays for housekeeping genes (all Applied Biosystems, Appendix Table H). A common threshold value of 0.1 was set for all TaqMan assays to enable comparison. Primers for SYBR Green expression assays are listed in Appendix Table K. Expression of total *MAPT*, *RBM4* and *PTBP1* were determined as 2^–(Assay C_T – housekeeper geometric mean). Expression of *MAPT* isoforms was normalised to total *MAPT* instead of housekeepers, with exon % inclusion determined by the formula [2^–(*MAPT* isoform assay C_T – Total *MAPT* C_T)]*100.

Table 2.12: Conditions for qRT-PCR with TaqMan Gene Expression Master Mix.

PCR component	Volume per reaction (µl)	Final concentration
Water	3	-
TaqMan Gene Expression Master Mix (2X)	10	1X
Tau probe/primer mix (20X) FAM	1	1X
Housekeeper probe/primer mix (20X) VIC	1	1X
cDNA (1 or 2 ng/µl)	5	5 or 10 ng
TOTAL	20	-
Cycling Conditions		
Temperature	**Time**	**Cycles**
50°C	2 min	1
95°C	10 min	1
95°C	15 s	40
60°C	1 min	

Table 2.13: Conditions for qRT-PCR with Fast SYBR Green Master Mix.

PCR component	Volume per reaction (µl)	Final concentration
Water	3	-
Fast SYBR Green Master Mix (2X)	10	1X
Primer Pair (2 µM forward, 2 µM reverse)	2	200 nM each
cDNA (1 or 2 ng/µl)	5	5 or 10 ng
TOTAL	20	-
Cycling Conditions		
Temperature	**Time**	**Cycles**
95°C	20 s	1
95°C	3 s	40
60°C	30 s	

Chapter 3: Generation and validation of a human dopaminergic reporter

3.1 Introduction

On a cellular level, pathologically confirmed PD is characterised by the progressive loss of dopaminergic neurons in the SNpc, and in most cases some of the remaining neurons exhibit aggregated deposits of alpha-synuclein formed into Lewy bodies (Spillantini et al. 1997). Despite the detection of Lewy bodies and Lewy neurites throughout the brain stem and later within cortical regions (Braak et al. 2003), the degree of cell loss observed in the SNpc is selective (Hirsch et al. 1988) and does not always correlate with the overall burden of Lewy body pathology (Parkkinen et al. 2011), suggesting that SNpc neurons themselves are particularly susceptible to the toxic processes of PD. Further, the pattern of cell loss within the SNpc is different to the loss seen in ageing (Fearnley and Lees 1991), so PD does not simply accelerate the process that occurs naturally.

The study of this critical cell type *in situ* in the brain has led to the generation of animal models to examine the effects of genetic mutations, environmental factors and toxic insults on the health of SNpc dopaminergic neurons as well as the impact of their loss, often induced through potent dopaminergic toxins e.g. 1-methyl-4-phenyl-1,2,3,6-tetrahydropyridine (MPTP) (Heikkila et al. 1984). However, the identification of these neurons by fluorescence while alive has been difficult, as this requires a cell-type specific promoter to drive the expression of a fluorescent protein.

Candidate promoters in mammals include the tyrosine hydroxylase gene (*TH* or *Th*) and the pituitary homeobox 3 gene (*PITX3* or *Pitx3*). The TH enzyme catalyses the addition of a hydroxyl group to L-tyrosine to yield L-dihydroxyphenylalanine (L-DOPA); this reaction forms

the rate-limiting step in the synthesis of dopamine as well as the other catecholamines noradrenaline and adrenaline that are produced by further metabolism from dopamine. As such this enzyme is crucial to all catecholaminergic neurons, although dopaminergic neurons of the SNpc that form the nigrostriatal pathway are anatomically separate from populations of noradrenergic and adrenergic neurons. Alternatively, PITX3 is a transcription factor that is involved in the regulation of midbrain dopaminergic neurons, and is more restricted in its expression than TH (Messmer et al. 2007).

Transgenic mice have been made carrying most of the human *TH* locus, comprising all exons and introns, 2.5 kb of 5' promoter and 0.5 kb downstream (Kaneda et al. 1991); expression generally matched that of mouse Th but there was some ectopic expression in non-catecholaminergic regions. Likewise, the use of limited portions of the human *TH* 5' promoter – 5 kb (Nagatsu et al. 1994) or 11 kb (Kessler et al. 2003) – to drive reporter gene expression in transgenic mice have also shown ectopic expression. Nevertheless, the 11 kb promoter construct has since been used to generate a GFP-expressing rat model with selection of a founder line showing minimal ectopic expression (Iacovitti et al. 2014).

In contrast to animal models, the study of these neurons in the brains of individuals with or without PD is for the most part restricted to non-invasive imaging techniques, e.g. positron emission tomography (PET), or functional magnetic resonance imaging (fMRI), which provide only very limited observational information and cannot be manipulated. The dawn of stem cell technology, first by differentiation of human ESCs and most recently by differentiation of iPSCs obtained from any donor of choice, allows the study of this critical neuronal cell type *in vitro*, with a large toolkit of manipulations and experimental designs available for use.

Identification of live dopamine neurons within iPSC-derived cultures has so far been impossible due to the lack of a reliable fluorescence reporter, whether engineered into the genome of individual clones or delivered by viral means. Nevertheless, recently a human ESC

line has been engineered to express EGFP from one allele of *PITX3* and showed >90% co-localisation of EGFP with dopaminergic markers following differentiation to dopaminergic neuronal cultures (Watmuff et al. 2015); this followed similar reports made in a mouse ESC line (Zhao et al. 2004; Hedlund et al. 2008). However, the creation of genetically engineered reporter knock-in iPSC lines for each donor individual would be impractical, so ideally a reporter construct that can be delivered to any human cell culture would be employed. While a fragment of the mouse *Pitx3* 5' promoter has been used as a deliverable construct for human neuroblastoma culture (Castillo-Carranza et al. 2008), it showed low expression and no further reports have been made of constructs using this or the human *PITX3* promoter.

Further to the efforts described above using portions of the human *TH* locus in transgenic mice, one group attempted to generate a dopaminergic reporter for human cell culture using minimal portions of the human *TH* 5' promoter incorporated into a lentiviral construct. Following the identification of five conserved regions in the 5' promoter of human, mouse and rat, the five human regions were sequentially combined, yet the construct containing all five only showed 47% specificity in differentiated neuronal culture (Romano et al. 2005). Their further attempts with 6.3 kb of contiguous sequence comprising the latter three conserved regions plus the first intron of *TH* positioned 3' to the GFP reporter were not successful in cell culture using mixed TH+/TH- cells (Romano et al. 2007). Additional studies showed that polymorphic sequences in *TH* intron 1 assist in regulating gene expression (Meloni et al. 1998; Albanèse et al. 2001); for example, replacement of both exon 1 and intron 1 of endogenous mouse *Th* produced reporter expression in proportionally few cells, some of which were non-catecholaminergic (Kelly et al. 2006).

The above attempts to produce a minimal human *TH* promoter were directed by the 9 kb limit for packaging RNA into lentiviral particles. However, the use of such designs requires

the removal of sequence that may still assist in regulation of gene expression. The distance upstream of the *TH* translation start site before reaching the next defined locus is 95 kb and this region could contain additional distal promoter elements beyond those that have already been identified within the first 11 kb of 5' promoter (Kessler et al. 2003). Ideally, a whole genomic locus with full promoter sequence would be used to generate a reporter that is regulated in the same physiological manner as the endogenous gene; however, genomic loci comprising all coding and regulatory sequences usually exceed the packaging limit for lentiviruses so require an alternative strategy. Whole genomic loci can be cloned into bacterial artificial chromosomes (BACs) or P1-derived artificial chromosomes (PACs) up to a few hundred kilobases long. Herpes simplex virus-1 (HSV-1) amplicons, which can package 152 kb of any DNA construct containing the viral packaging signal, are therefore suitable for packaging of large BACs/PACs for cellular delivery of entire genomic loci (Wade-Martins et al. 2001). This enables the use of an entire genomic locus rather than minimal promoter elements to drive reporter gene expression. Further, manipulation of large DNA constructs such as BACs/PACs requires particular tools, namely homologous recombination by Red/ET recombination (Zhang et al. 2000) rather than restriction digest and ligation, and separation of DNA by pulsed-field gel electrophoresis (PFGE).

Despite the difficulty of manipulating and utilising BAC/PAC constructs, they are invaluable as a tool for studying gene expression and for enabling expression of alternatively spliced gene products. For this reason they have been widely used to generate stable transgenic animal models that maintain the physiological regulation of the donor locus. However, studies also support a physiological regulation of expression when BAC/PAC constructs are delivered to animals and cell culture by HSV-1 amplicon transduction. For example, physiological regulation of splicing has been shown by delivery of the *CDKN2* region to glioma cells that rescued expression of three correctly-spliced encoded mRNAs along with concomitant growth inhibition (Inoue et al. 2004), and by delivery of the human *MAPT* locus

to mouse primary cultures that subsequently expressed splice isoforms corresponding to both 3R and 4R tau (± exon 10) (Peruzzi et al. 2009). Cell-type specific expression has been shown through delivery of the gonadotropin-releasing hormone gene *GnRH* to the brains of *ΔGnRH* mice where expression was generally restricted to the expected brain regions unlike constitutive GFP expression (Jeong et al. 2007); this concept has been shown further by the expression of *lacZ* from glutamatergic neuron-specific promoters (*PAG*, *VGLUT1*) and a GABAergic neuron-specific promoter (*GAD67*), which each showed ~90% cell-type specificity of expression when injected into rat cortex (Rasmussen et al. 2007). Finally, HSV-1 amplicons are capable of demonstrating expression that is dependent on cell state, as evidenced by the delivery of the low density lipoprotein receptor (*LDLR*) locus to *ΔLdlr* cells whereby the levels of expressed LDLR were capable of being repressed by sterols as would be seen with endogenous expression (Lufino et al. 2007), supporting the concept that episomal genomic DNA constructs can exert physiological gene expression.

3.1.1 Aims of the Chapter

- To detail the generation of a deliverable dopaminergic neuronal reporter using the entire genomic locus of human *TH* to control expression. This novel PAC-based approach includes all regulatory elements found in the 5' promoter, exons, introns and 3' downstream sequences, replacing only the coding portion of exon 1 with a self-contained fluorescent protein cassette. As a result, the expression of the fluorescence reporter is driven by the native *TH* promoter but does not allow transcription from the remaining exons of *TH* contained within the PAC.
- To detail efforts to validate expression from the construct in TH+ and TH- immortalised cell lines and in iPSC-derived dopaminergic neuronal cultures.

3.2 Methods

3.2.1 Plasmids and primers used in the construction of TH-*PAC reporters*

For full lists of plasmids and primers used in this chapter, see Appendix Tables A-C. Of special mention, BAC RP11-542J6 containing the human *TH* locus from chr11p15.5 was previously sub-cloned into a PAC by Mr S.P. Shorkey to eliminate the remaining loci (*IGF2*, *INS*, *ASCL2*, *C11orf21* and *TSPAN32* as per UCSC Genome Browser GRCh38/hg38 Assembly), leaving ~70 kb upstream of the translation start site and 0.7 kb downstream of the 3' untranslated region (3' UTR) (S.P. Shorkey, MSc Dissertation, Hilary Term 2012).

3.2.2 Retrofitting of plasmids with HSV-1 amplicon sequences

Reporter constructs were retrofitted with HSV-1 amplicon sequences by Cre-mediated recombination with retrofitting plasmids pEHHG (Wade-Martins et al. 2001) or pH-FRT-Hy (Alegre-Abarrategui et al. 2009) by a modified method of Lufino et al. (2011). Inverted ratio combinations of 50-100 ng PAC-based reporter construct and 1-2 µg retrofitting plasmid were used in 30 µl reactions in 1X Cre buffer with 1 µl Cre recombinase (Novagen). Reactions were incubated (37°C, 1 hour) then heat-inactivated (70°C, 5 min) before dialysing on 0.025 µm VSWP filters (Millipore) over MilliQ water for 2 hours then electroporated into *E. coli* (15 µl reaction, 20 µl bacteria; see section 2.6.1) for selection by both the antibiotic(s) of the reporter construct and the ampicillin resistance of the retrofitting plasmids.

3.2.3 Production and use of HSV-1 based amplicons

(i) Packaging of HSV-1 based amplicons

Improved helper virus-free packaging (Saeki et al. 2001) was performed according to published protocols (Lufino et al. 2011). Briefly, $1x10^6$ Vero 2-2 cells were seeded in 6 cm dishes in DMEM Complete medium (without G418), six dishes per retrofitted *TH*-PAC construct and three dishes per unmodified retrofitting plasmid for controls due to the increased transfection efficiency of and viral titres from these smaller constructs. After 24 hours, each dish of Vero 2-2 cells was co-transfected with 1.8 µg retrofitted *TH*-PAC (or 0.6 µg unmodified retrofitting plasmid for controls), 2 µg fHSVΔpacΔ27 0++ (Saeki et al. 2001) and 0.2 µg pEBHICP27 (Saeki et al. 2001); all DNA was incubated with 10 µl/dish PLUS reagent (Invitrogen) in 250 µl/dish OptiMEM (Gibco) followed by drop-wise addition of 23 µl/dish Lipofectamine (Invitrogen) in 250 µl/dish OptiMEM and incubation for 30-40 min for complex formation then topped up with OptiMEM to a final volume of 1.5 ml/dish. Cells were washed twice with 2.5 ml OptiMEM before replacement with diluted complexes. After four hours, cells were washed three times with 2.5 ml OptiMEM then replaced with 3.5 ml packaging medium (DMEM high glucose [Sigma], 6% [v/v] foetal bovine serum, 1X penicillin-streptomycin, 1X L-glutamine, 25 mM HEPES [all Gibco]). After 72 hours, cells were detached by scraping and cells and medium were pooled in a 50 ml Falcon tube for all dishes per amplicon then frozen on dry ice. Tubes were thawed in water (~30°C) prior to sonication to break cell membranes (50% amplitude, 30 s for six dishes or 20 s for three dishes). Debris was removed by centrifugation (2450 RCF, 15 min, 4°C) then the supernatant was filtered (0.22 µm) into a SW32Ti ultracentrifuge tube with additional ice-cold PBS and an underlay of 5 ml ice-cold 30% sucrose in PBS before ultracentrifugation (SW32Ti, 22,000 RPM, 2 hours, 4°C). After rapid aspiration of the supernatant the pellet was

resuspended in 250 µl medium (DMEM Complete medium or base for Final medium from iPSC differentiation without growth factors) and stored as aliquots at -80°C.

(ii) Titration of HSV-1 based amplicons

Titration of amplicons was carried out in G16.9 cells (Inoue et al. 2004) with detection either by EGFP fluorescence (pEHHG-retrofitted) or X-gal staining (pH-FRT-Hy) also as described (Lufino et al. 2011). Briefly, $4x10^5$ G16.9 cells were seeded per well of 24-well plates in DMEM Complete medium (without Hygromycin B). After 24 hours, medium was replaced with the following volumes of amplicons diluted to 250 µl in titration medium (DMEM high glucose [Sigma], 2% foetal bovine serum, 1X penicillin-streptomycin, 1X L-glutamine, 25 mM HEPES [Gibco]): 5 µl, 2 µl, 0.5 µl, 0.1 µl, 0.02 µl, 0.004 µl. For EGFP-expressing constructs, fluorescence was examined after 24 hours and counted as described below. For *lacZ*-expressing constructs, cells were fixed with 250 µl 2% formaldehyde, 0.05% glutaraldehyde in PBS for 10 min, washed twice with PBS, then incubated overnight (37°C) with X-gal solution (PBS with 1 mg/ml 5-bromo-4-chloro-3-indolyl-β-D-galactopyranoside, 5 mM potassium ferricyanide, 5 mM potassium ferrocyanide, 2 mM $MgCl_2$). EGFP+ or X-gal+ cells were counted in six fields of view across the well using the eyepieces of a Nikon Eclipse TE-2000U inverted fluorescence microscope. The calculation for titre was as follows for a chosen dilution with fewer than ~100 positive cells per field of view, where the area of the well corresponds to 151 fields of view:

$$\frac{\text{Mean number of transduced cells} \times 1000 \times 151}{\text{µl virus in the counted well}} = \text{number of transducing particles/ml}$$

Later testing and modification of the protocol resulted in the following changes. Lipofectamine LTX (20 µl) was used in place of Lipofectamine (23 µl) with only 10-15 min incubation to form complexes; complexes did not require removal by washing so after four

hours medium was topped up to 3.5 ml per dish with packaging medium. Finally, resuspended amplicons were briefly centrifuged (1000 RCF, 5 min, 4°C) to pellet any remaining debris before application to cells, providing a marked visual improvement.

(iii) Transduction using HSV-1 based amplicons

Cultures of immortalised cells or iPSC-derived dopaminergic neurons were transduced with HSV-1 based amplicons by first diluting amplicons in culture medium according to the desired multiplicity of infection (MOI) and then using this to replace the medium already on the cells. As the titres of amplicons were usually low, this necessitated the MOI to be <2 and often <1. The additional method of 'spinoculation' assisted in concentrating the amplicons closer to the cell layer: after adding the diluted amplicons to the cells, culture plates were centrifuged (20 min, 1500 RCF, 30°C; then 40 min, 700 RCF, 30°C). Amplicons were incubated with cells for 24 hours to maximise transduction.

3.2.4 Nucleofection of induced pluripotent stem cells

Attempts were made to nucleofect iPSCs with mCherry-3'UTR *TH*-PAC pEHHG by Amaxa nucleofection (Lonza), with pmaxGFP (Lonza) and pEHHG as controls. ROCKi was added to iPSCs 1-2 hours before use. iPSCs were washed with DPBS, incubated with TrypLE (3 min, 37°C) then added to 9 ml DPBS with ROCKi. After counting by Scepter, the cells to be nucleofected ($8x10^5$-$1x10^6$) were pelleted by centrifugation (115 RCF, 3 min). Wells of Geltrex-coated plates were prepared with mTeSR1/penicillin-streptomycin/ROCKi; non-nucleofected cells were then added to their wells. For nucleofection, pelleted cells were re-suspended in 100 µl Amaxa Nucleofector Solution, followed by the addition of 2-5 µg endotoxin-free DNA in ≤10 µl water, prepared by NucleoBond Xtra Maxi EF (Machery-Nagel).

The cell:DNA mix was electroporated using an Amaxa Nucleofector I (Lonza) on programme B-16. Cells were immediately diluted with 500 µl pre-warmed mTeSr1/penicillin-streptomycin/ROCKi and transferred to the prepared Geltrex-coated well. After 24 hours, medium was changed to remove ROCKi and changed daily.

3.3 Results

3.3.1 Generation of 1st generation TH-*PAC reporters*

A first generation *TH*-PAC reporter was constructed in two stages: construction of a fluorescent protein reporter cassette containing a selectable resistance marker; replacement of the coding portion of *TH* exon 1 with the reporter cassette by homologous recombination (Fig. 3.1).

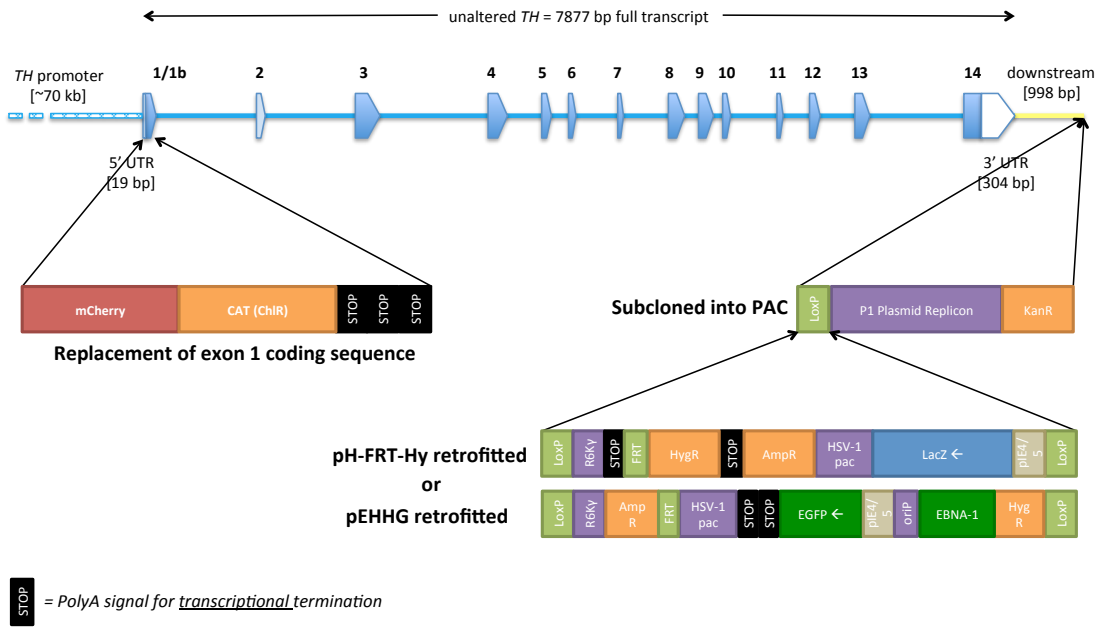

Figure 3.1: 1st generation human *TH* fluorescent reporter constructs.
Schematic of the overall process to generate a PAC-based fluorescent reporter to visualise cells that normally express tyrosine hydroxylase, i.e. dopaminergic neurons. 'Retrofitting' denotes a recombination with a plasmid containing the packaging signal of herpes simplex virus-1 (HSV-1) in order to make infectious BAC/PAC amplicons (iBACs). The initial strategy was designed by Dr E. Hartfield.

First, the fluorescent protein reporter cassette was constructed in pGEM-T containing three polyadenylation (polyA) signals. To add a new resistance marker, the chloramphenicol acetyltransferase sequence inclusive of bacterial promoter was amplified by high-fidelity PCR and ligated into *Sac*II-*Spe*I digested pGEM-T/PolyAx3 plasmid (Fig. 3.2A). Correct

colonies selected on chloramphenicol were confirmed by *Nco*I and *Pvu*II analytical digests (Fig. 3.2B). To insert the mCherry sequence, pGEM-T/PolyAx3 was double digested with *Apa*I and *Sac*II (Fig. 3.2C) and the product of mCherry high-fidelity PCR (Fig. 3.2D) was ligated in, with correct bacterial colonies confirmed by *Apa*LI analytical digest (Fig. 3.2E).

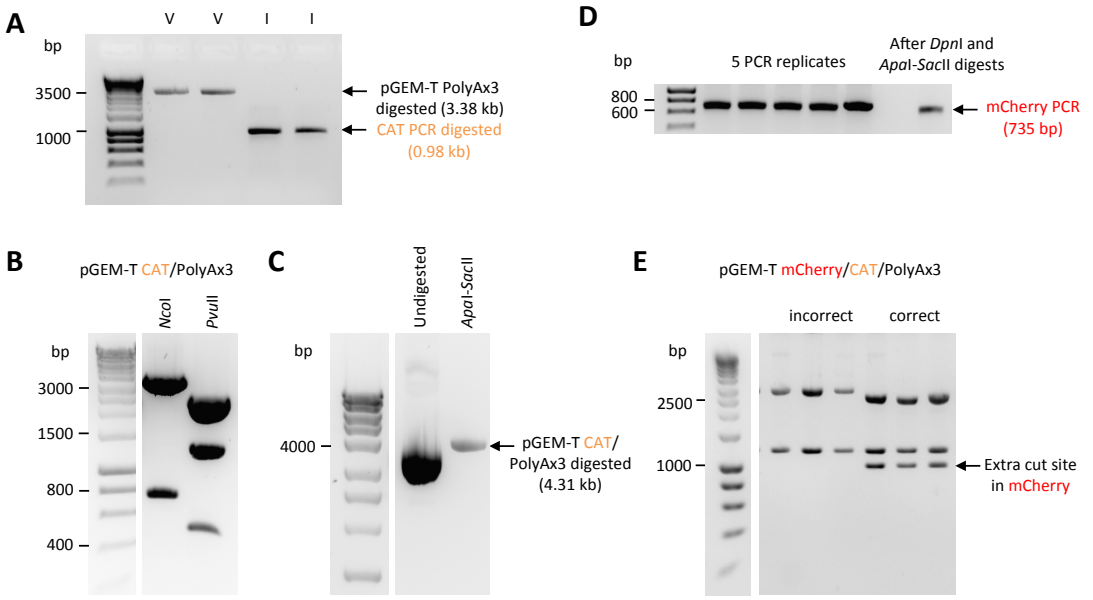

Figure 3.2: Incorporation of the chloramphenicol and mCherry sequences by restriction digest and ligation to form the 1st generation reporter cassette.
(A) Purified pre-ligation components after *Sac*II-*Spe*I digestion: V, vector pGEM-T PolyAx3; I, insert PCR of full chloramphenicol acetyl-transferase (CAT) sequence, including promoter, from the BAC backbone (pBACe3.6) of RP11-542J6 BAC.
(B) *Nco*I and *Pvu*II analytical restriction digests of plasmid maxiprep from a colony with correctly ligated pGEM-T CAT/PolyAx3. Each enzyme cuts once within the CAT sequence to show correct insertion, as well as one (*Nco*I) or two (*Pvu*II) cuts in the vector backbone. *Nco*I digest bands: 3610 bp, 736 bp. *Pvu*II digest bands: 2564 bp, 1297 bp, 485 bp.
(C) Gel purification of the acceptor vector, *Apa*I-*Sac*II digested pGEM-T CAT/PolyAx3, prior to mCherry ligation.
(D) Insert PCR of mCherry sequence from an mCherry expression plasmid (gift from Roger Tsien laboratory) with subsequent *Apa*I-*Sac*II digestion of the PCR ends ready for ligation.
(E) *Apa*LI analytical restriction digests of plasmid minipreps following ligation to insert mCherry. Correctly ligated pGEM-T mCherry/CAT/PolyAx3 has 3 digest fragments due to a restriction site within mCherry. *Apa*LI digest bands for incorrect pGEM-T/CAT/PolyAx3: 3100 bp, 1246 bp. *Apa*LI digest bands for correct pGEM-T/mCherry/CAT/PolyAx3: 2767 bp, 1246 bp, 1020 bp.

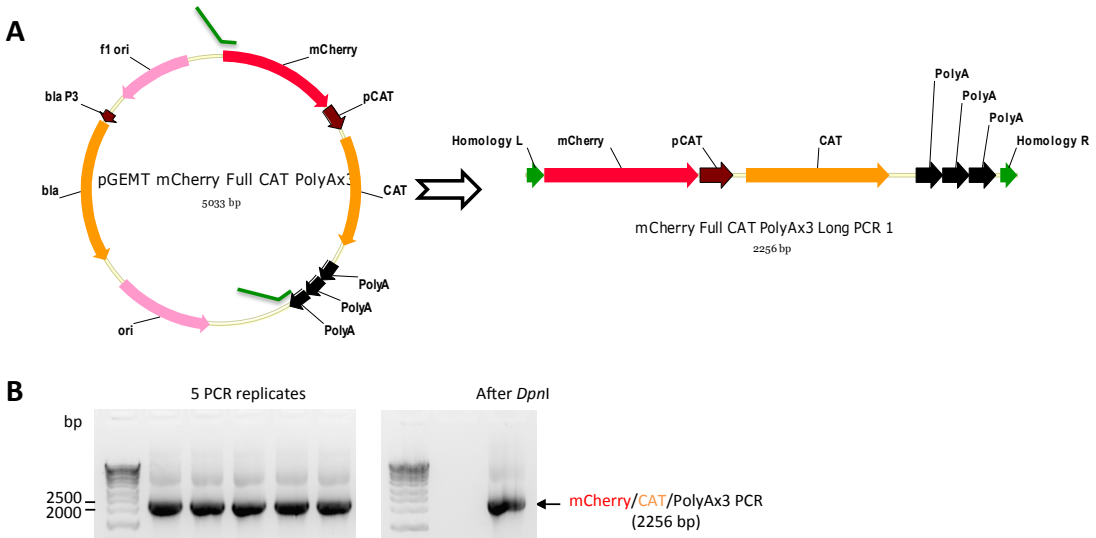

Figure 3.3: Long-range PCR of the 1st generation mCherry cassette for homologous recombination with *TH*-PAC.
(A) Schematic of the PCR amplification of the entire mCherry cassette using primers that each add 80 bp of sequence homologous to the sequences flanking the coding portion of human *TH* exon 1.
(B) Long-range PCR of mCherry/CAT/PolyAx3 before and after *Dpn*I digest and purification.

The second step was to insert the reporter cassette into *TH*-PAC by homologous recombination. The sequence-verified fluorescence cassette was amplified by high-fidelity long-range PCR (Fig. 3.3) and electroporated into *E. coli* containing the subcloned *TH*-PAC and plasmid pRed/ET, which encodes both a 5'-3' exonuclease and a single-stranded DNA binding protein that are required for homologous recombination. Subsequent growth at 37°C caused the loss of pRed/ET and permitted homologous recombination to produce mCherry-*TH* PAC; selection with chloramphenicol allowed only correct recombinants containing the mCherry/CAT/PolyAx3 cassette to grow. Colonies with the correct presence of both 5' and 3' insert junctions (Fig. 3.4A), insert sizes (Fig. 3.4B) and overall analytical digest patterns (Fig. 3.4C) were sequenced to obtain a verified intact reporter construct 90 kb in length that had maintained the remaining *TH* exons 2-14 (Fig. 3.4D).

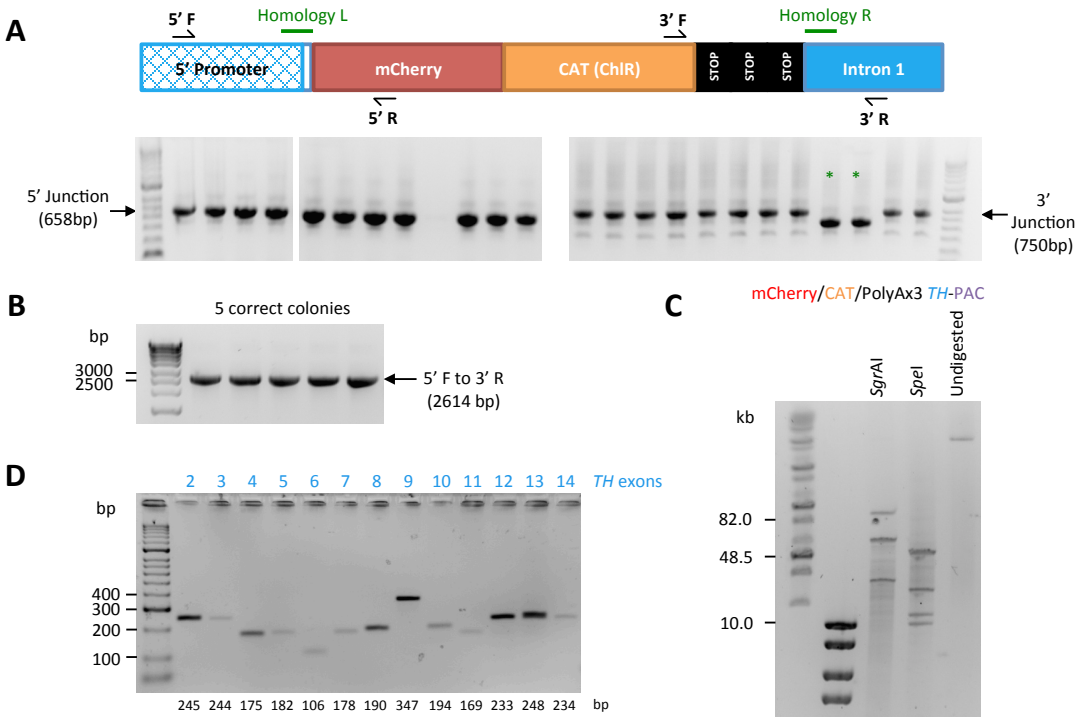

Figure 3.4: Verification of the identity of 1st generation recombinants by analytical PCR and restriction digest.
(A) Junction PCR to show the presence of the recombined cassette. Schematic shows the positions of the 5' (left) and 3' (right) junction primers that span the junction of homologous recombination. * represents a colony that has lost one PolyA signal.
(B) Pre-sequencing PCR to amplify the entire inserted region using primers 5' F and 3' R on the schematic in (A).
(C) Pulsed-field gel showing *Sgr*AI and *Spe*I analytical restriction digests of maxiprep from a colony with sequence-verified correctly recombined mCherry-*TH* PAC. Each enzyme cuts once within the mCherry cassette to show correct insertion, as well as one (*Sgr*AI) or three (*Spe*I) cuts in the *TH* promoter. Note that the *Sgr*AI digest lane still shows some linearised plasmid with one cut only (90 kb band). *Sgr*AI digest bands: 61 kb, 29 kb. *Spe*I digest bands: 50 kb, 19 kb, 11 kb, 10 kb.
(D) PCR to show the continued presence of all remaining exons of *TH* in mCherry-*TH* PAC.

To increase the efficiency of delivery to cell types that are difficult to transfect, the reporter construct was enhanced by the addition of *cis* sequences required for packaging as herpes simplex virus 1 (HSV-1) amplicons; the process of adding the HSV-1 sequences is referred to hereafter as retrofitting. These sequences are present on plasmids pEHHG (Wade-Martins et al. 2001) and pH-FRT-Hy (Alegre-Abarrategui et al. 2009) along with constitutive reporters EGFP and *lacZ* respectively under the control of the HSV-1 IE4/5 promoter (Fig. 3.5A). The benefits of having a constitutive reporter are two-fold: first, it is necessary for quantification

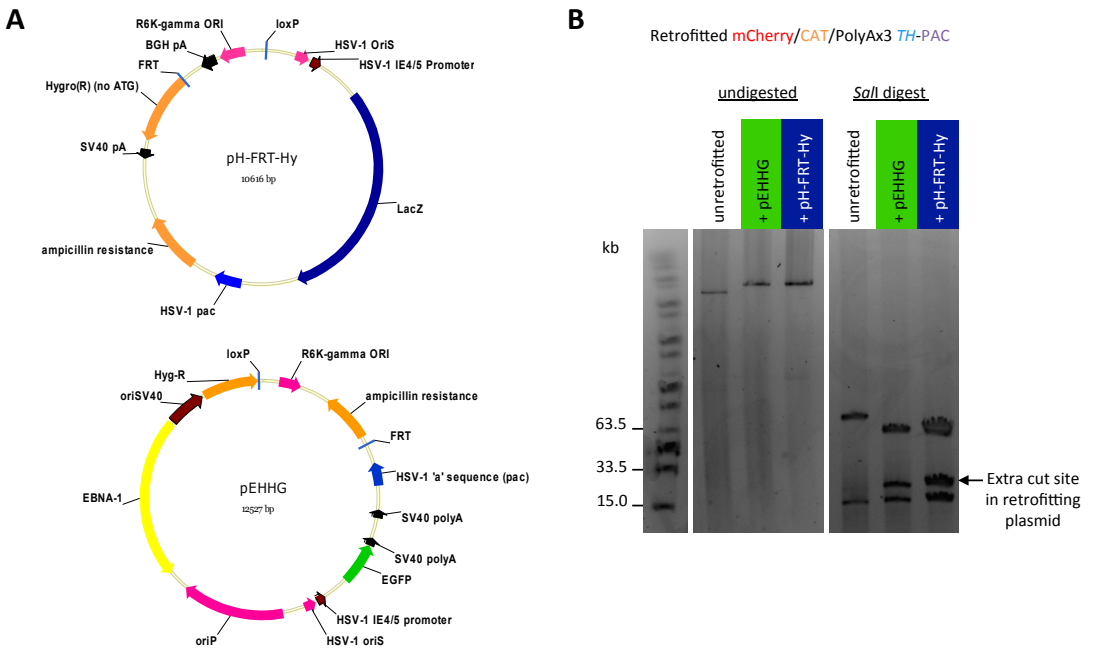

Figure 3.5: 'Retrofitting' of 1st generation mCherry-*TH* PAC by Cre-mediated recombination.
(A) Schematics of HSV-1 amplicon retrofitting plasmids pH-FRT-Hy and pEHHG, carrying reporter sequences *LacZ* and EGFP respectively.
(B) Pulsed-field gel showing *Sal*I analytical restriction digests of maxipreps of unretrofitted and retrofitted mCherry-*TH* PAC. *Sal*I enzyme cuts once within the retrofitting plasmid to show correct recombination without concatamerisation, in addition to two cuts in the *TH* promoter. *Sal*I digest bands for unretrofitted mCherry-*TH* PAC: 72 kb, 18 kb. *Sal*I digest bands for mCherry-*TH* PAC pEHHG: 61 kb, 24 kb, 18 kb. *Sal*I digest bands for mCherry-*TH* PAC pH-FRT-Hy: 59 kb, 24 kb, 18 kb.

of viral titres, wherein X-gal staining for *lacZ* may be used without reducing the number of fluorescence channels available in downstream experiments; second, in the case of cell-type specific reporters, such as the one generated here, it allows determination of which cells have received the construct, from which to determine the proportion of cells that express both the constitutive and cell-type specific reporter. Therefore, mCherry-*TH* PAC was retrofitted by addition of either pEHHG or pH-FRT-Hy through Cre-mediated recombination at loxP sites with successful colonies selected by three antibiotics: ampicillin for the retrofitting plasmid, kanamycin for the PAC backbone and chloramphenicol for the mCherry/CAT/PolyAx3 cassette (Fig. 3.5B). Many permutations of ratios of PAC to retrofitting plasmid were attempted for the reactions, which are also sensitive to DNA

quality, and it was found that the inverse molar ratio, i.e. high excess of small plasmid, e.g. 50 ng PAC : 1 µg plasmid (approximately 1:180 molar ratio) was the most successful. However, even after several attempts, the pEHHG-retrofitted reporter could only be obtained as a concatamer (data not shown), and was subsequently 'de-retrofitted' using Cre-mediated recombination without the addition of other plasmids in order to leave only one copy of pEHHG within the final construct as per correct *Sal*I analytical digest (Fig. 3.5B).

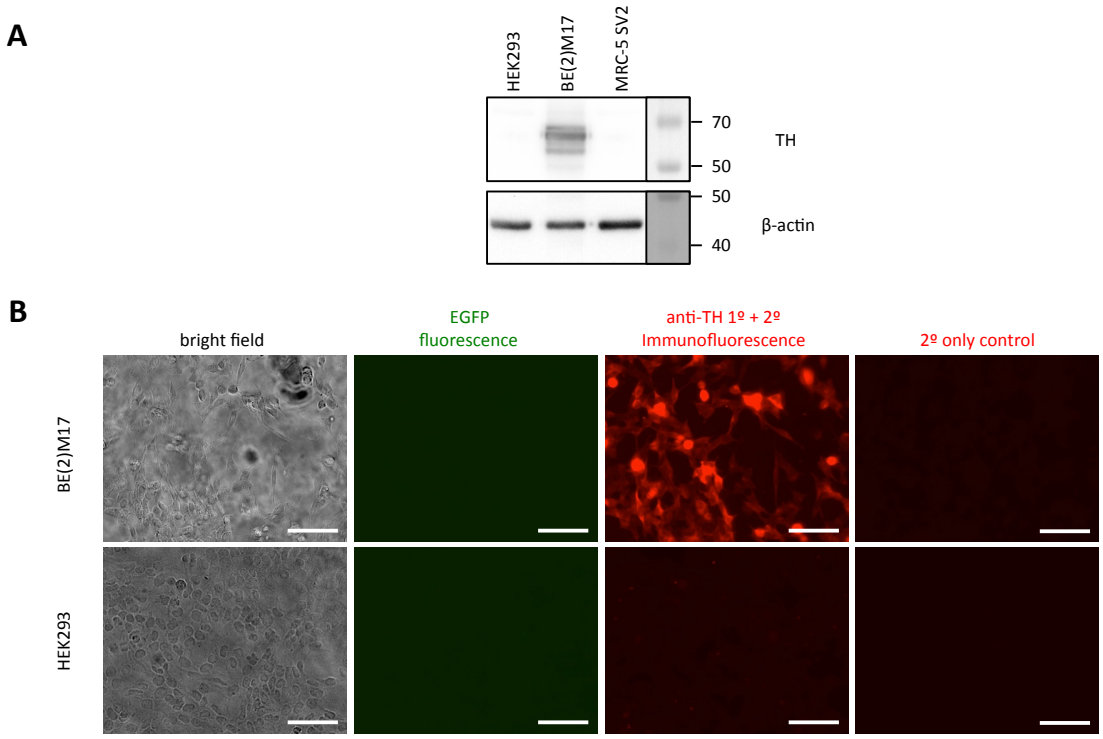

Figure 3.6: Identification of TH-positive and TH-negative immortalised cell lines.
(A) TH immunoblot of immortalised cell lines to identify positive and negative controls for testing of reporter specificity. Immunostaining for rabbit anti-TH (Millipore, AB152), followed by re-probing with rabbit anti-beta actin (abcam, ab8227).
(B) TH immunocytochemistry of BE(2)M17 and HEK293 lines to confirm 100% and 0% TH^+ identity respectively. No endogenous EGFP fluorescence was detected as these are untransfected cells. Secondary antibody only controls included to show specificity of fluorescent signal. Bright field and fluorescence images. Scale bars, 100 µm.

3.3.2 Testing of 1st generation TH-*PAC reporters*

The expression and specificity of 1st generation *TH*-PAC reporter constructs were tested in immortalised cell lines. Three human cell lines were examined for their expression of TH by Western blot (Fig. 3.6A) and immunocytochemistry (Fig. 3.6B): BE(2)M17 cells, a dopaminergic cell line derived from a neuroblastoma that had metastasised to bone marrow, were confirmed as wholly TH+; MRC-5 SV2 cells, foetal lung fibroblasts transformed with SV40 virus, and HEK293 cells, embryonic kidney cells transformed with a portion of Adenovirus 5 DNA, were both confirmed as TH-. Transfection of the pre-retrofitted mCherry-*TH* PAC reporter construct into both BE(2)M17 cells and HEK293 cells yielded a small number of red fluorescent mCherry-expressing cells (Fig. 3.7). This confirmed that the construct was capable of promoting mCherry expression; however, it did not suggest that it was specific to TH+ cells.

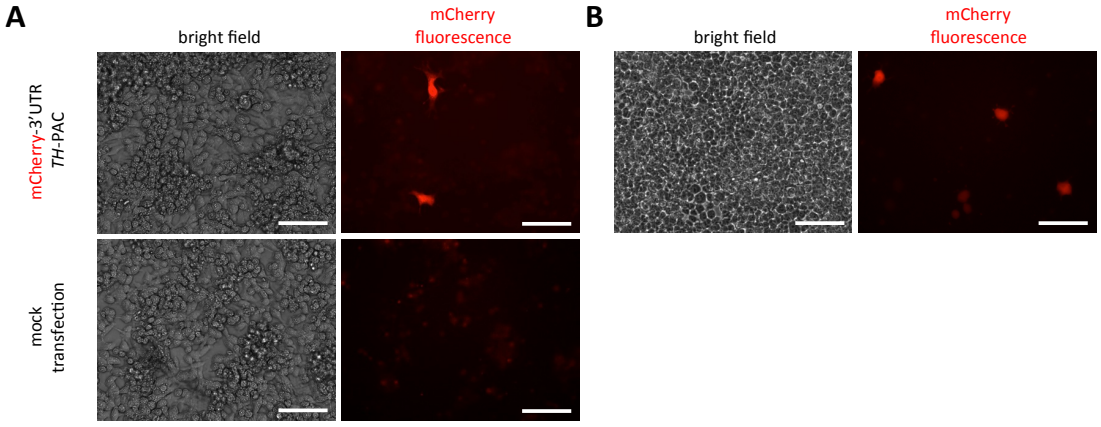

Figure 3.7: Transfection of 1st generation unretrofitted mCherry-*TH* PAC showed expression of mCherry by fluorescence microscopy.
Bright field and fluorescence images for (A) BE(2)M17 and (B) HEK293 cells. Live fluorescence of mCherry expression is seen in both TH+ and TH- cell lines. Scale bars, 100 µm.

Following retrofitting of mCherry-*TH*-PAC with pH-FRT-Hy and subsequent production of HSV-1 amplicons, transduction did not yield detectable mCherry fluorescence in an initial test of infected cells (data not shown). However, retrofitting with pEHHG followed by plasmid transfection of BE(2)M17 and HEK293 cells produced constitutive EGFP-expressing cells with 18% and 43% of these co-expressing mCherry respectively (Fig. 3.8-3.9). These data revealed two problems with the construct: first, the degree of expression from the *TH* promoter was poor, as it was expected that all BE(2)M17 cells expressing EGFP should co-express mCherry given that all cells are TH+; second, the construct lacked specificity in that mCherry expression was produced even in a TH- cell line.

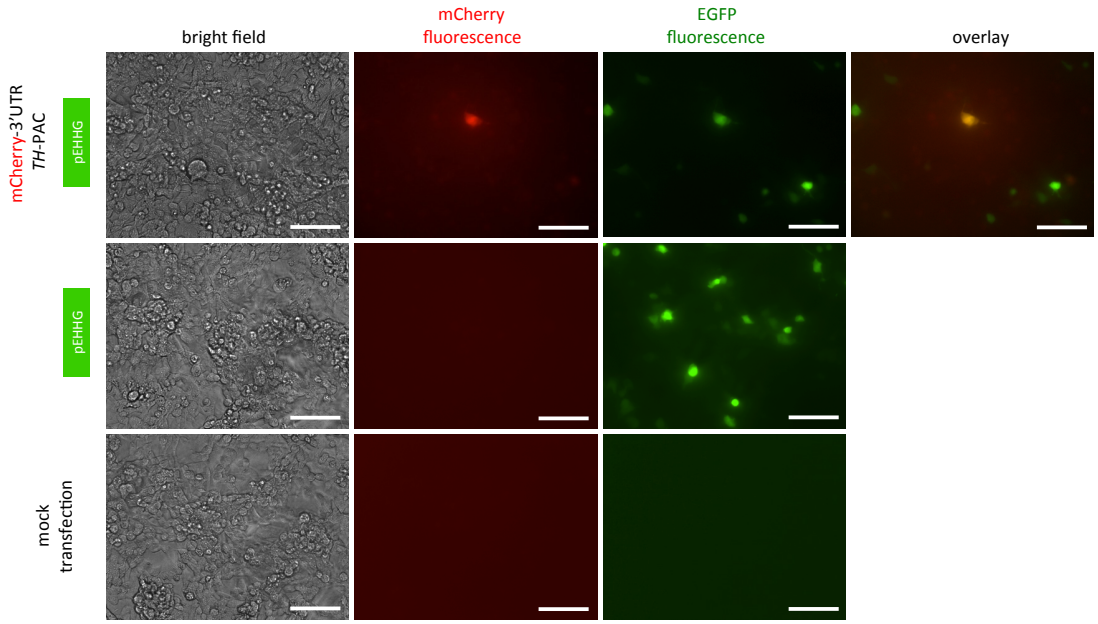

Figure 3.8: Transfection of BE(2)M17 cells with 1st generation pEHHG-retrofitted mCherry-*TH* PAC showed partial co-expression of mCherry and EGFP by fluorescence microscopy.
Bright field and fluorescence images for BE(2)M17 cells. Transfection with the dual-coloured reporter construct generated mCherry/EGFP co-expressing cells representing 18% of EGFP expressing cells. Transfection with the EGFP-containing pEHHG retrofitting plasmid alone only showed EGFP expression. Scale bars, 100 µm.

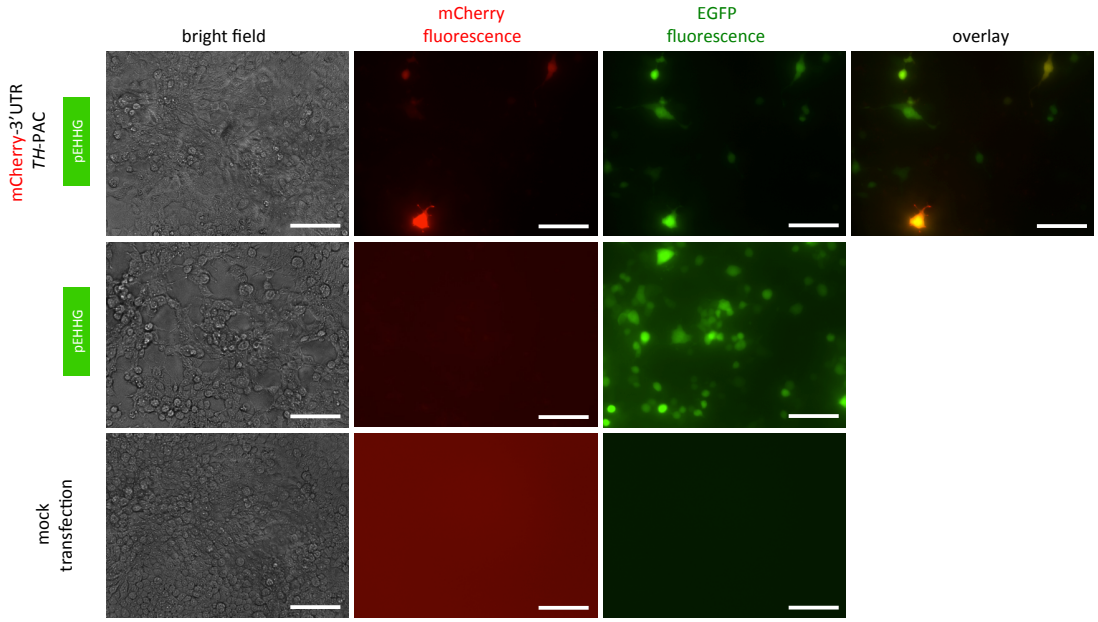

Figure 3.9: Transfection of HEK293 cells with 1st generation pEHHG-retrofitted mCherry-*TH* PAC showed partial co-expression of mCherry and EGFP by fluorescence microscopy.
Bright field and fluorescence images for HEK293 cells. Transfection with the dual-coloured reporter construct generated mCherry/EGFP co-expressing cells representing 43% of EGFP expressing cells. Transfection with the EGFP-containing pEHHG retrofitting plasmid alone only showed EGFP expression. Scale bars, 100 µm.

3.3.3 *Generation of 2nd generation* TH-*PAC reporters*

It was hypothesised that the problem of poor expression of mCherry from the *TH* promoter could be due to transcription continuing beyond the mCherry sequence and into the bacterial promoter and chloramphenicol acetyltransferase sequence before reaching a signal for polyadenylation. The fluorescent reporter cassette was redesigned to incorporate a 3'UTR with polyadenylation signal after the mCherry coding sequence to separate it from the neighbouring bacterial elements (Fig. 3.10). Given the need to begin the reporter construction again from an early stage, the opportunity was taken to generate an alternative reporter using EGFP in place of mCherry. The EGFP sequence was amplified by high-fidelity PCR (Fig. 3.11A) and ligated into *Apa*I-*Sac*II digested pGEM-T CAT/PolyAx3 (Fig. 3.11B), then

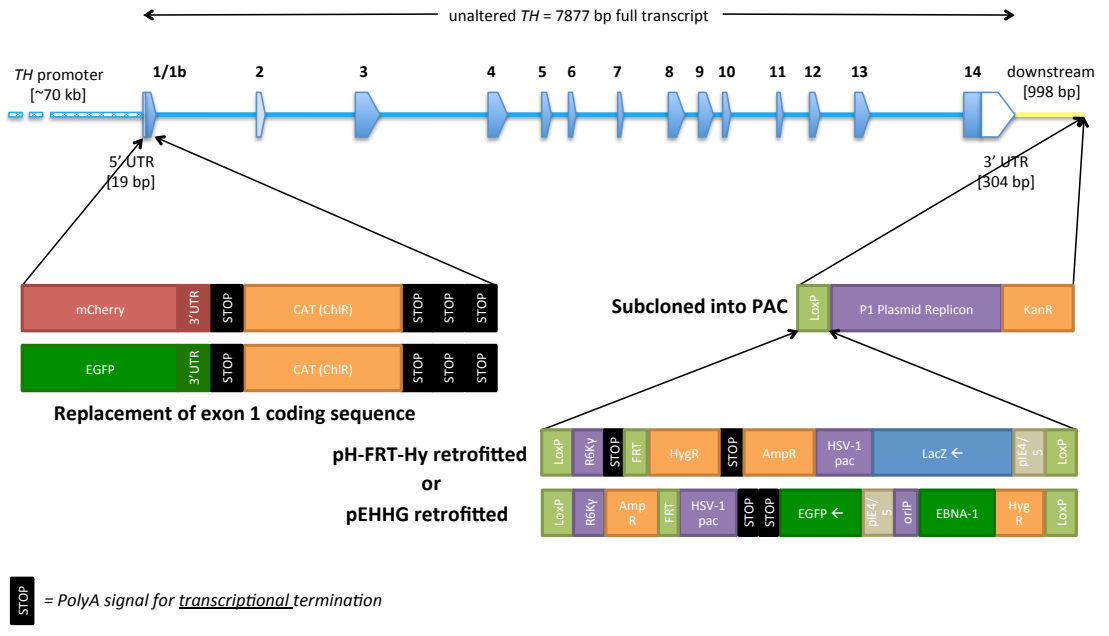

Figure 3.10: 2nd generation human *TH* fluorescent reporter constructs.
Schematic of the overall process to generate 2nd generation PAC-based fluorescent reporters to visualise cells that normally express tyrosine hydroxylase, i.e. dopaminergic neurons. Both mCherry and EGFP versions were designed, as shown by two possible cassettes for replacement of the coding portion of exon 1. These cassettes differed from the 1st generation cassettes by the incorporation of a 3' UTR-polyadenylation sequence after the mCherry or EGFP coding sequences, which required a repeat of the construction from an early stage. 'Retrofitting' denotes a recombination with a plasmid containing the packaging signal of HSV-1 in order to make infectious BAC/PAC amplicons (iBACs).

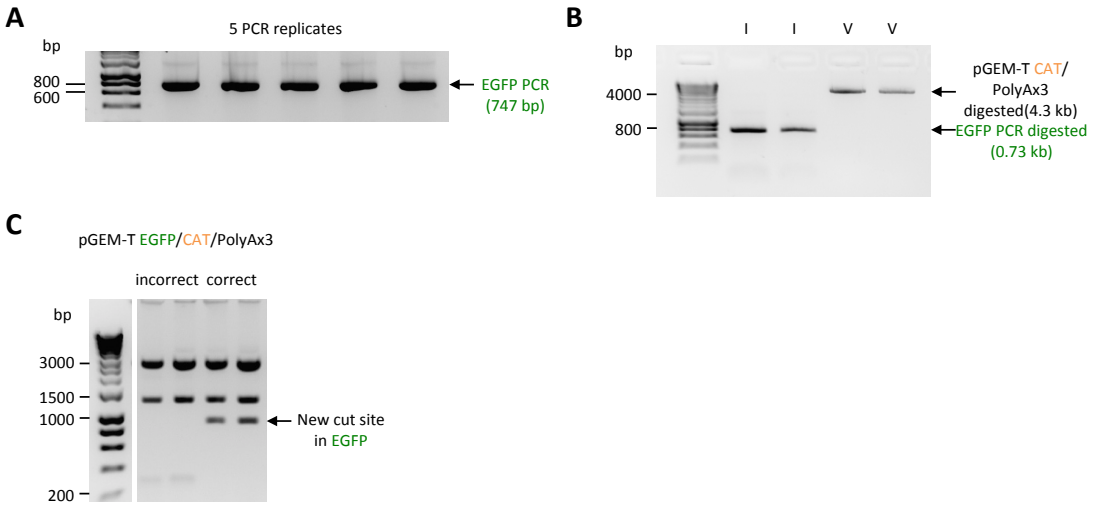

Figure 3.11: Incorporation of the EGFP sequence by restriction digest and ligation.
(A) Insert PCR of EGFP sequence from pEHHG with subsequent *Apa*I-*Sac*II digestion of the PCR ends ready for ligation.
(B) Purified pre-ligation components after *Apa*I-*Sac*II digestion: I, insert PCR of EGFP; V, vector pGEM-T CAT/PolyAx3.
(C) *Bgl*I-*Bsr*GI analytical restriction digests of plasmid minipreps following ligation to insert EGFP. Correctly ligated pGEM-T EGFP/CAT/PolyAx3 has a diagnostic 898 bp fragment due to a restriction site within EGFP replacing one lost by *Apa*I-*Sac*II. *Bgl*I-*Bsr*GI digest bands for incorrect pGEM-T CAT/PolyAx3: 2819 bp, 1318 bp, 209 bp. *Bgl*I-*Bsr*GI digest bands for correct pGEM-T EGFP/CAT/PolyAx3: 2826 bp, 1318 bp, 898 bp.

colonies displaying the correct *Bgl*I-*Bsr*GI analytical digest pattern (Fig. 3.11C) were sequenced to verify correct insertion of EGFP. To select a suitable insert to follow mCherry or EGFP, the sequences of all of the available DsRed2 and mCherry expression plasmids available from Clontech were compared to identify the 3'UTR and polyadenylation sequence that is common to all. This sequence was amplified by high-fidelity PCR (Fig. 3.12A) and ligated into *Sac*II-digested pGEM-T/mCherry/CAT/PolyAx3 (Fig. 3.12B) and pGEM-T/EGFP/CAT/PolyAx3 (Fig. 3.12C). Colonies with the insert in the correct orientation were identified by analytical digest: *Swa*I-*Nco*I for the mCherry construct (Fig. 3.12D) and *Swa*I-*Bgl*I for the EGFP construct (Fig. 3.12E). Long-range PCR of the mCherry (Fig. 3.13A) and EGFP (Fig. 3.13B) constructs was performed prior to electroporation into *E. coli* containing *TH*-PAC and pRed/ET with chloramphenicol selection for the presence of the reporter cassette. As for the 1st generation construct, successful colonies were confirmed for both

mCherry-3'UTR *TH*-PAC (Fig. 3.14) and EGFP-3'UTR *TH*-PAC (Fig. 3.15) by verifying insert junctions (A), insert sizes (B), *Spe*I analytical digest (C) and the remaining presence of exons 2-14 (D) along with full verification by sequencing.

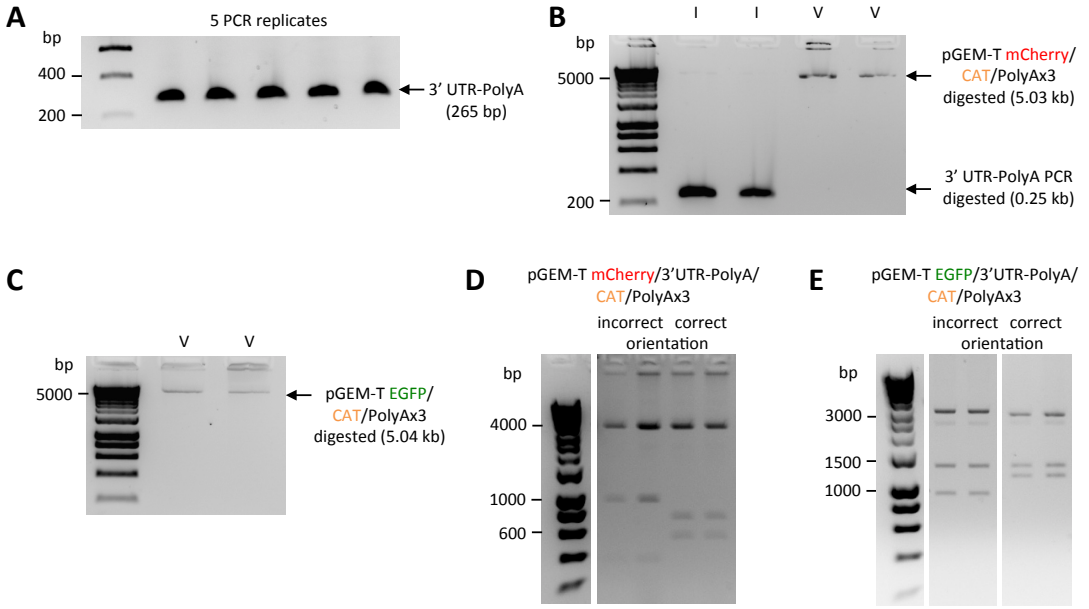

Figure 3.12: Incorporation of the 3' UTR-polyadenylation sequences into 2nd generation constructs by restriction digest and ligation.
(A) Insert PCR of 3' UTR-PolyA sequence from pDsRed2-C1 with subsequent *Sac*II digestion of the PCR ends ready for ligation.
(B) Purified pre-ligation components after *Sac*II digestion: I, insert PCR of 3' UTR-PolyA; V, vector pGEM-T mCherry/CAT/PolyAx3.
(C) Purified pre-ligation components after *Sac*II digestion: V, vector pGEM-T EGFP/CAT/PolyAx3.
(D) *Swa*I-*Nco*I analytical restriction digests of plasmid minipreps following ligation to insert 3' UTR-PolyA into the mCherry construct. As ligation was of ends cut with a single enzyme, the correct orientation was determined by the single *Swa*I cut. *Swa*I-*Nco*I digest bands for incorrect orientation: 4025 bp, 966 bp, 289 bp. *Swa*I-*Nco*I digest bands for correct orientation: 4025 bp, 735 bp, 520 bp.
(E) *Swa*I-*Bgl*I analytical restriction digests of plasmid minipreps following ligation to insert 3' UTR-PolyA into the EGFP construct. As ligation was of ends cut with a single enzyme, the correct orientation was determined by the single *Swa*I cut. *Swa*I-*Bgl*I digest bands for incorrect orientation: 3051 bp, 1318 bp, 920 bp. *Swa*I-*Bgl*I digest bands for correct orientation: 2820 bp, 1318 bp, 1151 bp.

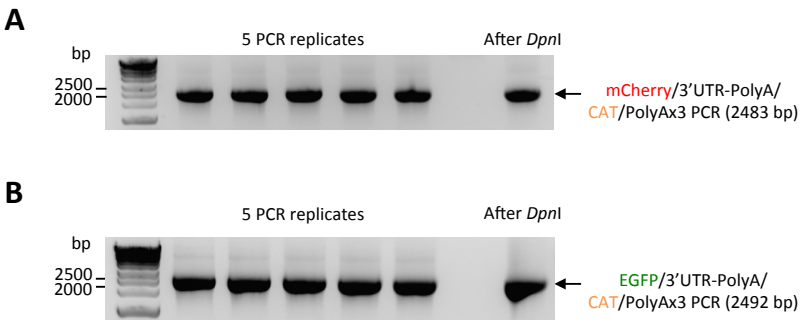

Figure 3.13: Long PCR amplification of the 2nd generation mCherry and EGFP cassettes for homologous recombination with *TH*-PAC.
(A) PCR of mCherry/3'UTR-PolyA/CAT/PolyAx3 before and after *Dpn*I digest and purification.
(B) PCR of EGFP/3'UTR-PolyA/CAT/PolyAx3 before and after *Dpn*I digest and purification.

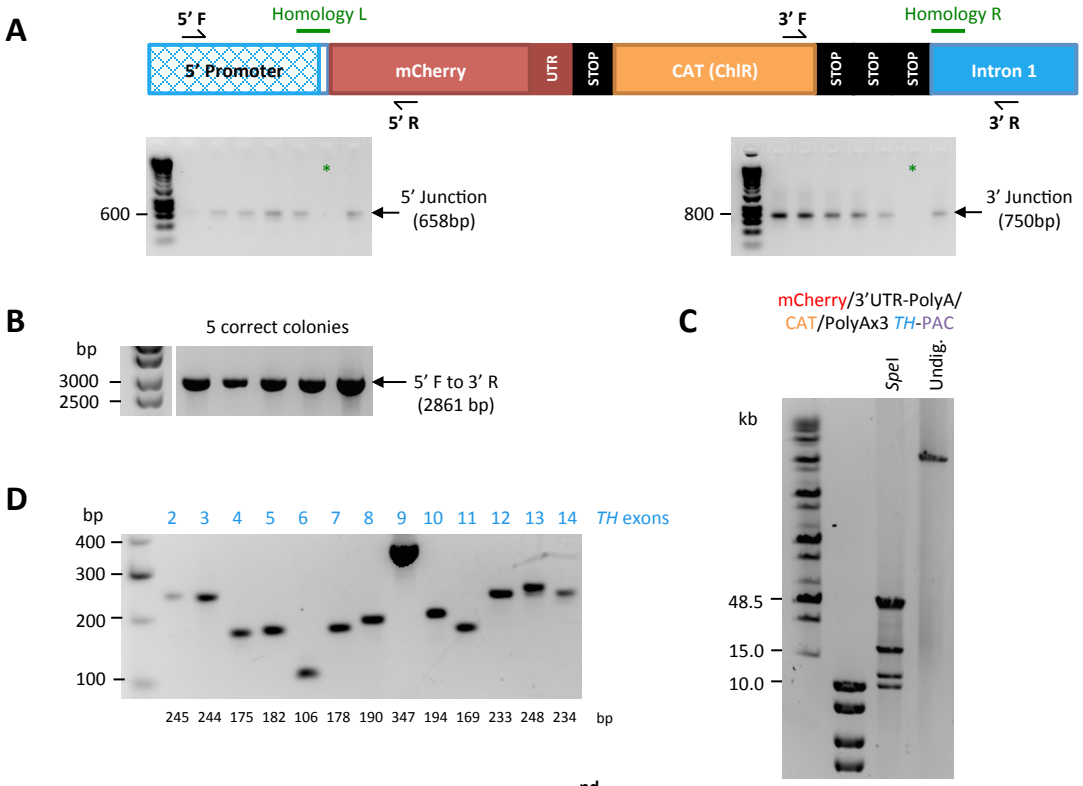

Figure 3.14: Verification of the identity of 2nd generation mCherry recombinants by analytical PCR and restriction digest.
(A) Junction PCR to show the presence of the recombined cassette. Schematic shows the positions of the 5' (left) and 3' (right) junction primers that span the junction of homologous recombination. * represents a colony lacking the junction.
(B) Pre-sequencing PCR to amplify the entire inserted region using primers 5' F and 3' R on the schematic in (A).
(C) Pulsed-field gel showing *Spe*I analytical restriction digests of maxiprep from a colony with sequence-verified correctly recombined mCherry-3'UTR *TH* PAC. The enzyme cuts once within the mCherry cassette to show correct insertion, as well as three cuts in the *TH* promoter. *Spe*I digest bands: 51 kb, 19 kb, 11 kb, 10 kb.
(D) PCR to show the continued presence of all remaining exons of *TH* in mCherry-3'UTR *TH*-PAC.

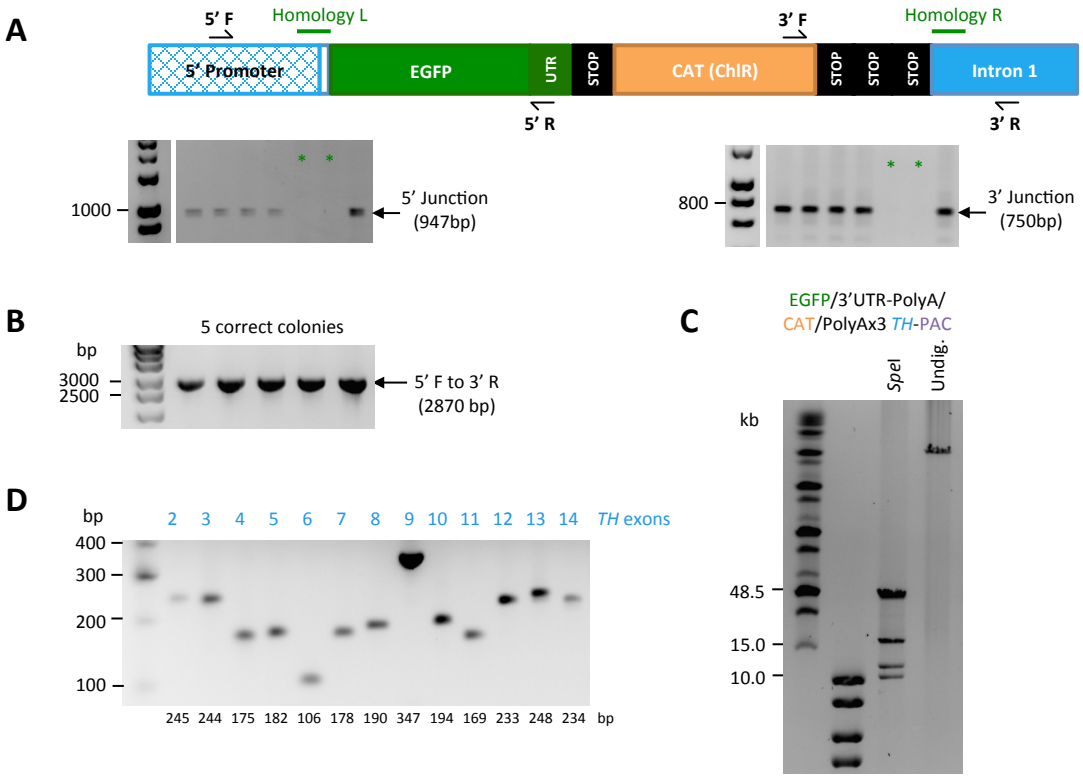

Figure 3.15: Verification of the identity of 2nd generation EGFP recombinants by analytical PCR and restriction digest.
(A) Junction PCR to show the presence of the recombined cassette. Schematic shows the positions of the 5' (left) and 3' (right) junction primers that span the junction of homologous recombination. * represents a colony lacking the junction.
(B) Pre-sequencing PCR to amplify the entire inserted region using primers 5' F and 3' R on the schematic in (A).
(C) Pulsed-field gel showing *Spe*I analytical restriction digests of maxiprep from a colony with sequence-verified correctly recombined EGFP-3'UTR *TH*-PAC. The enzyme cuts once within the EGFP cassette to show correct insertion, as well as three cuts in the *TH* promoter. *Spe*I digest bands: 51 kb, 19 kb, 11 kb, 10 kb.
(D) PCR to show the continued presence of all remaining exons of *TH* in EGFP-3'UTR *TH*-PAC.

Finally, Cre-mediated recombination was also repeated to generate dual-reporter constructs that were ready for packaging as HSV-1-based amplicons. The mCherry-3'UTR *TH*-PAC construct was retrofitted with pH-FRT-Hy and pEHHG (Fig. 3.16A-B), but due to the use of EGFP under the *TH* promoter, EGFP-3'UTR *TH*-PAC was only retrofitted with the *lacZ*-expressing plasmid pH-FRT-Hy (Fig. 3.16C).

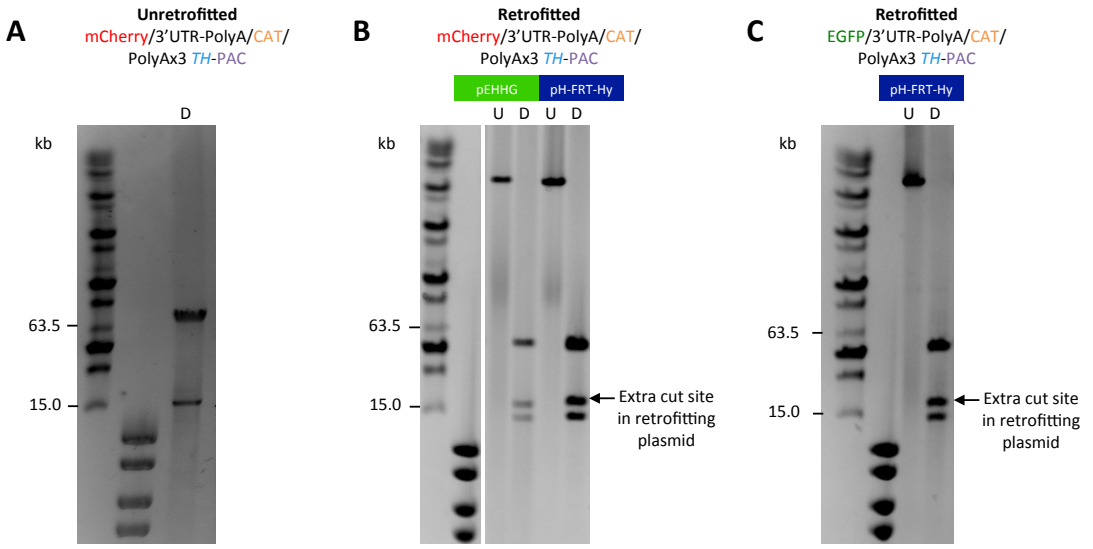

Figure 3.16: 'Retrofitting' of 2nd generation reporters by Cre-mediated recombination.
Pulsed-field gels showing *Sal*I analytical restriction digests of maxipreps of unretrofitted and retrofitted 2nd generation *TH*-PAC reporters. *Sal*I enzyme cuts once within the retrofitting plasmid to show correct recombination without concatamerisation, in addition to two cuts in the *TH* promoter.
(A) Unretrofitted mCherry-3'UTR *TH*-PAC. *Sal*I digest bands: 72 kb, 18 kb.
(B) pEHHG and pH-FRT-Hy retrofitted mCherry-3'UTR *TH*-PAC. *Sal*I digest bands for mCherry-3'UTR *TH*-PAC pEHHG: 61 kb, 24 kb, 18 kb. *Sal*I digest bands for mCherry-3'UTR *TH*-PAC pH-FRT-Hy: 59 kb, 24 kb, 18 kb.
(C) pH-FRT-Hy retrofitted EGFP-3'UTR *TH*-PAC. *Sal*I digest bands: 59 kb, 24 kb, 18 kb.

3.3.4 Testing of 2nd generation TH-*PAC reporters in neuroblastoma cells*

Transfection of all three 2nd generation *TH*-PAC reporters into BE(2)M17 cells yielded good reporter efficiency of expression (Fig. 3.17). This was particularly shown for the pEHHG retrofitted construct (top row) by the co-expression of constitutive EGFP and *TH*-promoted mCherry in 80% of transfected cells. Further, the two single-fluorescence constructs retrofitted with pH-FRT-Hy showed good expression of mCherry or EGFP respectively without any bleed-through between channels (middle rows) and no expression was detected in the mock transfection (bottom row). Interestingly, further testing of the dual-fluorescent reporter (mCherry-3'UTR *TH*-PAC pEHHG) in two TH- cell lines, MRC-5 SV2 and HEK293, also yielded high co-expression of mCherry with EGFP at approximately 90% (Fig. 3.18).

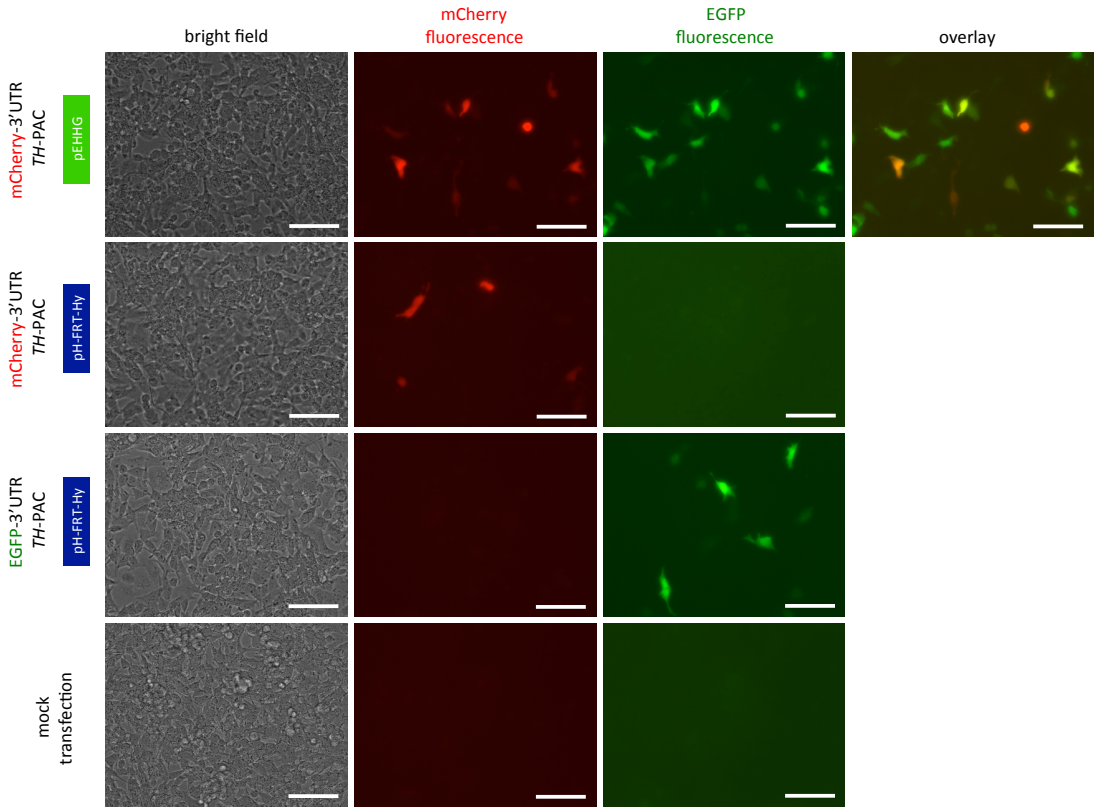

Figure 3.17: Transfection of BE(2)M17 dopaminergic cells with 2nd generation constructs. Bright field and fluorescence images for BE(2)M17 cells examined 72 hours after transfection. Transfection with the dual-coloured reporter construct generated mCherry/EGFP co-expressing cells representing 80% of EGFP expressing cells. Transfection with single-coloured reporter constructs expressing either mCherry or EGFP along with *lacZ* (encoded by the pH-FRT-Hy retrofitting plasmid portion) showed expression of only mCherry or EGFP respectively with no cross-talk between fluorescence channels. Scale bars, 100 µm.

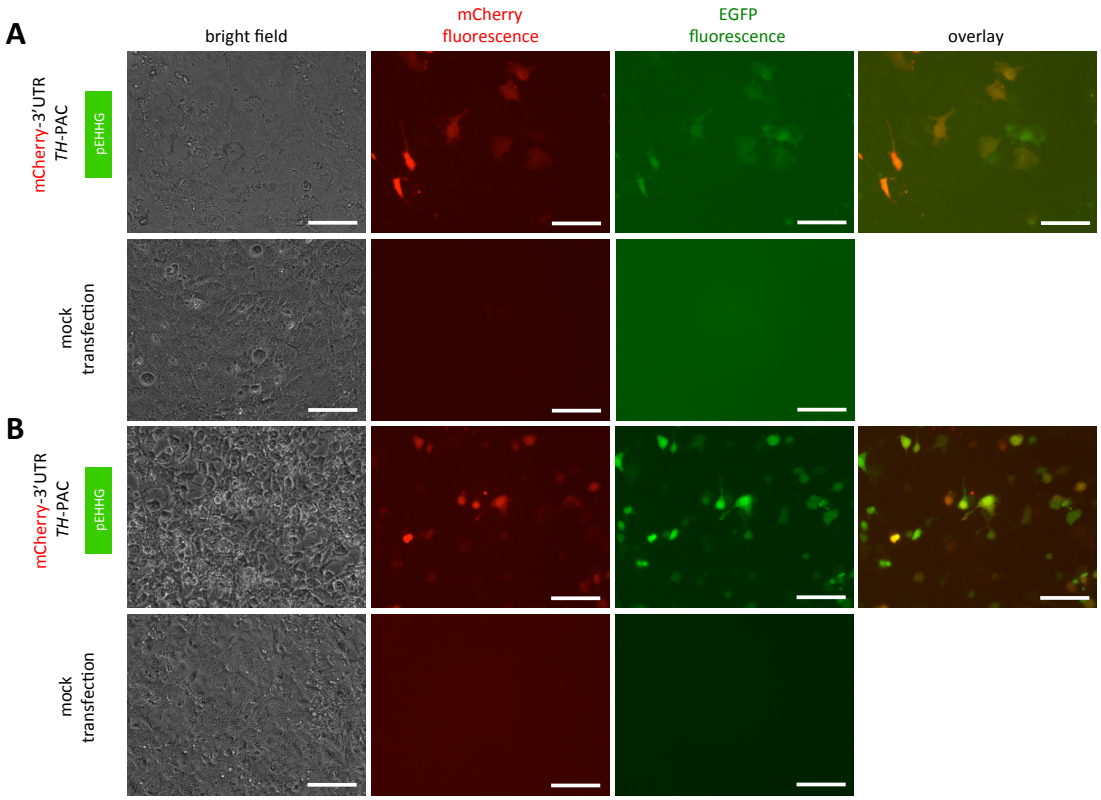

Figure 3.18: Transfection of MRC-5 SV2 and HEK293 non-dopaminergic cells with 2nd generation mCherry dual-fluorescence construct
Bright field and fluorescence images for (A) MRC-5 SV2 and (B) HEK293 cells, examined 72 hours after transfection. Transfection with the dual-coloured reporter construct generated mCherry/EGFP co-expressing cells representing 90% and 89% of EGFP expressing cells in MRC-5 SV2 and HEK293 cells respectively. Scale bars, 100 µm.

To investigate why mCherry under the *TH* promoter was ectopically expressed in TH- cell lines, the HEK293 TH- cell line was transfected with the unmodified *TH*-PAC containing the full genomic locus of *TH*. RT-PCR analysis using primers in non-adjacent exons designed only to amplify mRNA transcripts (Fig. 3.19A) verified that untransfected BE(2)M17 cells express *TH* transcripts and that untransfected HEK293 cells do not (Fig. 3.19B), which confirms the existing assignment of TH+ and TH- made at the protein level (Fig. 3.6). However, transfection of the full *TH* locus within the *TH*-PAC yielded detectable *TH* mRNA transcripts in HEK293 cells (Fig. 3.19B). As the *TH*-PAC is unmodified, these data show that the ectopic mCherry expression was not due to a hidden expression of endogenous *TH* mRNA that never

became detectable TH protein, but instead suggests that unphysiological bulk delivery of DNA by transfection can result in dysregulation of cell-type specific expression.

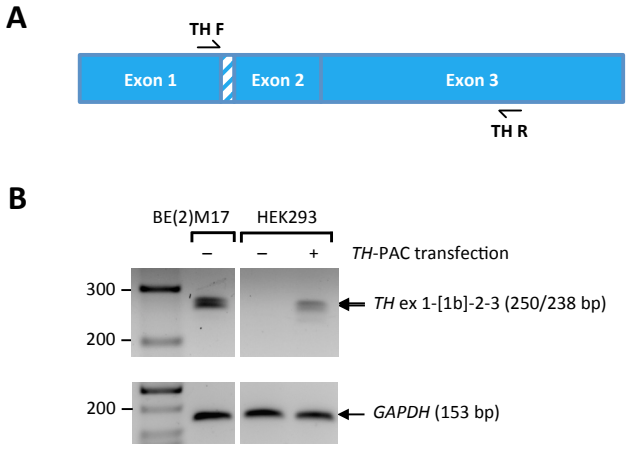

Figure 3.19: *TH* RT-PCR of MRC-5 SV2 and HEK293 non-dopaminergic cells transfected with unmodified *TH*-PAC.
(A) Schematic showing the location of PCR primers relative to the exons of human *TH* mRNA. Hatched segment represents exon 1b, an additional 12 bp at the end of exon 1 due to an alternative 5' splice site.
(B) End-point RT-PCR for human *TH* exons 1-3 in non-dopaminergic HEK293 cells with and without transfection with *TH*-PAC. BE(2)M17 cells used as a positive control for a TH+ expressing cell line. *GAPDH* used as a housekeeper control. Primer sequences in Appendix Table D.

3.3.5 Testing of 2nd generation TH-*PAC reporters in iPSC-derived dopaminergic neuronal cultures*

Testing in immortalised cell culture had confirmed that in the 2nd generation constructs, the *TH* promoter was capable of driving expression of the mCherry or EGFP reporter. As the purpose for these reporters was for use in iPSC-derived dopaminergic neuronal cultures that contain both dopaminergic neurons and non-dopaminergic cells, the remaining testing of the constructs was performed on these cultures.

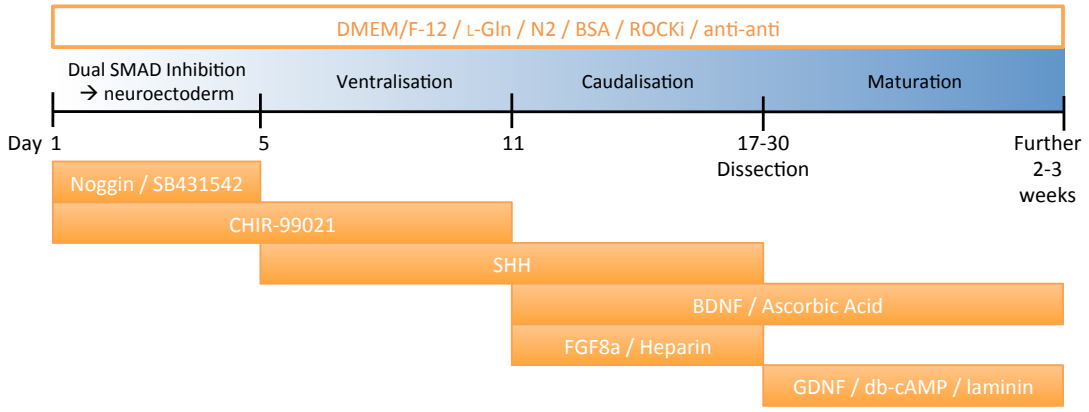

Figure 3.20: Differentiation of iPSC-derived embryoid bodies into midbrain-type dopaminergic neuronal cultures.
Timeline schematic for the method modified from Hartfield et al. (2014), showing the timing of the application of morphogens within the culture medium in order to restrict and determine cellular fate. This protocol is preceded by the formation of embryoid bodies from human iPSCs. SHH, sonic hedgehog; BDNF, brain-derived neurotrophic factor; FGF8a, fibroblast growth factor 8a; GDNF, glial cell-derived neurotrophic factor; db-cAMP, N^6,2'-*O*-dibutyryladenosine 3',5'-cyclic monophosphate.

(i) Generation of iPSC-derived dopaminergic neuronal cultures

Differentiation of iPSCs into dopaminergic neuronal cultures was first performed using a modification of the method of Hartfield et al. (2014) (Fig. 3.20). This method used iPSCs that had been grown first into embryoid bodies, rather than using iPSCs in two-dimensional culture. The Hartfield differentiation method generated neurons expressing both tyrosine hydroxylase (TH) and neuron-specific βIII-tubulin (Fig. 3.21A). However, partway through this study my laboratory commenced using a modified method of Kriks et al. (2011) (summarised in Fig. 4.2A) that uses iPSCs cultured in a monolayer before the application of factors promoting differentiation to dopaminergic neurons. Utilisation of this method also generated neurons expressing both tyrosine hydroxylase (TH) and neuron-specific βIII-tubulin (Fig. 3.21B).

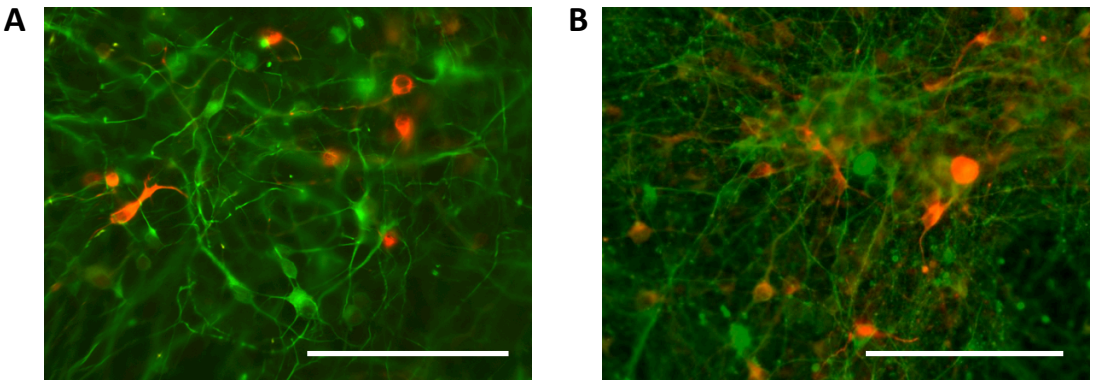

Figure 3.21: Differentiation of iPSCs generates neurons co-expressing dopaminergic markers TH and Tuj1.
(A-B) Immunocytochemistry showing the presence of TH+/Tuj1+ dopaminergic neurons within iPSC-derived cultures generated by the modified methods of (A) Hartfield et al. (2014) and (B) Kriks et al. (2011). Red, TH; Green, Tuj1. Scale bars, 100 µm.

(ii) Generation and use of HSV-1 amplicons

TH-PAC reporters were packaged into HSV-1 amplicons for delivery to iPSC-derived dopaminergic neurons. Production requires co-transfection of the ~100 kb *TH*-PAC constructs, ~178 kb modified HSV-1 genome (fHSVΔpacΔ27 0++) and 12.2 kb pEBHICP27 plasmid into the Vero 2-2 packaging cell line, a clone that contains a replacement copy of the HSV-1 ICP27 gene that has been removed from the HSV-1 genome. Prior to harvesting, EGFP was clearly expressed from Vero 2-2 cells that had been transfected with pEHHG or the pEHHG-retrofitted *TH*-PAC construct (Fig. 3.22A). Although the system is reported to produce yields up to 10^9 transducing units/ml (TU/ml) after ultracentrifugation (Saeki et al. 2001), titres of the *TH*-PAC constructs were consistently between $1x10^5$ and $1x10^6$ TU/ml, which made their use difficult for large numbers of cells or for anything but a low multiplicity of infection (MOI), usually <1. When the retrofitting plasmids pEHHG and pH-FRT-Hy were packaged, these gave titres between $1x10^6$ and $2x10^7$ TU/ml consistent with the theory that their smaller size would make transfection more efficient so that more cells received the DNA and also allow each cell to make more copies of that DNA by rolling-circular replication during the process of packaging. To improve the transfection conditions for the large *TH*-PAC

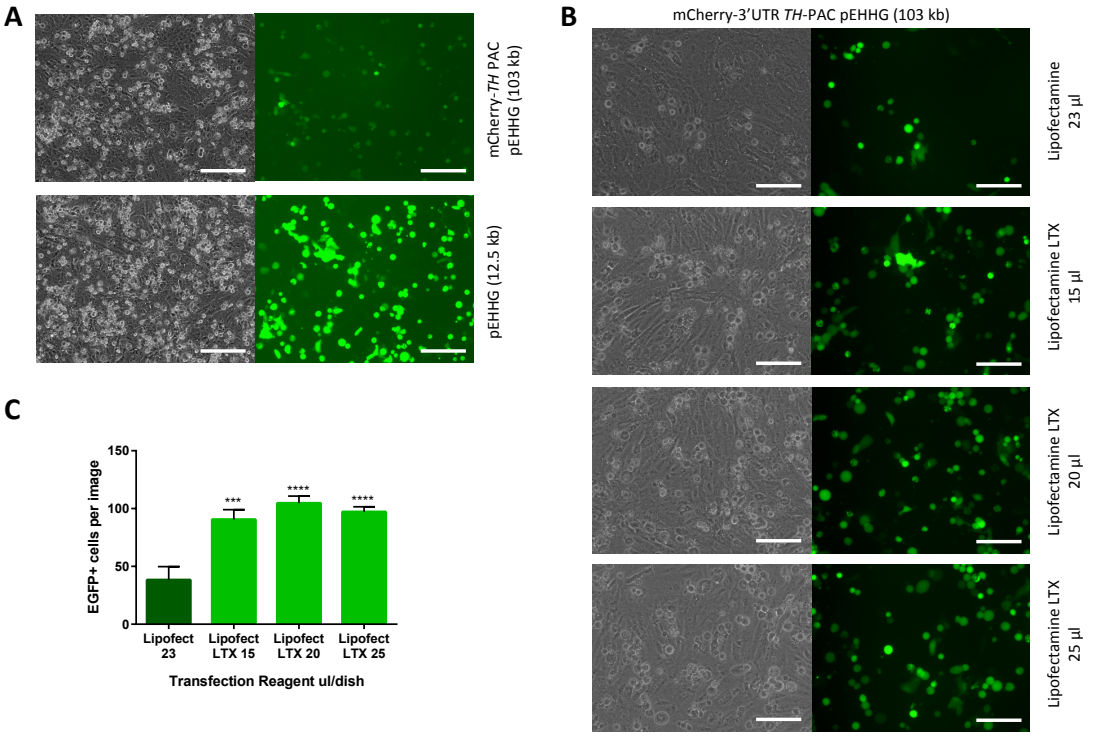

Figure 3.22: HSV-1 based amplicon production in Vero 2-2 cells.

(A) Bright field and fluorescence images of Vero 2-2 cells 72 hours after transfection for amplicon production using the standard method with Lipofectamine. Scale bars, 200 µm.

(B) Bright field and fluorescence images of Vero 2-2 cells 72 hours after transfection for mock production of amplicons to test transfection with Lipofectamine vs Lipofectamine LTX reagent. Scale bars, 200 µm.

(C) Graph of EGFP+ cell counts from transfection of Vero 2-2 cells with all plasmid components used in the production of amplicons to test transfection with Lipofectamine vs Lipofectamine LTX reagent. Mean ±SEM from count of n=7 images: Lipofectamine 23 µl, 38.3 ±11.6; Lipofectamine LTX 15 µl, 90.6 ±8.5; Lipofectamine LTX 20 µl, 104.7 ±6.1; Lipofectamine LTX 25 µl, 97.1 ±4.4. One-way ANOVA was statistically different (p<0.0001, F=13.83) and each Lipofectamine LTX condition was significantly different from Lipofectamine in Bonferroni's multiple comparison test: 15 µl, adjusted p=0.0004; 20 µl, adjusted p<0.0001; 25 µl, adjusted p<0.0001.

constructs, given the availability of newer transfection reagents since the protocol was first developed, four transfection conditions were tested in parallel and compared for the number of EGFP+ cells at the time point where harvesting would normally take place. The use of Lipofectamine LTX in place of Lipofectamine increased the number of EGFP+ cells in all three quantities tested (Fig. 3.22B-C). However, use of this modification in the packaging protocol subsequently showed only a possible minor improvement in amplicon titre at $7x10^5$ to $2x10^6$ TU/ml.

iPSC-derived dopaminergic neuronal cultures were transduced with 2nd generation *TH*-PAC reporter constructs to assess their expression and specificity. Unlike had been seen with transfection of immortalised cell lines, initial transductions of iPSC-derived cultures using the dual-fluorescent reporter showed differential expression of mCherry in a subset of EGFP+ neurons (Fig. 3.23). Subsequent transductions coupled with fixation 7 days after transduction and immunocytochemistry for TH, mCherry and EGFP showed that EGFP single-positive cells were a mixture of mostly TH- and some TH+, while the very small

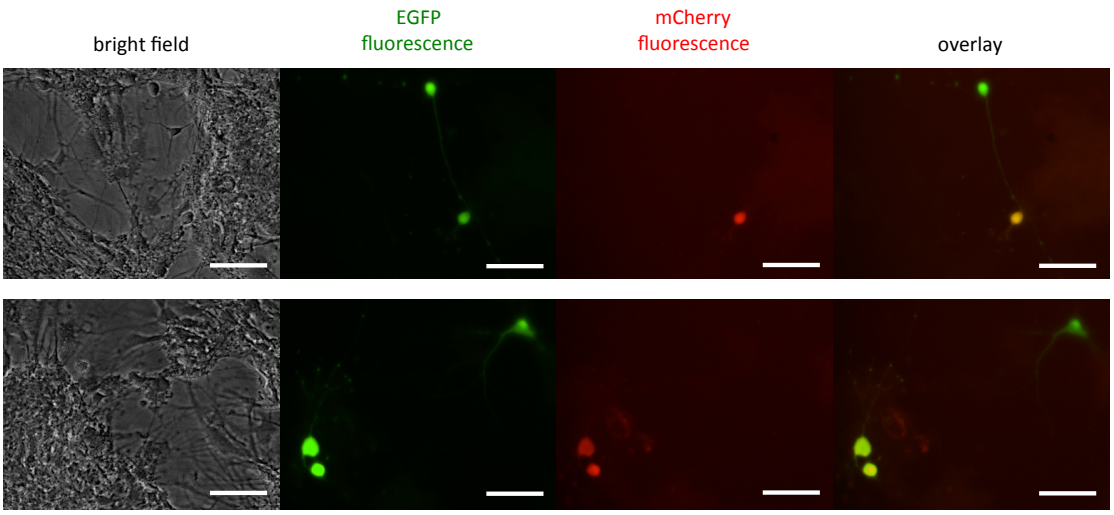

Figure 3.23: Transduction of iPSC-derived dopaminergic neuronal cultures with 2nd generation mCherry dual-fluorescence construct.
Bright field and live fluorescence images for iPSC-derived dopaminergic neuronal cultures examined 4 days after transduction. Differentiation was by the modified Hartfield method. Transduction with the dual-coloured construct results in differential expression of mCherry in a sub-set of EGFP+ cells. Scale bars, 100 µm.

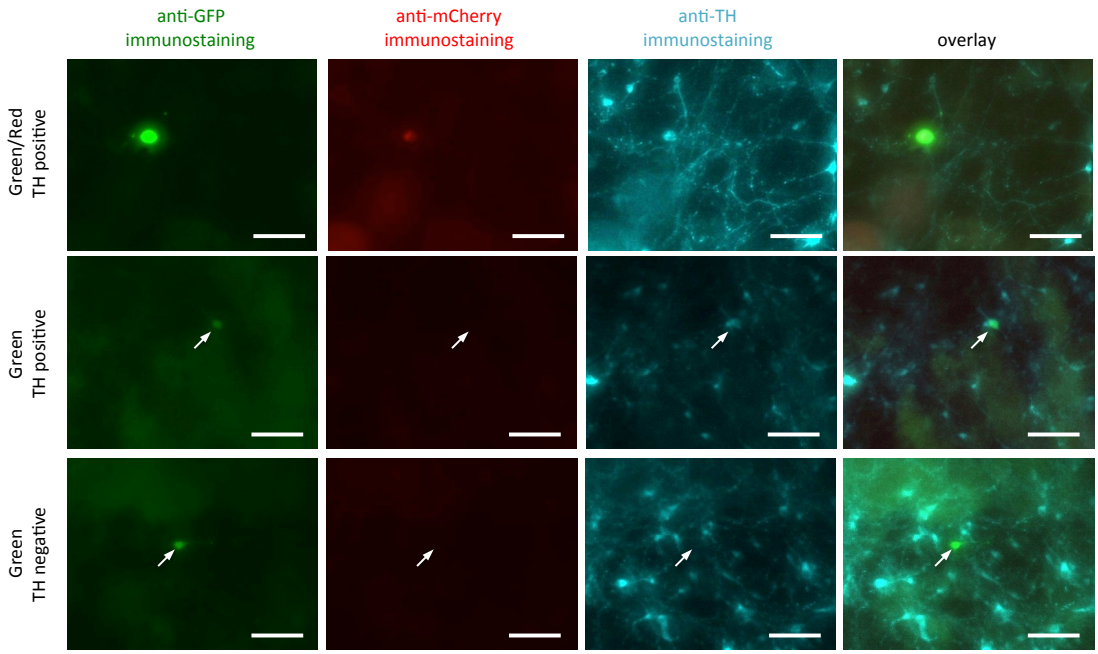

Figure 3.24: Immunocytochemistry of transduction of iPSC-derived dopaminergic neuronal cultures with 2nd generation mCherry dual-fluorescence construct.
Fluorescence images of immunocytochemistry for iPSC-derived dopaminergic neuronal cultures fixed 7 days after transduction (DIV27), showing examples of the three different combinations of EGFP/mCherry/TH co-expression seen following immunocytochemistry. Differentiation was by the method modified from Kriks et al. (2011). Arrows in the middle and lower rows point to the same cell in each image per row. Scale bars, 50 µm.

Table 3.1: Cell counts for immunocytochemistry of transduction of iPSC-derived dopaminergic neuronal cultures with 2nd generation mCherry dual-fluorescence construct.
Data from two experiments presented in adjacent sub-columns.

	Green		Green/Red	
TH negative	34	53	0	0
TH positive	5	17	2	1

% specificity (true negative rate)	100
% sensitivity (true positive rate)	12

number of mCherry+/EGFP+ cells were all TH+ (Fig. 3.24, Table 3.1). These data show that when delivered by transduction, the TH promoter is not active in all TH+ cells (sensitivity = 12%, Table 3.1), but the lack of any observed mCherry+ cells that were TH- suggests that the reporter is nevertheless specific (specificity = 100%, Table 3.1). However, the small numbers of mCherry+ cells detected in these experiments make it unable to prove conclusively.

(iii) Nucleofection of iPSCs

Given the poor yields of amplicons, I investigated the possibility of introducing the PAC-based reporter directly to iPSCs by nucleofection of DNA. iPSCs were nucleofected with the reporter that constitutively expresses EGFP under the HSV-1 intermediate-early 4/5 promoter (mCherry-3'UTR *TH*-PAC pEHHG) along with its companion retrofitting plasmid pEHHG, and pmaxGFP that expresses EGFP under a CMV promoter. Imaging 24 hours after nucleofection showed many EGFP+ cells for pmaxGFP (2 μg), indicating that nucleofection was generally successful (Fig. 3.25A), although with a small amount of cell death compared to non-nucleofected cells (Fig. 3.25B). Nucleofection with 3.9 μg pEHHG produced fewer EGFP+ cells in most fields of view (Fig. 3.25C) but nucleofection with 5 μg PAC-based reporter (Fig. 3.25D) yielded very few EGFP+ cells that required searching for, accompanied by substantial cell death, which worsened by 48 hours after nucleofection (data not shown). A further trial with 2 μg of each plasmid confirmed that delivery of the PAC-based construct was toxic to iPSCs; after 24 hours, while pmaxGFP showed a reasonable proportion of EGFP+ cells (Fig. 3.25E), very few EGFP+ cells were found for pEHHG (Fig. 3.25F) and only one EGFP+ cell for the PAC-based reporter when delivered as 2 μg (Fig. 3.25G) but not as 5 μg (Fig. 3.25H). Nucleofection of iPSCs with such a large construct was therefore deemed unsuitable.

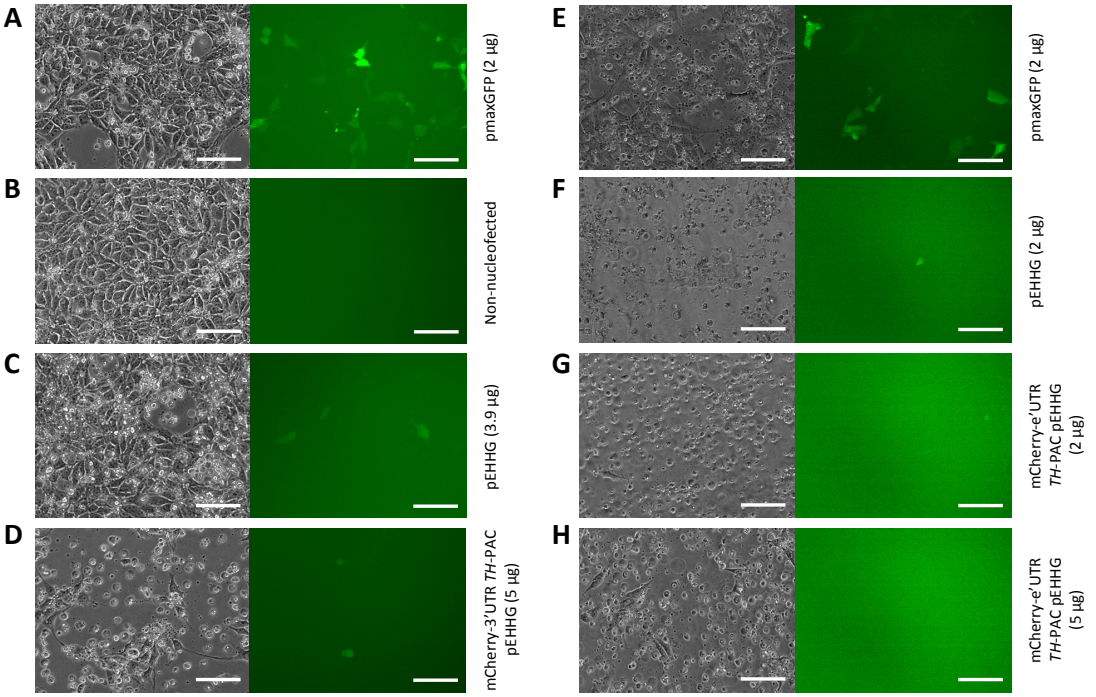

Figure 3.25: Nucleofection of iPSCs with EGFP-expressing plasmids.
Bright field and fluorescence images taken 24 hours after nucleofection. Scale bars, 100 µm.
(A-D) Four nucleofections from one experiment: (A) 2 µg pmaxGFP according to manufacturer's standard conditions; (B) non-nucleofected cells; (C) 3.9 µg pEHHG representing the maximum volume recommended; (D) 5 µg mCherry-3'UTR *TH*-PAC pEHHG representing the maximum mass of DNA recommended.
(E-H) Nucleofections from a further experiment where (E-G) 2 µg of each construct was used, except for (H) where 5 µg mCherry-3'UTR *TH*-PAC pEHHG was used as previously.

3.4 Discussion

3.4.1 Reporter construction and design

In this chapter I have presented the generation of several constructs towards the goal of producing a reporter of dopamine neurons for use in human cell culture models. These made use of the *TH* locus in its entirety with the exception of the exchange of the coding portion of exon 1 for a self-contained fluorescent protein cassette. A first generation human *TH* reporter expressing mCherry under the control of the *TH* genomic locus was successfully made using Red/ET homologous recombination. Expression of mCherry was sparse amongst transfected TH+ neuroblastoma cells, which could suggest that the mCherry/CAT/PolyAx3 cassette had problems with production and/or stability of transcripts. The first generation cassette lacked a specific 3'UTR for the mCherry portion, and the resultant transcripts would only reach a polyadenylation signal after reading through the bacterial promoter and chloramphenicol acetyltransferase sequence; it is possible that an element in these bacterial sequences causes RNA Polymerase II to pause. Critically, both the 3'UTR and polyadenylation signals of genes affect the stability of transcripts and are interconnected with transcription and mRNA processing more generally (Proudfoot 2011).

Subsequently, the reporter was redesigned to alter the cassette used to replace the coding portion of *TH* exon 1. These second generation constructs were made by the addition of a verified 3'UTR and polyadenylation sequence to separate mCherry from the bacterial promoter of chloramphenicol acetyltransferase so that there would be no significant read-through beyond the new polyadenylation sequence. Testing of these new constructs by transfection of immortalised cell lines showed near-complete co-expression of both the *TH*-driven mCherry and viral-driven EGFP reporters, showing that the redesign had overcome the problem of poor expression seen in first generation constructs.

While unproven, it would appear that the presence of the bacterial elements so close to the mCherry reporter sequence affected transcription or transcript stability. A better redesign for the construct would be to eliminate the bacterial elements altogether by using counter selection Red/ET recombination (Gene Bridges). This method employs two steps of homologous recombination to produce footprint-free modification of DNA constructs such as BACs and PACs; as such the reporter cassette used to replace the coding portion of exon 1 could be made to contain only the fluorescent protein sequence, a 3'UTR and polyadenylation sequences without the need for a bacterial resistance gene. Counter selection takes advantage of the fact that many widely used laboratory strains of *E. coli* are resistant to Streptomycin through a mutant *rpsL* gene that when augmented with a wild type *rpsL* gene will again confer sensitivity to Streptomycin. In such a strategy, the coding sequence of exon 1 would first be replaced with a cassette containing *rpsL-chl* (wild type *rpsL* and chloramphenicol acetyltransferase) by homologous recombination, with selection of recombinants performed on chloramphenicol. After verifying that recombinants are then sensitive to Streptomycin, a second homologous recombination step would be performed using the fluorescent reporter construct to replace the *rpsL-chl* cassette, with selection of recombinants performed on Streptomycin.

3.4.2 Reporter testing

(i) Transfection of immortalised cell lines

Testing of the second generation reporter by transfection of immortalised cell lines showed expression of mCherry in EGFP+ cells whether the cell line was TH+ or TH- (Fig. 3.18). Further investigation revealed that although untransfected TH- cells contain no *TH* transcripts, TH- cells transfected with unmodified *TH*-PAC did express *TH* transcripts (Fig. 3.19), despite the

TH-PAC construct being the wild type genomic locus that is already present in the genome of these cells. Similar findings were observed with a related construct made in this laboratory, where exon 1 of the mouse *Th* locus was replaced by an EGFP-L10a/3'UTR-PolyA/Amp^R cassette (Dr S. Janezic, DPhil thesis); while the construct expressed EGFP when transfected into HEK293 cells, region-specific expression was nevertheless demonstrated in the subsequently generated *Th*-bacTRAP mice. Further characterisation of these mice by Miss K. Wagner has shown that a subset of TH+ neurons correctly express the EGFP-L10a.

It has not been examined whether there are any genomic alterations to the *TH* locus in HEK293 or MRC-5 SV2 that would mask an otherwise TH+ phenotype, but the likelihood of this being the case for both cell lines is low. Rather the present data suggest that cell-type specificity of exogenous DNA constructs can be overridden when delivered by transfection as a large bolus of DNA. This could be particularly the case if the locus is tightly controlled by chromatin modifications, which would not immediately be established for newly-delivered constructs. Some studies have been performed on the epigenetic regulation of *TH*, notably that intron 1 includes a site for binding of the nuclear matrix/scaffold, and binding of the locus to nuclear matrix proteins was detected in TH+ adrenal medulla but not TH- liver samples (Lenartowski and Goc 2002); additionally the first exon, notably removed in the current study, contains a DNA methylation site that is specifically methylated in TH- cells and controls the binding of a transcriptional repressor (Arányi et al. 2005). Further studies into this area of regulation are warranted. An alternative possibility is that the transcription factors that inhibit expression from *TH* show limited expression, so that the delivery of additional binding sites upsets the balance of factors and loci. With either of these hypotheses it is possible that after sufficient time the correct regulation of expression could be established for loci delivered by transfection, requiring passaging of immortalised cell lines. Alternatively, further investigation of the reporter could be carried out in a set of

single-cell clones so that all cells would carry the reporter; however, this was not pursued in this study.

As detailed in the introduction of this Chapter, in principle, the delivery of genomic loci by HSV-1 amplicons allows physiological regulation of gene expression. Packaging of the unmodified *TH*-PAC into HSV-1 amplicons and subsequent delivery would inform as to whether the ectopic mRNA expression in TH- cell lines was an artefact of transfection or a possible problem with the *TH* locus itself. Certainly the *TH* locus is not straightforward in its regulation, evidenced by the failures of attempts to make a minimal promoter using conserved elements (Romano et al. 2005; Romano et al. 2007) and the complex regulatory architecture of the locus, including roles for the element in intron 1 in regulating expression (Meloni et al. 1998; Albanèse et al. 2001; Lenartowski and Goc 2002; Kelly et al. 2006).

(ii) Comparison of differentiation protocols

Both differentiation protocols used in this chapter employ similar principles to generate dopaminergic neurons from iPSCs. The Kriks method is now generally used throughout the field because it generates midbrain progenitors co-expressing FOXA2 and LMX1A. Both protocols used in the current study begin with neural induction by inhibition of two SMAD pathways: inhibition by SB431542 of the TGF-β pathway acting through Smad2/3 and inhibition of the BMP pathway acting through Smad1/5/8 (Chambers et al. 2009), the latter using noggin in the Hartfield protocol or the dorsomorphin derivative LDN-193189 in the Kriks protocol. These restrict patterning to a (neuro)ectodermal fate.

Next, both protocols induce patterning to a ventral midbrain fate. Through a modification to the Hartfield protocol by Dr J.L. Badger, both protocols used CHIR-99021 to inhibit GSK-3β, resulting in the de-inhibition of Wnt signalling, although employed at different times. Sonic

hedgehog (SHH), aided by CHIR-99021, promotes differentiation to a ventral fate, while delivery of FGF8a mimics release from the midbrain-hindbrain organiser (Rhinn and Brand 2001) to induce a more caudal identity. However, the Kriks protocol introduces both SHH and FGF8a at a much earlier time point (equivalent Day 2) instead of at days 5 and 11 respectively, and adds the Smoothened agonist purmorphamine to augment the effect of SHH in triggering the hedgehog pathway. As a result of the compressed patterning time, the Kriks protocol only has one maturation medium from equivalent day 12 onwards once patterning has been achieved.

For maturation, both protocols use growth factors BDNF and GDNF to offer trophic support to neurons, while the specific antioxidant ascorbic acid (Yan et al. 2001) and protein kinase A activator dibutyryl-cAMP (Mena et al. 1995) have been shown to increase dopaminergic differentiation. Additionally the Kriks protocol employs both TGF-β3 (Roussa et al. 2006) and the γ-secretase/Notch inhibitor DAPT (Crawford and Roelink 2007; Borghese et al. 2010) to promote neuronal maturation.

One particular advantage of the Kriks method is that it does not employ embryoid bodies, which have reduced accessibility of the interior cells to the soluble differentiation factors added in the medium and so generate more heterogeneous cultures (Bratt-Leal et al. 2009). Further, the manual dissection and re-plating steps in the Hartfield method are replaced by single-cell dissociation, counting and re-plating as a monolayer in the Kriks method, allowing for better penetration of viral particles, more accurate determination of cell number, and better ability to control cell density. The Kriks method also uses mitomycin C treatment to remove dividing cells, which improves the ability to keep cultures for long-term maturation. For these reasons, the Kriks method was employed in the remaining chapters of this thesis.

(iii) Transduction of iPSC-derived dopaminergic neuronal cultures

Second generation constructs were tested in iPSC-derived dopaminergic neuronal cultures by delivery of HSV-1 amplicons and showed very few cells expressing the fluorescent protein from the TH promoter, although all of these were TH+. The specificity of the construct when delivered by HSV-1 amplicons to human neuronal cultures as designed may therefore be correct, although the sensitivity is poor, i.e. not all TH+ cells that were EGFP+ also expressed mCherry. However, with such low numbers of transduced cells it cannot be ruled out that some TH- cells will ectopically express from the reporter; it has also not been confirmed that the entire construct is maintained intact on delivery to cells by performing a plasmid rescue experiment, as fragmented constructs could express one or both fluorescent proteins in a dysregulated manner, especially if integrated into the genome near to a promoter.

The attempts to verify cell-type specificity in iPSC-derived dopaminergic neuronal cultures were largely hampered by low yields of amplicons so that only low MOIs could be achieved. The helper-virus free system for HSV-1 amplicon production relies on co-transfection of the very large BAC containing the HSV-1 genome, the large *TH*-PAC reporter construct itself and a small additional plasmid. Even with small improvements in transfection capacity by changing the transfection reagents only had a numerical gain, not an increased order of magnitude of viral titres. It was noticed that while the transfection complexes can be left on cells with Lipofectamine LTX without the need to remove them after 4 hours, the adding of packaging medium at the 4 hour mark did not compensate for the volume already on the cells with respect to the concentrations of FBS, L-glutamine, HEPES etc.; it is possible that while more cells were transfected, the yield from each cell was not the optimal it could be. The quality of supercoiled DNA for transfection could also be improved by caesium chloride density gradient purification of DNA maxipreps. Further optimisations could be attempted for the packaging protocol, although these would be time-consuming to verify. The use of a

replication-deficient helper virus instead of the current helper-virus free system, in addition to producing amplicons contaminated with helper virus, would only improve yields for constructs that are smaller than 50 kb because the serial passaging of viral stocks only alters the ratio of products in favour of the target amplicon when the amplicon has a higher ratio of *ori*:genome length and so can replicate faster than the helper virus (Geller et al. 1990).

A final improvement would be to redesign the *TH*-PAC reporter to have a shorter promoter length so that it can be more easily transfected and packaged. The choice to use 70 kb of promoter was to be certain that long range regulation was included, and this amount of upstream sequence was available within the original BAC; however, given the difficulties of working with such a large construct and the lack of evidence that this length is required, a more manageable construct would be preferred. A BAC expressing mCherry as a fusion of the gene product of *FUS* made in this laboratory by Dr M. Thomas was 59 kb and showed significantly better transfection efficiency in immortalised cells when performed alongside the *TH*-PAC constructs (data not shown), and the smaller retrofitting plasmids likewise showed increased transfection efficiency and HSV-1 amplicon yields compared to the *TH*-PAC constructs (Fig. 3.22A).

3.4.3 Future directions for a dopaminergic reporter

Despite the benefits of genomic expression from HSV-1 amplicons, production of infectious lentiviral particles is a more ideal situation due to their higher viral titres and greater infectivity. However, the packaging limit for lentiviruses is 9 kb between the 5' and 3' long terminal repeats (LTRs), whereas HSV-1 amplicons can package up to 152 kb; as such, the promoter and reporter would need to be sufficiently small and simple to be accommodated within a lentiviral plasmid. Considering this, future efforts to produce a dopaminergic

reporter would be best served concentrating on the *PITX3* locus. Advantageously, this transcription factor is restricted to a more appropriate subset of dopaminergic neurons rather than the wider expression of *TH* in all catecholamine-producing cells (Messmer et al. 2007) so would theoretically be a more ideal target. Mice with knock-in expression of EGFP under the *Pitx3* locus yielded EGFP+ neurons that were >90% pure after fluorescence activated cell sorting (Hedlund et al. 2008), compared to the problems of ectopic expression in TH- cells seen by the same group using mice expressing EGFP from the rat *TH* promoter (Hedlund et al. 2007), although knock-in and transgenic promoters are not truly comparable. A fragment of the mouse *Pitx3* promoter has already been used in human cell culture, albeit with minimal characterisation (Castillo-Carranza et al. 2008), suggesting that a small portion of its promoter could be incorporated into a lentiviral vector. It is therefore hoped that the human *PITX3* locus would be amenable to the incorporation of its promoter into a lentiviral vector as a reporter construct for use in human iPSC-derived dopaminergic neuronal cultures.

Chapter 4: Allele-specific expression studies in iPSC-derived dopaminergic neuronal cultures

4.1 Introduction

Variation at the *MAPT* locus is associated with risk for PD as well as tauopathies in the spectrum of parkinsonism. The risk is conferred by an extended haplotype created by a chromosomal inversion within chromosome 17q21.31 (Stefansson et al. 2005) and the resulting linkage disequilibrium that maintains separation of the two principal haplotypes, H1 and H2 (Baker et al. 1999). Meta-analysis of genome-wide association studies has shown that in European populations where the H2 allele is present, the H1 haplotype is associated with risk for PD and the H2 haplotype with disease protection (Nalls et al. 2014). Interestingly the H2 allele also appears to be under positive selection (Stefansson et al. 2005). As the H1 allele is more common, representing approximately 75%, and is understood to be the human ancestral allele, it has significantly more variation than H2 resulting in H1 having many sub-haplotypes (Pittman et al. 2005; Fung, Xiromerisiou, et al. 2006; Vandrovcova et al. 2009). However, although the H1c sub-haplotype and rs242557 are associated with increased risk for PSP (Pittman et al. 2005; Höglinger et al. 2011), no sub-haplotype of H1 has been repeatedly associated with PD to narrow down the range of the association and provide insight into how the haplotype confers risk.

The coding portions of *MAPT* do not include any non-synonymous SNPs so the amino acid sequence of tau is unchanged from the two haplotypes. However, tau is not a single protein, but has expression of six major isoforms in adult human brain through the variable inclusion of exons 2, 3 and 10. As outlined in section 1.4, there are two candidate explanations for how the two *MAPT* alleles could differentially confer risk to PD (Caffrey and Wade-Martins

2012): haplotype sequence differences alter the overall expression of tau protein through changes in the promoter or 3'UTR; or haplotype sequence differences alter the expression of particular isoforms of tau protein by changing the regulation of alternative splicing.

Evidence on both sides has been presented. In summary, biochemical promoter studies in SK-N-MC cells suggested that the H1 promoter shows increased expression compared to H2 (Kwok et al. 2004); however, the isolation of this promoter sequence from the context of the *MAPT* locus and a relevant cellular context could affect the applicability of these findings. Curated analysis of exon array data and correlation with genotype suggested that there was no haplotype-specific alteration in total *MAPT* expression, but that isoforms containing exon 3 were more abundant with each allele of H2 in most brain regions examined (Trabzuni et al. 2012). However, a more powerful method for examining the effect of individual alleles is the use of PCR-based expression assays with allelic discrimination, either using single-base extension and detection or differential probe binding (Buckland 2004; Chen et al. 2008), because these can be performed using heterozygous samples and generate an internally-controlled ratio of expression between the two alleles. Previous studies from this laboratory used allelic discrimination to investigate *MAPT* haplotype expression in neuroblastoma cell lines and post-mortem human frontal cortex and globus pallidus (Caffrey et al. 2006; Caffrey et al. 2008). These studies found that post-mortem brain samples showed no difference in total *MAPT* expression between the two haplotypes, but did show haplotype-specific increases in exon 10 expression from the H1 allele and in exon 3 expression from the H2 allele.

4.1.1 Aims of the Chapter

- To detail the generation of dopaminergic neuronal cultures from human iPSCs with *MAPT* H1/H2 genotype, and the determination of culture conditions necessary for the expression of all six isoforms of *MAPT*.
- To present analysis of the expression of *MAPT* in human iPSC-derived dopaminergic neuronal cultures and post-mortem human midbrain, both in terms of general expression and expression from the individual haplotypes H1 and H2. Both sample sets represent the kind of dopaminergic neurons that die in PD.
- To describe efforts to isolate and characterise *MAPT* expression within a pure population of dopaminergic neurons to understand that specific cell type following fluorescence-activated cell sorting. This work includes the co-culture of human neurons with primary rat astrocytes to assess the effect on neuronal maturity.

4.2 Methods

4.2.1 Genotyping, sequencing and sub-cloning

Genomic DNA for 58 healthy individuals from the OPDC cohort was provided by Mr S. Evetts. *MAPT* H1/H2 genotyping reactions around the 238 bp indel in intron 9 (Appendix Table E) were performed as described in section 2.5.1.

For sub-cloning of individual alleles, products from allele-specific amplification of the region around *MAPT* exon 10 by AmpliTaq Gold (section 2.5.1) were ligated into pGEM-T Easy (section 2.3.2) and electroporated into NEB 10-beta Electrocompetent *E. coli* (section 2.6.1) prior to incubation (overnight, 37°C) on ampicillin-agar with IPTG/X-Gal for blue-white selection. Plasmids were isolated (section 2.2.1 *ii*) and sequenced (section 2.5.4).

4.2.2 RNA extraction from post-mortem human midbrain

Samples of frozen post-mortem human midbrain were obtained for *MAPT* H1/H2 individuals without signs of neuropathology from the UK MRC Control collection run by Oxford Brain Bank, University of Oxford. Samples were composed of several cryostat-generated horizontal sections that each included the *substantia nigra*. Samples were homogenised in RNeasy Buffer RLT with 1% 2-mercaptoethanol using a TissueRuptor (QIAGEN), centrifuged (16250 RCF, 3 min), then RNA was extracted from the lysate supernatant as per section 2.10.1 *ii*, beginning with the addition of 100% ethanol.

4.2.3 Bioanalyzer electrophoretic analysis of RNA

RNA integrity was evaluated by Eukaryotic Total RNA 6000 Pico assay on a 2100 Bioanalyzer (Agilent Technologies) according to manufacturer's instructions. Briefly, pico chips were assembled with gel by addition of 1 µl dye concentrate to 65 µl pre-filtered gel matrix, centrifugation to remove precipitates (10 min, 13,000 RCF) and even dispersal of 9 µl per chip using the chip priming station; 9 µl gel and 9 µl conditioning solution were then added to the respective marked wells. Pico marker was added to each sample/ladder well (5 µl) then 1 µl denatured RNA (70°C, 2 min) or 1 µl 1X ladder was added to each sample/ladder well before the chip was vortexed horizontally (1 min, 2400 RPM) and run on the Bioanalyzer.

4.2.4 Allele-specific qRT-PCR

Three pairs of TaqMan probes were used to discriminate allelic transcripts in *MAPT* at haplotype-tagging SNPs identified in Baker et al. (1999): (1) a pair validated by Dr M-C.Lai against SNP1 (rs17650901) (M.C. Lai, DPhil Thesis, Hilary Term 2016); (2) a pair designed in PrimerExpress software v3.0 (Applied Biosystems) against SNP9ii (rs17652121); (3) an additional pair against SNP9ii published by Myers et al. (2007a). Probe pairs were ordered as custom probe-only assays (both probes together) from Applied Biosystems; see Appendix Table J for all primer and probe sequences. Validation of specificity was performed using H1/H1, H1/H2 and H2/H2 genomic DNA, followed by the generation of a standard curve from 8:1 to 1:8 with *MAPT* H1 PAC (a gift from F. Denk) and *MAPT* H2 PAC (a gift from R. Wade-Martins) constructs, which was adjusted through the origin. Specificity for the reactions was achieved with 5X SNP1 probe concentration, 3X SNP9ii (Myers) probe concentration and 900 nM primers.

H1:H2 ratios were calculated as follows: 2^(-1.194*[(cDNA ΔC_T H1-H2) – (Mean genomic ΔC_T H1-H2)] for SNP1 and 2^(-1.043*[(cDNA ΔC_T H1-H2) – (Mean genomic ΔC_T H1-H2)] for SNP9ii. For midbrain samples, the mean of the genomic ΔC_T H1-H2 values for the eight iPSC clones was used. Specific H1:H2 ratios for inclusion of exon 3 and exon 10 in *MAPT* transcripts were determined by dividing by the respective H1:H2 ratio for total *MAPT* transcripts.

4.2.5 Co-culture of astrocytes with iPSC-derived dopaminergic neuronal cultures

A vial of rat primary cortical astrocytes (Invitrogen) containing $1x10^6$ cells was thawed into a T75 flask in DMEM, 25 mM glucose, 3.97 mM GlutaMAX, 1 mM sodium pyruvate (Gibco) supplemented with 15% FBS as per manufacturer's instructions. Medium was changed every 4-5 days until cells reached confluency at which point they were passaged into three 6-well plates pre-coated with Geltrex, being approximately timed to reach confluency by DIV20 of the differentiation protocol. Astrocyte culture medium was removed and re-plated neuronal cultures were added in neuronal maturation medium before being treated as standard neuronal cultures regarding mitomycin C treatment etc.

4.2.6 Intracellular staining and fluorescence-activated cell sorting

The following protocol was developed by Mr P. Robertson and detailed in Sandor and Robertson et al. (2016) (under review). Neuronal cultures or co-cultures (one 6-well plate per line) were rinsed briefly with DPBS and incubated with trypsin-EDTA (900 µl/well, 5 min) to detach cells. After addition of defined trypsin inhibitor (Gibco) with 6 U/ml DNase I (NEB) (1200 µl/well), cells were pooled and gently triturated to a single-cell suspension before passed through a 40 µm cell strainer rinsed with PBS with 3 U/ml DNase I. All subsequent

steps were performed on ice. Cells were centrifuged (4°C, 300 RCF, 5 min), resuspended in 1 ml PBS and centrifuged (4°C, 300 RCF, 5 min; standard from here). Dead cells were stained for 10 min with 1 ml 1:500 LIVE/DEAD Fixable Yellow Dead Cell Stain Kit (Molecular Probes) in PBS, which was stopped with addition of 200 µl 10% BSA in PBS. Cells were centrifuged, resuspended in 30 µl PBS and fixed for 10 min with addition of 200 µl 4% paraformaldehyde in PBS. Fixation was stopped by adding 25 µl 1 M glycine in PBS then 200 µl permeabilisation buffer with IgG (PB/IgG; PBS with 0.1% saponin, 2% BSA, 5 mM DTT, 100 U/ml Protector RNase inhibitor [Roche], 2 µg/ml normal goat IgG [Santa Cruz Biotechnology]). After centrifugation, cells were blocked by 10 min incubation in 200 µl PB/IgG and 25 µl 1 M glycine then divided 5:1 for TH and IgG_{2a} staining and centrifuged.

For staining with primary antibody or IgG_{2a} isotype control, cells were resuspended in 500 µl or 100 µl PB/IgG with the appropriate antibody (0.1 µg/ml TH F-11 or normal mouse IgG_{2a} [Santa Cruz Biotechnology]) and incubated rotating for 1 hour, 4°C, then centrifuged. For staining with secondary antibody, cells were resuspended in PRDB (PBS with 2% BSA, 5 mM DTT, 100 U/ml Protector RNase inhibitor) with 1:2000 goat anti-mouse IgG Alexa-Fluor 635 conjugate (Invitrogen) and incubated rotating for 15 min, 4°C, then centrifuged. After resuspension in 200 µl PRDB, centrifugation and final resuspension in 400 µl PRDB, cells were ready for sorting.

Staining controls were processed as follows. Unstained cells were only resuspended in PBS and centrifuged before fixation and neutralisation with glycine but not blocking with IgG (PB only). A ‘live’ population stained only with LIVE-DEAD stain was treated with all steps to fixation and neutralisation with glycine but not blocking with IgG (PB only). A ‘dead’ population was treated as the unstained cells above, then fully permeabilised by addition of PB (no IgG) and glycine again before incubation with LIVE-DEAD stain, which enters all cells,

and neutralisation with BSA. Following the above preparations, all controls were centrifuged and resuspended in PRDB before being used in sorting.

Cells were sorted on a BD FACSAria IIu at the Weatherall Institute of Molecular Medicine Flow Cytometry Facility by Dr S-A Clark, or a BD FACSAria III at the Experimental Medicine Division Flow Cytometry Facility by Dr H Ferry. Unstained cells were used to delineate the cell population from debris while 'live' and 'dead' controls were used to set the gating strategy for the LIVE-DEAD staining to select only cells that had been alive prior to fixation. Finally, the gating for the TH staining was determined using the IgG_{2a} isotype staining control and then the live TH+ population was identified on the initial forward-scatter side-scatter plot to further refine the area corresponding to live cells.

4.2.7 RNA isolation and cDNA synthesis from fixed cells

RNA was isolated from fixed cells using either the RNeasy micro kit as described in Chapter 2 with addition of proteinase K digestion step, or by RNeasy FFPE kit (QIAGEN). To add proteinase K digestion to the RNeasy micro protocol, samples in buffer RLT with 1% 2-mercaptoethanol were vortexed for 5 min and diluted 3-fold with RNase-free water and proteinase K (Sigma) to final concentration of 222 ng/µl before incubation at 56°C for either 15 min or 60 min then continuation with the standard protocol at the 70% ethanol step. The RNeasy FFPE kit was carried out as per manufacturer's instructions. Briefly, samples were resuspended in 150 µl buffer PKD and 10 µl proteinase K (>600 mAu/ml, QIAGEN) was added before incubation at 56°C for 15 min and 80°C for 15 min, or else 56°C for 60 min according to Thomsen et al. (2016). Samples were held on ice (3 min) and centrifuged (15 min, 20,000 RCF) before addition of 1/10 volume DNase booster buffer and 10 µl DNase I (2.73 U/µl) with incubation for 15 min at room temperature. Lysates were mixed with 320 µl

buffer RBC and 720 µl 100% ethanol before loading on the MinElute spin column by centrifugation. The columns were washed twice with 500 µl buffer RPE, spun again for 5 min to dry the columns, then samples were eluted with 14 µl RNase-free water.

RNA concentration was determined by Quant-iT RiboGreen kit (Molecular Probes) using the low-range assay as per manufacturer's protocol. Briefly, a standard curve was constructed with ribosomal RNA standard from 0 to 10 ng in 100 µl; samples were run as 1 µl or 0.2 µl neat sample diluted to 100 µl with 1X TE buffer. Standard/samples were run in duplicate in a flat-bottomed 96-well plate. After addition of 100 µl diluted RiboGreen reagent (2000-fold in 1X TE buffer), the plate was incubated for 2-5 min and read on a Synergy HT fluorescent microplate reader (BioTek) using 485/20 excitation filter, 528/20 emission filter and multiple gain settings to choose the one with results nearest the instrument's maximum.

cDNA synthesis was performed using the SeqPlex RNA Amplification kit (Sigma-Aldrich) according to manufacturer's instructions. Briefly, 15 ng of RNA, 1.8 µl library synthesis solution and water to 11.88 µl were incubated to denature RNA (70°C, 5 min) then held at 18°C to allow primer binding. To this, 1.8 µl library synthesis buffer, 1.44 µl library synthesis enzyme and water were added to make an 18 µl library synthesis reaction, which was incubated as follows: 18°C, 10 min; 25°C, 10 min; 37°C, 30 min; 42°C, 10 min; 70°C, 20 min; 4°C hold. Library samples were frozen at -20°C until amplification. On thawing, the amplification reaction was set up by addition of 15 µl 5X amplification mix, 0.75 µl amplification enzyme and water to 75 µl, then incubated for PCR in a thermal cycler as follows: 94°C, 2 min; 25 cycles of 94°C, 30 s and 70°C, 5 min; final step of 70°C, 30 min. Amplified cDNA was purified by QIAquick PCR Purification kit (QIAGEN) as described in section 1.2.3 *i*, with elution in 50 µl water.

4.2.8 Statistical analysis

All statistical analysis and graphical representation was performed in Prism version 7 (GraphPad Software). Specific tests are noted in each figure legend. For allele-specific expression studies, two-tailed one-sample *t*-tests were used to determine whether the mean H1:H2 ratio was significantly different from 1. Unpaired two-tailed *t*-tests were used to compare the expression levels of two groups. Pearson correlation was used to determine the correlation between *RBM4* and *PTBP1* expression.

4.3 Results

4.3.1 Generation of human iPSC-derived dopaminergic neuronal cultures

To enable study of the relationship between *MAPT* and PD, human iPSCs were differentiated into dopaminergic neuronal cultures as a cellular model of human dopamine neurons. The use of iPSC technology enables cultures to be made with specific genotypes of interest corresponding to those of their donors. Fifty-eight healthy controls within the Oxford Parkinson's Disease Cohort were screened to identify heterozygous individuals with a copy of both the *MAPT* H1 and H2 alleles by amplifying around the 238 bp indel in intron 9 (Fig. 4.1). Of the 58 individuals genotyped, 22 individuals (38%) were the desired H1/H2 genotype with 31 individuals (53%) homozygous for H1 and 5 individuals (9%) homozygous for H2 (Fig. 4.1B). Overall the H1 allele represented 72% of all alleles and the H2 allele represented 28% (Fig. 4.1C). The distributions of genotypes and alleles were not significantly different from those of a published UK control cohort (Goris et al. 2007).

From the available iPSC clones generated by Ms J. Vowles and Dr S.A. Cowley at the James Martin Stem Cell Facility, Oxford Stem Cell Institute, a total of eight iPSC clones were selected for use in this study, being made from three H1/H2 individuals (Fig. 4.1D, Appendix Table F). The three individuals were further genotyped by myself at 33 exonic SNPs in *MAPT*, *STH*, *SNCA*, *LRRK2*, *CRHR1* and *KANSL1* (see Appendix Table G). Many of the selected SNPs were chosen as they carry significant association with Parkinson's disease by large meta-analysis (Nalls et al. 2014), but only rs6673790 in *LRRK2* of individual 3 showed a differential presence of a risk allele (homozygous C in individual 3 vs. homozygous T in individuals 1-2), and all three individuals confirmed their H1/H2 status at additional SNPs in *MAPT*, *STH*, *CRHR1* and *KANSL1*.

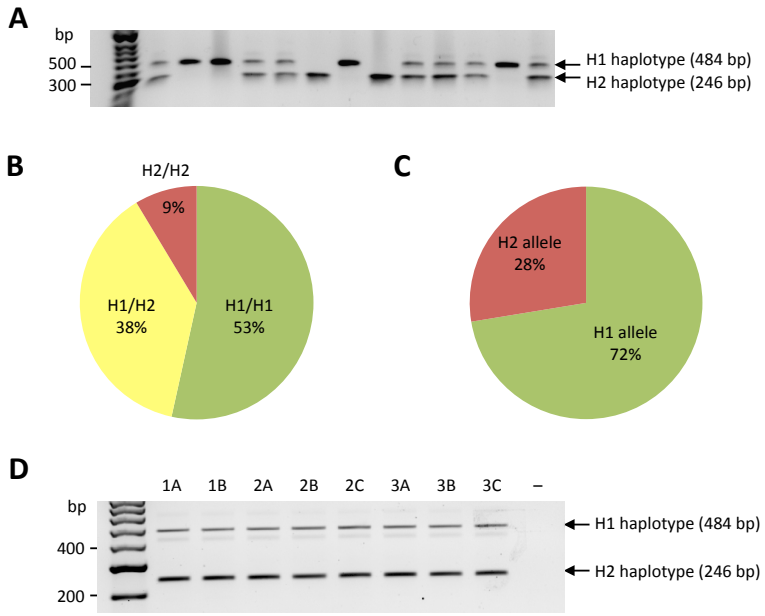

Figure 4.1: Determination of *MAPT* genotype of healthy control cohort.
Genotyping data for healthy controls in the OPDC cohort using PCR to distinguish the H1 and H2 alleles of *MAPT* by the 238 bp indel in intron 9.
(A) Representative agarose gel electrophoresis of the genotyping PCR showing the three genotypes, H1/H1, H1/H2 and H2/H2, in members of the OPDC cohort.
(B) Pie chart showing the percentage distribution of genotypes within the 58-individual cohort. Actual numbers: H1/H1, 31; H1/H2, 22; H2/H2, 5. UK control cohort from Goris et al. (2007) for comparison: H1/H1, 1241 (58%); H1/H2, 806 (37%); H2/H2, 106 (5%). OPDC control cohort distribution shows no significant difference from that of Goris et al. (2007) using a Chi-square test (χ^2=1.714, df=2, p=0.4244).
(C) Pie chart showing the percentage distribution of alleles within the 58-individual cohort. UK control cohort from Goris et al. (2007) for comparison: H1 allele, 3288 (76%); H2 allele, 1018 (24%). OPDC control cohort distribution shows no significant difference from that of Goris et al. (2007) using a Chi-square test (χ^2=0.9708, df=1, p=0.3245).
(D) Agarose gel electrophoresis of the genotyping PCR showing the H1/H2 genotype of eight selected iPSC clones. Clones are identified by the number of the individual donor (1-3) then by the clone generated from reprogramming of the fibroblasts of that individual (A-C).

Differentiation of iPSCs towards a midbrain fate (Fig. 4.2A) generated dopaminergic neuronal cultures (Fig. 4.2B) expressing neuron-specific beta-III tubulin (Tuj1) and the dopaminergic neuronal marker tyrosine hydroxylase (TH), identified by Western blot (Fig. 4.2C). Both markers were already present by DIV20 when the differentiated cells are re-plated in their final configuration. Immunocytochemistry confirmed the Western blot data, showing that 60% of cells were Tuj1-positive, with up to 50% of those co-expressing TH (Figs. 4.2D and 4.3). Further, at later time points during maturation some cultures had

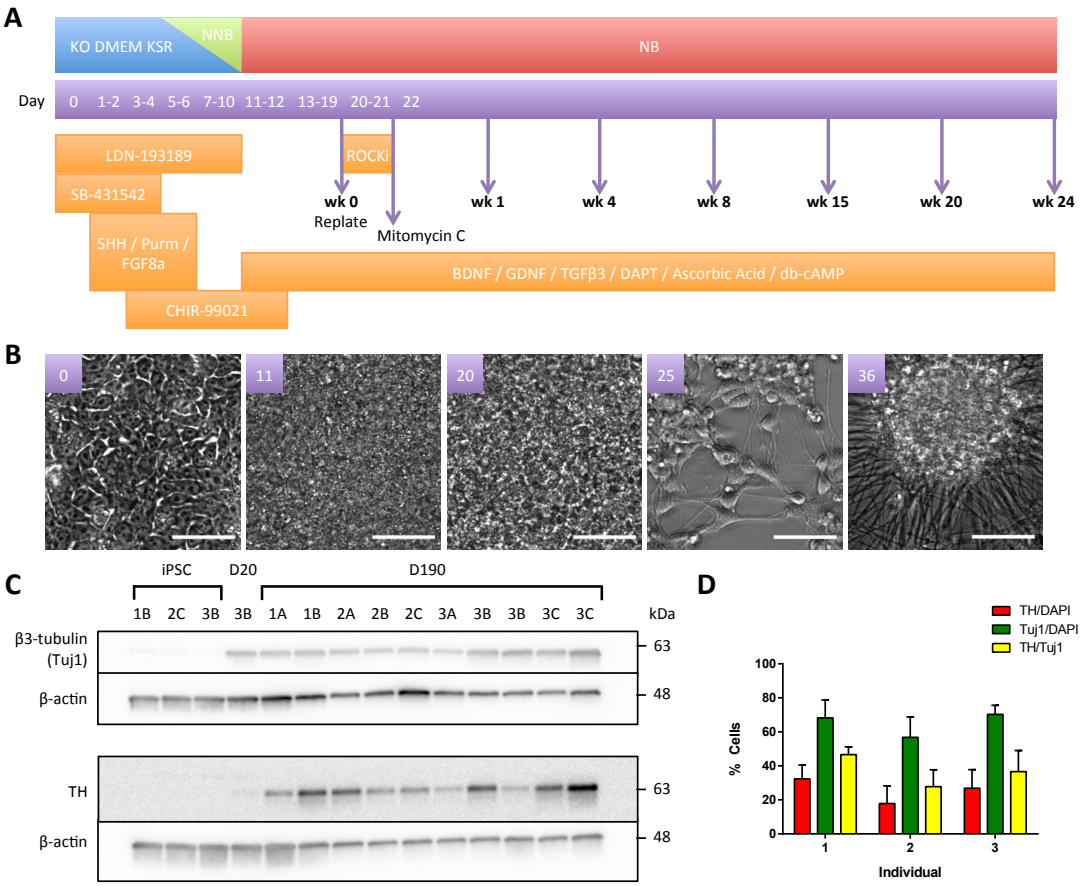

Figure 4.2: Differentiation of induced pluripotent stem cells with MAPT H1/H2 genotype into dopaminergic neuronal cultures.

(A) Schematic of the differentiation protocol to generate dopaminergic neuronal cultures and their subsequent maturation as used in this study. Orange boxes denote the differentiation and trophic factors added to the medium on each day (purple boxes). Base media are shown in the bar at the top. Following re-plating on DIV20 (maturation week 0), time point samples were taken as shown by purple arrows up to a maturation of 24 weeks (DIV190). For full details see section 2.7.3 *ii*.

(B) Phase contrast images of a representative differentiation from iPSCs (DIV0) to dopaminergic neuronal cultures at DIV36. Each image shows DIV in the top left. Scale bars, 50 µm.

(C) Western blots showing differentiation into cultures expressing Tuj1 and TH. Clone numbering as described in Fig. 4.1D; clones 3B and 3C include samples from two differentiations. iPSC stage and DIV20 (week 0; re-plating) samples are included as comparisons for the DIV190 samples.

(D) Bar chart of cell counts following immunostaining for tyrosine hydroxylase (TH) and beta-III tubulin (Tuj1). Counts were performed on cultures fixed between one and four weeks following re-plating. Mean ±SEM of n=2 or n=3 clones per individual; 4 images per clone.

spontaneously differentiated a very small number of glial fibrillary acidic protein (GFAP)-positive astrocytes, but these were estimated to be <1% of all cells (Fig. 4.4). Expression of the *MAPT* gene is both spatially and developmentally regulated, being primarily expressed in neurons, but although astrocytes express a small amount of tau (Papasozomenos and Binder 1987; Müller et al. 1997), the small number of contaminating astrocytes is unlikely to make a significant impact on *MAPT* expression data generated from these cultures.

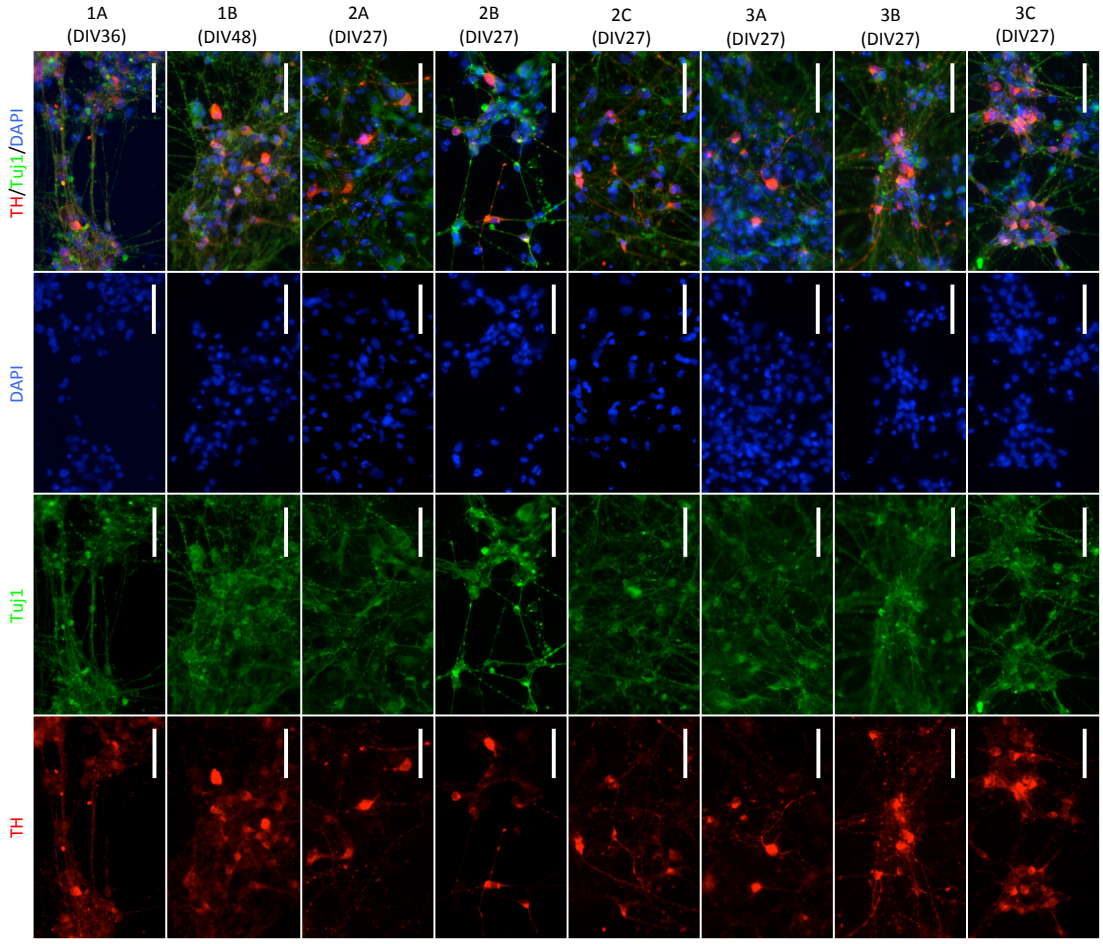

Figure 4.3: Immunostaining of iPSC-derived dopaminergic neuronal cultures showing the generation of dopaminergic neurons.
Immunostaining of representative dopaminergic neuronal cultures from each clone fixed between 1 week (DIV27) and 4 weeks (DIV48) after re-plating with separate channels and merged image. Each clone generated dopaminergic neurons shown by co-expression of TH+/Tuj+ but with different efficiencies, as quantified in Fig. 4.2D. Scale bar, 50 µm.

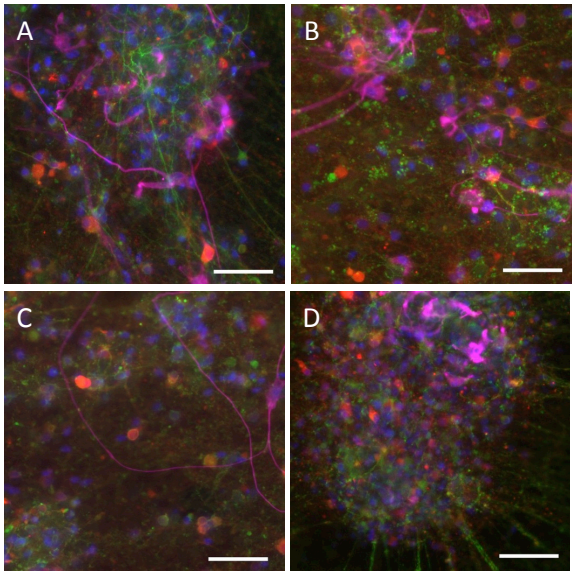

Figure 4.4: Immunostaining of iPSC-derived dopaminergic neuronal cultures showing the spontaneous generation of a small number of astrocytes.
(A-D) Selected images of a small number of glial fibrillary acidic protein (GFAP)-positive cells by immunostaining at various points in the time course, weeks numbered beyond re-plating at DIV20: (A) clone 2A, 15 weeks; (B) clone 2B, 15 weeks; (C) clone 1B, 15 weeks; (D) clone 3A, 4 weeks. Merged images with GFAP (magenta), Tuj1 (green), TH (red) and DAPI (blue). Scale bar, 50 µm.

4.3.2 Development of allele-specific quantitative RT-PCR expression assays

The principal aim of the work detailed in this chapter was to characterise the level of *MAPT* isoforms expressed from the two haplotypes, H1 and H2, within iPSC-derived dopaminergic neuronal cultures. The overall expression of the different isoforms was determined using existing quantitative real-time PCR (qRT-PCR) assays but these cannot distinguish allelic transcripts. Rather, allele-specific expression assays distinguish the provenance of transcripts from an individual allele using a single nucleotide polymorphism (SNP). A set of TaqMan-based qRT-PCR allele-specific expression assays was developed using SNPs in exon 1 (rs17650901) (M.C. Lai, DPhil Thesis, Hilary Term 2016) and exon 9 (rs17652121) of *MAPT* to distinguish between transcripts deriving from H1 and H2 alleles (Fig. 4.5A-B). These assays amplify the desired portion of cDNA (primers in exons shown in purple in Fig. 4.5A-B) or genomic DNA (one primer in an intron shown in orange in Fig. 4.5A-B) without allelic

discrimination, but rely on a pair of TaqMan probes whose sequences differed at a haplotype-tagging SNP to distinguish the allelic origin of each molecule. The output of these assays is a ratio of H1:H2 transcripts for a given PCR amplicon, whereby a ratio greater than 1 represents more expression from the H1 allele than from the H2 allele and vice versa.

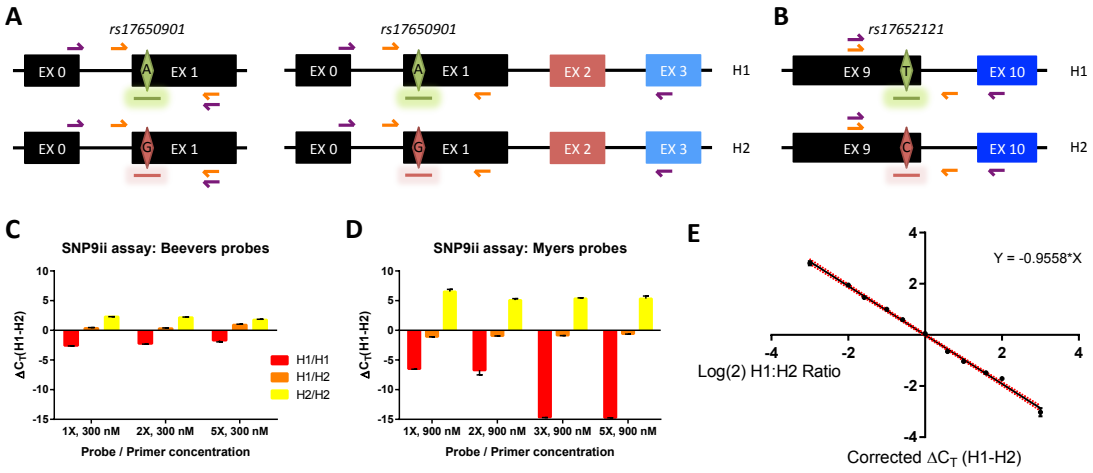

Figure 4.5: Schematics and validation of allele-specific *MAPT* qRT-PCR expression assays.
(A-B) Schematics of the allele-specific TaqMan-based expression assays exploiting the haplotype-tagging SNP in (A) *MAPT* exon 1 (SNP1, rs17650901) or (B) *MAPT* exon 9 (SNP9ii, rs17652121), shown as a green or red diamond denoting the H1 or H2 allele respectively. TaqMan probes bearing FAM (green) or VIC (red) are shown as coloured lines below the SNP. Arrows denote primers to amplify from genomic DNA (orange) or cDNA (purple).
(C-D) Validation of specificity for the two pairs of allele discriminating probes for SNP9ii (rs17652121). The concentration of probe pairs was increased to try to improve specificity (greater ΔC_T H1-H2 value) when only one allelic sequence was present (ie homozygous H1 or H2). Mean ±SEM, n=2 wells.
(E) Standard curve for the allele-specific expression assay using SNP9ii (rs17652121), generated using *MAPT* H1 PAC and *MAPT* H2 PAC in ratios from 8:1 to 1:8. The values of ΔC_T (H1-H2) were plotted against log(2) H1:H2 ratio, then corrected after linear regression to remove the value of the y-intercept (to bring the graph through the origin). To use as a standard curve for cDNA expression assays, cDNA values of ΔC_T (H1-H2) were first corrected relative to a genomic DNA sample before reading the corresponding log(2) H1:H2 ratio from the standard curve using the graph equation, ΔC_T(H1-H2) = -0.9558 * log(2)H1:H2 ratio. Mean ±SEM, n=3 wells, linear regression R^2=0.997. Red dashed line, 95% confidence interval.

The allele-specific probes against SNP9ii (rs17652121) that I designed were tested for their specificity using genomic DNA from H1/H1, H1/H2 and H2/H2 individuals and showed that while the three genotypes could be distinguished sufficiently for genotyping purposes (the goal of the design software) the signal generated from the non-present allele in each case was too great (Fig. 4.5C). Despite increasing the concentration of probes from 1X up to 5X, the ΔC_T (H1-H2) values for H1/H1 were -2.56, -2.23 and -1.69 with increasing probes and for H2/H2 were 2.29, 2.17 and 1.79 with increasing probes (Fig. 4.5C). As this degree of specificity was unsuitable for the construction of a standard curve for allele dilution, the probes designed and used by Myers et al. (2007a) were obtained and tested likewise. The Myers probes showed greater specificity, which further increased with increasing probe concentration, so that the ΔC_T (H1-H2) values for H1/H1 were -6.49, -6.72, -14.64 and -14.72 and for H2/H2 were 6.54, 5.10, 5.36 and 5.35 (Fig. 4.5D). The probe pair has an inherent bias so that the H1 probe is more prone to incorrectly bind to the H2 sequence than the H2 probe is to incorrectly bind to the H1 sequence, as shown by the negative ΔC_T (H1-H2) values when the template is H1/H2 heterozygous genomic DNA (Fig. 4.5D). Notwithstanding, the Myers probes were suitable for construction of a standard curve of allele dilution from 8:1 to 1:8 with H1 and H2 PAC DNA (Fig. 4.5E). By adjusting the ΔC_T (H1-H2) values by the value of the y-intercept, the graph passed through the origin, correcting for the inherent bias, and allowing for subsequent cDNA samples to be compared to the standard curve following correction with a genomic DNA sample.

4.3.3 Establishment of expression of adult tau isoforms in neuronal cultures

Adult human brain expresses six principal isoforms of tau generated through the splicing of exons 2, 3 and 10 (Fig. 1.2B) while the human foetus expresses only the shortest isoform, lacking exons 2, 3 and 10. An initial time course study of the first four weeks after re-plating

(up to DIV48) showed that each of the principal alternatively-spliced exons of *MAPT* could be detected in RNA transcripts (Fig. 4.6A), revealing the presence of the following isoforms: foetal tau (0N and 3R) from week 0; 1N tau from week 0; 2N tau, i.e. exon 3 inclusion, from week 1; 4R tau, i.e. exon 10 inclusion, from week 2.

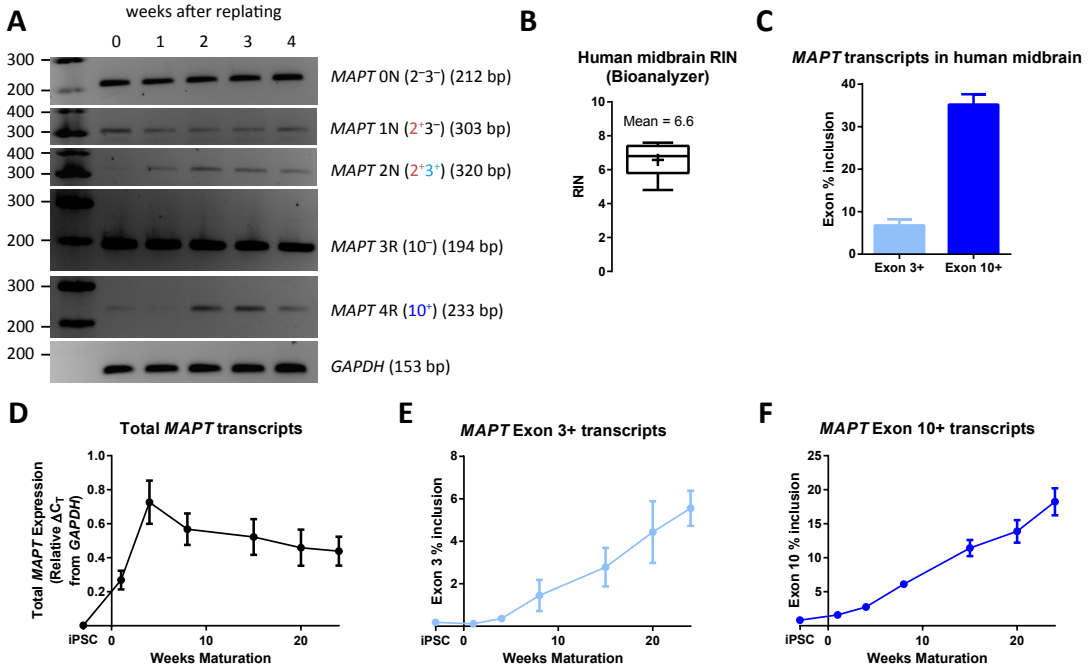

Figure 4.6: *MAPT* adult isoforms increase in expression over a six-month differentiation.
(A) Agarose gel electrophoresis of end-point RT-PCR on samples from a short time course of maturation of iPSC-derived dopaminergic neuronal cultures from the week 0 (DIV20), the day of re-plating, to week 4 (DIV48) following re-plating.
(B) RNA integrity values for RNA extracted from slices of frozen post mortem human midbrain containing the substantia nigra, from individuals of H1/H2 genotype (n=9). Box and whisker plot showing minimum and maximum (bars), quartiles (box), median (centre line) and mean (+).
(C) *MAPT* exon inclusion from TaqMan-based quantitative RT-PCR expression assays performed on human midbrain cDNA. Mean ±SEM, n=5 individuals; exon 3+ mean = 6.79 ±1.43; exon 10+ mean = 35.22 ±2.43.
(D-F) Data from TaqMan-based quantitative RT-PCR expression assays on samples from a time course of maturation of dopaminergic neuronal cultures from week 1 (DIV27) to week 24 (DIV190) as per time points shown in Fig. 4.2A, as well as the iPSC stage (representative of DIV0). Each graph shows mean ±SEM, n=7 clones (all clones except 1A). For each graph, linear regression performed using all data points from weeks 4-24 with F-test confirming that each slope is significantly different from zero: (D) y = -0.01303*x + 0.7279, F= 4.615, p=0.0391; (E) y = 0.2553*x - 0.7078, F= 23.32, p<0.0001; (F) y = 0.7416*x - 0.05151, F=96.28, p<0.0001.

As a comparison for the data to be generated from iPSC-derived dopaminergic neuronal cultures, RNA was extracted from nine post-mortem human midbrain samples, shown to be of adequate quality (Fig. 4.6B) and quantified by qRT-PCR (Fig. 4.6C). The average inclusion of exon 3 in post-mortem adult midbrain was 6.8% and of exon 10 was 35.2% (Fig. 4.6C). Publications estimate that adult brain has a 3R:4R ratio of approximately 1:1, i.e. 50% inclusion of exon 10; however, this is most commonly determined in human cortical samples (Goedert and Jakes 1990; Hong et al. 1998) and so may reasonably be different in the midbrain, as evidenced by other published regional differences in this ratio within control individuals (Majounie et al. 2013).

Using qRT-PCR, iPSC-derived dopaminergic cultures were examined over a six-month time course of maturation as outlined in Fig. 4.2A. During this period the expression of total *MAPT* transcripts relative to *GAPDH* peaked at four weeks after re-plating (DIV48; Fig. 4.6D). Over the period from DIV48 to DIV190, cultures exhibited a 15-fold increase in the expression of adult isoforms containing exon 3, reaching an inclusion of 5.6%, a similar level to that of adult midbrain (Fig. 4.6E). Adult isoforms containing exon 10 showed a 6.6-fold increase in expression over the same period (Fig. 4.6F), rising towards the level seen in post-mortem human midbrain (18.2% vs. 35.2%). Data from the inclusion of exons 3 and 10 are clear evidence of cell maturation, but also show that further maturation would be required to reach equivalent adult midbrain levels of exon 10 inclusion.

In addition to quantification of transcripts by qRT-PCR, the presence of all six tau protein isoforms was examined by Western blot with dephosphorylation to allow accurate identification of isoforms. An initial time course reaching 25 weeks (DIV197) after re-plating showed the presence of 0N4R tau from 8 weeks (DIV76) and 1N4R tau and both 2N isoforms by 25 weeks (DIV197) (Fig. 4.7). Cultures of all eight clonal iPSC lines were subsequently matured to six months after re-plating (DIV190). Although included on this blot, the batch of

iPSCs used for clone 1A was discovered to have a duplication in chromosome 1q so was excluded from further expression analysis. Western blot analysis of six-month cultures confirmed that for all remaining lines the inclusion of exons 3 and 10 at the transcript level led to the presence of all six isoforms at the level of tau protein, detected by either a pan-tau antibody or antibodies probing for 4R and 2N tau isoforms (Fig. 4.8). In contrast, only a small amount of foetal tau (0N3R), the smallest isoform, was detected at DIV20, the day of re-plating following the period of midbrain patterning and initial differentiation (Fig. 4.8, lane 5) and none in iPSCs before commencing differentiation (Fig. 4.8, lanes 2-4). Overall, these data show that by six months, iPSC-derived dopaminergic neuronal cultures already show significant adult-like maturity, recapitulating expression patterns seen in adult midbrain, and are a valuable model for the study of *MAPT* biology.

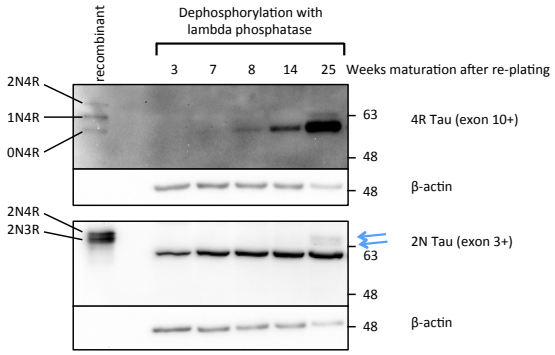

Figure 4.7: Tau adult isoforms increase in expression over a six-month differentiation.
Western blots showing the increasing presence of isoforms of mature tau protein in an initial time course of iPSC-derived dopaminergic neuronal cultures (clone 3A) from DIV41 to DIV200, as detected by antibodies against total tau (TAU5) or just specific isoforms (4R Tau, 2N Tau) and beta-actin loading control. All sample lanes included dephosphorylation treatment with lambda phosphatase. Left lane, ladder of all six recombinant tau protein isoforms. 2N Tau blot: central bands indicated by blue arrows represent the two 2N Tau isoforms; additional lower band is of unknown identity. The positions of the 63 kDa and 48 kDa bands from BLUeye Prestained Protein Ladder (GeneFlow) are shown on the right.

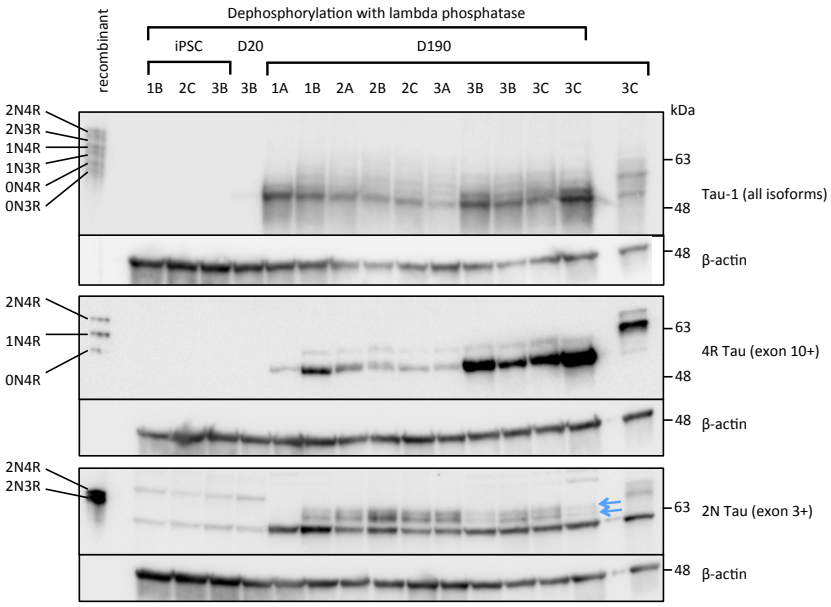

Figure 4.8: All major tau protein isoforms expressed in iPSC-derived dopaminergic neuronal cultures differentiated for six months.

Western blots showing the presence of all six major isoforms of mature tau protein in dopaminergic neuronal cultures at DIV190, as detected by antibodies against total tau (Tau-1) or just specific isoforms (4R Tau, 2N Tau) and beta-actin loading control. Sample details as Fig. 4.2C; all sample lanes included treatment with lambda phosphatase except the far right lane as an untreated duplicate sample. Although the sample for clone 1A is included on this blot, it was generated from a batch containing a duplication of chromosome 1q and was subsequently removed from further analysis. Far left lane, ladder of all six recombinant tau protein isoforms. 2N Tau blot: central bands indicated by blue arrows represent the two 2N Tau isoforms; additional upper and lower bands are of unknown identity. The positions of the 63 kDa and 48 kDa bands from BLUeye Prestained Protein Ladder (GeneFlow) are shown on the right.

4.3.4 Haplotype-specific expression of MAPT *in human iPSC-derived dopaminergic neuronal cultures*

Following the design of allele-specific assays detailed in section 1.3.2, analysis of *MAPT* expression was performed in both a general and haplotype-specific manner in iPSC-derived dopaminergic neuronal cultures matured for six months to model the critical cell type that degenerates in PD. Samples from the same six-month cultures of the eight clonal iPSC lines that had been examined previously by Western blotting (Fig. 4.8) were analysed by qRT-PCR. The levels of total *MAPT* transcripts showed no significant difference between individuals (Fig. 4.9A). Transcripts containing exon 3 also showed no significant difference between individuals, with the average inclusion of exon 3 for all seven clones being 9.1% (Fig. 4.9B). However, following a trend seen at the protein level (Fig. 4.8) individual 3 showed a 42% higher inclusion of exon 10 in *MAPT* mRNA transcripts compared to individuals 1 and 2 (p=0.0005; Fig. 4.9B).

The expression of all *MAPT* transcripts combined, measured by amplifying transcripts between constitutive exons 0 and 1, was 23% greater from H1 than from H2 in DIV190 dopaminergic neuronal cultures (Fig. 4.9C). In the same assay, total *MAPT* expression in post-mortem human midbrain did not differ significantly from an allelic ratio of 1 (Fig. 4.9C).

The average H1:H2 allelic ratio of *MAPT* transcripts containing exon 3 was 0.56 across all iPSC-derived dopaminergic culture sample sets as well as 0.51 in the midbrain sample set (Fig. 4.9D). This signifies that the H2 allele expresses approximately twice as many transcripts containing exon 3 as the H1 allele. These data from dopaminergic neuronal cultures and midbrain agree with those of other brain regions and cell types examined previously (Caffrey et al. 2008) and it is expected that this haplotype-specific difference in the regulation of exon 3 inclusion would be displayed in most CNS neurons.

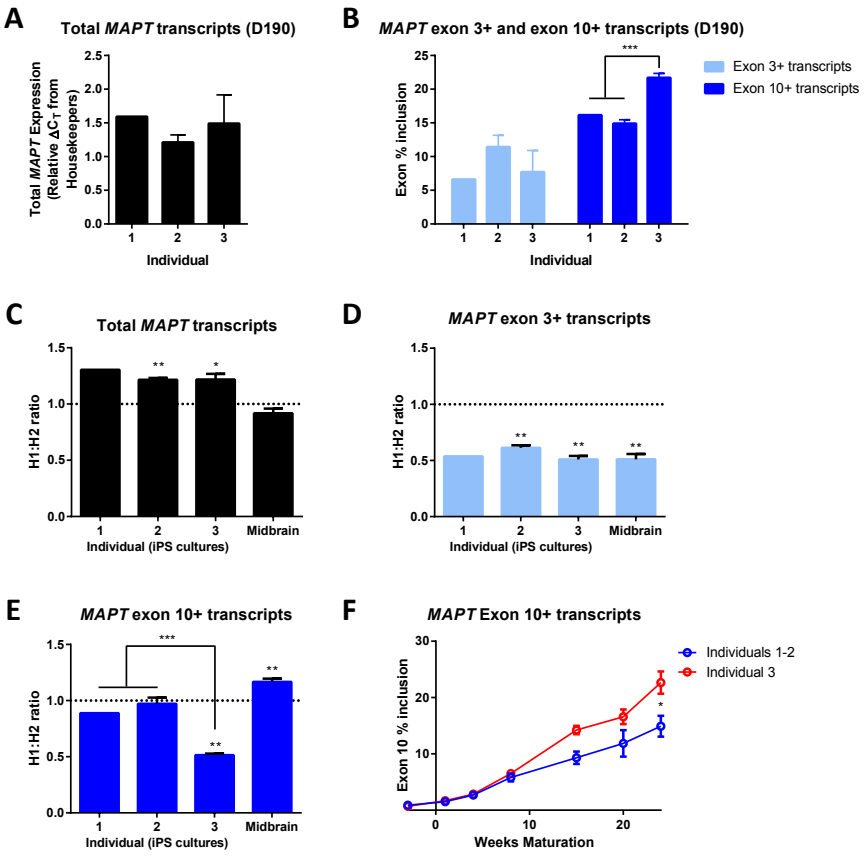

Figure 4.9: Dopaminergic neuronal cultures extended to six months exhibit significant differences in isoform expression from H1 and H2 alleles.

Data from TaqMan-based qRT-PCR expression assays on samples at DIV190 (week 24) matching those analysed by Western blot in Fig. 4.2C and Fig. 4.8. Following the discovery that the batch of iPSCs for clone 1A had a duplication of chromosome 1q, these data were removed from analysis but are included below for reference. Mean ±SEM; individual 1, n=1 clone; individuals 2 and 3, n=3 clones each; 3 cDNA samples per clone, except clones 3B and 3C where 6 cDNA samples were averaged to generate the clonal mean (two differentiations of 3 cDNA samples each).

(A-B) Standard *MAPT* expression assay results combined by individual. (A) Total *MAPT* expression reported as relative ΔC_T of geometric mean of three housekeeper genes (*GAPDH*, *HPRT1*, *ACTB*). No difference between individuals using one-way ANOVA with Fisher's least significant difference test using all comparisons. Clone 1A, 1.64. (B) Asterisk denotes significant statistical difference between groups in an unpaired *t*-test: $mean_{1\text{-}2}$=15.23 ± 0.50, $mean_3$=21.69 ± 0.65, *p*=0.0005, *t*=8.019, df=5. Clone 1A: exon 3, 0.60%; exon 10, 4.79%.

(C-E) Allele-specific expression assays distinguishing transcripts of H1 and H2 allelic origin, presented as H1:H2 ratio, i.e. values >1 show higher H1 expression. Data from analysis of human midbrain cDNA are additionally included: (C) n=9 individuals; (D) n=5 individuals that passed qPCR threshold criteria; (E) n=9 individuals. RIN data for midbrain samples are shown in Fig. 4.6B. For exon 3+ and exon 10+ transcripts (D-E), the H1:H2 ratio is normalised to the H1:H2 ratio of total *MAPT* transcripts per sample. Asterisks on individual samples denote significant statistical difference from a hypothetical mean of 1 in a one-sample *t*-test: (C) individual 1, 1.304, (n=1); individual 2, mean=1.216 ± 0.017, *p*=0.0059, *t*=12.92, df=2; individual 3, mean=1.218 ± 0.049, *p*=0.0471, *t*=4.445, df=2; midbrain, mean=0.917 ± 0.041, n.s.; (D) individual 1, 0.536, (n=1); individual 2, mean=0.613 ± 0.022, *p*=0.0032, *t*=17.64, df=2; individual 3, mean=0.509 ± 0.031, *p*=0.0040, *t*=15.71, df=2; midbrain, mean=0.511 ±

0.048, p= 0.0020, t=10.29, df=3; (E) individual 1, 0.888, (n=1); individual 2, mean=0.972 ± 0.055, n.s.; individual 3, mean=0.514 ± 0.014, p= 0.0008, t=34.87, df=2; midbrain, mean=1.167 ± 0.029, p=0.0005, t=5.698, df=8. Asterisks above the bracket in (E) denote significant statistical difference between groups in an unpaired t-test: $mean_{1\text{-}2}$=0.951 ± 0.044, $mean_3$=0.514 ± 0.014, p=0.0005, t=8.115, df=5. Excluded values for clone 1A: (C) 1.143; (D) 0.419; (E) 0.832.
(F) Subdivision of Fig. 4.6F (time course qRT-PCR) to separate out individual 3, which showed a distinct increase in exon 10 inclusion by quantitative RT-PCR. Individuals 1-2, n=4 clones; individual 3, n=3 clones. Asterisk denotes significant statistical difference between groups in a multiple one-sample t-test with Sidak-Bonferroni multiple comparison correction: $mean_{1\text{-}2}$=14.91 ±1.85, $mean_3$=22.66 ±1.98, p=0.000133, t=4.36, df=31.

Finally, when the allelic ratios of *MAPT* transcripts containing exon 10 were determined, the ratio was not different from 1 for DIV190 dopaminergic neuronal cultures from individuals 1-2 (Fig. 4.9E); however, cultures from individual 3 showed a marked shift to a ratio of 0.51 (Fig. 4.9E). Consistent with previous observations in other brain regions and cultured cells (Caffrey et al. 2008), post-mortem human midbrain exhibited an H1:H2 ratio for exon 10+ transcripts of 1.2 (Fig. 4.9E). As the data from individual 3 showed a distinct phenotype compared to individuals 1-2, the data from the six-month qRT-PCR time course was re-analysed and confirmed that individual 3 showed a greater inclusion of exon 10 than individuals 1-2, a difference that reached statistical significance by 24 weeks as a 52% increase (Fig. 4.9F).

Having established the extent of haplotype-specific expression differences in iPSC-derived dopaminergic neuronal cultures matured for six months, samples from three selected time points from the time course of culture maturation were also examined in these new assays to determine whether haplotype-specific expression changes over time while cultures are maturing (Fig. 4.10). For total *MAPT* transcripts, no difference was seen at 4 weeks after re-plating but H1 expressed 11% more than H2 at 15 weeks, and 31% more than H2 at 24 weeks, (Fig. 4.10A). For exon 3+ transcripts, no difference was seen at 4 weeks due to low overall expression of exon 3, but the phenotype of strong H2 expression was clear at 15 weeks (H1:H2 ratio 0.59) and 24 weeks (H1:H2 ratio 0.52) (Fig. 4.10B). Finally, analysis of

exon 10+ transcripts confirmed that individual 3 consistently showed an H1:H2 ratio of <0.5 at all three time points (Fig. 4.10C).

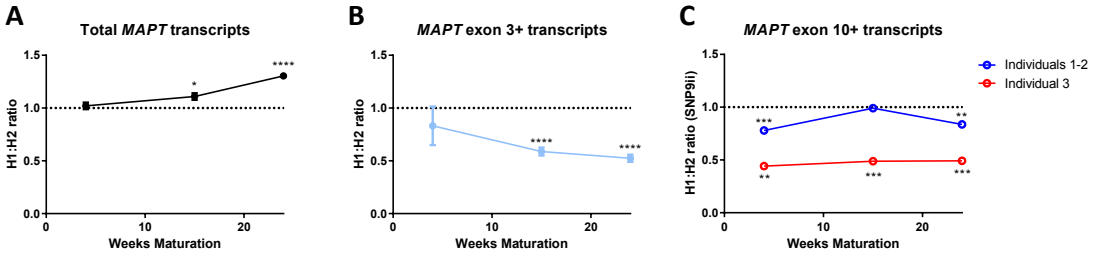

Figure 4.10: Time-course graphs of allele-specific *MAPT* qRT-PCR expression assays on iPSC-derived dopaminergic neuronal cultures.
Data from allele-specific TaqMan-based quantitative RT-PCR expression assays on samples from three points of a time course of maturation of dopaminergic neuronal cultures: week 4 (DIV48), week 15 (DIV124) and week 24 (DIV190) as per time points shown in Fig. 4.2A. Graph C shows individual 3 separated out to highlight the consistent and distinct phenotype relative to exon 10. Each graph shows mean ±SEM; (A-B) n=7 clones (all clones except clone 1A); (C) individuals 1-2, n=4 clones; individual 3, n=3 clones. Asterisks denote significant statistical difference from hypothetical mean of 1 in a one-sample *t*-test: (A) week 4, mean=1.020 ±0.031, n.s.; week 15, mean=1.109 ±0.031, p=0.0132, t=3.478, df=6; week 24, mean=1.305 ±0.024, p<0.0001, t=12.58, df=6; (B) week 4, mean=0.832 ±0.183, n.s.; week 15, mean=0.588 ±0.038, p<0.0001, t=10.97, df=6; week 24, mean=0.524 ±0.034, p<0.0001, t=13.95, df=6; (C) individuals 1-2 week 4, mean=0.780 ±0.013, p=0.0005, t=16.50, df=3; individuals 1-2 week 15, mean=0.991 ±0.030, n.s.; individuals 1-2 week 24, mean=0.837 ±0.014, p=0.0013, t=11.74, df=3; individual 3 week 4, mean=0.441 ±0.019, p=0.0011, t=29.85, df=2; individual 3 week 15, mean=0.488 ±0.006, p=0.0002, t=81.41, df=2; individual 3 week 24, mean=0.492 ±0.006, p=0.0002, t=81.39, df=2. Although there was a discrepancy between the samples of individuals 1-2 in (C) and the corresponding main six-month sample set (Fig. 4.9E), wherein the time course samples showed a significant reduction in H1:H2 ratio, the main set had a larger sample size and more cDNA analysis replicates so was taken to be the more reliable result.

4.3.5 Identification of a novel variant that alters the inclusion of MAPT *exon 10*

The three clones from individual 3 in this study were significantly different from the four clones made from individuals 1 and 2 with respect to the biology of *MAPT* exon 10. In summary, individual 3 showed a 2-fold increase in expression of exon 10+ transcripts from the H2 allele (Fig. 4.9E) and over 40% more inclusion of exon 10 (Fig. 4.9B). To investigate the root of these phenotypes, *MAPT* exons 9 and 10 and their flanking regions were

sequenced for all three individuals. Individuals 1 and 2 showed the expected wild-type sequence but an indel was detected in individual 3 that resulted in a disrupted read formed by overlapping sequences from the mismatch of the two alleles (Fig. 4.11A). Whether using the read from reverse sequencing primer or subtracting the known wild-type sequence from the overlapping portion, both methods identified the indel as a deletion of three nucleotides (ΔCTT) at positions +102 to +104 of intron 10.

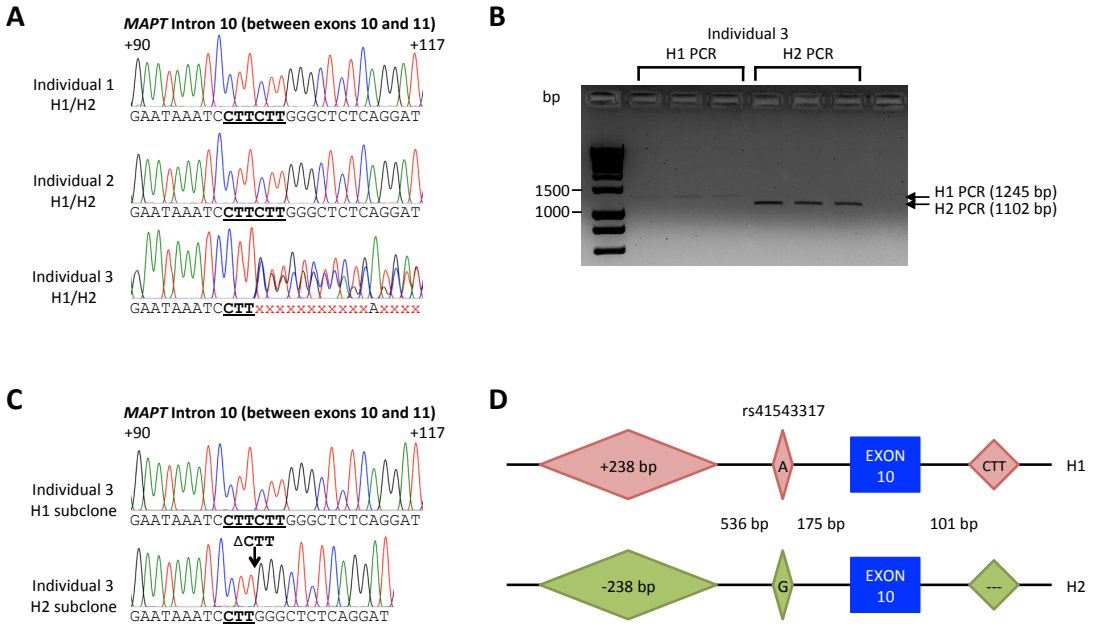

Figure 4.11: Discovery of a novel deletion in *MAPT* intron 10.
(A) Sequencing results within *MAPT* intron 10 (base positions after exon 10 at top) showing reads from genomic DNA (both H1 and H2 alleles together) for individuals 1-3. Red x's represent unclear reads from two overlapping sequences caused by an indel on one allele. **(B)** Agarose gel electrophoresis of products of PCRs amplifying the region around *MAPT* exon 10 from each separate allele, H1 and H2, by virtue of a forward primer either flanking or contained within the 238 bp indel in the preceding intron. The PCR products were subsequently sub-cloned into the pGEM-T Easy vector system to facilitate reading of the two isolated sequences.
(C) Sequencing results within *MAPT* intron 10 (base positions after exon 10 at top) showing clean reads from sub-cloned single allelic genomic DNA from individual 3. The H2 subclone showed a ΔCTT that has not previously been reported.
(D) Schematic of the region around *MAPT* exon 10 showing the sequence differences between H1 and H2 alleles from individual 3.

To identify on which allele the deletion was present, long PCRs were designed to stretch from beyond the indel in intron 10 back to the 238 bp haplotype-tagging indel in intron 9 that could be used to anchor the PCR to a specific allele by having the primer positioned either within (H1) or spanning (H2) the 238 bp indel (Fig. 4.11B). Allele-specific PCR products were subsequently sub-cloned into pGEM-T Easy vector for screening of colonies with the expected insert before direct sequencing. Sequencing of individual H1 or H2 allelic sub-clones confirmed the identity of the ΔCTT variant and revealed that it was present only on the H2 allele of individual 3 (Fig. 4.11C). A schematic of the sequence variation in the vicinity of *MAPT* exon 10 for individual 3 is shown in Fig. 4.11D. This ΔCTT variant does not exist on any public database of genetic variation so is a novel variant. As the deletion was present on the allele that showed increased exon 10 inclusion, this strongly suggests that this novel ΔCTT variant causes increased inclusion of exon 10 in agreement with the altered H1:H2 ratio.

To examine possible functional mechanisms for the increased inclusion of exon 10 in transcripts that include the ΔCTT variant, an *in silico* search of splice factor binding sites was performed on the intronic sequence with/without the ΔCTT variant using *SpliceAid 2* (Fig. 4.12) (Piva et al. 2012). *SpliceAid 2* uses only experimentally confirmed binding motifs from human cells/tissues to predict binding, and can be further refined to the level of tissues/cell types to reflect the complement of splicing factors expressed therein. Using all available splicing factors, two binding sites were predicted to be lost by the ΔCTT variant: RBM4, which is predicted to enhance inclusion of exon 10 (Kar et al. 2006), and PTBP1 (PTB/hnRNP I), which is predicted to promote exclusion of exon 10 (Wang et al. 2004). In the presence of the ΔCTT variant the predicted binding site for RBM4 would be reduced from 9 bp to 6 bp and that of PTBP1 from 6 bp to only 3 bp.

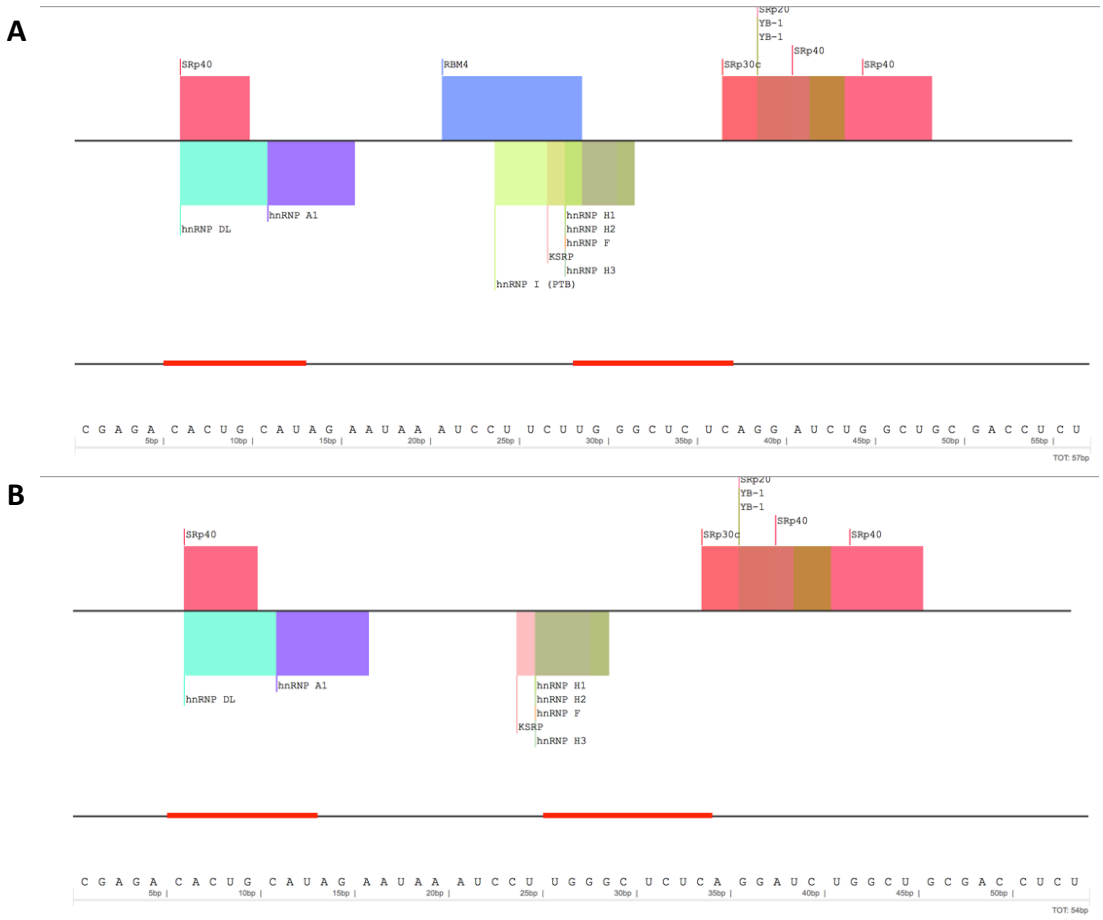

Figure 4.12: The novel ΔCTT deletion in *MAPT* intron 10 is predicted to decrease binding of factors that regulate exon 10 splicing.
Screen shots of splice factor binding site analysis with and without the novel deletion in *MAPT* intron 10 using *Splice Aid 2* online tool (http://193.206.120.249/splicing_tissue.html, version February 2013, 71 splicing factors, 2339 RNA binding sites, accessed February 2016) (Piva *et al.* 2012). Analysis performed with input of a portion of **(A)** the normal sequence of *MAPT* intron 10 and **(B)** the ΔCTT sequence as in control 3. Splice factors that promote exon inclusion or exclusion are shown as blocks respectively above or below the central line. Unlike the normal sequence, the ΔCTT variant sequence is not predicted to be bound by RBM4 (blue box above) or hnRNP I (PTB; light green box below). All known splicing factors were included in this search, rather than restricting by tissue type.

qRT-PCR for *RBM4* and *PTBP1* confirmed the expression of both of these splicing factors in cultures of clones from each of the three individuals across the period of the time course (Fig. 4.13A-B). Furthermore, the expression of *RBM4* and *PTBP1* appeared to be correlated in these samples (Fig. 4.13C). From week 4 after re-plating (DIV48) the expression levels of both genes appears to be relatively stable, rather than matching the observed increase in inclusion of exon 10 over time. Importantly, if the levels seen in individuals 1 and 2 are taken

as examples of normal variation in the expression of *RBM4* and *PTBP1*, there is no significant difference in the levels seen in individual 3 that could otherwise explain the phenotype of individual 3.

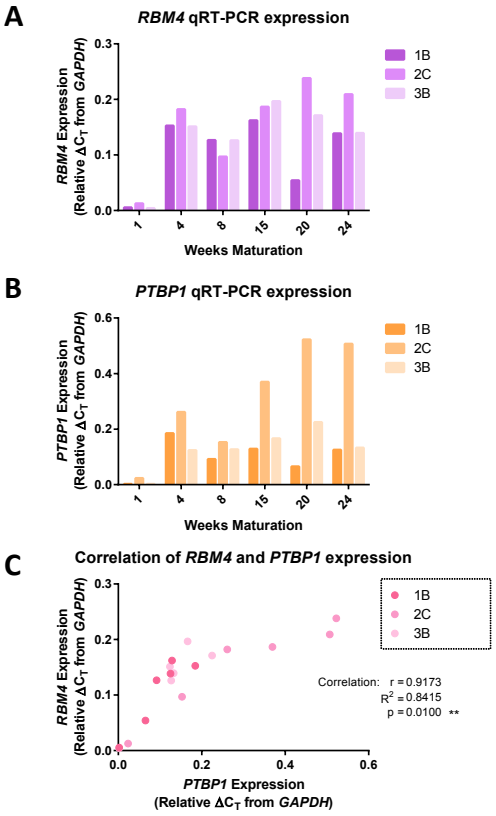

Figure 4.13: Splice factor expression analysis in a time course study of dopaminergic neuronal cultures matured up to six months.
(A-B) Quantitative RT-PCR expression for *RBM4* and *PTBP1* (PTB/hnRNP I) over the time course of maturation for dopaminergic neuronal cultures from week 1 (DIV27) to week 24 (DIV190). Both splice factors are significantly expressed at the RNA level from at least week 4 (DIV48) onwards but show no correlation with the rising inclusion of exon 10 (see Fig. 4.5F). No significant difference is observed for control 3. Bars represent mean of three technical values of n=1 cDNA sample, with each of the three individuals (one clone per individual) represented as a separate bar.
(C) Alternative representation of the data from graphs A-B to reveal correlation of the expression of *RBM4* and *PTBP1* transcripts across the time course; statistical results for Pearson correlation are presented on the graph.

4.3.6 Isolation of dopaminergic neurons from mixed neuronal culture by fluorescence-activated cell sorting

The above expression studies were performed on iPSC-derived dopaminergic neuronal cultures where dopamine neurons are not the only type of neuron or cell. While these data are highly valuable and informative, I undertook to augment these with cell-type specific data from dopaminergic neurons alone. A method for isolation of dopaminergic neurons from mixed cultures using fluorescence-activated cell sorting (FACS) coupled with an intracellular staining protocol was already developed in this laboratory by Mr P. Robertson. These techniques have been used previously to isolate dopaminergic neurons from the same kind of iPSC-derived cultures for analysis by RNA-seq (Sandor and Robertson et al., 2016, under review).

One additional use for this FACS protocol is to permit assessment of the development of co-cultures by retrieving only the desired cells afterwards. I have already shown that even after six months of maturation, iPSC-derived dopaminergic neuronal cultures still only generate approximately half the inclusion of *MAPT* exon 10 seen in post-mortem human midbrain and the required time to reach this maturation complicates their potential widespread use through high maintenance costs. I determined to investigate the potential of astrocyte co-culture to stimulate a more rapid maturation of the neurons. However, given that astrocytes express a small amount of tau (Papasozomenos and Binder 1987; Müller et al. 1997), the introduction of a relatively large proportion of astrocytes into the cultures would contaminate the signal from neurons if expression in the cultures were to be analysed without first separating the cells.

Initial attempts to isolate TH+ neurons from iPSC-derived dopaminergic neuronal cultures produced low numbers of TH+ cells stained as 'live' before fixation; most occasions retrieved fewer than $1x10^5$ cells when the initial cell plating was of $1.7x10^7$. In particular, a noticeable

problem was that large clumps of cells were difficult to dissociate, and the efforts to do so could have been damaging those that did dissociate sufficiently. Three alternative treatments for dissociating cells were tested in parallel and analysed by flow cytometry: the standard protocol with trypsin-EDTA (5 min) stopped with defined trypsin inhibitor and DNase I; TrypLE Express (10 min) or Accutase (10 min) stopped by dilution with PBS and DNase I. However, the two alternative treatments provided no improvement between conditions in terms of the percentage of cells stained as 'live' before fixation (trypsin-EDTA, 52.2% live; TrypLE, 49.6% live; Accutase, 46.0% live) so the standard protocol continued to be used.

iPSC-derived dopaminergic neuronal cultures with and without astrocyte co-culture were matured for 15 weeks and exhibited highly dense neuronal morphology (Fig. 4.14A). When examined at an earlier time point (DIV36), co-cultures of neurons and astrocytes exhibited some altered network morphology compared to the single cultures, demonstrated by greater fasciculation of processes with less overall density (Fig. 4.14B), but it is not clear what specific effect the astrocytes were having on the cultures and whether this was an advantage or disadvantage.

Cultures were dissociated, stained, analysed by initial examination on the cell sorter and then sorted. Three staining controls were used to set up initial gating (Fig. 4.15A): one without any staining and two with only the LIVE-DEAD viability stain, one of which was first fixed and permeabilised to make all cells appear as dead. For each sample to be sorted an immunoglobulin isotype control (IgG_{2a}) treated sample was used to determine the level of background antibody binding; both the IgG_{2a} and anti-TH stained plots are shown in Fig. 4.15B for three clones. TH-positive and TH-negative populations were collected for each sample.

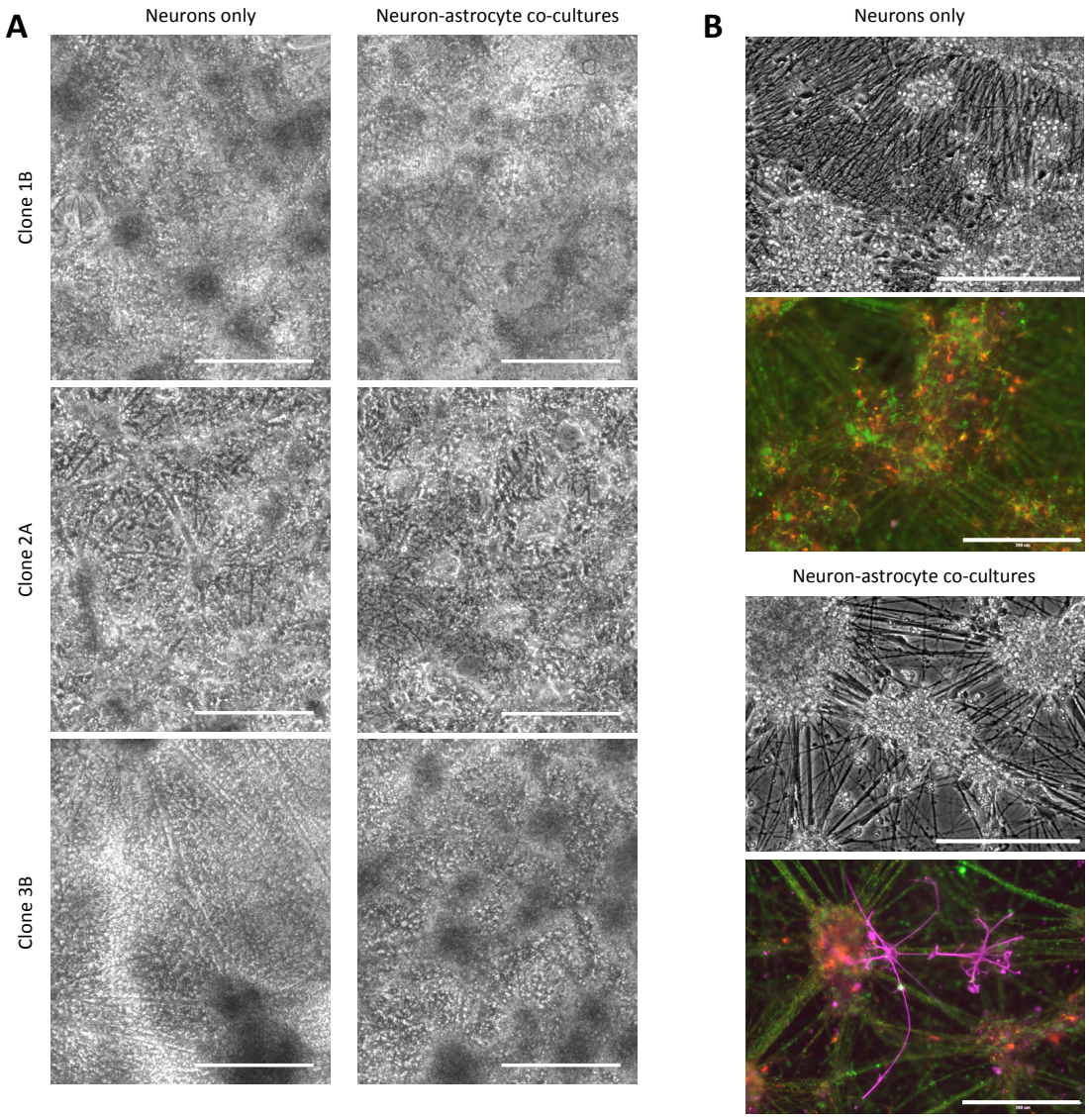

Figure 4.14: iPSC-derived dopaminergic neuronal cultures and co-cultures with astrocytes.
(A) Phase contrast images of iPSC-derived dopaminergic neuronal cultures matured for 15 weeks (DIV104) after re-plating, taken prior to harvesting for FACS. Due to the density of cultures, images were taken at low magnification to enable visualisation of large clumps of cells and the formations between them. Scale bars, 500 µm.
(B) Images from preliminary testing of co-culture of iPSC-derived dopamine neuronal cultures with rat primary cortical astrocytes. The same cell density of neurons was plated either onto a layer of astrocytes on Geltrex or onto Geltrex alone at DIV20 of the dopamine neuron differentiation protocol. Phase contrast images were taken at DIV36, followed by fixation and immunostaining for glial fibrillary acidic protein (magenta), beta-III tubulin (green) and tyrosine hydroxylase (red). Scale bars, 200 µm.

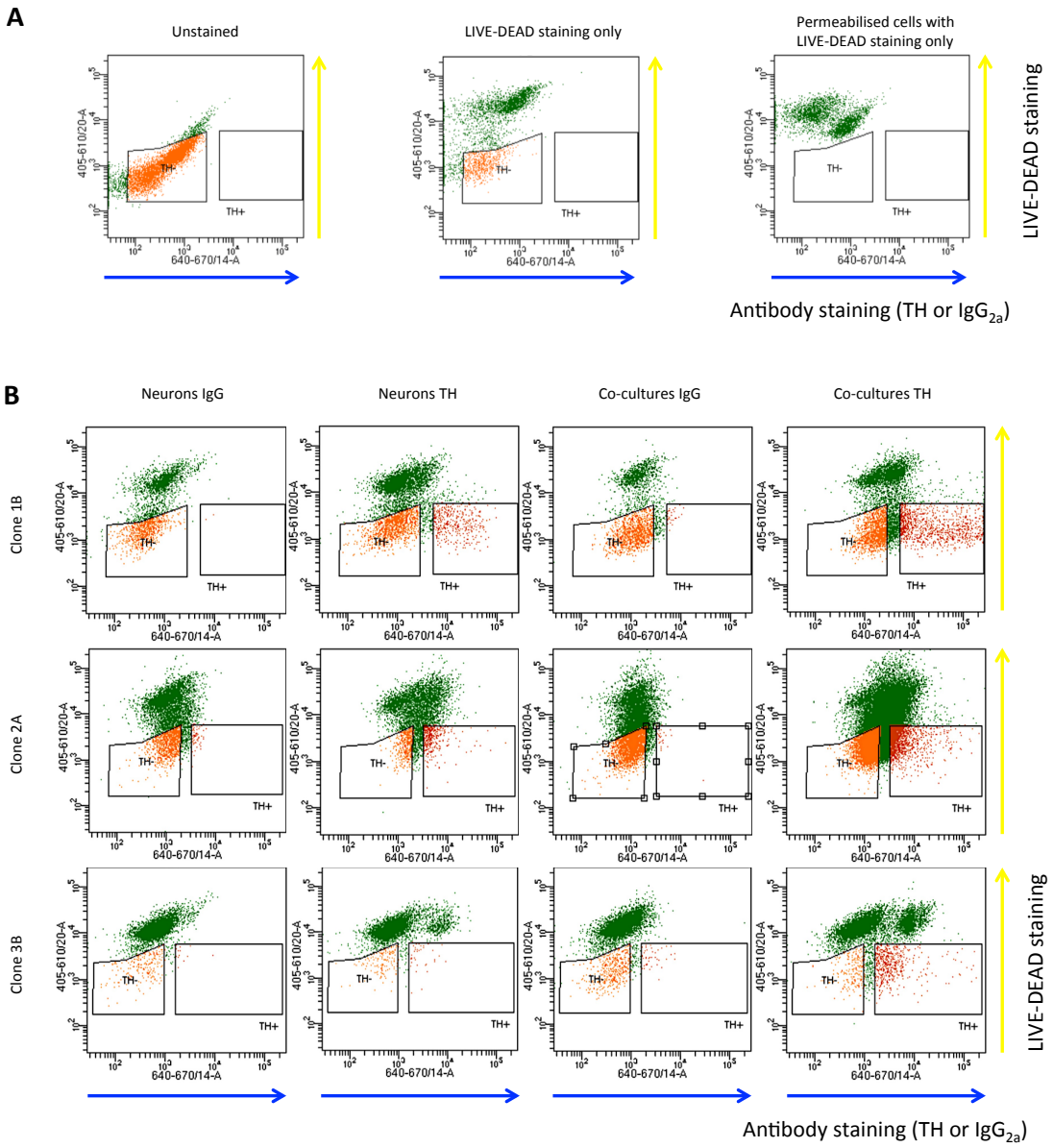

Figure 4.15: Scatter plots from flow cytometry of iPSC-derived dopaminergic neuronal cultures.

Scatter plots of cells analysed by flow cytometry immediately prior to sorting. Plots show logarithmic scale of LIVE-DEAD staining on the y-axis against logarithmic scale of Alexa-Fluor 635 secondary antibody staining coupled to primary antibody staining of tyrosine hydroxylase or immunoglobulin IgG_{2a} isotype staining control on the x-axis. Polygons on each plot mark the selected TH-negative (left) and TH-positive (right) populations to be collected.

(A) Scatter plots for controls to set the initial gating parameters: unstained cells; cells stained with LIVE-DEAD stain only; cells fixed and permeabilised before staining with LIVE-DEAD stain only, i.e. all staining as 'dead'.

(B) Scatter plots for samples to be sorted, arranged with the three clonal lines in successive rows, and the four conditions in successive columns: neuronal cultures with IgG_{2a} or TH staining; co-cultures with IgG_{2a} or TH staining. IgG_{2a} staining was used to establish the level of background from non-specific antibody binding, and forms an intermediate between the LIVE-DEAD only stained samples and the real TH stained samples.

Post-hoc analysis of the FACS plots by dividing into four quadrants determined the number of cells in each of the four categories (clockwise from top left): dead TH-, dead TH+, live TH+, live TH-. From this the overall percentages of TH+ cells and live cells were determined (Fig. 4.16A). Comparison between standard neuron-only cultures and neuron:astrocyte co-cultures showed a trend towards greater percentage of TH+ cells (Fig. 4.16B) and a significant increase in live cells in the co-culture samples (Fig. 4.16C).

A

	% TH+		% Live	
Clone	**Neurons**	**Co-cultures**	**Neurons**	**Co-cultures**
1B	19.07	29.91	41.55	57.02
2A	28.79	32.26	33.64	49.58
3B	10.12	31.32	5.05	12.03

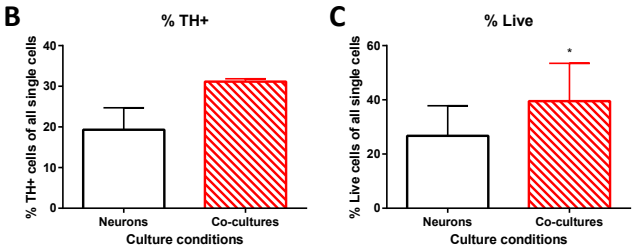

Figure 4.16: Cell percentages from flow sorting of iPSC-derived dopaminergic neuronal cultures.

Comparison of the percentage of single cells determined to be TH-positive or Live, in both standard neuronal cultures and neuron:astrocyte co-cultures.

(A) Table of percentages shown graphically in B and C.

(B) No significant difference between culture conditions for percentage of TH-positive cells as a proportion of all single cells, using paired two-tailed *t*-test (p=0.148, t=2.302, df=2, $mean_{neurons}$=19.33 ±5.39, $mean_{co\text{-}cultures}$=31.16 ±0.68). Mean ±SEM, n=3 clones.

(C) Asterisk denotes statistically significant difference between culture conditions for percentage of live cells as a proportion of all single cells, using paired two-tailed *t*-test (p=0.0481, t=4.395, df=2, $mean_{neurons}$=26.75 ±11.09, $mean_{co\text{-}cultures}$=39.54 ±13.92, effective pairing p=0.0167, r=0.9986). Mean ±SEM, n=3 clones.

4.3.7 Analysis of gene expression in flow sorted samples

In order to perform intracellular staining prior to FACS, samples require fixation before permeabilisation. Aldehyde fixation of cells forms cross-links between molecules throughout the cell; this includes cross-linking of RNA to the proteins that are bound with it, which hinders subsequent extraction of the RNA. A selection of RNA extraction methods were tested on fixed HEK293 cells to examine which releases the most RNA. All of these methods utilised proteinase K digestion to remove bound proteins. The first pair of methods employed proteinase K digestion for 15 or 60 minutes before using the QIAGEN RNeasy micro kit, as had been used in Sandor and Robertson et al. (2016, under review). The other pair of methods used the QIAGEN RNeasy FFPE kit, designed for use on fixed samples, either with the standard digestion protocol (15 min at 60°C then 15 min at 80°C) or an extended digestion protocol (60 min at 60°C only) described by Thomsen et al. (2016). When the standard RNeasy extraction protocol with buffer RLT was used without proteinase K there was only a negligible yield of RNA, but addition of a proteinase K digestion step of either length led to approximately 8-fold greater yield of RNA (Fig. 4.17A). Further still, use of the RNeasy FFPE kit released 7-fold more RNA than the two RLT/PK conditions (Fig. 4.17A). However, it was noted that the Bioanalyzer traces for samples generated by the RNeasy FFPE kit did show increased presence of small RNA fragments <100 nt compared to those generated from the RNeasy kit (Fig. 4.14B). The method of Thomsen et al. (2016) was chosen.

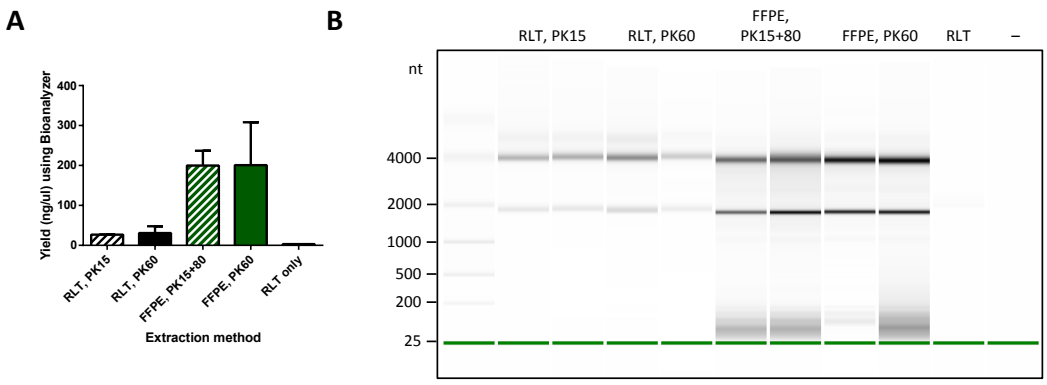

Figure 4.17: RNA yield and Bioanalyzer gel pseudo-images for RNA extracted from fixed HEK293 cells.

Analysis of RNA extracted from HEK293 cells after aldehyde fixation, using five different methods performed in duplicate, from left to right being: RNeasy micro kit with addition of proteinase K digestion for 15 min, 56ºC; RNeasy micro kit with addition of proteinase K digestion for 60 min, 56ºC; RNeasy FFPE kit with standard proteinase K digestion for 15 min, 56ºC then 15 min, 80ºC; Thomsen et al. (2016) modification of RNeasy FFPE kit with proteinase K digestion for 60 min, 56ºC only; unmodified RNeasy micro kit (single sample only).

(A) Graph of RNA yield, represented as concentration of a 12 µl sample. Concentration was determined by Bioanalyzer then multiplied by the dilution factor to achieve a concentration for undiluted RNA.

(B) Bioanalyzer gel pseudo-images. Scaling mode set to Global to enable comparison between quantity in lanes, which are loaded with equal dilutions of each sample. 18S and 28S ribosomal subunits appear as bands running at approximately 2000 and 4000 nt respectively.

The numbers of sorted cells obtained by FACS are shown in Table 4.1. Extraction of RNA from sorted cells produced a range of yields from 1.2 pg/cell to 11.3 pg/cell (Table 4.1). The yield and RIN were noticeably lower for samples from clone 3B, which had been delayed for sorting for 24 hours (Table 4.1, Fig. 4.18). However, while some degradation had occurred with all samples, they did not show a significant amount of small fragments (Fig. 4.18) like those that had been seen for the fixed HEK293 samples extracted by the same method (Fig. 4.17B, lanes 6-9). RNA yields from TH+ samples were 43% higher per cell than for TH- samples (Fig. 4.19A).

Table 4.1: Yields of cells and RNA from flow sorted iPSC-derived dopaminergic neuronal cultures.

Clone	Sample Name	Cell yield	RNA yield (ng/µl in 12 µl)	RNA yield (pg per cell)	RIN from Bioanalyzer
1B (6 wells)	Neurons TH+	37,414	23.5	7.5	9.1
	Neurons TH-	152,444	53.5	4.2	7.0
	Co-cultures TH+	67,182	50.1	8.9	9.3
	Co-cultures TH-	132,353	75.5	6.8	9.4
2A (4 wells)	Neurons TH+	12,761	9.5	8.9	8.0
	Neurons TH-	27,511	13.9	6.1	9.3
	Co-cultures TH+	4,579	4.3	11.3	8.9
	Co-cultures TH-	16,457	13.9	10.1	8.9
3B (6 wells)	Neurons TH+	6,096	1.7	3.3	7.2
	Neurons TH-	56,340	5.6	1.2	6.6
	Co-cultures TH+	25,738	9.0	4.2	6.8
	Co-cultures TH-	24,771	5.0	2.4	6.6

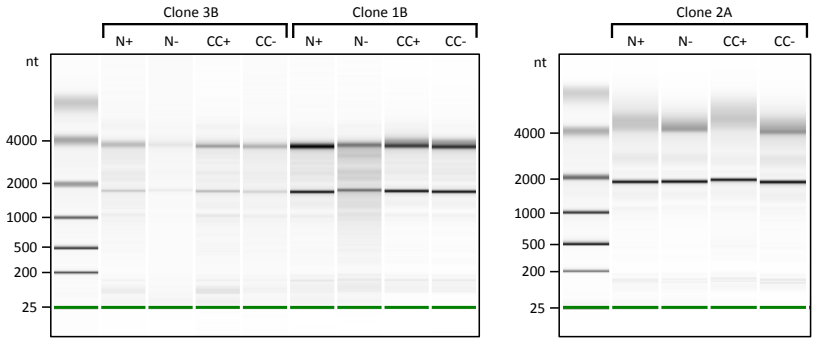

Figure 4.18: Bioanalyzer gel pseudo-images for flow sorted iPSC-derived dopaminergic neuronal cultures.
Scaling mode set to Individual because each sample was diluted differently according to the concentration of RNA determined by RiboGreen quantification. 18S and 28S ribosomal subunits appear as bands running at approximately 2000 and 4000 nt respectively.

cDNA was synthesised from all samples using the SeqPlex RNA Amplification kit (Sigma-Aldrich), which adds a universal primer sequence to cDNA during reverse transcription allowing unbiased amplification of all synthesised cDNA in successive PCR cycles. Additionally, some samples with sufficiently high yield were also converted to cDNA using the standard SuperScript VILO kit to permit verification.

qRT-PCR analysis of samples yielded unexpected and variable results (Fig. 4.19B-F). For exon 3+ transcripts, the inclusion of exon 3 was over 10-fold higher in some samples than for the bulk unsorted samples taken at the same time (Fig. 4.19B). Further, for the one clone that yielded sufficient cells and RNA to allow cDNA synthesis to be performed on the same samples with both the standard and amplification methods (Superscript VILO and SeqPlex) these values were not closely comparable (black dots). For exon 10+ transcripts the samples were also variable; however, the clone bearing the ΔCTT variant did show approximately equivalent exon 10 inclusion to its bulk unsorted sample, but was not the highest of the three clones like would have been expected (Fig. 4.19C). Allele-specific expression analysis of total *MAPT* transcripts was reasonably unvaried but showed no differences between samples (Fig. 4.19D). However, for exon 3+ transcripts – what should be the most consistent of all allele-specific phenotypes – the ratios were highly variable and were not around the expected mean of 0.5 (Fig. 4.19E). Finally, the allele-specific data for exon 10+ transcripts did not properly recapitulate the lower ratio for clone 3B with the ΔCTT variant (Fig. 4.19F). In summary, the quality of the data did not produce confidence in any of the results from the fixed sorted cells, whether the cDNA was amplified or not, and strongly suggests that RNA from fixed cells is unsuitable for these assays.

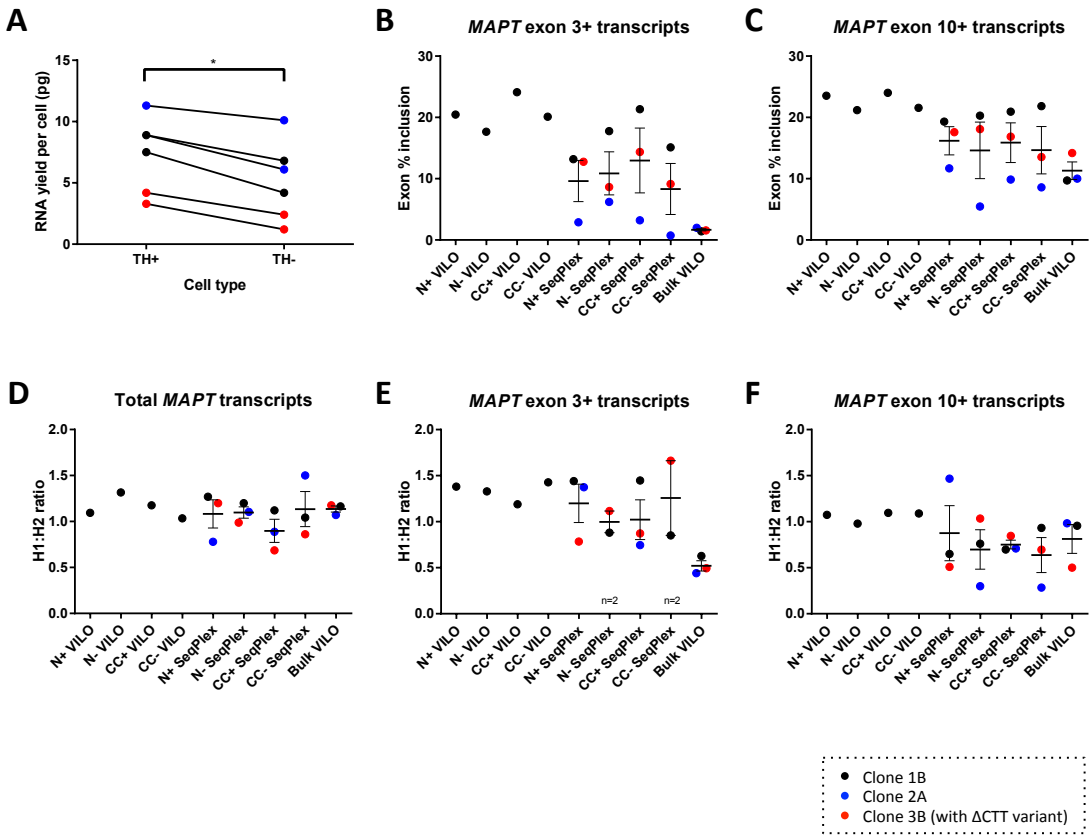

Figure 4.19: RNA yield and qRT-PCR data from flow sorted iPSC-derived dopaminergic neuronal cultures.

Legend at bottom right of figure.

(A) RNA yield per cell, as also shown in Table 4.2, showing a statistically significant difference between the RNA yield from sorted TH+ neurons vs sorted TH- cells. Ratio paired *t*-test: p=0.0126, t=3.799, df=5, mean_{TH+}=7.35 ±1.25, mean_{TH-}=5.13 ±1.32 (mean ±SEM), effectiveness of pairing p=0.0002, r=0.9853.

(B-F) *MAPT* qRT-PCR expression assay results. RNA from flow sorted fixed samples at 15 weeks maturity was converted to cDNA either using SuperScript VILO (no amplification) or by SeqPlex RNA Amplification kit. cDNA made from bulk unsorted unfixed samples using SuperScript VILO is shown as a comparison. Lines indicate mean ±SEM; each point represents the mean of technical qRT-PCR replicates. (B-C) Standard *MAPT* expression assays showing exon inclusion comparative to total *MAPT* transcripts. (D-F) Allele-specific expression assays distinguishing transcripts of H1 and H2 allelic origin, presented as H1:H2 ratio, i.e. values >1 show higher H1 expression. For exon 3+ and exon 10+ transcripts (E-F), the H1:H2 ratio is normalised to the H1:H2 ratio of total *MAPT* transcripts per sample. (E) PCRs for clone 2A N- SeqPlex and CC- SeqPlex did not reach threshold so no blue points are shown.

4.4 Discussion

In this chapter I have described the generation of human iPSC-derived dopaminergic neuronal cultures expressing mature isoforms of tau and the analysis of general and haplotype-specific expression of *MAPT* within them. I have also presented efforts to isolate dopaminergic neurons from mixed cultures for specific expression analysis in this key cell type.

4.4.1 Utility and maturity of iPSC-derived neuronal cultures

This is the first study to specifically use iPSC models to study *MAPT* haplotypes. iPSC models are particularly invaluable to the study of human neurodegenerative diseases as they offer the ability to generate cultures of human neurons that could not be obtained otherwise, and further still, each cell will bear the genotype of the donor. This also allows a wider range of genetic diversity to be observed within experiments than with the use of cancer cell lines (Agholme et al. 2010) or inbred animal lines, as the background of each individual is unique. Given the sizes of the chromosomal inversion around *MAPT* (970 kb) and the region of extended linkage disequilibrium (1.8 Mb), there is scope for significant diversity between individuals of the same haplotype, and indeed many sub-haplotypes have been identified (Oliveira et al. 2004; Pastor et al. 2004; Skipper et al. 2004; Fung, Xiromerisiou, et al. 2006; Tobin et al. 2008; Vandrovcova et al. 2009). Additionally, one of the three individuals with H1/H2 genotype selected for use in this study contained a novel variant that impacted on *MAPT* expression.

Independent iPSC clones derived from the same individual show variability beyond the genetic diversity seen between individuals and this is particularly evident when integrating viruses are used in the initial generation of those clones. In this study, six of the eight clones

were generated by retroviral delivery of the Yamanaka factors, with the remaining two clones (3B and 3C) generated by the cytoplasmic CytoTune-iPS system based on Sendai virus that is subsequently eliminated following reprogramming. Clones differed in their ability to differentiate to dopaminergic neurons, evident in the cell count data (Fig. 4.2D), and showed some differences in overall appearance of the cultures (Fig. 4.3) including whether or not they spontaneously generated astrocytes (Fig. 4.4). However, the choice to use multiple clones from a small number of individuals allowed both inter- and intra-individual clonal variation to be accounted for, and ultimately permitted the discovery of the novel variant through having n=3 clones showing the same phenotypes.

One of the greatest achievements of this study is to show production of all six isoforms of mature tau for the first time in iPSC-derived dopaminergic neuronal cultures, after maturation of up to six months following initial patterning and differentiation. This was shown first at the transcript level where the inclusion of the alternative exons 3 and 10 increases steadily across a time course of six months maturation (Fig. 4.6) and further by specific detection of all six isoforms at the protein level (Figs. 4.7 and 4.8).

Other groups have generated different types of stem cell-derived neurons also expressing mature tau isoforms. Iovino et al. (2010) reported the use of human embryonic stem cells (hESCs) and foetal neural precursors to generate forebrain neuronal cultures. These cultures produced all six isoforms of tau protein by DIV56, notably from the already partially differentiated foetal neuronal precursors, although the evidence for expression of the largest isoform (2N4R) was not clear. Further work from the same authors suggested that iPSC-derived cortical neurons express all six tau isoforms by DIV150, particularly from 4R-promoting mutant N279K lines, although again the data were not clear for every individual isoform (Iovino et al. 2015). In contrast, another group reported that only foetal tau (0N3R) is expressed in iPSC-derived cortical cultures by DIV100 unless bearing a

mutation affecting exon 10 inclusion (10+16) and that it takes a year of maturation for iPSC-derived cortical cultures to visibly express all six isoforms (Sposito et al. 2015). In light of these studies, the ability of iPSC-derived dopaminergic neuronal cultures to express mature isoforms so relatively quickly is either inherently due to the difference in cell type, or else is a product of the factors delivered during differentiation and maturation. It is interesting that the compound DAPT was used for 96 hours "to enhance neuronal maturation" in the experiments of Iovino et al. (2015), and is used continually from DIV11 in the dopaminergic neuronal protocol used here but never in the experiments of Sposito et al. (2015). Application of DAPT halts the self-renewal of hESC-derived neural stem cells, promoting differentiation and improving the electrophysiological maturity of neurons that are produced (Borghese et al. 2010). However, as an inhibitor of γ-secretase, continuous use of DAPT would have to be precluded from any experiments requiring amyloid-beta.

A strength of the current study is the use of quantitative RT-PCR to assess *MAPT* expression. Assessment of the ratio of 3R to 4R *MAPT* transcripts is frequently performed by standard end-point RT-PCR followed by quantitation of the two bands separated on a gel (Boutajangout et al. 2004; Iovino et al. 2010); however, this method is not wholly quantitative and generates two sizes of PCR products from the same primers, which biases amplification of the smaller product. Another publication utilised qRT-PCR TaqMan assays for exon 10- vs. exon 10+ transcripts to look at only the 3R:4R ratio (Iovino et al. 2015) and a further used Affymetrix exon array datasets, carefully curated to remove probe sets that are affected by *MAPT* haplotype, to enable a high-volume study to reveal regional differences in isoform expression that correlated with *MAPT* genotype (Trabzuni et al. 2012). The validated quantitative RT-PCR TaqMan assays used in this chapter enabled determine of exon inclusion by comparison of exon-specific and total *MAPT* quantitation. In particular, precise determination of exon 3 inclusion, rarely examined in detail, revealed that cultures matured for six months express approximately the levels found in adult midbrain (Fig. 4.6C, E).

Further, in post-mortem human midbrain, transcripts containing exon 10 constituted an average of 34% of all *MAPT* transcripts (Fig. 4.6C), rather than nearer to 50%. It is frequently stated that normal human brain expresses approximately equal quantities of 3R and 4R tau; however, while many Western blot data generally agree with this statement (Goedert and Jakes 1990; Hong et al. 1998; Trabzuni et al. 2012), some published images appear to show greater expression of 3R isoforms than 4R isoforms (Boutajangout et al. 2004; Iovino et al. 2010). One analysis of *MAPT* isoform expression by qRT-PCR in post-mortem frontal cortex from control individuals found an average 4R:3R ratio of 0.48, equivalent to 32.4% exon 10 inclusion, in contrast to FTLD and PSP brains that had ratios of 1.32 and 1.12 (equivalent to 56.9% and 52.8% exon 10 inclusion) (Ingelsson et al. 2007). Certainly there is variation in isoform expression in different brain regions (Luk et al. 2009; Trabzuni et al. 2012; Majounie et al. 2013), and the midbrain data here may reflect that.

4.4.2 Haplotype-specific analysis of gene expression

High inclusion of alternatively spliced exons of *MAPT* in mature iPSC-derived cultures permitted reliable quantitation of allele-specific expression in a set of qRT-PCR assays developed in this laboratory. Allele-specific expression analysis of heterozygotes has the significant advantage of being internally controlled and permits small differences in expression to be detected; with the H2 haplotype being such a common variant, many heterozygous H1/H2 samples were available for use. The TaqMan-based allele-specific assays used here were established according to the description of Chen et al. (2008) who developed expression assays for individuals with heterozygous variants in *BRCA1* and *BRCA2*. A less-developed form of the SNP9ii assay had been used previously to show greater 4R tau expression in carriers of the H1c sub-haplotype (Myers et al. 2007a), and the probe sequences from that report were used in this study. Previous work in our laboratory had

employed the Sequenom platform to quantify single base extensions of PCR products by mass spectrometry (Caffrey et al. 2006; Caffrey et al. 2008). Although other forms of allele-specific expression assay also exist (Buckland 2004), including notably the use of SNaPshot technology to quantify single base extension (Bray et al. 2004; Bray et al. 2003a; Bray et al. 2003b), the ability to perform relatively inexpensive assays on available equipment on a short timescale made the qRT-PCR form of allelic assay ideal. A final alternative method has been employed by Majounie and colleagues, where SNP specificity was achieved in standard qRT-PCR using primers containing a locked nucleic acid base at the position of the SNP (Majounie et al. 2013); however, the present method offers the advantage of unbiased amplification of all transcripts, with only the probe binding as a means of distinguishing allelic origin.

(i) Exon 3+ transcripts

The new assays showed a robust haplotype-specific difference in the inclusion of exon 3, with H2 expressing two-fold more than H1 in iPSC-derived cultures from all individuals and also post-mortem human midbrain (Fig. 4.9D). This is in complete agreement with previous findings in the human neuronal cell line SK-N-F1, post-mortem frontal cortex and globus pallidus (Caffrey et al. 2008) as well as from comparison of exon 3 expression in several brain regions in H1/H1, H1/H2 and H2/H2 individuals (Trabzuni et al. 2012).

With the strong association of increased exon 3 expression with the protective H2 allele it is possible that 2N tau is particularly advantageous to neurons. The inclusion of exon 3 increases the length of the projection domain from 168 to 197 amino acids. This could be expected to increase the spacing between microtubules, following the pattern seen with three microtubule-associated proteins possessing different sized projection domains (Chen et al. 1992). Microtubule spacing has been proposed to mitigate the efficiency of organelle

transport (Marx et al. 2000; Shahpasand et al. 2012), notably by kinesin-1 (Conway et al. 2014). It is also particularly interesting that, unlike most of the projection domain, exon 3 contains a portion that is basic, which may be involved with charge-charge interactions between tau projection domains on adjacent microtubules (Chung et al. 2016). 2N tau isoforms showed reduced kinetics of aggregation than 1N tau isoforms (Zhong et al. 2012). The presence of both N-terminal inserts (2N4R) also appeared to inhibit acetylation of tau residue K163 by CREB-binding protein compared to 0N4R tau (Cohen et al. 2016); however, the impact of acetylation of this residue is yet to be explored. Finally, it has been proposed that the segment encoded by exon 3 may be involved in signal transduction (Trabzuni et al. 2012) following interaction of the projection domain with either the plasma membrane (Brandt et al. 1995; Pooler and Hanger 2010; Pooler et al. 2012) or src-family kinases such as Fyn (Ittner et al. 2010); in light of this, apolipoprotein A1 (ApoA1) was shown to interact specifically with the 2N isoform of tau in adult mouse brain by co-immunoprecipitation so 2N tau may impact on the regulation of lipid metabolism (Liu et al. 2016).

(ii) Total MAPT *transcripts*

iPSC-derived cultures showed a shifted H1:H2 ratio representing 1.2-fold increased expression of total *MAPT* transcripts from the H1 allele, but no allelic effect on the inclusion of exon 10 (Fig. 4.9C, E). In contrast, H1:H2 ratios in post-mortem human midbrain samples showed no difference from 1 for total *MAPT* transcripts but a ratio of 1.2 for exon 10+ transcripts. The midbrain samples were in concert with other cell culture and post-mortem samples from our laboratory analysed using the Sequenom platform (Caffrey et al. 2006); however, it should be noted that the cell culture samples in that study did show a small but significant increase in expression of total *MAPT* that wasn't seen in the post-mortem

samples and so was not highlighted. It is unknown to what extent the general conditions of cell culture can impact on haplotype-specific regulation of *MAPT* expression.

On the question of whether the H1 haplotype increases total *MAPT* expression there is evidence on both sides, although mostly suggesting that there is no difference. Using *MAPT* promoter-reporter studies, one group suggested that the H1 allele expresses more total *MAPT* (Kwok et al. 2004), while others showed only a non-significant trend towards increased expression unless additional SNPs were changed (Myers et al. 2007a). Quantitative trait loci analyses comparing gene expression with genotype initially claimed to support increased total expression from the H1 locus (IPDGC et al. 2011) but after the removal of expression probes that included H1:H2 SNPs the association was claimed to be no longer significant (Trabzuni et al. 2012; Latourelle et al. 2012). Further, SNaPshot analysis in three brain regions by another group showed no difference in total *MAPT* expression (Hayesmoore et al. 2009). However, a study in cerebellum and temporal cortex of Alzheimer's patients showed significant association between the H2 haplotype and decreased expression of total *MAPT* (Allen et al. 2014), and the association of the H2/H2 genotype with reduced total *MAPT* was shown in dorsolateral pre-frontal cortex in a new RNA-seq study (Valenca et al. 2016). Given the fresh evidence from the current study in favour of increased total expression from H1 in at least some contexts, it is hard to neatly reconcile the two different possibilities of total expression vs. isoform-specific expression alone being at the root of disease risk. However, one possibility is the age of the samples; Hayesmoore et al (2009) noted a negative correlation between H1:H2 ratio at the rs1052553 SNP in *MAPT* exon 7 and age, so that with increased age comes decreased H1:H2 ratio. Despite their expression of mature isoforms of tau, iPSC-derived neuronal cultures may represent a biologically much younger sample than post-mortem adult brains.

(iii) Exon 10+ transcripts

There is good support for the hypothesis that the H1 haplotype increases the inclusion of exon 10, seen by allele-specific differences in neuroblastoma cells (Caffrey et al. 2006), and brain regions in control individuals: frontal cortex and globus pallidus (Caffrey et al. 2006); temporal cortex and cerebellum (Majounie et al. 2013). Additionally a new RNA-seq study showed that H2/H2 individuals had lower expression of 1N/4R transcripts (Valenca et al. 2016), which are the most common of the three 4R isoforms in human brain (Hong et al. 1998). Oddly, one study that also used the Myers probes to perform allele-specific quantification only found an increased H1:H2 ratio for exon 10+ transcripts in samples from PD patients and not controls (Williams-Gray et al. 2009). Greater allele-specific differences have been shown with measurements of the effect of the H1c haplotype vs. non-H1c haplotypes (Myers et al. 2007a; Majounie et al. 2013). The increased H1 allelic expression in post-mortem midbrain of exon 10+ transcripts encoding 4R tau, even if not matched in the iPSC-derived cultures, is in line with the hypothesis that increased 4R tau is associated with neurodegenerative disease. This is notably the case with the 4R tauopathies (PSP, CBD, some cases of FTDP-17), some cases of which are due to mutations around exon 10 of *MAPT* that lead to increased inclusion of exon 10 (Hutton et al. 1998; Hasegawa et al. 1999), while other mutations affect the likelihood of tau to detach from microtubules and/or form aggregates (Grover et al. 2003).

The discussion of the effect of 4R tau is normally conducted in the context of these tauopathies, where aggregated filaments of 4R tau becomes incorporated into a range of deposits such as neurofibrillary tangles (see Table 1.3). However, given the general lack of aggregated tau in PD, other roles of 4R tau would be more likely candidates to mediate the specific disease association.

The presence of the additional repeat in 4R tau strengthens binding to microtubules (Gustke et al. 1994), and the spacer (KVQIINKK) and repeat encoded by exon 10 appear to be more capable than those encoded by exon 12 at microtubule binding and nucleation (Goode and Feinstein 1994; Gustke et al. 1994; Mukrasch et al. 2007). Further, evidence is emerging for different roles of 3R and 4R tau in the regulation of microtubule dynamics, although the story is not clear. 4R tau not only stimulates the growth of microtubules more rapidly than does 3R tau (Panda et al. 2003), which at low concentrations actually inhibits growth (Levy et al. 2005), but 4R tau is also better at promoting a 'turbo boost' to switch microtubules into a faster grade of assembly (Levy et al. 2005). However, 4R tau increased stability of microtubules, i.e. reduced the rate of shortening, both near steady state and when microtubules were diluted below the critical concentration for polymerisation, whereas 3R tau had little effect (Panda et al. 2003). Additional possible roles for 4R tau in affecting axonal transport are discussed in chapter 5.

It is likely that there is a healthy balance in the amount of 4R vs. 3R tau, and specifically it has been proposed that there is a window for healthy microtubule dynamics, outside of which can be pathogenic to neurons (Panda et al. 2003). It can be expected that the differences are subtle and cumulative with age to only manifest as disease symptoms in old age. A final possibility to address is that 4R tau is capable of auto-acetylation at position K280 within the repeat encoded by exon 10; this acetylation increases the propensity to self-generate tau fragments in a process catalysed by internal cysteine residues, one of which also lies within the exon 10 sequence (Cohen et al. 2016). However, more firm evidence of their production in human brain is required before a role is ascribed to these newly discovered tau fragments.

4.4.3 Effect of the ΔCTT novel intronic variant

Through the use of qRT-PCR and Western blotting I showed that clones from individual 3 expressed greater levels of 4R tau and had reduced H1:H2 expression ratios for exon 10+ transcripts. The discovery of a novel ΔCTT variant in *MAPT* intron 10 of the H2 allele within a sequence that had been previously identified to play a role in exon 10 splicing (Kar et al. 2006) makes it highly likely that this variant is functional and is responsible for the observed changes.

In silico analysis from *SpliceAid 2* showed that two binding sites were predicted to be disrupted in the variant allele compared to the wild type allele: RBM4 and PTBP1 (PTB/hnRNP I). Both have already been identified to have roles in the splicing of exon 10. Such a role for RBM4 was reported by Kar et al. (2006) after they performed a screen with a human brain cDNA library using a splicing reporter construct that would only express GFP when *MAPT* exon 10 was included to make the downstream GFP sequence in frame. Exon 10 inclusion was increased with overexpression of *RBM4* and reduced with *RBM4*-targeting shRNA treatment, while overexpression of RBM4 lacking the RNA recognition domain showed no effect (Kar et al. 2006). Further, RBM4, either as extract from cells overexpressing it or as recombinant protein, bound to RNA containing the putative binding site downstream of exon 10, but the binding was disrupted either by competitor RNA or by mutating all pyrimidines to purines in the putative binding site (UCCUUCUUG), though a small amount of binding persisted even with the mutant binding site (Kar et al. 2006). RBM4 performs a parallel role of promoting exon inclusion for the α-tropomyosin gene, but is antagonised by the binding of PTBP1 as both share an overlapping binding site (Lin and Tarn 2005) that is similar to the one found in *MAPT* (Kar et al. 2006). As the novel ΔCTT variant forms part of the sequence that was mutated in the study of Kar et al. (2006), this is strong evidence that ΔCTT indeed disrupts a common binding site for RBM4 and PTBP1.

As the ΔCTT variant is present on the H2 allele and individual 3 shows H1:H2 expression ratios of approximately 0.5 for exon 10+ transcripts, this means that the variant results in increased expression of exon 10 from the H2 variant allele than from the H2 wild type allele borne by individuals 1 and 2. The overall shift towards more splicing is feasible either by more enhancer action or less suppressor action. Given that the variant is predicted to reduce binding, I predict that a partial loss of binding of RBM4 and near abrogation of binding of PTBP1 would swing the balance more in the favour of inclusion of exon 10 in transcripts originating from the ΔCTT H2 allele. Alternatively the complete loss of binding of both factors could leave the balance of remaining factors shifted more towards that of promoting exon 10 inclusion. Further work to investigate the binding of RBM4 and PTBP1 could include RNA pull-down assays with wild type and mutant RNA probes along with either cell extracts or recombinant RBM4/PTBP1 to confirm the effect of the ΔCTT variant on splice factor binding.

As the ΔCTT variant increases the inclusion of exon 10, only time will tell if individual 3 is unfortunate enough to develop a 4R tauopathy such as FTDP-17. Performing a thought experiment on my existing data, if ΔCTT doubles exon 10 expression from the H2 allele, then in the heterozygous state exon 10 expression would be increased by 50%; using the midbrain data point of 34% exon 10 inclusion, a ΔCTT heterozygote could be expected to have a midbrain exon 10 inclusion that is 50% higher, i.e. 51%, and a 4R:3R ratio of 1.04. This is just below the published mean 4R:3R ratios for sets of FTLD and PSP samples, within the range of variation shown for cases (Ingelsson et al. 2007).

4.4.4 Cell-type specific analysis with sorted populations

In order to truly understand the nature of *MAPT* expression in dopamine neurons I wanted a way of studying this type of neuron as a pure population. To select an individual population by FACS, the ideal situation is to have that population express a fluorescent protein so that no antibody staining is required. This has been possible with transgenic animals (Hedlund et al. 2008; Roessler et al. 2014; Iacovitti et al. 2014) but has been more difficult with human cell culture. With the unsuitability of the dopaminergic reporter from Chapter 3, an alternative approach was required to select dopaminergic neurons. This was first pursued in my laboratory by Mr P. Robertson, who developed the FACS method with intracellular TH staining utilised here. One previous attempt of his was the use of a fluorescent false neurotransmitter as a dopamine analogue that would be taken up specifically by cells expressing the dopamine transporter (Rodriguez et al. 2013); however, those experiments did not produce satisfactory and cell-specific results suitable for sorting of the cells by FACS. Using his new method, iPSC-derived dopaminergic neuronal cultures from three control individuals and three individuals bearing *LRRK2* G2019S mutation were sorted and the extracted RNA used for RNA-seq (Sandor and Robertson et al. 2016, under review). Using the method he obtained a significant enrichment of TH expression by qRT-PCR (>8-fold) between unsorted and sorted populations, showing that the method was successful at selecting dopamine neurons.

Other groups have used FACS with extracellular staining protocols to enrich for dopaminergic neuronal precursors before the final plating, particularly those desiring purer populations for transplantation. The first published study performing this on human cells used the glycoprotein neural cell adhesion molecule (NCAM) to enrich for neurons from human iPSC-derived dopaminergic neuronal cultures before transplantation into rats (Hargus et al. 2010). However, as this is not a specific dopaminergic marker this would not

have been sufficient for use in this experiment, although it could have been used to select against astrocytes from co-cultures. A more successful approach likely requires the use of arrays of several markers in concert, none of which is cell-type specific on its own but each of which is highly expressed and so confers specificity in combination. This was apparently achieved with human cells in a protocol divided into two stages of FACS: the first at day 11 of the Kriks protocol to select for midbrain dopaminergic progenitors with NCAM+/CD133+ gating and subsequently at day 32 to select for midbrain dopaminergic neurons with gating for NCAM+/CD24+/CD15-/CD184- (Woodard et al. 2014); however, these are not recognised markers for dopaminergic neurons and confirmation by other groups is still awaited. For rodent cells, midbrain dopaminergic progenitors have been selected from mouse ESC-derived differentiations using Otx2 and Corin (Chung et al. 2011), and from rat midbrain using Alcam, Chl1, Gfra1 and Igsf8 (Bye et al. 2015).

In this chapter I used FACS to separate dopaminergic neurons from neuron:astrocyte co-cultures with the aim to investigate the effect of the astrocytes on neuronal expression of *MAPT*. The use of neuron:astrocyte co-cultures to increase maturity of cultured neurons has been demonstrated in human iPSC-derived cortical neuronal cultures, in which the expression of mature neuronal markers is increased when cultured with astrocytes (Muratore et al. 2014). Even without intentional co-culture, astrocytes can be generated in significant frequency during maturation of iPSC-derived cortical neuronal cultures (Muratore et al. 2014), although evidence from the present study suggests that iPSC-derived dopaminergic neuronal cultures only have low level spontaneous generation of astrocytes.

The one meaningful result that was obtained in the present study using FACS was that co-culture with astrocytes enabled a greater proportion of the cells to remain alive through the first portion of the dissociation and staining protocol. A few possibilities exist to explain this. It could represent a favourable effect of the astrocytes on the health of the cultures so

that there were either fewer dead cells already or that the cells were more robust and so less susceptible to damage through the protocol. Alternatively, the cultures could have become less dense early in the co-culture protocol, such as (i) through astrocyte-derived stimulation to form an altered network morphology, (ii) by an initial toxic effect of the astrocytes on the progenitors when they were first introduced in co-culture, or (iii) that the astrocytes permitted the pruning of some of the dead cells after mitomycin C treatment rather than those cells remaining adhered within clumps due to tangles of DNA. If the cultures were less dense, as observed at DIV36, it would make dissociation easier, resulting in fewer cells becoming mechanically damaged.

An alternative method for separation of neuron:astrocyte co-cultures has been described using application of a jet of ice cold PBS (Goudriaan et al. 2014), which would be worth attempting in future to enable separation of the two populations without fixation, even if only to have a bulk neuronal sample free of astrocytes instead of fully-purified dopaminergic neurons; this would then be comparable to the single culture samples used throughout the rest of the chapter. Another approach has been to grow the neurons on a separate surface suspended above the astrocytes but sharing medium (Jones et al. 2012); however, this only allows the sharing of secreted factors and not any direct cell-cell interactions.

Finally, the results from cDNA analysis of the fixed sorted samples were not internally reliable and made it difficult to form any firm conclusions. The qRT-PCR results deviated from the few expectations that were set, namely that at least one group (TH+ or TH-) would approximate that of the unfixed bulk samples, particularly in terms of the strong allele-specific ratio phenotypes for exon 3+ transcripts for all samples and for exon 10+ transcripts for clone 3B. Instead, the exon inclusions were considerably inflated, many of the ratios for exon 3+ transcripts were in favour of more expression from H1, and clone 3B did not segregate from the other clones for exon 10+ transcripts. As the deviations were seen both

from the cDNA made using SuperScript VILO and from the amplified cDNA kit, this suggests that the problem was with the initial RNA quality and not just due to stochastic levels with the low amounts of starting RNA in each amplification reaction. RNA from fixed cells is more likely to be suitable for downstream analysis by RNA-seq as this requires pre-fragmentation and performs reads on all fragments without the need for specific sequences or extended lengths. However, other groups have claimed that the RNA extracted from fixed cells after FACS is of sufficient quality for qRT-PCR without significant bias (Hrvatin et al. 2014; Thomsen et al. 2016). It is hoped that the generation of a lentiviral-based fluorescent dopaminergic reporter using the human *PITX3* promoter will allow identification of live dopaminergic neurons that can be reliably isolated by FACS without fixation or extended staining protocols, and that this will enable detailed cell type-specific expression studies using qRT-PCR and Western blotting to confirm the findings from bulk cultures containing dopaminergic neurons.

Chapter 5: Axonal Transport in iPSC-derived dopaminergic neuronal cultures with knockdown of *MAPT*

5.1 Introduction

The *MAPT* H2 allele is associated with a protective effect from Parkinson's disease. In chapter 4 I outlined how the presence of the H2 haplotype could result in lower amounts of neuronal 4R tau compared to the H1 allele through lower expression of total *MAPT* transcripts or lower inclusion of exon 10. However, it is unclear what the impacts of such differences are on neuronal functionality, and in particular what cellular function is performed by 4R tau isoforms. No studies have investigated the role of tau and its isoforms in dopaminergic neurons in order to probe the features underlying genetic risk for Parkinson's disease.

One way to interrogate the function or otherwise pathogenic effect of a protein of interest is to perturb the cellular levels of that protein through augmentation or depletion. Tau, as a microtubule-associated protein, binds to microtubules and uses its three or four microtubule-binding repeats to contribute to microtubule assembly and stability (Fellous et al. 1977; Cleveland et al. 1977; Gustke et al. 1994; Panda et al. 2003). Delivery of surplus tau protein or its specific isoforms has shown that excess tau can hinder microtubule-related processes including kinesin-mediated transport, observed in CHO cell culture (Ebneth et al. 1998; Trinczek et al. 1999), differentiated N2a neuroblastoma neuron-like cells (Ebneth et al. 1998; Dubey et al. 2008) and neurons (Mandelkow et al. 2004; Zhang et al. 2005a), particularly when 4R tau isoforms are overexpressed (Stoothoff et al. 2009). However, overexpression studies, while informative about an induced pathogenic state, do not necessarily reveal the normal cellular role. Other studies have adopted an approach of tau

depletion, either by utilising tau knockout animals to investigate the effect in neurons that have never expressed tau (Dawson et al. 2001; Yuan et al. 2008; Vossel et al. 2010; Vossel et al. 2015) or by employing a knockdown methodology to reduce but not completely abrogate endogenous tau expression (Sapir et al. 2012; DeVos et al. 2013; Vossel et al. 2015). However, none of these studies has applied knockdown to cultures containing dopaminergic neurons to relate tau function to the key cell type of PD.

Virtually all previous studies into the cellular functions of the isoforms of tau have been limited to the selective overexpression of particular isoforms *in vivo* or delivery of recombinant isoforms *in vitro*. Only two studies have performed selective knockdown of mammalian tau isoforms with phenotypic analysis: one used antisense oligonucleotides to reduce 4R tau, which destabilised microtubules in non-neuronal pancreatic cells (Kalbfuss et al. 2001) while another study made mice lacking *Mapt* exon 10, which displayed a mild effect on sensorimotor functionality when adult mice expressed only 3R tau (Gumucio et al. 2013).

Altered expression of 4R tau isoforms is already proven to have a pathogenic effect as evidenced by some cases of frontotemporal dementia and parkinsonism linked to chromosome 17 (FTDP-17), in which mutations in splice sites of *MAPT* are sufficient to cause disease by significantly altering the inclusion of *MAPT* exon 10 (Hutton et al. 1998; Spillantini et al. 1998a; Hasegawa et al. 1999). The magnitude of the effect of *MAPT* exon 10 splice-site mutations in FTDP-17 was first reported as a 2-fold or greater increase in exon 10 inclusion (Hutton et al. 1998). The allele-specific data presented in chapter 4 revealed that common variation at the *MAPT* locus associated with PD causes a smaller increase in expression of 4R tau transcripts from the H1 allele of approximately 20%. It is therefore expected that the physiological effects of increased expression from the H1 allele will be less pronounced than those seen due to FTDP-17 *MAPT* splicing mutations and hence that the H1 allele

contributes to disease susceptibility rather than directly causing disease. Additionally, as a tauopathy, FTDP-17 is characterised by aggregation of tau protein, and cases with exon 10 splicing mutations show a predominance of 4R tau within insoluble deposits (Iovino et al. 2014). The general lack of insoluble tau pathology in PD suggests that tau contributes to PD in other ways than through aggregation. More work is needed to understand the role of tau isoforms outside of the formation of aggregates and through examination in a more physiological setting than with protein overexpression.

Very little is understood about the cellular function of 2N tau isoforms, but as the projection domain is involved in microtubule spacing (Chen et al. 1992) there is scope for a role for 2N tau in axonal transport if it reduces the likelihood of the steric hindrance of motors within bundles of microtubules (Marx et al. 2000; Shahpasand et al. 2012; Conway et al. 2014). In chapter 4 the protective H2 allele showed a robust two-fold increase in expression of transcripts encoding 2N tau in all samples, agreeing with previous reports (Caffrey et al. 2008; Trabzuni et al. 2012) so it is hypothesised that knockdown of 2N tau would have a negative effect on axonal transport in neurons.

5.1.1 Aims of the Chapter

- To describe the design, generation and testing of novel RNA interference tools to knockdown tau protein and its isoforms. This includes design of siRNA and shRNA molecules and the incorporation of shRNA sequences into lentiviral plasmids for improved delivery to cells in culture.
- To detail the investigation of the roles of tau protein and its isoforms, notably 4R tau, in axonal transport in iPSC-derived dopaminergic neuronal cultures using isoform-specific shRNA tools.

5.2 Methods

5.2.1 Design of short interfering RNAs

Short interfering RNAs (siRNAs) were designed according to instructions provided by Life Technologies (Life Technologies, www.lifetechnologies.com/uk/en/home/references/ambion-tech-support/rnai-sirna/general-articles/-sirna-design-guidelines.html, accessed 28-Apr-2014), whereby candidate sequences of 21 nt beginning with AA, were checked by NCBI BLAST search (National Center for Biotechnology Information, www.ncbi.nlm.nih.gov/blast/, accessed 28-Apr-2014) to have no more than a stretch of 15 or 16 nucleotides in common with other human RefSeq RNA sequences. Alignments of *MAPT* exons 9-12 as amino acid and DNA sequences were performed using CLUSTAL 2.1 (http://www.clustal.org/clustal2/) (Larkin et al. 2007) with delineation of the microtubule-binding repeats of *MAPT* and *MAP4* as per Chapin & Bulinski (1992). Custom synthesized Silencer Select siRNAs were obtained from Life Technologies, in addition to non-targeting control (Silencer Negative Control No 1, #AM4611).

5.2.2 siRNA transfection of cell culture

BE(2)M17 cells were seeded as $1.2x10^5$ cells per well of 12-well plate. On day 2, transfection mixtures were made with 100 nM siRNA and 1% (v/v) Lipofectamine 2000 (Invitrogen) in OptiMEM (Gibco) and incubated to form complexes (20 min, room temperature). Cells were washed twice with OptiMEM before adding 1 ml OptiMEM and 200 µl siRNA:Lipofectamine mix to cells. After 6 hours, 600 µl OptiMEM with 30% foetal bovine serum (Gibco) was added. On day 3, medium was replaced with OptiMEM Complete. Cell pellets were harvested 72 hours post-transfection. cDNA synthesis was performed with SuperScript III (section 2.10.2 *i*) with 1 µg RNA.

BLOCK-iT Alexa Fluor Red Fluorescent Control (Ambion) was used in place of siRNA in transfection of BE(2)M17 cells to enable determination of transfection efficiency with 100 nM siRNA. NucBlue Live ReadyProbes Reagent (Molecular Probes) was added as 2 drops per well 24 hours post-transfection to visualise nuclei, then cells were imaged with a Nikon Eclipse TE-2000-U fluorescent microscope.

For delivery of siRNA to iPSC-derived dopaminergic neurons, transfection mixtures were made as above but with 3% (v/v) Lipofectamine 2000. Cultures in 12-well plates (DIV41) that had been seeded at $3x10^5$ cells/cm^2 on DIV20 were washed with PBS before adding 900 µl OptiMEM and 100 µl siRNA:Lipofectamine mix. After 6 hours, medium was replaced with standard maturation medium. Cell pellets were harvested 72 hours post-transfection. cDNA synthesis was performed with SuperScript III (Life Technologies) followed by qRT-PCR where SYBR Green housekeeper genes (*SDHA*, *GAPDH*, *HPRT1*) were used for normalisation.

5.2.3 Design and construction of short hairpin RNA lentiviral constructs

Short hairpin RNAs (shRNAs) were designed from siRNA sequences using the BLOCK-iT RNAi Designer (Life Technologies, http://rnaidesigner.lifetechnologies.com/) with additional instructions from http://rnaidesigner.lifetechnologies.com/rnaiexpress/help/convert_sirna_to_shrna.htm (accessed Jul-2014) and using the standard CGAA loop to form the hairpin. Three siRNA sequences against total *MAPT* that comprise Ambion #4392420 were determined from the positions of the central nucleotide in each 21 nt sequence in transcript NM_01123066.3 (s8508, central nt 2316; s8509, central nt 2342; s8510, central nt 1461). A non-targeting control was generated as a scrambled version of MAPTx3_1 using siRNA Wizard (www.sirnawizard.com/scrambled.php, accessed Jul-2014) on the 19 nt following the

initial AA dinucleotide. The resulting scrambled sequence was further verified using NCBI BLAST against the human RefSeq RNA database.

Lentiviral constructs to express short hairpin RNAs (shRNAs) were made using Gibson Assembly Master Mix (NEB) with the following DNA molecules: pRRL.sin.wpre fragment of *Spe*I-HF/*Sal*I-HF double digest (NEB) of pRRL.sin.U6.shRNA.cPPT.CMV.EGFP.wpre (kind gift from Dr Óscar Cordero Llana); PCR of U6 promoter from the same construct, adding each specific shRNA sequence with a long reverse primer (Harper and Davidson 2005; Rinaldi et al. 2014); PCR of RRE.cPPT.pEF1α from CSii-EF-MCS (a gift from Dr H. Miyoshi, RIKEN BioResource Center DNA Bank); PCR of EBFP2 from pBAD-EBFP2 (a gift from Robert Campbell, Addgene plasmid #14891). Primers for PCR (see Appendix Table L) were designed to incorporate ≥20 nt overlapping sequence between PCR/digest fragments to enable Gibson Assembly. PCRs were performed using KAPA HiFi HotStart ReadyMix (KAPA Biosystems). All DNA molecules were separated by agarose gel electrophoresis (2% for shRNA PCRs and 1% for all others), purified by QIAquick Gel Extraction Kit (QIAGEN) and quantified by Nanodrop. Gibson Assembly was performed as per manufacturer's instructions. Digested vector ($3x10^{-14}$ mol) and a three-fold molar excess of the three PCR products ($9x10^{-14}$ mol each) were incubated in a 20 µl reaction with Gibson Assembly Master Mix (50°C, 15 min) then stored on ice. Assembly products were diluted three-fold with water and 1 µl was used to transform One Shot TOP10 Chemically Competent *E. coli* (Invitrogen) before growth and selection. Following verification and sequencing (see Appendix Table M), validated plasmids were used to transform One Shot Stbl3 Chemically Competent *E. coli* (Invitrogen) for lower risk of recombination. Verification experiments were performed using plasmids prepared by PureLink HiPure Miniprep (section 2.2.1 *iii*).

5.2.4 Transfection of shRNA lentiviral constructs

BE(2)M17 cells were transfected with shRNA-bearing lentiviral constructs as per siRNA transfections except with 1 μg plasmid DNA instead of siRNA, and cells were harvested 48 hours post-transfection.

5.2.5 Generation and use of lentiviral particles

(i) Production of lentiviral particles

Third-generation lentiviral plasmids (Dull et al. 1998) were constructed, permitting the generation of self-inactivating lentiviruses as neither copy of the lentiviral long terminal repeats (LTRs) is wild-type: the 5' LTR is truncated and relies on a rous sarcoma virus promoter to drive transcription, while the 3' LTR is deleted in the U3 region (Zufferey et al. 1998). For production of lentiviral particles the following plasmids were prepared by PureLink HiPure Plasmid Maxiprep kit (section 2.2.2 *iii*) with transfection quantities shown per 15 cm dish: 10 μg shRNA/EBFP2 lentiviral vector; 10 μg pMDLg/pRRE (a gift from Didier Trono, Addgene plasmid #12251); 2 μg pRSV-Rev (a gift from Didier Trono, Addgene plasmid #12253); 3.4 μg pMD2.g (a gift from Didier Trono, Addgene plasmid #12259) encoding vesicular stomatitis virus glycoprotein (VSV-G) for lentiviral pseudotyping.

HEK293T cells ($8x10^6$ cells seeded per 15 cm dish the previous day with 20 ml medium; typically 12 dishes per lentiviral preparation) were transfected by calcium phosphate transfection: the above DNA was incubated with 125 mM $CaCl_2$, 25 mM HEPES, 140 mM NaCl, 0.75 mM Na_2HPO_4 for 30 min before adding 2.4 ml transfection mix per dish. On day two, culture medium was replaced (16 ml per dish), containing 10 mM sodium butyrate; eight hours later the medium was replaced (16 ml per dish) and kept to form the

first harvest (stored 4°C). A second harvest of medium was performed at the end of day three and pooled with the first harvest.

(ii) Concentration of lentiviral particles

To concentrate viral particles, harvested medium was centrifuged to remove debris (1,000 RCF, 5 min), 0.45 µm filtered, then centrifuged overnight to pellet viral particles (JLA-10.500 rotor, 6,000 RCF, 4°C). On day four the pellet was re-suspended in ice-cold PBS, ultra-centrifuged (SW32.1Ti rotor, 20,000 RPM, 90 min, 4°C) and finally re-suspended in a volume of TSSM buffer (20 mM Tris base, 100 mM NaCl, 10 g/l sucrose, 10 g/l D-mannitol) representing a 2000X reduction in original volume; brief centrifugation (1000 RCF, 5 min, 4°C) removed persistent debris before aliquoting for -80°C storage.

(iii) Titration of lentiviral particles

Viral titres were determined by transduction of HEK293T cells with serial dilutions, followed by flow cytometry determination of the percentage of EBFP2-positive cells 72 hours post-transduction. On day one, HEK293T cells were seeded $1x10^5$ cells per well in 12-well format. On day two, a representative well was trypsinised (200 µl trypsin-EDTA; 800 µl DMEM Complete to neutralise) and counted by Scepter in 1 ml volume to determine the starting number of cells per well. Serial dilutions were prepared representing $5x10^2$ (positive control aiming for 100% transduction), $1x10^3$, $1x10^4$ and $1x10^5$ dilutions (500 µl/well) with at least duplicate wells per condition. After 3-4 hours, 500 µl DMEM Complete was added to each well. On day four, 72 hours post-transduction, cells were washed with PBS, trypsinised as above, centrifuged (2880 RCF, 3 min), washed with PBS, centrifuged, resuspended in 100 µl PBS then fixed by addition of 400 µl 4% (w/v) paraformaldehyde in PBS for 10-15 min.

PFA was diluted by the addition of 900 µl PBS, centrifuged, resuspended in PBS, centrifuged and finally resuspended in 1% BSA (w/v) in PBS. Cell suspensions were analysed using a CyAn ADP Analyzer (Beckman Coulter) after setting the gating strategy for the FL6 channel parameters with the ~100% transduction condition ($5x10^2$ dilution factor) and untransduced cells. Allowing 10,000 cells to pass through the initial gate set up to remove debris, the proportion of cells showing as positive for EBFP2 per condition was used to calculate viral titres (transducing units/ml). The estimate for viral titre per condition was calculated as:

$$\frac{\%\ EBFP2^{+}\ cells \times original\ cell\ count \times 100}{transduction\ volume \times dilution\ factor}$$

then averaged for all estimates where EBFP2 percentage was between 5% and 60%.

(iv) Lentiviral transduction of cell culture

BE(2)M17 cells ($3.75x10^4$) were seeded in 24-well plates in OptiMEM Complete on day one. On day two, culture medium was replaced with 250 µl OptiMEM Complete containing lentiviral particles to an MOI of 10 or 20, based on the seeding density of day one. Medium was topped up to 500 µl after four hours. Cells were harvested 72-hours post-transduction (MOI 10) or 96-hours post-transduction (MOI 20).

iPSC-derived dopamine neuronal cultures were transduced on DIV20 shortly after re-plating, by addition of a small volume of lentiviral particles directly into the culture medium at MOI 2.5 or 5. The remainder of the protocol inclusive of treatment with Mitomycin C was as normal, and cells were harvested on DIV36.

5.2.6 Mitochondrial axonal transport imaging

Cultures of iPSC-derived dopaminergic neuronal cultures were re-plated onto Geltrex-coated coverslips on DIV20 and transduced with shRNA-bearing lentiviral particles. Cultures were maintained until four weeks post re-plating or five months post re-plating before imaging. Cultures were incubated with MitoTracker Deep Red (Invitrogen) for 30 min then washed with Hanks Balanced Salt Solution with calcium and magnesium (Invitrogen). Cultures were imaged on a Nikon Eclipse TE-2000-U fluorescent microscope with heated chamber at 37°C and delivery of 5% CO_2/Air for up to one hour with a 60X immersion objective (Nikon Plan APO VC, 60x/1.40 oil, 0.17, DIC, N2). Time-lapse imaging with Cy5 channel was performed using Volocity software to generate 150 images at 1 s intervals with 110 ms exposure (Vossel et al. 2015). Single EBFP2 images were taken on the DAPI channel to identify transduced neurons for each video.

5.2.7 Image analysis

Kymograph time-space plots were generated from blinded videos in Fiji software (National Institutes of Health) using the Multiple Kymograph plugin and the tsp050706 macro according to its protocol (http://www.embl.de/eamnet/html/body_kymograph.html). For transduced coverslips, only EBFP2-positive axons were chosen for analysis. Within the multiple kymograph, a segmented line was drawn along the path of each mitochondrion and velocities were determined using the 'read velocities from tsp' macro. Mitochondria were classed as motile if they moved more than 2 µm during the imaging period, corresponding to the approximate length of a mitochondrion (Vossel et al. 2015). Pauses were determined as individual parts of the path where a mitochondrion moved 0-1 pixels and/or had a velocity <0.12 pixels/s (<0.0139 µm/s) corresponding to the minimum velocity needed to reach the

overall threshold of motility in the 150 s imaging window. Motility and pause number data are presented as the average per neuron. Velocity data are presented as average velocity (μm/s) for the measured period and also the same average velocity calculation but with pause periods removed.

5.3 Results

5.3.1 Generation of RNA interference tools to reduce MAPT *expression*

(i) Short interfering RNAs to target MAPT isoforms

As an initial strategy for investigating the role of tau isoforms, a set of short interfering RNA (siRNA) molecules was designed to target *MAPT* transcripts containing exon 3 or exon 10. Target sequences in *MAPT* exon 3 (Fig. 5.1A) having suitable GC% were checked by BLAST search; MAPTx3_1 and MAPTx3_3 were chosen for testing as the BLAST search confirmed them to have no more than 16 nt contiguous sequence with other loci. However, it was noted that MAPTx3_3 shared 15 nt contiguous with the 1N isoforms of *MAPT*. For *MAPT* exon 10, which encodes one of the four microtubule-binding domain repeats, the translations of the four imperfect repeat exons were first aligned to determine the region of greatest divergence, which was shown to be the spacer sequences (Fig. 5.1B). From the DNA alignment of the *MAPT* spacer sequences, three siRNA target sequences were designed (Fig. 5.1C) then checked by BLAST search; MAPT10_1 and MAPT10_3 were chosen for testing, and had 15 nt contiguous with one locus and three loci respectively. In addition, the sequences for the spacers and repeats of the non-neuronal microtubule-associated protein MAP4 were examined and verified to be sufficiently dissimilar to those of *MAPT*, sharing only 50% sequence identity between the *MAPT* exon 10 spacer and the *MAP4* equivalent (Fig. 5.1D). Sequences of siRNAs selected for testing are shown in Table 5.1.

BE(2)M17 cells were transfected with siRNAs and the effect of knockdown was determined by qRT-PCR (Fig. 5.2A-C, Table 5.2). Transfection efficiency was estimated at >99% as shown by a fluorescent siRNA control being present in every cell (Fig. 5.2D). Both siRNAs targeting *MAPT* exon 3 (represented throughout as light blue bars) had a large and exclusive effect on exon 3+ transcripts, knocking them down by 79% and 84% respectively compared to

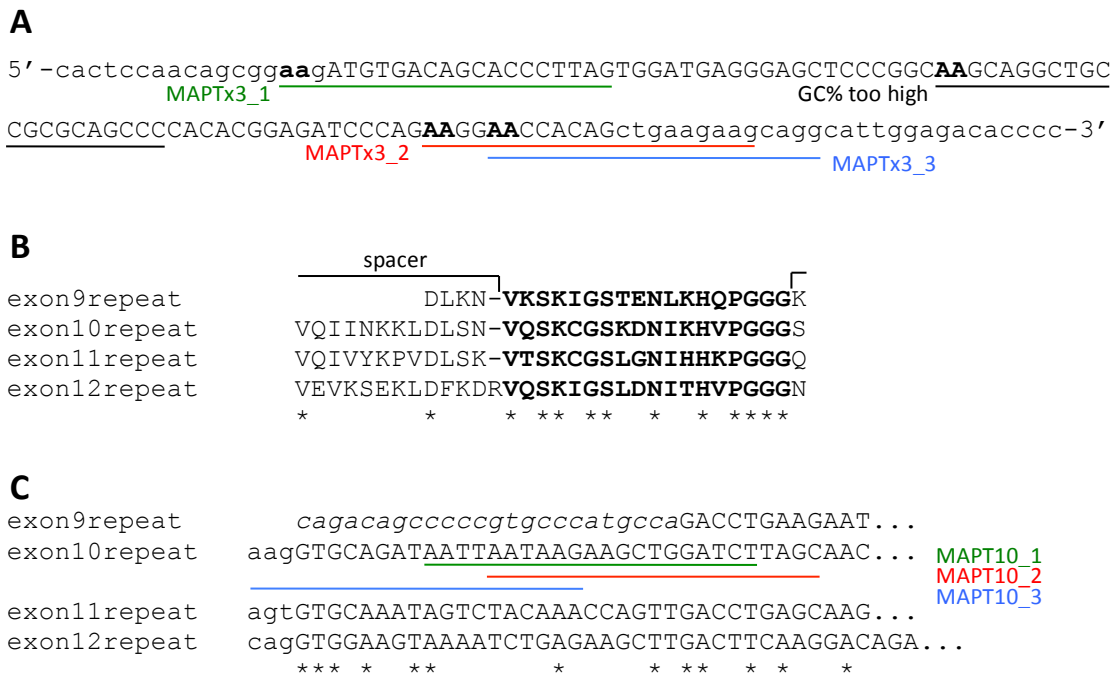

Figure 5.1: Design of short interfering RNA target sequences for *MAPT* isoforms.
(A) Partial sequence of *MAPT* mRNA (NM_005910.5 encoding 2N4R) showing exon 3 (uppercase) flanked by the adjacent portions of exons 2 and 4 respectively (lowercase). Four potential siRNA target sequences commencing with AA are shown underlined, with GC content (in order): 47.6%, 76.1% (unsuitable), 47.6%, 52.3%.
(B) CLUSTAL 2.1 alignment of the amino acid sequence of microtubule-binding domain repeats (bold) and spacer sequences encoded by *MAPT* exon 9-12, as denoted by Chapin & Bulinski (1992). Asterisks denote amino acids common to all of the sequences.
(C) CLUSTAL 2.1 alignment of the DNA sequence of the variable spacers shown in (B), plus additional sequence of exon 9 shown in lowercase italics. The three nucleotides of spacer sequence at the end of each exon are included in lowercase. Asterisks denote nucleotides common to all of the sequences (not including the portion of exon 9 shown in italics). Three potential siRNA target sequences commencing with AA are shown underlined, with GC content (in order): 28.5%, 38.1%, 28.5%.
(D) Alignment of the *MAPT* exon 10 spacer sequence with the equivalent sequence from *MAP4* (NM002375.4). Asterisks denote nucleotides common to both sequences.

Table 5.1: siRNA sequences (5'-3') tested in cell culture.

MAPTx3_1	
Target RNA sequence	AAGAUGUGACAGCACCCUUAG
Sense sequence (passenger strand)	gAUGUGACAGCACCCUUAGuu
Antisense sequence (guide strand)	***CUAAGGGUGCUGUCACAUCUU***
MAPTx3_3	
Target RNA sequence	AACCACAGCUGAAGAAGCAGG
Sense sequence (passenger strand)	CCACAGCUGAAGAAGCAGGuu
Antisense sequence (guide strand)	***CCUGCUUCUUCAGCUGUGGUU***
MAPT10_1	
Target RNA sequence	AAUUAAUAAGAAGCUGGAUCU
Sense sequence (passenger strand)	UUAAUAAGAAGCUGGAUCUuu
Antisense sequence (guide strand)	***AGAUCCAGCUUCUUAUUAAUU***
MAPT10_3	
Target RNA sequence	AAGGUGCAGAUAAUUAAUAAG
Sense sequence (passenger strand)	GGUGCAGAUAAUUAAUAAGuu
Antisense sequence (guide strand)	***CUUAUUAAUUAUCUGCACCUU***
Silencer Negative Control No 1 (Ambion, # AM4611) – non-targeting	

Silencer1 negative control (represented throughout by light grey bars) (Fig. 5.2A) but showing no effect on the levels of exon 10+ (Fig. 5.2B) or total *MAPT* transcripts (Fig. 5.2C). Both siRNAs targeting *MAPT* exon 10 (represented throughout as dark blue bars) had a clear effect on exon 10+ transcripts, knocking them down by 83% and 94% respectively compared to Silencer1 negative control (Fig. 5.2B). There was also a 43% and 57% knockdown effect respectively on exon 3+ transcripts (Fig. 5.2A) and a 38% (not significant with Bonferroni correction) and 47% knockdown effect respectively on total transcripts (Fig. 5.2C). The effect on exon 3+ transcripts could be explained by a combination of factors: first by a mirroring of the partial knockdown effect seen on total transcripts; second by the fact that some exon 10+ transcripts would also be exon 3+. It is unclear why the exon 10-targeting constructs produced partial knockdown of total transcripts; part of this will be by of the degree of exon 10 inclusion, but this is only estimated to be 7% of all *MAPT* transcripts in untransfected BE(2)M17 cells (Fig. 5.2E). Off-target interference is unlikely as the 21 nt siRNA sequences shared only 10 or 13 nt with the exon 11 and exon 12 spacer sequences (Fig. 5.1C).

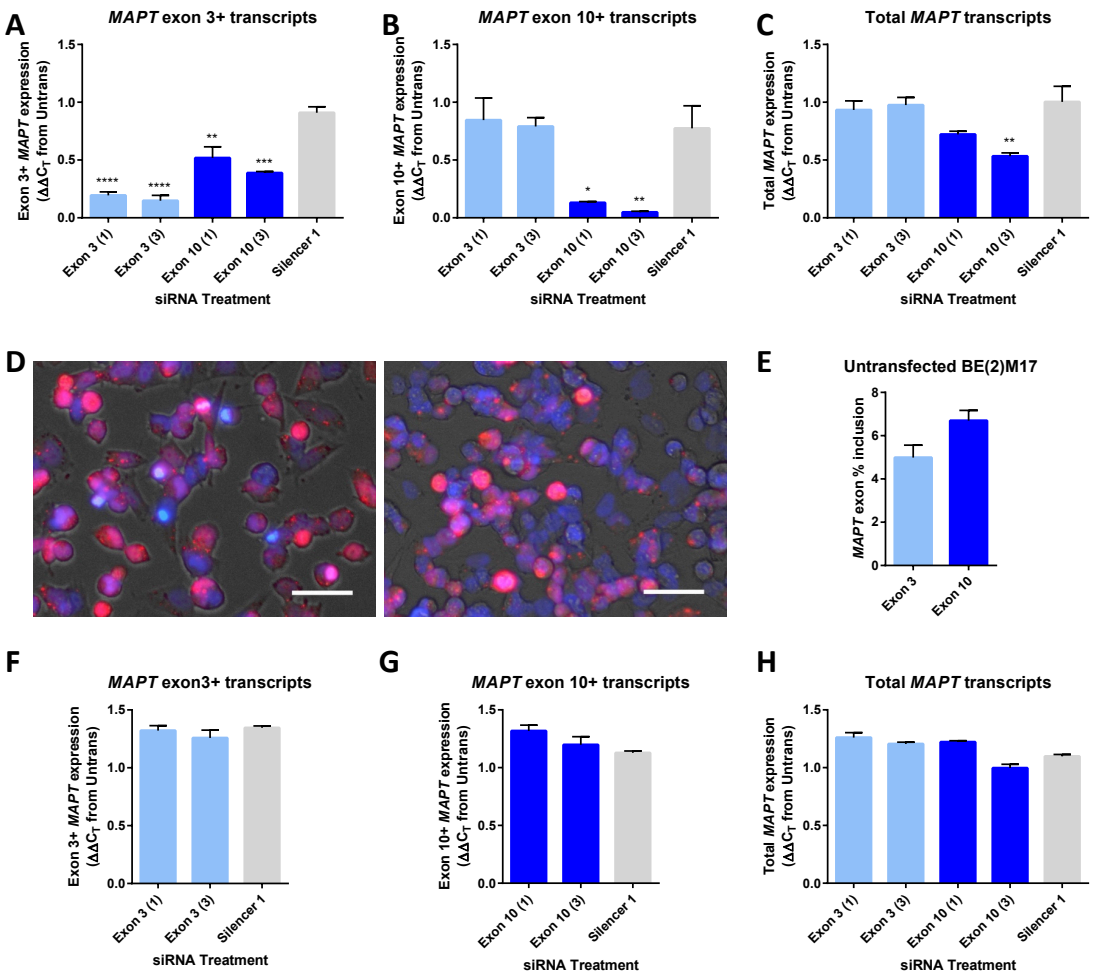

Figure 5.2: *MAPT* expression by qRT-PCR after siRNA delivery to BE(2)M17 cells and iPSC-derived dopaminergic neuronal cultures.

(A-C) qRT-PCR data for siRNA transfection of BE(2)M17 cells, measuring the effect of each siRNA treatment on (A) exon 3+ transcripts, (B) exon 10+ transcripts and (C) total *MAPT* transcripts. Mean ±SEM, n=3 independent transfections. Asterisks denote significant statistical difference from Silencer 1 negative control in a one-way ANOVA followed by Bonferroni's multiple comparisons test; see Table 5.2 for statistical data.

(D) Images of BE(2)M17 cells transfected with BLOCK-iT Alexa Fluor Red Fluorescent siRNA (red), with nuclei stained live with NucBlue (blue) and background phase contrast image. Scale bars 50 µm.

(E) Exon % inclusion for untransfected/untransduced BE(2)M17 cells. Mean ±SEM, n=9 independent experiments. Exon 3, 4.99% ±0.57%; exon 10, 6.70% ±0.47%.

(F-H) qRT-PCR data for siRNA transfection of iPSC-derived dopaminergic neuronal cultures, examining the effect of each attempted siRNA delivery on (F) total *MAPT* transcripts, (G) exon 3+ transcripts and (H) exon 10+ transcripts. Mean ±SEM from n=3 qPCR wells with cDNA from n=1 transfection.

Table 5.2: Statistical data for *MAPT* expression by qRT-PCR after siRNA delivery to BE(2)M17 cells (Fig. 5.2).

	siRNA Treatment	Mean expression ($\Delta\Delta C_T$)	SEM	Multiple comparison to Silencer 1			
				Adjusted *p*	*t*	df	Significance Summary
Fig. 5.2A (Exon 3+ transcripts)	Exon 3 (1)	0.194	0.030	< 0.0001	8.24	9	****
	Exon 3 (3)	0.148	0.047	< 0.0001	8.77	9	****
	Exon 10 (1)	0.518	0.097	0.0059	4.51	9	**
	Exon 10 (3)	0.389	0.012	0.0008	6.00	9	***
	Silencer 1	0.909	0.052	-	-	-	-
Fig. 5.2B (Exon 10+ transcripts)	Exon 3 (1)	0.846	0.191	> 0.9999	0.40	10	ns
	Exon 3 (3)	0.791	0.076	> 0.9999	0.09	10	ns
	Exon 10 (1)	0.131	0.009	0.0201	3.58	10	*
	Exon 10 (3)	0.048	0.009	0.0094	4.04	10	**
	Silencer 1	0.774	0.195	-	-	-	-
Fig. 5.2C (Total *MAPT* transcripts)	Exon 3 (1)	0.933	0.079	> 0.9999	0.63	10	ns
	Exon 3 (3)	0.975	0.067	> 0.9999	0.25	10	ns
	Exon 10 (1)	0.722	0.028	0.1198	2.53	10	ns
	Exon 10 (3)	0.533	0.029	0.0069	4.24	10	**
	Silencer 1	1.003	0.136	-	-	-	-

iPSC-derived dopaminergic neuronal cultures (clone 1A) were also transfected with siRNAs and analysed for knockdown by qRT-PCR. However, no knockdown effect was observed (Fig. 5.2F-H). Other attempts in the laboratory to deliver nucleic acids to iPSC-derived neurons by transfection had also been unsuccessful, including siRNAs targeting *SNCA* (F. Zambon, personal communication), so the strategy for tau knockdown was changed to one that could be undertaken using viral particles.

(ii) Short hairpin RNAs to target MAPT isoforms

To enable efficient delivery of RNA interference particularly to neurons, siRNA sequences were converted to shRNA sequences for incorporation into lentiviral vectors (Table 5.3). These comprise conversions from the four isoform-specific *MAPT* siRNA sequences, three siRNA sequences against total *MAPT* previously used in the laboratory and a scrambled non-targeting control generated from MAPTx3_1.

Table 5.3: shRNA sequences incorporated into lentiviral constructs.

shRNA Name	shRNA sequence (5'-sense-loop-antisense-3')
sh1 – MAPTx3_1	AAGATGTGACAGCACCCTTAGCGAACTAAGGGTGCTGTCACATCTTTTTT
sh2 – MAPTx3_3	AACCACAGCTGAAGAAGCAGGCGAACCTGCTTCTTCAGCTGTGGTTTTTT
sh3 – MAPT10_1	AATTAATAAGAAGCTGGATCTCGAAAGATCCAGCTTCTTATTAATTTTTT
sh4 – MAPT10_3	AAGGTGCAGATAATTAATAAGCGAACTTATTAATTATCTGCACCTTTTTT
sh5 – s8508 (*MAPT* exons 11-12)	AACATCCATCATAAACCAGGACGAATCCTGGTTTATGATGGATGTTTTTT
sh6 – s8509 (*MAPT* exon 12)	CCAGGTGGAAGTAAAATCTGACGAATCAGATTTTACTTCCACCTGGTTTTTT
sh7 – s8510 (*MAPT* exon 5)	GCATGGTCAGTAAAAGCAAAGCGAACTTTGCTTTTACTGACCATGCTTTTTT
sh8 – NT (non-targeting control; scrambled MAPTx3_1)	AAGAAGGCTCGTCGCACTAATCGAAATTAGTGCGACGAGCCTTCTTTTTT

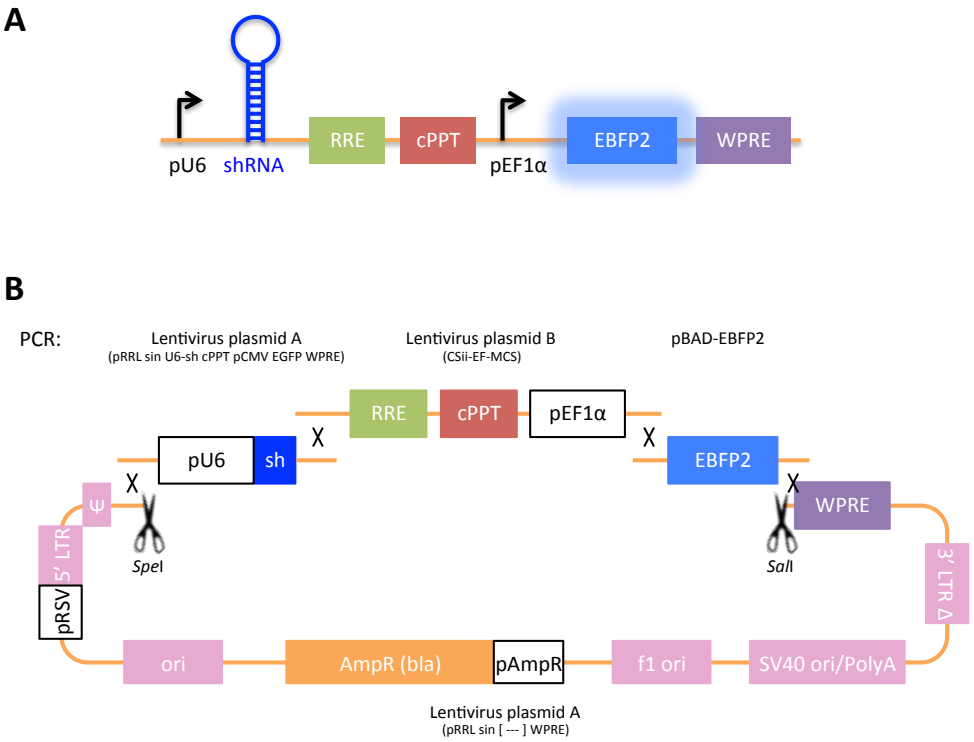

Figure 5.3: Schematics of lentiviral constructs.
(A) Schematic of the internal sequence of the shRNA-bearing lentiviral constructs, between the two long terminal repeats (LTRs).
(B) Schematic of the components of the four-fragment Gibson Assembly used to generate the constructs. The lentiviral backbone (lentivirus plasmid A) contains the standard plasmid replication machinery plus the lentiviral long terminal repeats (LTRs) that flank the insert region. Ψ, HIV-1 packaging sequence. Scissors represent digestion with restriction endonucleases. X represents regions of homology where 3' single-stranded overhangs created by 5' exonuclease during Gibson Assembly permit annealing of complementary sequence before repair by DNA polymerase and DNA ligase (Gibson et al. 2009).

(iii) Construction of shRNA lentiviral vectors

Lentiviral constructs were designed to express an shRNA from the mouse U6 promoter along with an enhanced blue fluorescent protein (EBFP2) (Ai et al. 2007) reporter driven by the human translation elongation factor 1α promoter (pEF1α), terminating with the woodchuck hepatitis virus post-transcriptional regulatory element (WPRE) (Fig. 5.3A). Eight shRNA constructs were made by Gibson Assembly (Gibson et al. 2009) (Fig. 5.3B). PCR fragments were amplified with high-fidelity polymerase (Fig. 5.4A-C) and assembled with digested backbone (Fig. 5.4D). PCR of the pU6-shRNA fragments showed a doublet band (Fig. 5.4A), thought to be the result of altered electrophoretic mobility of cruciform structured DNA where the shRNA sense and antisense sequences are complementary on the same strand. Colonies with correct digest patterns (Fig. 5.4E) were sequenced along the entire insert (>3.5 kb) and correct plasmids were used to transform stable *E. coli*. Newly transformed colonies maintained correct digest patterns (Fig. 5.4F) and sequences.

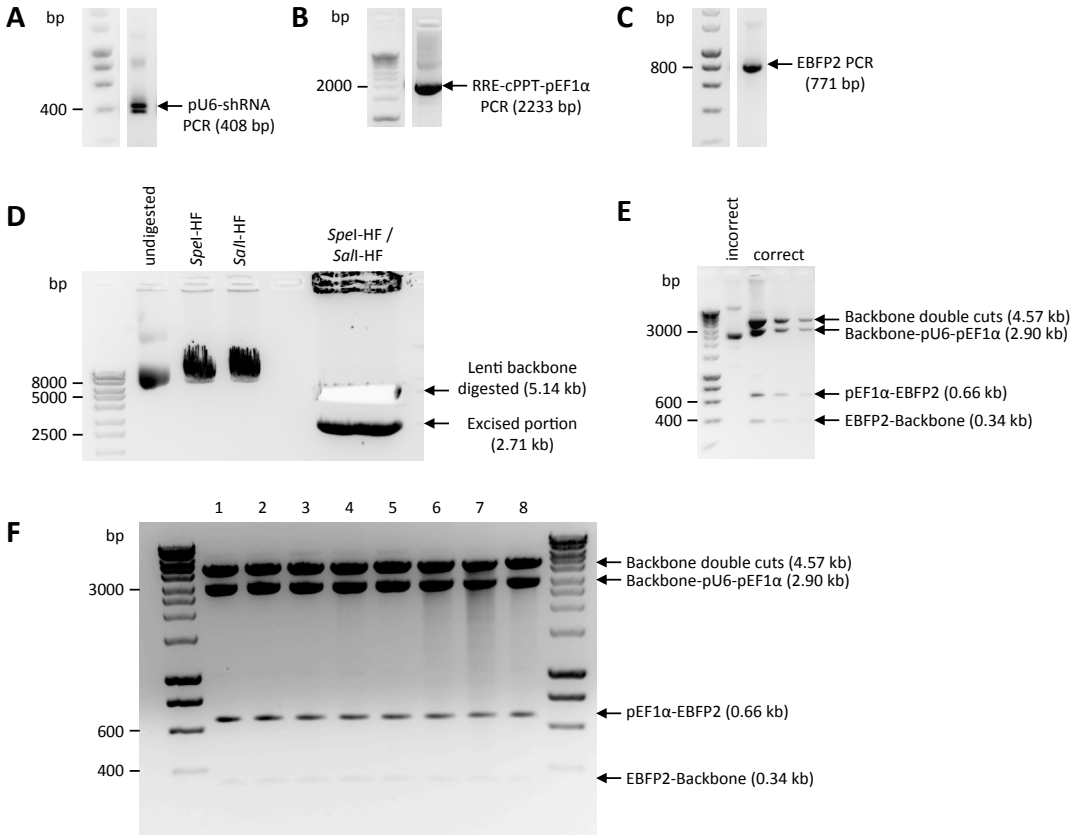

Figure 5.4: Construction of shRNA-bearing lentiviral constructs by four-fragment Gibson Assembly.
(A) Representative insert PCR of one of the eight different pU6-shRNA fragments before gel purification. The upper band of the doublet is the correct size, though both are of the correct sequence (data not shown).
(B) Insert PCR of RRE-cPPT-pEF1α before gel purification.
(C) Insert PCR of EBFP2 before gel purification.
(D) Pre-ligation *Spe*I-HF / *Sal*I-HF cloning restriction digest of pRRL.sin.pU6-sh.cPPT.pCMV.EGFP.WPRE to remove the undesired 2.71 kb portion from pU6 to EGFP. Undigested and single digest lanes are shown to confirm integrity of double digest. This image was taken after excision of the correct double digest fragment from the gel but a small portion remains visible.
(E-F) *Sfo*I-*Sal*I-HF analytical restriction digests of constructed lentiviral plasmid minipreps (E) following Gibson Assembly and (F) following transformation of Stbl3 bacteria. Correctly assembled lentiviral constructs have four digest fragments with cut sites shown. Minipreps in (F) are numbered as Table 5.3.

(iv) Validation of shRNA lentiviral constructs

The eight newly-generated lentiviral plasmids were tested for their ability to knockdown their respective targets of *MAPT* using transfection of BE(2)M17 cells. All eight constructs expressed EBFP2 by 24 hours post-transfection to identify transfected cells (Fig. 5.5A). As

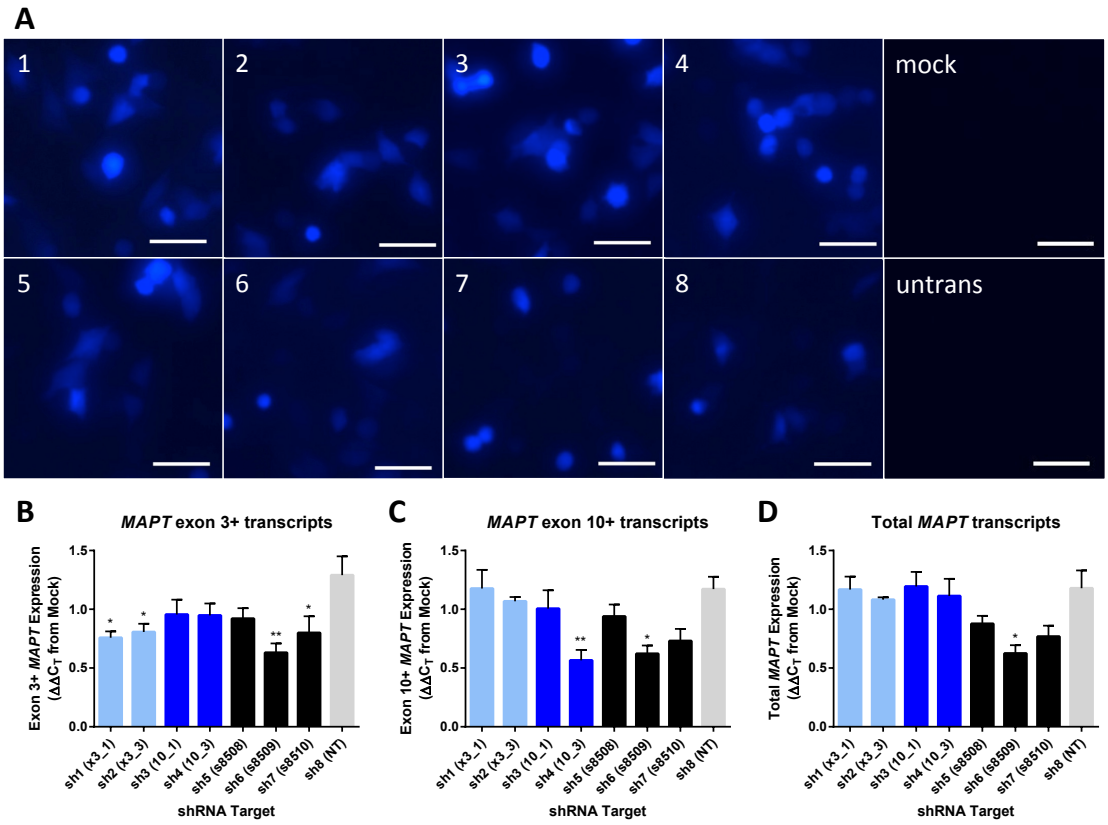

Figure 5.5: Transfection of BE(2)M17 cells with shRNA-bearing lentiviral plasmids.
(A) Images of EBFP2 expression 24 hours post-transfection on EVOS FL AUTO using TagBFP filter cube. Images 1-8, shRNA constructs (sh1-sh8); mock, transfection reagents without DNA; untrans, untransfected BE(2)M17 cells. Scale bars 50 µm.
(B-D) qRT-PCR data measuring the effect of each shRNA on (B) exon 3+ transcripts, (C) exon 10+ transcripts and (D) total *MAPT* transcripts. Mean ±SEM, n=3 independent transfections. Asterisks denote significant statistical difference from non-targeting shRNA control in a one-way ANOVA followed by Bonferroni's multiple comparisons test; see Table 5.4 for statistical data.

these initial transfections were considered a screen, in the analysis of *MAPT* qRT-PCR data, Bonferroni's multiple comparisons test was employed for the purpose of multiple testing correction to minimise the possibility of selecting false positives for lentiviral production. Both of the constructs targeting exon 3 significantly and selectively reduced exon 3+ transcripts (construct sh1, 41%; construct sh2, 37% decrease; Fig. 5.5B, Table 5.4) but not exon 10+ (Fig. 5.5C) or total transcripts (Fig. 5.5D). Construct sh4, targeting exon 10, reduced exon 10+ transcripts alone (52% decrease), but its partner construct sh3 had no effect in any assay (Fig. 5.5B-D). Of the three shRNA constructs targeting constitutive *MAPT* exons (sh5,

sh6, sh7), only construct sh6 significantly reduced all three kinds of *MAPT* transcripts (exon 3+, 51% decrease, Fig. 5.5B; exon 10+, 47% decrease, Fig. 5.5C; total *MAPT*, 47% decrease, Fig. 5.5D). None of the other seven constructs significantly affected total *MAPT* transcripts beyond a downward trend for constructs sh5 and sh7 (Fig. 5.5D), while construct sh7 reduced exon 3+ transcripts by 38% (Fig. 5.5C). From these data, I proceeded with production of lentiviral particles containing the best plasmid for each condition: construct sh1 (x3_1), construct sh4 (10_3), construct sh6 (s8509) and construct sh8 (non-targeting).

Table 5.4: Statistical data for *MAPT* expression by qRT-PCR after transfection of BE(2)M17 cells with shRNA-bearing lentiviral plasmids (Fig. 5.5).

	shRNA target	Mean expression ($\Delta\Delta C_T$)	SEM	Multiple comparison to non-targeting			
				Adjusted *p*	*t*	df	Significance Summary
Fig. 5.5B (Exon 3+ transcripts)	sh1 (x3_1)	0.758	0.054	0.022	3.47	16	*
	sh2 (x3_3)	0.807	0.070	0.0432	3.15	16	*
	sh3 (10_1)	0.956	0.127	0.31	2.18	16	ns
	sh4 (10_3)	0.948	0.101	0.2828	2.23	16	ns
	sh5 (s8508)	0.920	0.090	0.1968	2.41	16	ns
	sh6 (s8509)	0.631	0.079	0.0039	4.30	16	**
	sh7 (s8510)	0.799	0.141	0.0389	3.20	16	*
	sh8 (NT)	1.290	0.161	-	-	-	-
Fig. 5.5C (Exon 10+ transcripts)	sh1 (x3_1)	1.177	0.160	> 0.9999	0.03	16	ns
	sh2 (x3_3)	1.068	0.037	> 0.9999	0.68	16	ns
	sh3 (10_1)	1.006	0.156	> 0.9999	1.07	16	ns
	sh4 (10_3)	0.566	0.089	0.0086	3.92	16	**
	sh5 (s8508)	0.939	0.102	> 0.9999	1.51	16	ns
	sh6 (s8509)	0.622	0.071	0.0184	3.56	16	*
	sh7 (s8510)	0.731	0.102	0.081	2.85	16	ns
	sh8 (NT)	1.172	0.105	-	-	-	-
Fig. 5.5D (Total *MAPT* transcripts)	sh1 (x3_1)	1.168	0.110	> 0.9999	0.07	16	ns
	sh2 (x3_3)	1.082	0.020	> 0.9999	0.64	16	ns
	sh3 (10_1)	1.194	0.124	> 0.9999	0.10	16	ns
	sh4 (10_3)	1.113	0.147	> 0.9999	0.44	16	ns
	sh5 (s8508)	0.877	0.067	0.4334	2.01	16	ns
	sh6 (s8509)	0.624	0.070	0.0138	3.69	16	*
	sh7 (s8510)	0.768	0.092	0.1032	2.73	16	ns
	sh8 (NT)	1.179	0.152	-	-	-	-

Lentiviral particles were produced by packaging the above four plasmids in HEK293T cells. Viral titres achieved following purification and concentration are shown in Table 5.5. BE(2)M17 cells transduced with these four lentiviral particle preparations showed EBFP2 expression when imaged 72 hours post-transduction, prior to harvesting (Fig. 5.6A). Particles expressing shRNA targeting exon 3 produced only a small downward trend in exon 3+ transcripts corresponding to a 22% decrease (Fig. 5.6B, Table 5.6). Particles expressing shRNA targeting exon 10 significantly and selectively reduced exon 10+ transcripts by 44% (Fig. 5.6C) with no detectable effect on exon 3+ or total *MAPT* transcripts (Fig. 5.6B, D). For particles expressing shRNA targeting constitutive exons, knockdown was significant for exon 3+ transcripts (39% knockdown; Fig. 5.6B) but was close to the statistical cut-off for exon 10+ transcripts (p=0.0541, 39% knockdown; Fig. 5.6C) and total *MAPT* transcripts (p=0.0501, 40% knockdown; Fig. 5.6D). No other construct discernably affected total *MAPT* transcripts (Fig. 5.6D). While BE(2)M17 cells are useful as a model for short-term culture of dopamine-producing cells, they are not neurons and may react in different ways to treatment by lentiviral particles; therefore, further functional validation of all constructs was still required.

Table 5.5: Titres from lentiviral particle production.

Lentiviral particle identity	Measured titres (TU/ml)
sh1 (exon 3)	7.0×10^8
sh4 (exon 10)	1.3×10^9
sh6 (Total)	Batch 1: 4.7×10^8 Batch 2: 1.9×10^9
sh8 (Non-targeting)	Batch 1: 1.5×10^8 Batch 2: 2.0×10^9

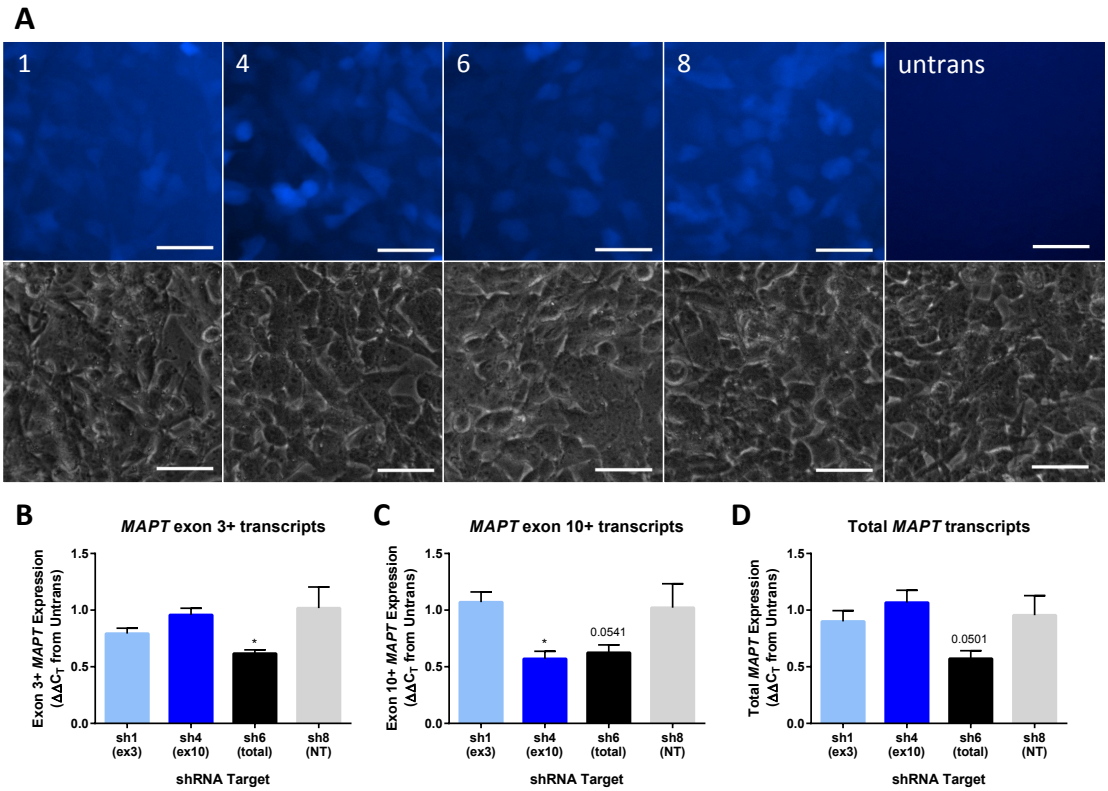

Figure 5.6: Transduction of BE(2)M17 cells with shRNA-bearing lentiviral particles.
(A) Images of EBFP2 expression 72 hours post-transfection on Nikon Eclipse TE-2000-U using DAPI filter cube with corresponding phase contrast images beneath. Numbering corresponds to shRNA constructs sh1-sh8; untrans, untransduced cultures. Scale bars 50 µm.
(B-D) qRT-PCR data measuring the effect of each shRNA on (B) exon 3+ transcripts, (C) exon 10+ transcripts and (D) total *MAPT* transcripts. Mean ±SEM, n=3 independent transductions. Asterisks denote significant statistical difference from non-targeting shRNA control in Fisher's Least Significant Difference test and the numerical values represent *p*-values close to significance; see Table 5.6 for statistical data.

Table 5.6: Statistical data for *MAPT* expression by qRT-PCR after transduction of BE(2)M17 cells with shRNA-bearing lentiviral particles (Fig. 5.6).

	shRNA target	Mean expression ($\Delta\Delta C_T$)	SEM	Multiple comparison to non-targeting			
				Adjusted *p*	*t*	df	Significance
Fig. 5.6B (Exon 3+ transcripts)	sh1 (ex3)	0.793	0.048	0.1571	1.56	8	ns
	sh4 (ex10)	0.958	0.059	0.6866	0.42	8	ns
	sh6 (Total)	0.618	0.032	0.0239	2.78	8	*
	sh8 (NT)	1.018	0.187	-	-	-	-
Fig. 5.6C (Exon 10+ transcripts)	sh1 (ex3)	1.071	0.090	0.787	0.28	8	ns
	sh4 (ex10)	0.571	0.066	0.0338	2.56	8	*
	sh6 (Total)	0.624	0.069	0.0541	2.26	8	ns
	sh8 (NT)	1.022	0.212	-	-	-	-
Fig. 5.6D (Total *MAPT* transcripts)	sh1 (ex3)	0.901	0.095	0.7469	0.33	8	ns
	sh4 (ex10)	1.067	0.109	0.5254	0.66	8	ns
	sh6 (Total)	0.572	0.069	0.0501	2.31	8	ns
	sh8 (NT)	0.956	0.172	-	-	-	-

Final testing of the lentiviral constructs was undertaken in iPSC-derived dopaminergic neuronal cultures to verify the suitability of the constructs for use in modelling tau function in a physiological setting. Cultures were transduced at DIV20 shortly after re-plating, in order to maximise transduction capacity while the cells formed a monolayer and existed predominantly as a soma without neurites. Prior to harvesting at DIV36, 16 days post-transduction, the cultures expressed EBFP2 (Fig. 5.7A).

Similar to transduction of BE(2)M17 cells, transduction of neuronal cultures with the exon 3-targeting construct showed no effect on exon 3+ transcripts compared to the non-targeting 'scrambled' construct (Fig. 5.7B, Table 5.7). Likewise the exon 3-targeting construct had no effect on exon 10+ transcripts (Fig. 5.7C), but strangely increased total *MAPT* transcripts by 36% (Fig. 5.7D). As these results were unsatisfactory in both BE(2)M17 cells and neuronal cultures, experiments with the exon 3-targeting shRNA construct were not pursued further.

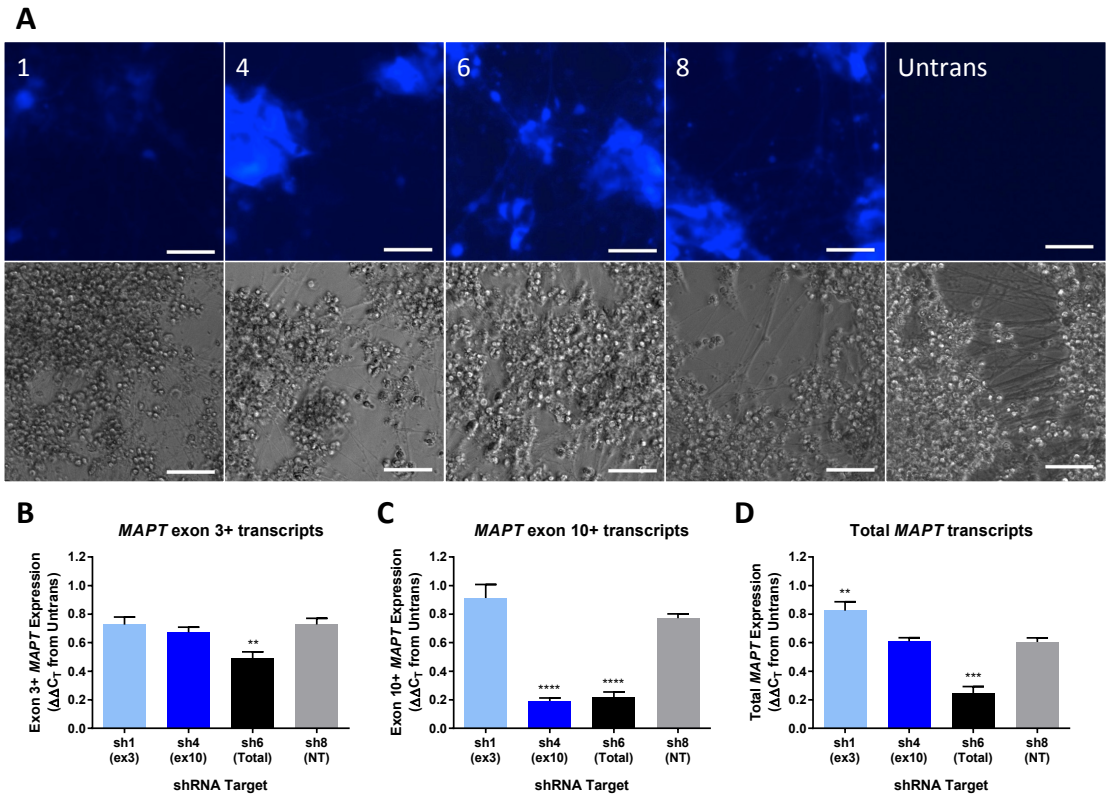

Figure 5.7: Transduction of iPSC-derived dopaminergic neuronal cultures with shRNA-bearing lentiviral particles.
(A) Images of EBFP2 expression at DIV36 on EVOS FL AUTO using TagBFP filter cube with corresponding phase contrast images beneath. Numbering corresponds to shRNA constructs sh1-sh8; untrans, untransduced cultures. Scale bars 50 µm.
(B-D) qRT-PCR data measuring the effect of each shRNA at DIV36 on (B) exon 3+ transcripts, (C) exon 10+ transcripts and (D) total *MAPT* transcripts. Mean ±SEM, n=3 transductions. Asterisks denote significant statistical difference from non-targeting shRNA control in Fisher's Least Significant Difference test; see Table 5.7 for statistical data.

The remaining two constructs performed well. Knockdown by lentiviral delivery of the exon 10-targeting construct selectively reduced exon 10+ transcripts by 75% (Fig. 5.7C) and not exon 3+ (Fig. 5.7B) or total transcripts (Fig. 5.7D), demonstrating that the effect on total transcripts seen as siRNAs (Fig. 5.2C) was not a consistent problem with this chosen target sequence. Knockdown by lentiviral delivery of the total *MAPT* shRNA construct reduced exon 3+ transcripts by 33% (Fig. 5.7B), exon 10+ transcripts by 72% (Fig. 5.7C) and total transcripts by 59% (Fig. 5.7D). In summary, the exon 10-targeting and total *MAPT* targeting constructs showed excellent knockdown compared with the non-targeting construct and

were suitable for use in studying axonal transport (remainder of this chapter) and additional disease-related phenotypes (Chapter 6).

Table 5.7: Statistical data for *MAPT* expression by qRT-PCR after transduction of iPSC-derived dopaminergic neuronal cultures with shRNA-bearing lentiviral particles (Fig. 5.7).

	shRNA target	Mean expression ($\Delta\Delta C_T$)	SEM	Multiple comparison to non-targeting			
				Adjusted *p*	*t*	df	Significance
Fig. 5.7B (Exon 3+ transcripts)	sh1 (ex3)	0.726	0.054	0.9866	0.02	8	ns
	sh4 (ex10)	0.672	0.036	0.4184	0.85	8	ns
	sh6 (Total)	0.488	0.048	0.0059	3.72	8	**
	sh8 (NT)	0.727	0.043	-	-	-	-
Fig. 5.7C (Exon 10+ transcripts)	sh1 (ex3)	0.913	0.095	0.1016	1.85	8	ns
	sh4 (ex10)	0.192	0.021	< 0.0001	7.60	8	****
	sh6 (Total)	0.218	0.036	< 0.0001	7.26	8	****
	sh8 (NT)	0.772	0.030	-	-	-	-
Fig. 5.7D (Total *MAPT* transcripts)	sh1 (ex3)	0.825	0.062	0.0066	3.64	8	**
	sh4 (ex10)	0.610	0.025	0.9322	0.09	8	ns
	sh6 (Total)	0.248	0.045	0.0004	5.90	8	***
	sh8 (NT)	0.605	0.029	-	-	-	-

5.3.2 Effects of reduced tau expression on axonal transport

With the tools to reduce tau expression in neurons established, iPSC-derived dopaminergic neuronal cultures were prepared for live imaging of axonal transport with tau knockdown. Two time points were studied: a short-term maturation of four weeks with knockdown of total tau, and a longer maturation of five months with knockdown of total tau or 4R tau encoded by exon 10+ transcripts. Transduction was performed at DIV20 shortly after re-plating onto imaging coverslips.

(i) Axonal transport with total tau knockdown during short-term maturation

At four weeks post-transduction, cultures were incubated with MitoTracker Deep Red and imaged as time-lapse videos (Fig. 5.8A). Transduced neurons continued to express EBFP2 under the EF1α promoter after four weeks (Fig. 5.8B) allowing axonal transport measurements to be restricted to this sub-set. Kymograph time-space plots were generated in order to measure the movement of individual mitochondria (Fig. 5.8C). Knockdown of tau protein at four weeks was confirmed as 65% (Fig. 5.8D).

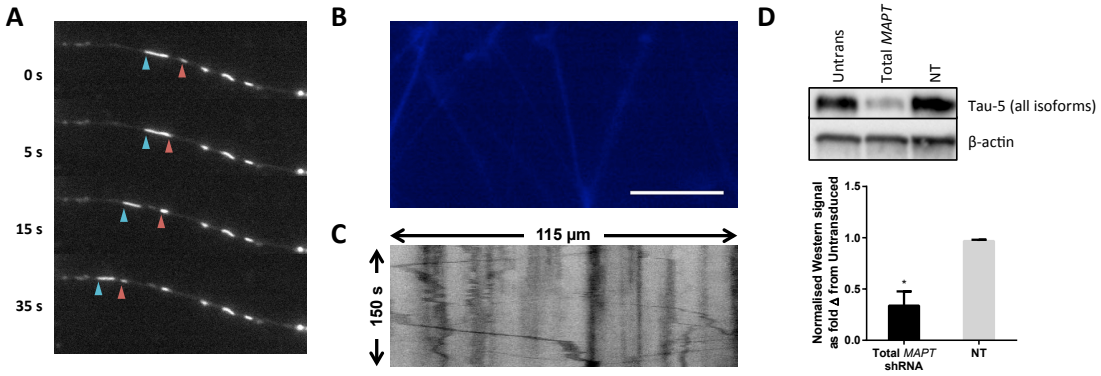

Figure 5.8: Mitochondrial axonal transport in dopaminergic neuronal cultures.
(A) Selected time-lapse fluorescence microscopy images of axonal mitochondria in dopaminergic neuronal cultures stained with MitoTracker Deep Red. Arrows show motile mitochondria.
(B) Image of EBFP2 expression during axonal transport live imaging on Nikon Eclipse TE-2000-U. Scale bar 25 µm.
(C) Kymograph time-space plot of a trace along the linear path of an axon, from which motility parameters can be determined.
(D) Representative western blots showing knockdown of tau protein (Tau-5 antibody) in dopaminergic neuronal cultures matured for four weeks, with beta-actin loading control. Quantification of duplicate blots shown below; mean ±SEM. Asterisk denotes significant statistical difference from non-targeting shRNA control in an unpaired *t*-test: *MAPT* 0.338 ±0.139, NT 0.969 ±0.012, p=0.0457, t=4.517, df=2.

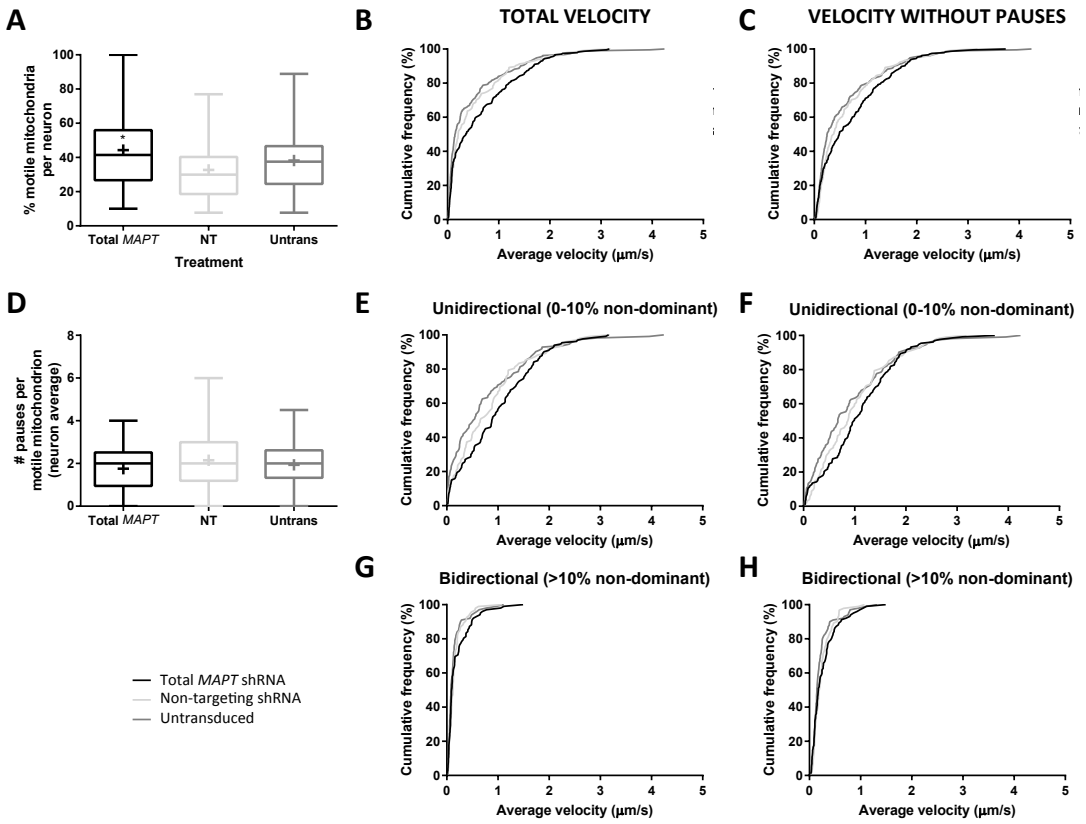

Figure 5.9: Mitochondrial axonal transport data for iPSC-derived dopaminergic neuronal cultures around four weeks post-transduction.

Legend for all parts at bottom left of figure.

(A) Box and whisker plots (minimum to maximum; centre line, median; '+', mean) of percentage motility of mitochondria per neuron. Asterisk represents significant statistical difference from non-targeting shRNA control in Kruskall-Wallis test with Dunn's multiple comparisons post-test [mean±SEM, median (IQR)]: total *MAPT* shRNA 44.28% ±3.32%, 41.43% (29.25%), n=50 neurons, adjusted *p*=0.015; non-targeting shRNA 32.70% ±2.32%, 29.97% (21.68%), n=54 neurons; untransduced n=54 neurons.

(B-C) Cumulative frequency (%) graphs of average mitochondrial velocity in dopaminergic neuronal cultures. (B) Average total velocity of each measured motile mitochondrion; (C) average velocity of each measured motile mitochondrion after removal of time when paused. Median velocities (IQR): (B) total *MAPT* shRNA, 0.358 (0.972) μm/s; non-targeting shRNA, 0.210 (0.708) μm/s; untransduced, 0.149 (0.573) μm/s; (C) total *MAPT* shRNA, 0.489 (0.988) μm/s; non-targeting shRNA, 0.383 (0.734) μm/s; untransduced, 0.251 (0.715) μm/s. Both graphs showed a statistically significant difference between median values in Kruskall-Wallis nonparametric tests: (B) *p*=0.0033, KW statistic=11.42; (C) *p*=0.0200, KW statistic=7.826. However, Dunn's multiple comparisons post test showed no statistical difference from non-targeting shRNA control (total *MAPT* shRNA, adjusted *p*=0.3277). Number of motile mitochondria per condition: total *MAPT* shRNA, 235; non-targeting shRNA, 195; untransduced, 212.

(D) Box and whisker plots of the number of pauses per mitochondrion (mean per neuron). No significant statistical difference between medians by Kruskall-Wallis test (*p*=0.3923, KW statistic=1.872).

(E-H) Cumulative frequency (%) graphs of average mitochondrial velocity in dopaminergic neuronal cultures after stratification by directionality. (E) Total velocity measurements for unidirectional mitochondria; (F) velocity without pause periods for unidirectional

mitochondria; (G) Total velocity measurements for bidirectional mitochondria; (H) velocity without pause periods for bidirectional mitochondria. Median velocities (IQR): (E) total *MAPT* shRNA, 0.882 (1.187) µm/s; non-targeting shRNA, 0.658 (0.908) µm/s; untransduced, 0.530 (1.139) µm/s; (F) total *MAPT* shRNA, 0.992 (1.011) µm/s; non-targeting shRNA, 0.869 (0.965) µm/s; untransduced, 0.671 (1.134) µm/s; (G) total *MAPT* shRNA, 0.096 (0.182) µm/s; non-targeting shRNA, 0.121 (0.130) µm/s; untransduced, 0.080 (0.092) µm/s; (H) total *MAPT* shRNA, 0.173 (0.256) µm/s; non-targeting shRNA, 0.195 (0.202) µm/s; untransduced, 0.146 (0.141) µm/s. Kruskall-Wallis test found a significant statistical difference between medians for (E) (p=0.0097, KW statistic=9.264) but Dunn's multiple comparisons post test showed no statistical difference from non-targeting shRNA control (total *MAPT* shRNA, adjusted p=0.2327). Kruskall-Wallis tests for (F-H) found no significant difference between medians: (F) p=0.0502, KW statistic=5.984; (G) p=0.1458, KW statistic=3.851; (H) p=0.1786, KW statistic=3.445. Number of mitochondria per condition (unidirectional/bidirectional): total *MAPT* shRNA, 133/102; non-targeting shRNA, 102/93; untransduced, 112/100.

Initial analysis identified motile vs. non-motile mitochondria, with motile mitochondria defined as those that have been displaced by ≥2 µm during the imaging period (Vossel et al. 2010); motility is therefore a measure of how many mitochondria are moving and how many are stationary. Knockdown showed a significant difference in the mean percentage of mitochondria per neuron that were motile (44% for knockdown, 33% for non-targeting control; Fig. 5.9A). However, when tau protein was reduced in these young neurons the average velocity of motile mitochondria was not significantly different from the non-targeting shRNA control (Fig. 5.9B). The data were further analysed by identifying the periods during which each motile mitochondrion had paused. When these pause periods were removed from the calculations of average velocity, the average motile velocity of motile mitochondria remained not significantly different with tau knockdown (Fig. 5.9C), nor was there a difference in the average number of pauses per mitochondrion (Fig. 5.9D).

Mitochondrial velocity was unable to be separated by direction (anterograde/retrograde), as the positions of the cell bodies were not determined in the relatively dense cultures. However, further stratification was performed by separating mitochondria that had >90% of their movement in a single direction (unidirectional) from those that were bidirectional. The

median velocities of unidirectional mitochondria (Fig. 5.9E-F) were between 4.5-fold and 9.2-fold higher than those of bidirectional mitochondria (Fig. 5.9G-H), but no significant difference was observed between knockdown and non-targeting conditions.

(ii) Axonal transport with 4R and total tau knockdown during five-month maturation

The later time point of five months maturation permitted the study of 4R tau function in axonal transport. In chapter 4 I described a progressive increase in *MAPT* exon 10 inclusion over a six-month period, resulting in detectable 4R tau protein at later time points (Figs. 4.6-4.7). The mature cultures used here expressed 4R tau isoforms that were detectable by Western blot (Fig. 5.10A). Quantification of Western blots showed that protein knockdown by the total *MAPT* shRNA persisted at a reduction by 55% of total tau, while the 4R *MAPT* shRNA knocked down 4R tau by 81% (Fig. 5.10A). Additionally, EBFP2 expressed under the EF1α promoter was also still strong after five months so as to permit identification of transduced neurons for quantification (Fig. 5.10B).

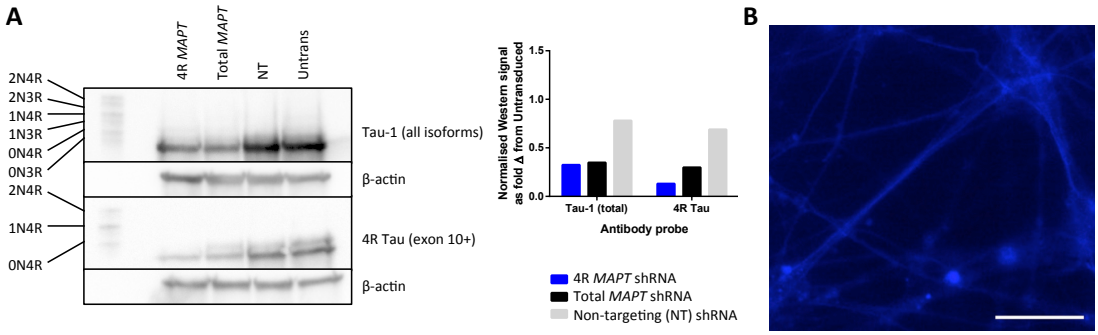

Figure 5.10: Knockdown of tau isoforms in iPSC-derived dopaminergic neuronal cultures five months post-transduction.
(A) Western blots after protein dephosphorylation with lambda phosphatase showing knockdown of tau protein (Tau-1 antibody) and 4R tau isoforms (4R tau antibody) in iPSC-derived dopaminergic neuronal cultures five months post-transduction, with beta-actin loading control. Far left lane, ladder of all six recombinant tau protein isoforms. Quantification of blots shown.
(B) Image of EBFP2 expression during axonal transport live imaging on Nikon Eclipse TE-2000-U. Scale bar 25 µm.

Unlike in the short-term knockdown, older neurons showed no difference in the percentage motility of mitochondria per neuron whether total or 4R *MAPT* transcripts were targeted (Fig. 5.11A). However, in these older neurons where the complement of tau proteins is more adult-like and knockdown conditions had persisted for longer, knockdown of 4R tau by targeting exon 10+ transcripts caused a significant increase in median (IQR) mitochondrial velocity from 0.148 (0.399) µm/s to 0.574 (0.935) µm/s (adjusted p=0.0007, Fig. 5.11B). When pause periods were removed from the velocity calculations, both knockdown of total tau and 4R tau showed a significant increase in median (IQR) mitochondrial velocity compared to the non-targeting shRNA control, from 0.272 (0.565) µm/s for non-targeting to 0.793 (0.937) µm/s and 0.519 (0.732) µm/s for 4R and total *MAPT* knockdown respectively (4R *MAPT* adjusted p=0.0002; total *MAPT* adjusted p=0.0191; Fig. 5.11C); however, again there was no observed difference in the actual number of pauses per motile mitochondrion (Fig. 5.11D).

When mitochondria were stratified by directionality, as was observed for younger neurons the median velocities of unidirectional mitochondria (Fig. 5.11E-F) were between 3.7-fold and 10.4-fold higher than those of bidirectional mitochondria (Fig. 5.11G-H). Knockdown of 4R tau resulted in a significant increase in velocity for mitochondria moving in one direction only, with or without inclusion of paused periods (Fig. 5.11E: median velocity (IQR), 4R *MAPT* 0.760 (0.752) µm/s, NT 0.344 (0.573) µm/s, p=0.0048; Fig. 5.11F: median velocity (IQR), 4R *MAPT* 0.990 (0.626) µm/s, NT 0.641 (0.827) µm/s, p=0.0033), but showed no difference in velocity of bidirectional mitochondria (Fig. 5.11G-H), showing that the overall effect seen by 4R tau knockdown was carried by unidirectional mitochondria. In contrast, knockdown of total tau resulted in increased velocity of both unidirectional and bidirectional mitochondria, but only when pause periods were removed (Fig. 5.11F: median velocity (IQR), total *MAPT* 0.946 (1.056) µm/s; NT, 0.641 (0.827) µm/s, p=0.0078; Fig. 5.11H: median velocity (IQR), total *MAPT* 0.294 (0.389) µm/s; NT 0.184 (0.154) µm/s, p=0.0327).

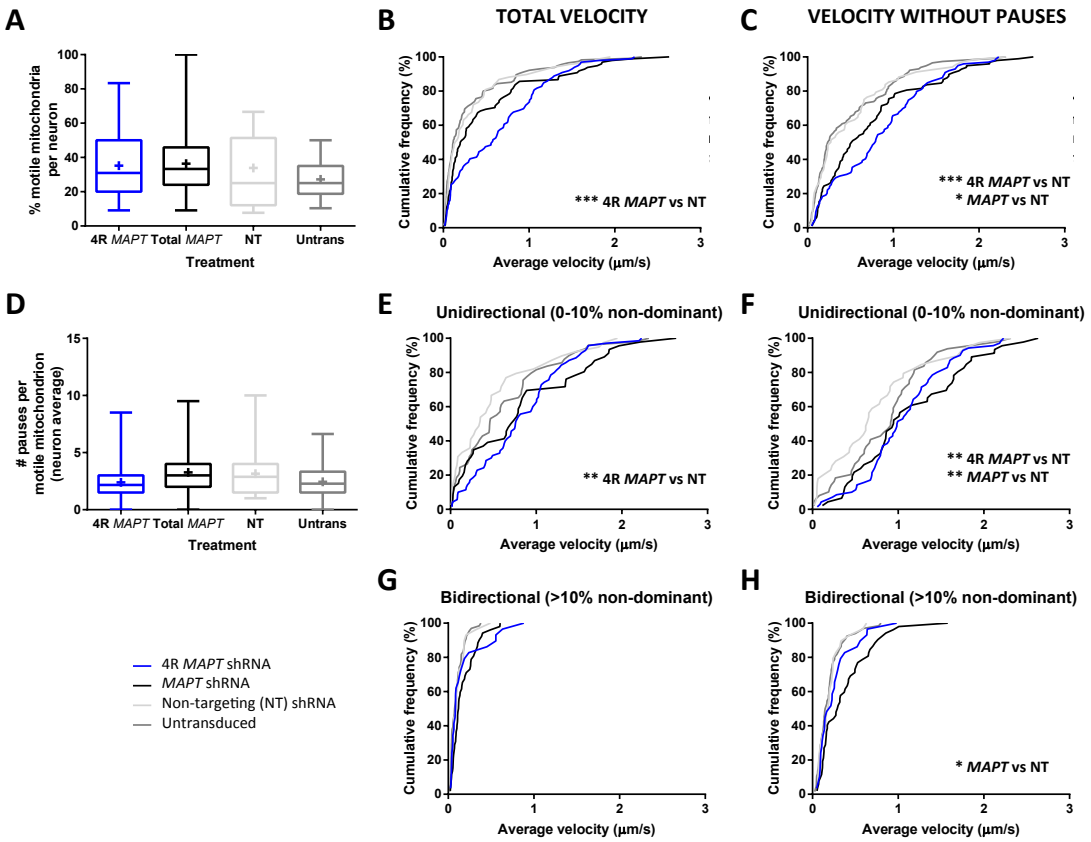

Figure 5.11: Mitochondrial axonal transport data for iPSC-derived dopaminergic neuronal cultures five months post-transduction.

Legend for all parts at bottom left of figure.

(A) Box and whisker plots (minimum to maximum; centre line, median; '+', mean) of percentage motility of mitochondria per neuron. No significant statistical difference between medians by Kruskall-Wallis test (p=0.1877, KW statistic=4.791). Number of neurons per condition: 4R *MAPT* shRNA, 38; total *MAPT* shRNA, 45; non-targeting shRNA, 26; untransduced, 39.

(B-C) Cumulative frequency (%) graphs of average mitochondrial velocity in dopaminergic neuronal cultures. (B) Average total velocity of each measured motile mitochondrion; (C) average velocity of each measured motile mitochondrion after removal of time when paused. Median velocities (IQR): (B) 4R *MAPT* shRNA, 0.574 (0.935) µm/s; total *MAPT* shRNA, 0.204 (0.588) µm/s; non-targeting shRNA, 0.147 (0.399) µm/s; untransduced, 0.116 (0.338) µm/s; (C) 4R *MAPT* shRNA, 0.793 (0.937) µm/s; total *MAPT* shRNA, 0.519 (0.732) µm/s; non-targeting shRNA, 0.272 (0.565) µm/s; untransduced, 0.239 (0.673) µm/s. Both graphs showed a statistically significant difference between median values in Kruskall-Wallis nonparametric tests: (B) p<0.0001, KW statistic=27.28; (C) p<0.0001, KW statistic=30.75. Asterisks represent significant statistical difference from non-targeting shRNA control in Dunn's multiple comparisons post test: (B) 4R *MAPT* shRNA, adjusted p=0.0007; (C) 4R *MAPT* shRNA, adjusted p=0.0002; total *MAPT* shRNA, adjusted p=0.0191. Number of motile mitochondria per condition: 4R *MAPT* shRNA, 99; total *MAPT* shRNA, 98; non-targeting shRNA, 68; untransduced, 115.

(D) Box and whisker plots of the number of pauses per mitochondrion (mean per neuron). No significant statistical difference between medians by Kruskall-Wallis test (p=0.0949, KW statistic=6.372).

(E-H) Cumulative frequency (%) graphs of average mitochondrial velocity in dopaminergic neuronal cultures after stratification by directionality. (E) Total velocity measurements for unidirectional mitochondria; (F) velocity without pause periods for unidirectional mitochondria; (G) Total velocity measurements for bidirectional mitochondria; (H) velocity without pause periods for bidirectional mitochondria. Median velocities (IQR): (E) 4R *MAPT* shRNA, 0.760 (0.752) µm/s; total *MAPT* shRNA, 0.723 (1.202) µm/s; non-targeting shRNA, 0.344 (0.573) µm/s; untransduced, 0.458 (0.718) µm/s; (F) 4R *MAPT* shRNA, 0.990 (0.626) µm/s; total *MAPT* shRNA, 0.946 (1.056) µm/s; non-targeting shRNA, 0.641 (0.827) µm/s; untransduced, 0.913 (0.660) µm/s; (G) 4R *MAPT* shRNA, 0.085 (0.131) µm/s; total *MAPT* shRNA, 0.120 (0.193) µm/s; non-targeting shRNA, 0.093 (0.113) µm/s; untransduced, 0.076 (0.106) µm/s; (H) 4R *MAPT* shRNA, 0.214 (0.215) µm/s; total *MAPT* shRNA, 0.294 (0.389) µm/s; non-targeting shRNA, 0.184 (0.154) µm/s; untransduced, 0.153 (0.145) µm/s. Kruskall-Wallis tests found significant statistical differences between medians for all graphs: (E) p=0.0075, KW statistic=11.97; (F) p=0.0030, KW statistic=13.96; (G) p=0.0113, KW statistic=11.09; (H) p=0.0022, KW statistic=14.59. Asterisks represent significant statistical difference from non-targeting shRNA control in Dunn's multiple comparisons tests: (E) 4R *MAPT* shRNA, p=0.0048; (F) 4R *MAPT* shRNA, p=0.0033; total *MAPT* shRNA, p=0.0078; (G) no significance in post test; (H) total *MAPT* shRNA, p=0.0327. Number of mitochondria per condition (unidirectional/bidirectional): 4R *MAPT* shRNA, 70/29; total *MAPT*, 52/46; non-targeting shRNA, 39/29; untransduced, 49/66.

5.4 Discussion

5.4.1 RNA interference of MAPT

In this study a set of RNA interference tools was designed, constructed and tested for their capacity to reduce expression of tau and its isoforms before using these tools to interrogate the role of tau in axonal transport. First, siRNA molecules to target *MAPT* transcripts containing either exon 3 or exon 10 were designed and tested in immortalised cell culture, where they successfully reduced expression of these transcripts by between 79% and 94% (Fig. 5.2). Despite the success of the siRNA approach in immortalised cell culture, the requirement for transfection ruled out its utility in iPSC-derived neuronal cultures.

Following conversion of siRNA sequences to shRNA sequences, new constructs were made to deliver RNA interference by lentiviral transduction to a wider range of cell types and for a longer period of time, as recipient cells can continuously express the molecules. Testing of these constructs by transfection and transduction in both BE(2)M17 cells and iPSC-derived dopaminergic neuronal cultures identified two constructs that could successfully reduce either exon 10+ transcripts or all *MAPT* transcripts in addition to a non-targeting control construct (Figs. 5.5-5.7). However, neither of the constructs designed to target exon 3+ transcripts appeared functional as lentivirally-delivered shRNAs. Differences between siRNA and shRNA functionality may be due to the loss of the chemical modifications made to siRNA molecules to help bias the inclusion of the guide strand into the RNA-induced silencing complex (RISC) or due to the ability of the specific shRNA sequence to be expressed due to its secondary structure (Rao et al. 2009).

The purpose of the non-targeting control construct was to account for any effects caused by delivery of lentiviral constructs, such as toxicity, or by general expression of shRNAs and EBFP2. While the non-targeting shRNA did not closely match any known RefSeq RNA, it is

still possible that delivery of the lentiviral construct expressing the non-targeting control shRNA had an effect on tau levels. For example, as the first viral titre for the non-targeting control was lower than for the other constructs (Table 5.5), this required a greater volume for the same MOI, which may have influenced toxicity levels. Oddly, iPSC-derived cultures transduced with the non-targeting construct showed tau expression levels at 60-70% of the untransduced cultures (Fig. 5.7); if delivery of the non-targeting construct conferred more toxicity than the exon 3 targeting construct, this could explain the increased levels of total and exon 10+ *MAPT* transcripts in exon 3 knockdown cultures relative to non-targeted cultures (Fig. 5.7). Further, off-target effects of RNA interference were not examined for any constructs in this study. Although all constructs were carefully designed to be theoretically independent of other transcripts according to standard criteria, in practice even some transcripts sharing only 7 nt have been altered by RNA interference (Lin et al. 2005). Any further studies using these novel shRNA constructs would benefit from adding duplicate constructs for each condition, including non-targeting control, to confirm absolutely that findings are due to knockdown of the correct target and not some other factor.

5.4.2 Tau protein and mitochondrial motility

Knockdown of total tau for four weeks in iPSC-derived cultures increased mitochondrial motility (Fig. 5.9A); however, no motility phenotype was observed after five months of knockdown of either 4R or total tau (Fig. 5.11A). In agreement with this, reduced mitochondrial motility has been reported as a phenotype of tau overexpression (Ebneth et al. 1998; Trinczek et al. 1999; Stamer et al. 2002), principally that of reduced anterograde transport by kinesin. To the contrary, some studies have shown that tau knockdown (Sapir et al. 2012) or tau knockout (Rapoport et al. 2002) also impair mitochondrial motility (Sapir et al. 2012), likely through the destabilisation and increased dynamics of microtubule

networks (Rapoport et al. 2002); consistent with these, primary cultures from tau knockout show deficiencies in neurite outgrowth (Dawson et al. 2001). Other studies, however, have found no effect of tau presence, absence or overexpression on measures of axonal transport (Morfini et al. 2007; Yuan et al. 2008; Vossel et al. 2010; Yuan et al. 2013), including one where only the expression of a pseudohyperphosphorylated form of tau reduced mitochondrial motility in human ESC-derived neurons (Mertens et al. 2013).

Of particular interest is the study published by Iovino et al. (2015), who measured mitochondrial axonal transport in iPSC-derived cortical neurons from patients with *MAPT* N279K or P301L mutations compared to control lines. The N279K mutation increases exon 10 inclusion so that more 4R tau is expressed; this resulted in a decrease in mitochondrial motility shown by more stationary mitochondria and there was a more pronounced decrease on anterograde motility than on retrograde motility (Iovino et al. 2015). The P301L mutation is encoded in exon 10 but does not alter splicing; rather it affects a conserved sequence within the microtubule-binding domain repeats (Hutton et al. 1998). The negative effect of the P301L mutation on mitochondrial motility was more pronounced than for N279K, and may be due to destabilising effects on microtubules (Iovino et al. 2015). Although this study did not specifically manipulate the levels of tau or its isoforms other than how the mutation does so, it supports a role for 4R tau isoforms in modulation of axonal transport.

It is likely that these two particular aspects of tau must be in balance, i.e. that there is enough present to stabilise microtubules but not so much as to hinder kinesin-dependent anterograde transport. For example, APP trafficking is disrupted both by tau knockdown (Lei et al. 2012) and tau overexpression (Stamer et al. 2002). The levels of tau reduction in the present study must be sufficient to observe unencumbered transport while maintaining microtubule stability at four weeks. However, at five months motility is reduced in all

conditions (Fig. 5.11), which may be due to the more mature complement of isoforms. Finally, despite increased motility at four weeks, no change in the number of pauses was observed (Fig. 5.9D).

5.4.3 Tau protein and mitochondrial velocity

While knockdown of total tau for four weeks showed no change in average mitochondrial velocity (Fig. 5.9), after five months average velocity without pause times was increased for all mitochondria (Fig. 5.11). It should be noted that most studies have calculated velocity solely as average velocity including pause times, but Trinczek et al. (1999) is an example of one that set a criterion threshold for pauses (<0.3 μm/s step velocity) in order to calculate the "velocity of active motion", i.e. average velocity without pauses. Mouse cortical cultures transfected with overexpression constructs of 3R or 4R tau isoforms showed decreased average velocity that was principally from a reduction in anterograde velocity (Stoothoff et al. 2009). However, most previous studies have shown that the presence or expression level of tau has no effect on the specific velocity of movement, only on the degree of motility of cargoes. Notably this was examined using *in vitro* motility assays where only recombinant proteins are present (Seitz et al. 2002; Dixit et al. 2008), though the use of such a highly controlled environment limits the application of some findings.

In light of the lack of an *in vitro* velocity phenotype there are three interrelated hypotheses to explain the results observed in the present study that I will now discuss.

(i) Specificity of cell type

The first hypothesis is that this is a cell type-specific phenotype requiring the specific subset of neurons generated by differentiation to dopaminergic neuronal cultures. Certainly findings from non-neuronal cells, e.g. CHO cells (Trinczek et al. 1999), have a limited application to phenotypes in neuronal axons. The differences seen could also be specific to human neurons. The studies of Vossel et al. (2010; 2015) made use of mouse hippocampal neurons either from the range of tau knockout mice (*Tau*$^{+/+}$, *Tau*$^{+/-}$, *Tau*$^{-/-}$) or using a similar lentiviral-delivered shRNA knockdown approach to the one described here, but saw no effect on velocity of mitochondria or TrkA receptor unless coupled with delivery of Aβ or amyloid precursor protein (APP). Interestingly, adult mice express only the three 4R isoforms of tau (McMillan et al. 2008; Gumucio et al. 2013), so may have evolved mechanisms to evade any intrinsic negative effects that 4R tau confers, particularly as the presence of murine 4R tau counteracts the formation of pathology otherwise seen with expression of the six isoforms of human tau in htau mice (Andorfer et al. 2003).

(ii) Specificity of developmental stage

The second hypothesis is that this is a developmental stage-specific phenotype, requiring mature neurons in order to observe a difference in velocity. This is in light of the observation that knockdown of total tau for five months rather than for four weeks results in a statistically significant increase in mitochondrial velocity (Fig. 5.11 compared to Fig. 5.9), despite the degree of knockdown being equivalent (Fig. 5.10A compared to Fig. 5.8D). qRT-PCR time course data in Chapter 4 showed that cultures matured for four weeks had 0.4% inclusion of *MAPT* exon 3 and 2.8% inclusion of *MAPT* exon 10, compared to 4.4% and 13.9% respectively at 20 weeks (Fig 4.6), equivalent to the later axonal transport time point.

It is not surprising that the transport phenotype was not revealed after four weeks when little but 0N3R tau was present in non-knockdown conditions.

(iii) Secondary effect via an intermediate effector

The third hypothesis is that altered transport velocity is a secondary effect of tau knockdown, whereby a decrease in tau alters an intermediate effector, which in turn affects transport, rather than tau affecting the transport directly. Such a role for tau would not be observed in an *in vitro* model containing only tau and other specified MAPs, motor proteins and microtubules (Seitz et al. 2002; Dixit et al. 2008). This hypothesis can encompass the others because rather than the maturity of the neurons *per se*, the length of knockdown could allow sufficient time for other processes to have a visible effect, such as the gradual accumulation or decline of effectors. As an illustration, complete tau knockout reduces the neuronal trafficking of APP, which has a role in neuronal iron export, to the plasma membrane, leading to cellular iron accumulation that is only visible behaviourally after 12 months (Lei et al. 2012); partial knockdown would be expected to have a slower accumulation of iron.

One candidate for an intermediate between tau and mitochondrial velocity is the organisation of actin filaments. Even in axons, mitochondrial movement has an actin-mediated component, which is generally slower (<0.3 μm/s) (Morris and Hollenbeck 1995), and disturbance of the actin network using cytochalasin increases mitochondrial velocity (Morris and Hollenbeck 1995). Tau induces co-localisation of actin with microtubules (Griffith and Pollard 1978, 1982; Elie et al. 2015), so reduced levels of tau could, over time, diminish the mutual proximity of these networks within axons and increase mitochondrial velocity.

It has been proposed that the amount of tau is co-regulated with the amount of tubulin, and that where microtubules are organised as bundles in axons the resulting higher density of microtubules may inhibit the movement of mitochondria (Shahpasand et al. 2012). Indeed, *in vitro* experiments examining kinesin-1 motility found that microtubules that were adequately spaced fostered improved motor movement (Conway et al. 2014).

Additionally, the amount of the individual motor proteins can influence velocity of movement, as shown with kinesin-1 concentration-dependent movement of APP vesicles or peroxisomes in *Drosophila*, whereby more active bound molecules result in a higher velocity than has been observed *in vitro* with single molecules (Kural et al. 2005; Reis et al. 2012). Another set of candidates comprises the adaptor proteins, such as Miro1 (MacAskill et al. 2009) and syntabulin (Cai et al. 2005), both of which are necessary for mitochondrial anterograde transport using kinesin and retrograde transport using dynein at least in *Drosophila* (Russo et al. 2009), but neither of which have a known link with tau expression, although over-stabilisation of Miro1 is implicated in sporadic and genetic PD through mutant PINK1, parkin and LRRK2 (Hsieh et al. 2016).

A final potential candidate is glycogen synthase kinase 3 beta (GSK3β). In addition to being a kinase that phosphorylates tau, GSK3β is required alongside tau for impairment of axonal transport induced by amyloid-beta toxicity (Vossel et al. 2015) or by delivery of either tau filaments or just the monomeric N-terminus of tau (LaPointe et al. 2009). One proposed mechanism was that tau brings protein phosphatase 1 to microtubules (Liao et al. 1998) where it can be activated, in turn activating GSK3β (LaPointe et al. 2009); active GSK3β in the vicinity of microtubules could subsequently phosphorylate kinesin to induce detachment from cargo (LaPointe et al. 2009). Reduction in tau levels would therefore be proposed to reduce the likelihood of such activations, although detachment of kinesin would more likely manifest in changes in motility and not in actual velocity.

5.4.4 Stratification of transport directionality

The stratification of mitochondrial transport into unidirectional vs. bidirectional (Fig. 5.9, Fig. 5.11) generated two pools that are reminiscent of the kinesin and dynein-dynactin kymographs respectively shown in Dixit et al (2008); however, no definitive distinction between motors can be made without knowledge of axonal orientation. Kinesin produces movement solely in the anterograde direction, whereas cytoplasmic dynein, while predominantly a retrograde motor, is capable of reversing and so functions bidirectionally (Dixit et al. 2008). Further, some cargoes bind both kinesin and dynein simultaneously (Pilling et al. 2006; Schuster et al. 2011a; Schuster et al. 2011b), possibly as a result of the dependence of dynein on kinesin for its function (Pilling et al. 2006), so that some bidirectional mitochondria may be representative of a switch in which motor is active. In the present study it is particularly interesting that knockdown of 4R tau for five months increases velocity of unidirectional mitochondria (most likely to be kinesin bound) but not of bidirectional mitochondria, suggesting that 4R tau may predominantly inhibit anterograde transport in these neurons.

5.4.5 Conclusion

In conclusion, the increase in mitochondrial velocity conferred in mature iPSC-derived dopaminergic neuronal cultures on knockdown of 4R tau or total tau is an acute mimic of the overall lower expression of 4R tau or total tau from the H2 allele compared to the H1 allele. In the complementary situation, increased levels of tau expression from the H1 allele compared to the H2 allele would be expected to decrease mitochondrial velocity. Thus individuals with the PD risk haplotype H1 may be expected to have some relative perturbation in axonal transport compared to those with the protective haplotype H2. The

use of mature neuronal cultures has been critical for determining these phenotypes, which could not have been achieved using primary rodent cultures. Further studies of axonal transport in mature iPSC-derived neurons utilising the intronic variant discovered in chapter 4 would be particularly useful in comparing the effects of the relative levels of 4R tau between lines with and without the ΔCTT variant.

Axonal transport is one of several intracellular trafficking pathways that may be perturbed early in the pathogenesis of PD, as part of a unified hypothesis underlying neuronal dysfunction in PD (Hunn et al. 2015). Indeed, SNpc dopaminergic neurons of both early and late-stage PD brains showed reduced immunostaining for axonal transport motors, particularly conventional kinesin (Chu et al. 2012). The correct maintenance of this delivery pathway to enable needed organelles, vesicles and other cargoes to reach the distal tips of the axonal arbour is essential, in addition to the necessary return of damaged organelles and proteins by retrograde transport for their subsequent degradation. It is not specifically known whether faster or slower mitochondrial velocity is beneficial for the cell, especially as mitochondria need to be located at particular points along the length of the axon, such as synaptic boutons. However, it is assumed that with the massive axonal arbour of SNpc dopaminergic neurons (Pissadaki and Bolam 2013) it would be beneficial to improve transport from the soma to the synapses throughout the arbour so that the demands of synapses for energy and calcium buffering can be met (Sheng 2014). Thus impaired axonal transport could contribute to synaptic dysfunction of SNpc dopaminergic neurons, reducing dopamine levels in the striatum before triggering their eventual death (Janezic et al. 2013) with the accompanying motor manifestations of PD.

Chapter 6: Knockdown of *MAPT* in *GBA* N370S iPSC-derived dopaminergic neuronal cultures

6.1 Introduction

One of the genes most highly associated with Parkinson's disease is *GBA*, encoding glucosylceramidase beta, more commonly known as β-glucocerebrosidase. Severely reduced enzymatic activity of β-glucocerebrosidase by loss-of-function mutations in *GBA* results in Gaucher's disease (Brady et al. 1966), a lysosomal storage disorder that has effects on the mononuclear phagocytic system, including enlargements of the spleen and liver, and skeletal problems via bone marrow (Sidransky and Ginns 1993). Some Gaucher's patients additionally experience neurological effects, so that the disease can be divided into non-neuronopathic (type 1) and neuronopathic forms, with the latter being divided into acute (type 2) and chronic (type 3) presentations (Sidransky and Ginns 1993). Common mutations in *GBA* that cause Gaucher's disease include N370S in exon 9, that is found more in type 1 patients (Tsuji et al. 1988) and L444P in exon 10 that is found more in neuronopathic-type patients (Tsuji et al. 1987); however, there is still significant heterogeneity of genotype-phenotype combinations so that mutations are not restricted to a particular disease presentation (Sidransky et al. 1994; Charrow et al. 2000; Koprivica et al. 2000). Both alleles of *GBA* need to be affected to cause Gaucher's disease so that mutations are found in either homozygous or double heterozygous states, and in some individuals a portion of one allele has undergone recombination with the *GBA* pseudogene (Koprivica et al. 2000).

An association was made between Gaucher's disease and PD on observing that parkinsonism was sometimes manifested in patients with Gaucher's (Tayebi et al. 2003). Further, an increased prevalence of parkinsonism amongst relatives of patients with Gaucher's (Goker-

Table 6.1: Top loci associated with Parkinson's disease listed on PDGene in October 2013.

#	Gene	Polymorphism	Ethnicity	OR (95% CI)	P-value
1	MAPT/STH	MAPT_H1H2	Caucasian	0.78 (0.75-0.80)	3.54E-52
2	SNCA	rs356220	All	1.30 (1.25-1.34)	3.06E-49
3	**GBA**	**GBA_N370S**	**All**	**3.37 (2.67-4.29)**	**1.11E-24**
4	LRRK2	rs34778348	Asian	2.23 (1.89-2.63)	2.97E-21
5	PM20D1	rs11240572	All	0.74 (0.69-0.80)	1.01E-14
6	GAK	rs1564282	All	1.29 (1.20-1.38)	6.54E-13
7	MCCC1	rs11711441	All	0.84 (0.80-0.89)	8.72E-12
8	STK39	rs2102808	All	1.28 (1.19-1.38)	1.54E-11
9	BST1	rs4698412	All	0.87 (0.83-0.91)	2.28E-10
10	GPNMB	rs156429	All	0.89 (0.86-0.93)	2.69E-10
11	SETD1A	rs4889603	All	1.14 (1.09-1.19)	4.68E-10
12	GWA_8p22	rs591323	All	0.89 (0.86-0.93)	2.59E-09
13	SYT11/RAB25	chr1:154105678	All	1.67 (1.41-1.98)	5.70E-09
14	FAM47E	rs6812193	All	0.89 (0.85-0.93)	1.07E-07
15	HLA-DRB5	chr6:32588205	All	0.75 (0.68-0.84)	2.90E-07
16	CCDC62/HIP1R	rs12817488	All	1.17 (1.09-1.25)	2.99E-06
17	ACMSD/TMEM163	rs6710823	All	1.40 (1.2-1.63)	1.61E-05
18	MED13	rs8081812	All	1.13 (1.07-1.2)	6.09E-05

Alpan et al. 2004), i.e. those that are in the carrier state for a Gaucher's mutation, suggested a possible association of single heterozygous mutations in *GBA* with PD. This hypothesis was validated by identification of *GBA* mutations in 12 members of a cohort of 57 autopsied PD cases, being a higher frequency than expected from the general population (Lwin et al. 2004), and ultimately confirmed by a large multi-centre analysis of 5691 PD patients vs 4898 controls where the frequency of *GBA* mutations was greater in PD patients than controls in virtually every population, so that *GBA* mutations conferred an odds ratio of 5.43 (Sidransky et al. 2009). Before the release of the meta-GWAS (Nalls et al. 2014), the *GBA* N370S mutation was ranked the third highest for association with PD on PDGene and showed the highest odds ratio amongst the top genes (Table 6.1); as the mutation is not one of the SNPs examined by GWAS the association is no longer included on PDGene.org, which is now solely an output for the meta-GWAS data from Nalls et al. (2014). However, despite the strong association between PD and the carrier state for *GBA* mutations, the disease-causing penetrance of heterozygous mutations is still low (Sidransky and Lopez 2012) so that heterozygous *GBA* mutations are best considered as risk variants rather than specific

disease-causing mutations. Nevertheless, in the multi-centre study, heterozygous *GBA* mutations were detected in 7% of PD cases from non-Ashkenazi Jewish ethnicities where the whole *GBA* locus was sequenced (Sidransky et al. 2009).

It is particularly interesting that carriers of heterozygous mutations in *GBA* should be at risk of developing PD, a disease that is significantly different from Gaucher's disease, and also that the N370S mutation should be a large part of the association when this is a mutation that is more generally seen in non-neuronopathic Gaucher's patients. Further, while Gaucher's disease is caused by the loss of enzymatic activity through loss-of-function mutations, the role of *GBA* mutations in the pathogenesis of PD is not clear; *GBA* mutations have been proposed to play either a loss-of-function role, e.g. by reducing lysosomal function with subsequent accumulation of alpha-synuclein, or a gain-of-function role, e.g. by accumulation of the mutant protein, blocking pathways for protein synthesis and degradation (Sidransky and Lopez 2012).

A number of PD patients within the Oxford Parkinson's Disease Cohort have been identified carrying heterozygous N370S and L444P mutations, and iPSC clones have been made from several individuals. A study performed predominantly by Dr H.R. Fernandes in this laboratory compared iPSC-derived dopaminergic neuronal cultures made from individuals in the cohort bearing *GBA* N370S with those from healthy controls (Fernandes et al. 2016). Principal findings from this study relating to the *GBA* N370S/wt genotype were: (1) impaired autophagy shown by increased levels of the autophagosomal marker LC3B-II, lysosomal markers LAMP1 and LAMP2A, and the autophagic chaperone protein p62/Sequestosome-1; (2) activation of endoplasmic reticulum (ER) stress through misfolding of mutant β-glucocerebrosidase enzyme, evidenced by upregulation of chaperones BiP and calreticulin, and effectors calnexin, IRE1α and PDI; (3) increased extracellular release of α-synuclein into the surrounding medium; (4) increased LC3+ puncta and larger lysosomal area within TH+

neurons (Fernandes et al. 2016). In summary, these findings were interpreted in the context that the *GBA* N370S mutation resulted in both gain and loss of function phenotypes, wherein blockage of mutant protein confers ER stress and reduced enzymatic activity results in autophagic deficits with the result that more α-synuclein is released from the cell instead of being degraded (Fernandes et al. 2016).

Some clinical presentations of PD in *GBA* mutation carriers overlap with features associated with *MAPT*. *GBA* mutation carriers are more likely to experience cognitive decline/dementia within PD (Brockmann et al. 2011; Setó-Salvia et al. 2012), which is additionally associated with the H1/H1 genotype (Williams-Gray et al. 2009); this suggests disease-modifying roles for both loci outside of the dopaminergic system. Multiple studies have also found associations of the *MAPT* H1 allele and *GBA* mutations with younger age of onset (Nichols et al. 2009; Sidransky et al. 2009; Benitez et al. 2016; Davis et al. 2016). Finally, dysregulated iron metabolism has been reported in Gaucher's patients (Stein et al. 2010), while brains and primary neurons of tau knockout mice showed increased iron accumulation as well as degeneration of SNpc dopaminergic neurons (Lei et al. 2012).

Despite the above, no clear association has been made between *GBA* and *MAPT*; however, as another protein associated with the same disease, tau may play an associative role in PD phenotypes already displayed in other models and may modify the penetrance of *GBA* mutations with respect to PD. In particular, tau is involved in axonal transport and trafficking within neurons and intracellular transport is critical for many neuronal processes including in bringing sub-cellular compartments together for autophagy and in secretion of vesicles. Notably, axonal transport and autophagy are interlinked: transport is required to bring autophagosomes and late endosomes back to the soma for degradation (Cai et al. 2010; Maday et al. 2012), while inhibition of lysosomal function has a negative effect on their axonal transport (Lee et al. 2011). With this in mind, some of the phenotypes displayed by

carriers of *GBA* mutations described above (Fernandes et al. 2016) involve processes that depend on axonal transport. I therefore reasoned that perturbing tau function in *GBA* N370S cells that already show PD-related phenotypes could enhance or suppress those phenotypes and thus reveal disease-related pathways in which tau plays a modulatory role.

6.1.1 Aims of the Chapter

- To describe the further use of the total *MAPT* shRNA construct generated in chapter 5 to perform short-term knockdown of *MAPT* in iPSC-derived dopaminergic neuronal cultures with and without heterozygous N370S mutation of *GBA*. This is to investigate a modulatory effect of tau on biochemical phenotypes seen in previous PD models (Fernandes et al. 2016).

6.2 Methods

6.2.1 Genotyping of GBA *N370S mutation*

Genotyping assays for the *GBA* c.1226A>G (p.N370S) mutation were performed as previously described (Aharon-Peretz et al. 2004) using a forward primer that introduces a *Xho*I restriction site by one nucleotide mismatch (see Appendix Table E with mismatch shown in red). AmpliTaq Gold PCR (section 2.5.1) was performed with an annealing temperature of 56°C, followed by *Xho*I analytical restriction digest and separation on a 3% (w/v) low-melt agarose gel.

6.2.2 Glucocerebrosidase enzyme activity assay

The enzyme activity of glucocerebrosidase was determined by cleavage of 4-methylumbelliferyl β-D-glucopyranoside (4-MUGlc) as previously described (Fernandes et al. 2016) with minor modifications. Briefly, protein extraction and BCA assay were performed as described in section 2.8.1, with the exception that instead of RIPA buffer, lysis was performed in 50 µl GCase lysis buffer (citrate phosphate buffer [22.2 mM citric acid, 55.6 mM dibasic sodium phosphate, pH 5.4] with 0.25% (v/v) Triton-X100, 0.25% (w/v) taurocholic acid and cOmplete Mini protease inhibitor cocktail [Roche]). Lysates were not frozen between protein extraction and the activity assay. For the activity assay, 0.5 µg protein in 10 µl GCase lysis buffer was added to quadruplicate wells of a 96-well flat-bottomed transparent plate. The irreversible glycosidase inhibitor conduritol B epoxide (CBE) was used to determine the background degradation of substrate without enzyme activity; 25 mM CBE (Enzo Life Sciences) in water was diluted 5X to 5 mM with GCase lysis buffer then 10 µl 5mM CBE was added to one well per sample and the remaining three wells received the equivalent 10 µl water/GCase lysis buffer. After incubation (37°C, 30 min) to

allow inhibition, 100 µl 5 mM 4-MUGlc in GCase lysis buffer was added to each well and the plate was incubated (37°C, 2 hours) for enzyme activity. Reactions were stopped by addition of 150 µl 50 mM glycine, 38.6 mM sodium hydroxide, pH 10.4. Fluorescence was read on a Synergy HT plate reader (BioTek) using excitation filter 360/40, emission filter 440/40, and multiple gain settings to get fluorescence values to around 30,000 units. Fluorescence from CBE-treated wells was subtracted from the remaining three wells to determine specific enzyme activity.

6.2.3 Western blotting

All protein samples were prepared for the β-glucocerebrosidase enzyme activity assay then frozen at -80°C until use for Western blotting. Subsequent dilutions were made with GCase lysis buffer prior to addition of Laemmli buffer, then Western blotting was performed as described in section 2.8.1 *iii*.

6.3 Results

6.3.1 Selection of human iPSC clones bearing GBA *N370S mutation*

The Oxford Parkinson's Disease Cohort includes individuals that have been identified bearing the N370S or L444P mutations in *GBA*. The *MAPT* genotype of these individuals was identified by distinguishing the H1 and H2 alleles using the 238 bp indel in intron 9, revealing that all of the N370S individuals were homozygous for the H1 allele. Matching sets of iPSC clones were chosen for each group: four H1/H1 clones with *GBA* N370S mutation designated GBA1, GBA2, GBA3 and GBA4, and four H1/H1 clones with wild type *GBA* designated Con1, Con2, Con3 and Con4 (Appendix Table F). Both groups consisted of one individual with a single clone reprogrammed by retroviruses, one individual with a pair of clones reprogrammed by retroviruses and one individual with a single clone reprogrammed by non-integrating Sendai virus. The *GBA* N370S (c.1226A>G) heterozygous mutation was confirmed in each of the eight clones by genotyping PCR with *Xho*I digestion, with the c.1226A>G mutation completing the restriction site only in the GBA1-4 clones (Fig. 6.1A). Confirmation of the H1/H1 genotype for all eight clones is shown (Fig. 6.1B) compared to the heterozygous H1/H2 clones detailed in chapter 4.

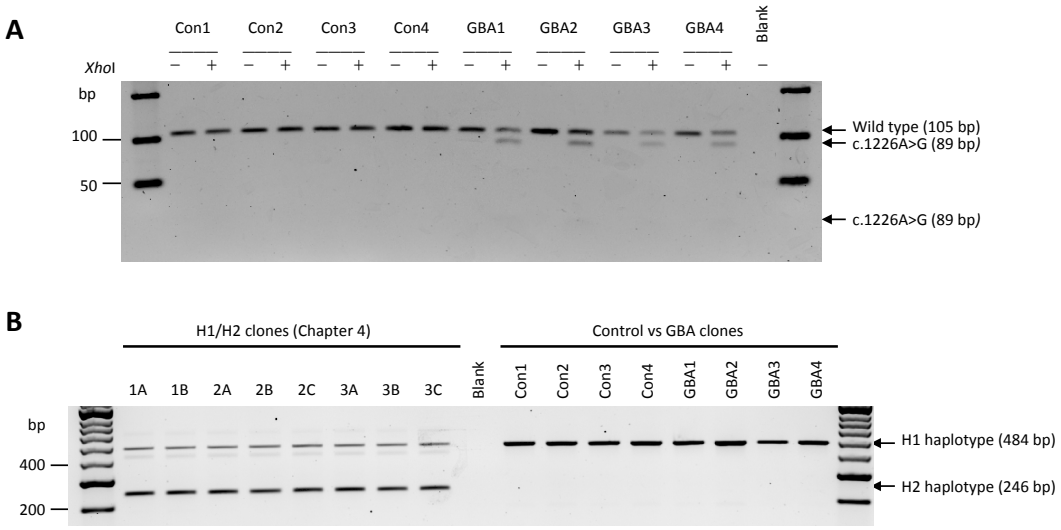

Figure 6.1: Genotyping of clones from controls and *GBA* N370S PD patients used in this study.
(A) Agarose gel electrophoresis of the genotyping PCR to distinguish the *GBA* c.1226A>G mutant allele (corresponding to N370S mutation of the protein) from the wild type allele. The presence of the mutation was revealed by *Xho*I digestion (lanes marked +) that cleaves mutant alleles only.
(B) Agarose gel electrophoresis of the genotyping PCR to distinguish the H1 and H2 alleles of *MAPT* by the 238 bp indel in intron 9. Lanes 2-9, the eight iPSC clones with H1/H2 genotype used in chapter 4 (see Fig. 4.1) included here to show the position of the two bands; lanes 11-18, the eight iPSC clones from part A showing that all were homozygous H1 genotype.

6.3.2 Characterisation of iPSC-derived dopaminergic neuronal cultures bearing GBA *N370S mutation following knockdown of tau protein*

The eight iPSC clones were differentiated into midbrain-type dopaminergic neuronal cultures, identified by cells co-expressing TH/Tuj1 in addition to the transcription factor FOXA2 (Fig. 6.2). Although there were some differences between individual clones in terms of efficiency of differentiation (Fig. 6.3A), overall the percentages of TH+, Tuj+ and TH+/Tuj+ cells were not significantly different between control and *GBA* N370S groups (Fig. 6.3B).

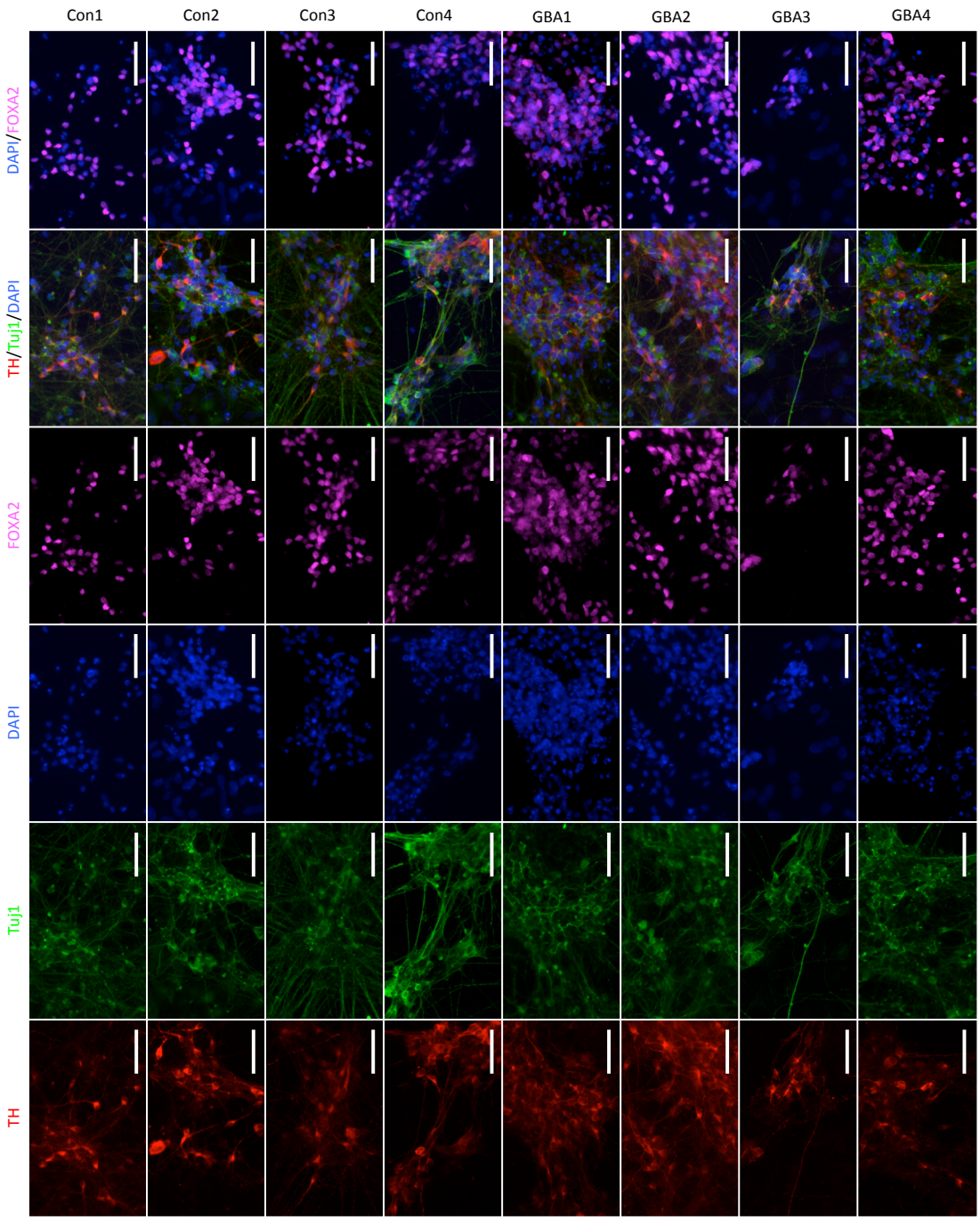

Figure 6.2: Immunocytochemistry of iPSC-derived dopaminergic neuronal cultures with *GBA* N370S mutation.

Fluorescence images of immunocytochemistry performed on cultures fixed at DIV36. All eight lines generated TH+/Tuj+ dopaminergic neurons and most nuclei were positive for the embryonic floor-plate marker FOXA2 confirming correct patterning to a ventral midbrain identity. Scale bars, 50 µm.

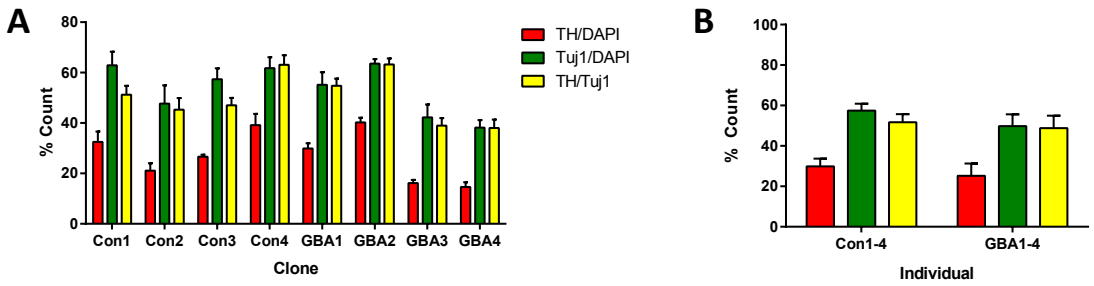

Figure 6.3: Cell counts of immunocytochemistry of iPSC-derived dopaminergic neuronal cultures with *GBA* N370S mutation.
(A-B) Percentage of cells expressing tyrosine hydroxylase (TH, red) or neuron-specific β3-tubulin (Tuj1, green) as a percentage of total cells counterstained by DAPI. Percentage of Tuj1+ cells co-expressing TH is shown in yellow. Counts shown (A) per clone and (B) per genotype. No significant difference between genotypes for any of the three counts using *t*-tests. Mean ±SEM percentages for Con1-4: TH/DAPI, 29.9% ±3.9%; Tuj1/DAPI, 57.4% ±3.5%; TH/Tuj1, 51.7% ±4.0%. Mean ±SEM percentages for GBA1-4: TH/DAPI, 25.2% ±6.1%; Tuj1/DAPI, 49.8% ±5.9%; TH/Tuj1, 48.8% ±6.2%.

Three differentiations were performed, each incorporating delivery on DIV20 of lentiviral particles encoding shRNA targeting total *MAPT* or a non-targeting (NT) shRNA control. Cells were harvested at DIV36 for analysis. Transduction with lentiviral particles at MOI 5 resulted in clear expression of the reporter protein EBFP2 in most cells (Fig. 6.4). Delivery of lentiviral particles had a visible effect on these cultures whether the particles encoded *MAPT* shRNA or NT shRNA, as evidenced by overall reduced density of neurites (Fig. 6.4).

All cell lysates were first processed for glucocerebrosidase enzyme activity assay. The assay confirmed the effect of the *GBA* N370S genotype on glucocerebrosidase enzyme activity, being at 68% of the level of control clones (one-way ANOVA effect of genotype, p=0.0017; Fig. 6.5). In contrast, no difference was observed with treatment (one-way ANOVA effect of treatment, p=0.3744), and within a treatment the proportional difference in enzyme activity between genotypes is similar between the three treatments (*GBA* N370S vs. control: untransduced, 67.5%; *MAPT* shRNA, 70.7%; NT shRNA, 66.2%).

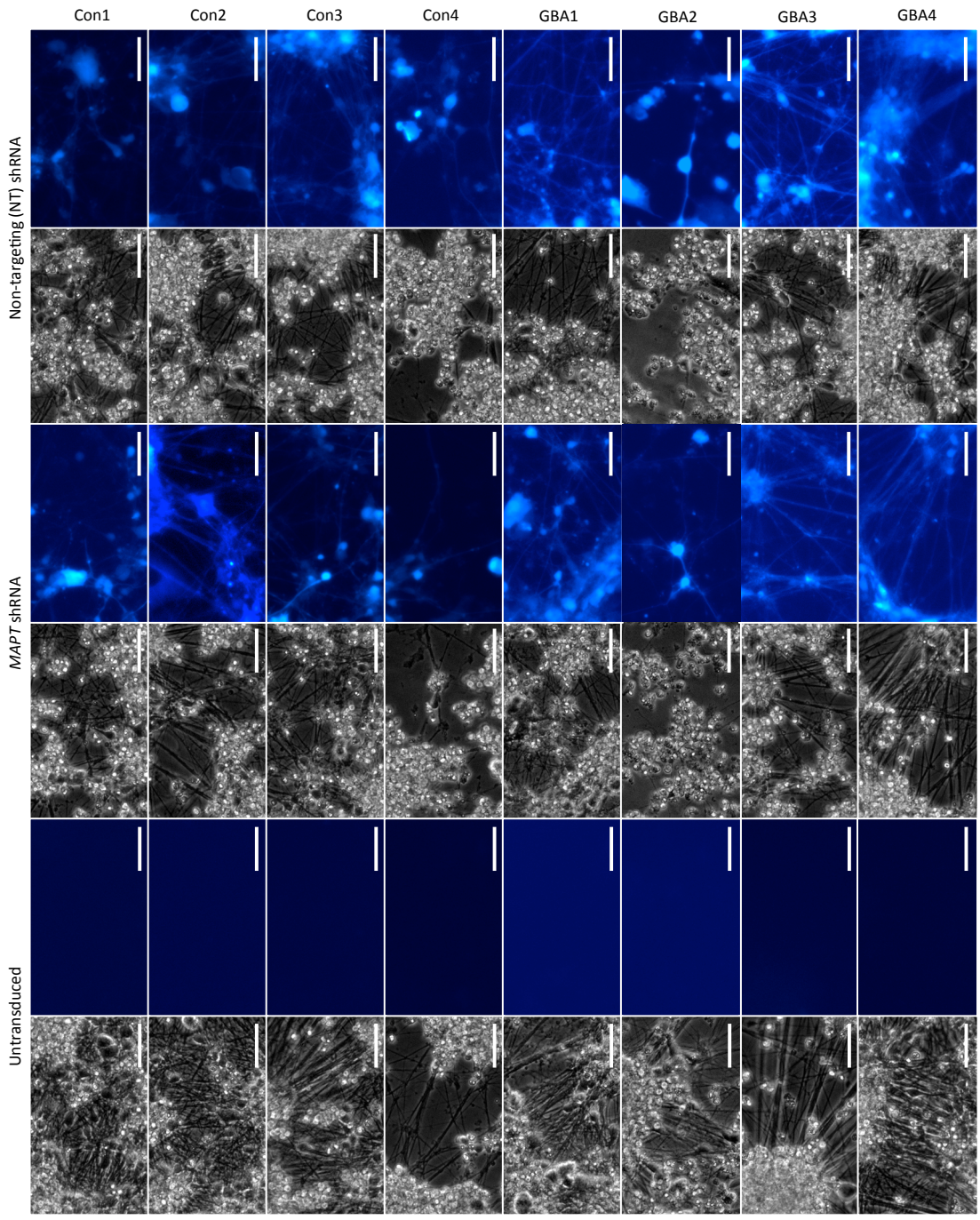

Figure 6.4: Transduction of iPSC-derived dopaminergic neuronal cultures with shRNA-bearing lentiviral particles.

Images of EBFP2 expression with corresponding phase contrast images, taken 16 days after transduction (DIV36) prior to harvesting. Images taken with EVOS FL AUTO using TagBFP filter cube. All transduced cultures expressed EBFP2 in most cells following delivery of lentiviral particles at MOI 5. The density of cells and neurites was noticeably reduced in all cultures treated with lentiviral particles compared to their untransduced controls showing that lentiviral treatment alone had an effect on these cultures. Scale bars, 50 µm.

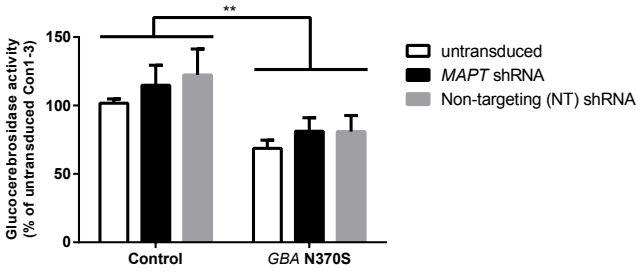

Figure 6.5: Glucocerebrosidase activity assay in iPSC-derived dopaminergic neuronal cultures transduced with lentiviral constructs expressing shRNA.
Combined enzyme activity assay results for clones Con1-4 and GBA1-4, expressed as percentage of untransduced Con1-3 in order to average across differentiations. Mean ±SEM, each bar n=4 clones, three independent differentiations except clones Con4 and GBA2 (two differentiations only). Asterisks represent statistically significant difference in two-way ANOVA: genotype, p=0.0017, F=13.60; treatment, p=0.3744, F=1.04; genotype x treatment, p=0.9285, F=0.074. Mean ±SEM: control untransduced, 101.7% ±3.1%; *GBA* N370S untransduced, 68.7% ±6.0% (67.5% of control untransduced); control *MAPT* shRNA, 114.8% ±14.6%; *GBA* N370S *MAPT* shRNA, 81.2% ±9.9% (70.7% of control *MAPT* shRNA); control NT shRNA, 122.3% ±19.1%; *GBA* N370S NT shRNA, 80.9% ±11.8% (66.2% of control NT shRNA); overall mean of all controls, 112.9% ±7.7%; overall mean of *GBA* N370S, 76.9% ±5.3% (68.1% of control).

Cell lysates were analysed for the levels of eight proteins by Western blotting (Figs. 6.6-6.7, Table 6.2): tau to determine shRNA-mediated knockdown, glucocerebrosidase, α-synuclein, the ER stress marker BiP, and autophagy markers LAMP1, LAMP2A, p62, and the lipidated form of LC3B (LC3B-II, either individually or as a ratio with the non-lipidated form LC3B-I). First, these data revealed that most proteins showed a high degree of inter-clone variability even in untransduced cultures. This is displayed by the spread of data points, each representing a single clone, particularly for the levels of tau (Fig. 6.7A), α-synuclein (Fig. 6.7C), LAMP1 (Fig. 6.7E), LAMP2A (Fig. 6.7F), p62 (Fig. 6.7G) and LC3B-II (Fig. 6.7H). Second, these data failed to show a difference between genotypes for any protein except GBA (Fig. 6.7B), which, other than tau and α-synuclein, is the only protein that was not expected to be different between genotypes (Fernandes et al. 2016). GBA levels in *GBA* N370S cultures were lower than in controls (two-way ANOVA, p=0.0005), and seen in each

treatment group (*GBA* N370S vs. control: untransduced, 71.2%; *MAPT* shRNA, 78.7%; NT shRNA, 83.1%). The GBA protein level data complicate the interpretation of the reduced glucocerebrosidase enzyme activity data (Fig. 6.5) as the reduced activity could be mostly explained by a reduction in GBA protein levels instead of a direct effect of the N370S mutation. Third, there was a statistically significant effect of treatment only on the levels of tau protein (two-way ANOVA, p=0.0023), although the high variability between clones prevented individual groups from reaching significance in the Bonferroni multiple comparisons test when all pairwise comparisons were made for the six groups.

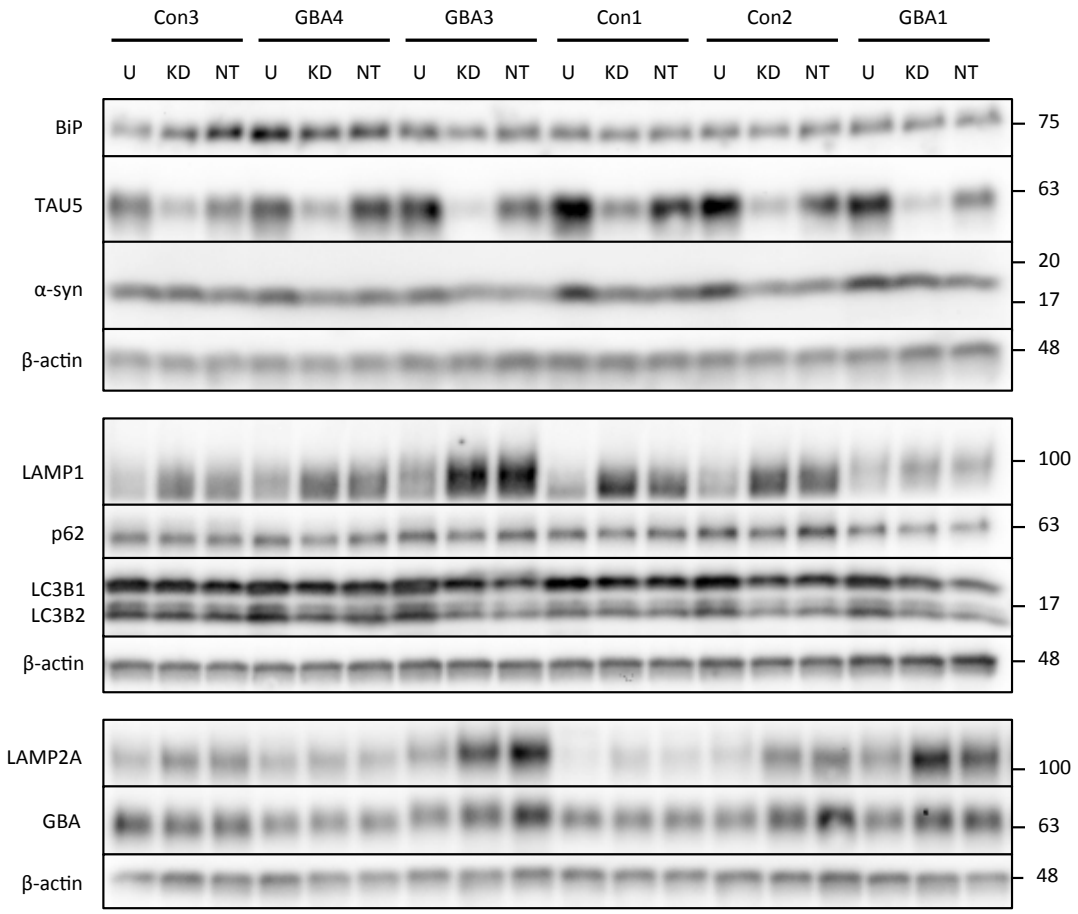

Figure 6.6: Western blot analysis in iPSC-derived dopaminergic neuronal cultures with *MAPT* knockdown and *GBA* N370S mutation.
Chemiluminescence images of representative Western blots against eight proteins of interest. U, untransduced; KD, *MAPT* shRNA; NT, non-targeting shRNA. Quantification of blots from three differentiations is presented in Fig. 6.7.

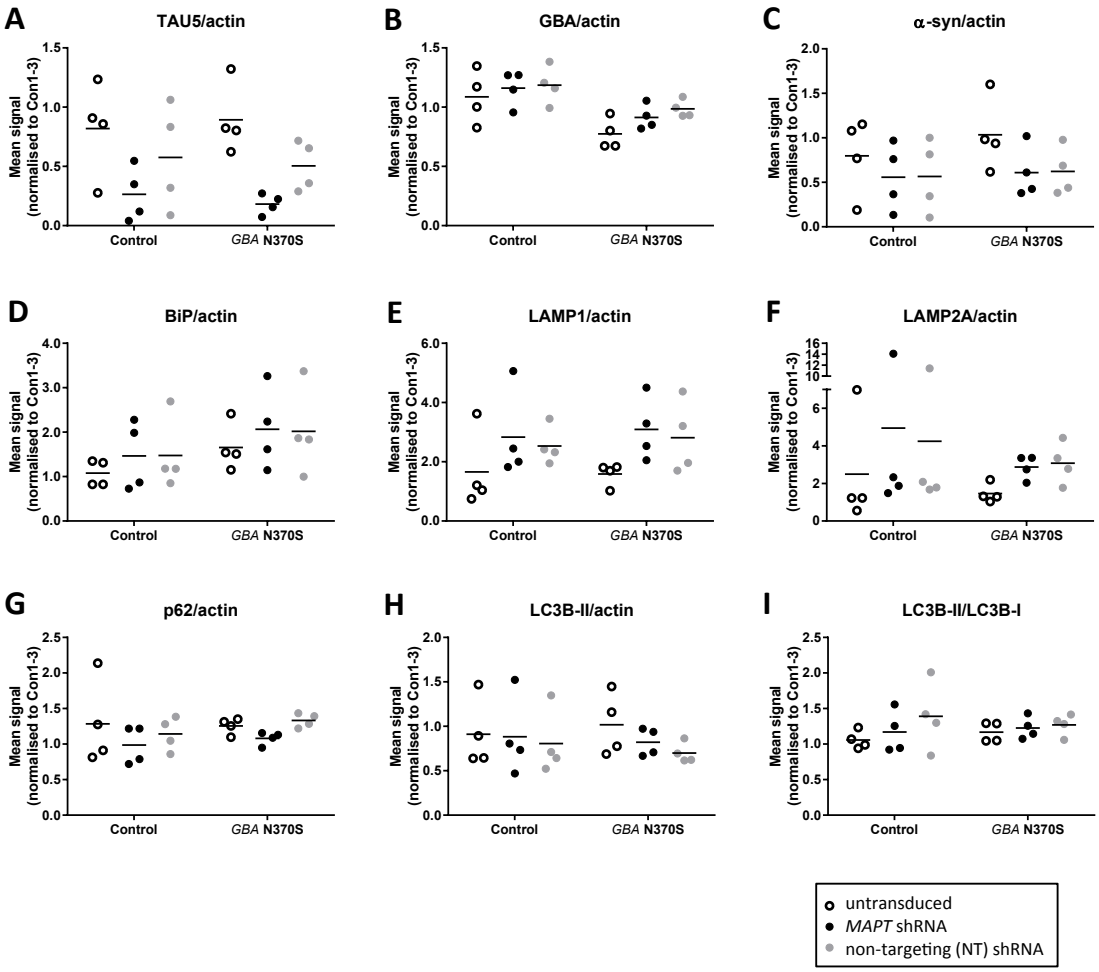

Figure 6.7: Quantification of Western blot analysis in iPSC-derived dopaminergic neuronal cultures with *MAPT* knockdown and *GBA* N370S mutation.

(A-I) Graphs of quantification of Western blots for (A) tau, (B) GBA, (C) α-synuclein, (D) BiP, (E) LAMP1, (F) LAMP2A, (G) p62, (H) LC3B-II and (I) LC3B-II as a ratio with LC3B-I. All quantification was performed with β-actin as a loading control. Lines represent mean of n=4 clones per genotype, with each clonal value shown as a dot being the mean from three independent differentiations except clones Con4 and GBA2 (two differentiations only). Data are normalised to the mean of untransduced Con1/Con2/Con3 from each blot to enable comparisons of blots/differentiations. Statistical data for these graphs are provided in Table 6.2.

Table 6.2: Two-way ANOVA statistics for quantification of Western blot analysis.

Protein	ANOVA Source of Variation	*p* value	*p* value summary	F
Tau	Genotype	0.8326	ns	0.046
	Treatment	**0.0023**	**	**8.667**
	Genotype x Treatment	0.8500	ns	0.164
GBA	**Genotype**	**0.0005**	***	**17.66**
	Treatment	0.1282	ns	2.307
	Genotype x Treatment	0.7482	ns	0.295
α-Syn	Genotype	0.4598	ns	0.571
	Treatment	0.1561	ns	2.063
	Genotype x Treatment	0.8510	ns	0.163
BiP	Genotype	0.0817	ns	3.402
	Treatment	0.5105	ns	0.698
	Genotype x Treatment	0.9972	ns	0.003
LAMP1	Genotype	0.7322	ns	0.121
	Treatment	0.0600	ns	3.303
	Genotype x Treatment	0.9389	ns	0.063
LAMP2A	Genotype	0.3246	ns	1.026
	Treatment	0.4885	ns	0.746
	Genotype x Treatment	0.9477	ns	0.054
p62	Genotype	0.4921	ns	0.492
	Treatment	0.2486	ns	0.249
	Genotype x Treatment	0.7597	ns	0.760
LC3B-II	Genotype	0.8818	ns	0.023
	Treatment	0.4551	ns	0.823
	Genotype x Treatment	0.7961	ns	0.231
LC3B-II/LC3B-I	Genotype	0.8871	ns	0.021
	Treatment	0.2667	ns	1.424
	Genotype x Treatment	0.6557	ns	0.432

To overcome the problem of clonal variability and to increase statistical power, the specific effects of shRNA treatment on each clone were determined as the fold change between *MAPT* shRNA and NT shRNA treatments and maintained in the two genotype groups (Fig. 6.8) with statistical analysis by one-sample *t*-test from a value of 1 (Table 6.3). Only two proteins were significantly and specifically altered by *MAPT* knockdown. Compared to NT shRNA, *MAPT* shRNA knocked down tau protein by 58% in controls and by 69% in *GBA* N370S cultures (Fig. 6.8A, Table 6.3). Further, p62 levels were significantly lower with *MAPT* shRNA treatment by 15% in *GBA* N370S cultures (Fig. 6.8G, Table 6.3). However, after Bonferroni correction, reducing the significance threshold to α=0.000277, only tau knockdown in *GBA* N370S cultures remained significant.

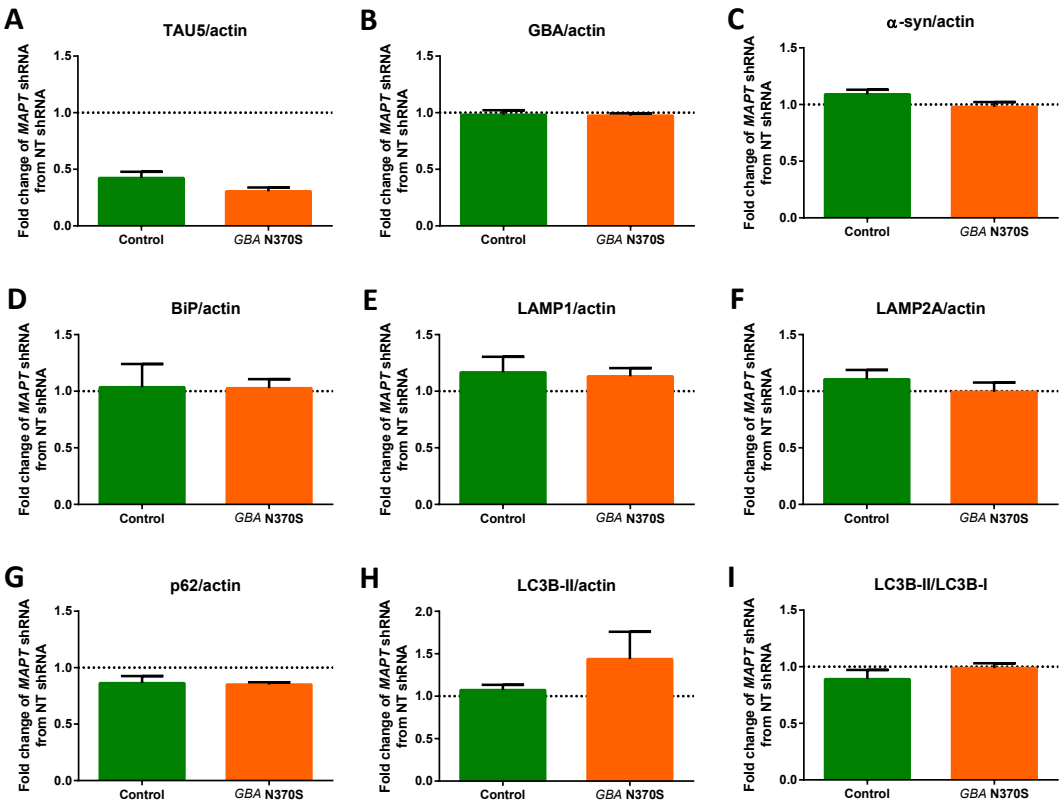

Figure 6.8: Determination of the effect of *MAPT* knockdown on Western blot data from iPSC-derived dopaminergic neuronal cultures with *GBA* N370S mutation.
Graphs showing the relative quantification of protein levels from Western blots in conditions of shRNA-mediated *MAPT* knockdown vs delivery of non-targeting shRNA.
(A-I) Western blot data for (A) tau, (B) GBA, (C) α-synuclein, (D) BiP, (E) LAMP1, (F) LAMP2A, (G) p62, (H) LC3B-II and (I) LC3B-II as a ratio with LC3B-I. All quantification was performed with β-actin as a loading control. Mean ±SEM, n=4 clones per genotype; clonal means derive from three independent differentiations except clones Con4 and GBA2 (two differentiations only). Statistical data for these graphs are provided in Table 6.3.

Table 6.3: One-sample *t*-test statistics for quantification of Western blot analysis.

Protein	Genotype	Mean	*p* value	*t*	df
Tau	Control	0.423	**0.0019**	10.47	3
	GBA N370S	0.306	**0.0002**	20.92	3
GBA	Control	0.982	0.6846	0.448	3
	GBA N370S	0.975	0.2886	1.286	3
α-Syn	Control	1.091	0.1016	2.336	3
	GBA N370S	0.979	0.6616	0.484	3
BiP	Control	1.035	0.8739	0.173	3
	GBA N370S	1.026	0.7664	0.325	3
LAMP1	Control	1.167	0.3145	1.205	3
	GBA N370S	1.132	0.1637	1.836	3
LAMP2A	Control	1.106	0.2864	1.294	3
	GBA N370S	0.994	0.9481	0.071	3
p62	Control	0.863	0.1179	2.175	3
	GBA N370S	0.851	**0.0046**	7.658	3
LC3B-II	Control	1.073	0.3199	1.189	3
	GBA N370S	1.437	0.2684	1.355	3
LC3B-II/LC3B-I	Control	0.891	0.2733	1.338	3
	GBA N370S	0.988	0.7946	0.284	3

As genotype was not a significant factor in the analysis of variance for any protein except GBA (Table 6.2), the effect of *MAPT* knockdown was examined in the eight clones regardless of genotype (Fig. 6.8, Table 6.4). With the power of eight clones, tau knockdown was highly significant ($p<0.0001$) with a mean reduction by 63.5% across the clones (Fig. 6.8, Table 6.4). The reduction of p62 protein with tau knockdown was also statistically significant ($p=0.0023$; Bonferroni adjusted $p=0.0207$), averaging 14.3% reduction compared to NT shRNA (Fig. 6.8, Table 6.4). No other proteins showed any significant difference due to tau knockdown.

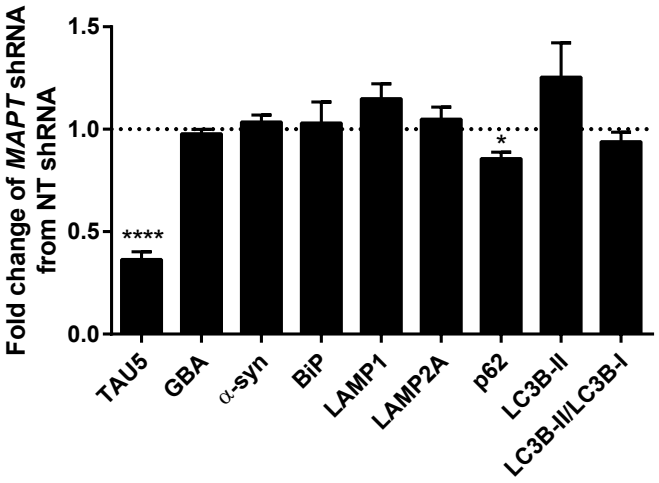

Figure 6.9: Determination of the effect of *MAPT* knockdown on Western blot data from iPSC-derived dopaminergic neuronal cultures regardless of genotype.
Combined graph of quantification of Western blots as per Figure 6.7 with the data for each protein combined regardless of genotype. Mean ±SEM, n=8 clones; clonal means derive from three independent differentiations except clones Con4 and GBA2 (two differentiations only). Statistical data for this graph are provided in Table 6.4.

Table 6.4: One-sample *t*-test statistics for quantification of Western blot analysis without segregation by genotype.

Protein	Mean	*p* value	*t*	df
Tau	0.365	**< 0.0001**	17.12	7
GBA	0.979	0.3310	1.044	7
α-Syn	1.035	0.3376	1.029	7
BiP	1.031	0.7713	0.302	7
LAMP1	1.149	0.0780	2.063	7
LAMP2A	1.050	0.4161	0.864	7
p62	0.857	**0.0023**	4.679	7
LC3B-II	1.255	0.1704	1.528	7
LC3B-II/LC3B-I	0.939	0.2325	1.307	7

6.4 Discussion

6.4.1 GBA *N370S phenotypes*

The phenotypes previously seen in *GBA* N370S heterozygous cultures (Fernandes et al. 2016) were not detected in the present study. Notably, the degree of variability in the protein expression data made it too difficult to observe smaller differences due to genotype.

There were three key differences between the published and present studies. First, the differentiation protocols used were not the same; in particular the present study used mitomycin C to remove proliferating cells and so generated a higher percentage of Tuj1+ neurons in the final cultures, those from the published study being on average <40% Tuj1+ (Fernandes et al. 2016) compared to the present study average of 50% Tuj1+. Second, some of the clones used in this study were different to those used in the published study, although it is not expected that this is the reason. Ideally a larger set of clones would have been tested first to identify those that differentiated equally well, but I chose to balance several factors including *MAPT* genotype, restricting the controls to H1 homozygotes to match the four *GBA* N370S clones. Third, the published study performed at least five differentiations per phenotype with several Western blots per differentiation set. If there had there been enough protein yield in the present study to run several blots per differentiation, this would have helped to reduce spread in the data from this semi-quantitative technique.

The activity of β-glucocerebrosidase enzyme was reduced in *GBA* N370S cultures as expected; however, the reduction was only to 68% of the level of controls instead of the reported 50%, and the level of β-glucocerebrosidase protein was a confounding issue wherein *GBA* N370S cultures showed a difference according to genotype (Fig. 6.7B, Table 6.2). Again this could be due to differences in the differentiation protocol, as another

study also using the Kriks protocol found that both enzyme activity and protein levels were reduced in patient lines (Woodard et al. 2014).

Some additional phenotypes have been observed in iPSC-derived dopaminergic neurons by other groups using the Kriks or Seibler differentiation protocols (Kriks et al. 2011; Seibler et al. 2011). Of note, lines with *GBA* N370S/wild-type or N370S/c.84dupG showed an increase in intracellular α-synuclein (Mazzulli et al. 2011; Woodard et al. 2014), and α-synuclein reduced β-glucocerebrosidase enzyme activity in the lysosome, whether with α-synuclein overexpression, the *GBA* N370S/c.84dupG Gaucher's disease line or idiopathic PD lines (Mazzulli et al. 2016).

6.4.2 Effects of tau knockdown

All subsequent analysis was performed by directly comparing *MAPT* shRNA and NT shRNA control to determine the effect of tau knockdown on protein levels of interest both with and without segregation by genotype. This reduced noise in the data and enabled clearer observation of phenotypes, notably the evident knockdown of tau itself. The ideal experiment would have used more than one shRNA to target *MAPT* to validate the effect of knockdown, although this is not always observed in practice. The data regarding p62 presented here ought to be confirmed with further knockdown experiments using multiple shRNA constructs and a pre-determined statistical design informed by the current data.

6.4.3 Tau, p62 and macroautophagy

p62, or sequestosome-1, is a protein adaptor that chaperones ubiquitinated proteins for degradation by macroautophagy (Lamark et al. 2009) or the proteasome (Seibenhener et al.

2004). Macroautophagy is the predominant route of autophagy wherein material to be degraded associates with a membrane bilayer called a phagophore that encloses the material in a double membrane bound autophagosome, later fusing with a lysosome to deliver the degradation machinery (Xie and Klionsky 2007). p62 remains bound to its targets and therefore is itself degraded by macroautophagy (Lamark et al. 2009) and a block in macroautophagy increases p62 levels (Bjørkøy et al. 2005).

Starvation on a timescale of a few hours leads to reduced levels of p62, which eventually return to normal levels on extended starvation (Sahani et al. 2014). Sahani and colleagues identified three factors controlling the levels of p62 during starvation: macroautophagy that reduces p62, starvation-induced increase in p62 mRNA, and the availability of the necessary amino acids to synthesise p62, themselves liberated by macroautophagy (Sahani et al. 2014). If reduced tau levels facilitated macroautophagy, this facilitation may reduce the levels of p62 without inducing increased transcription of p62. As the levels of LAMP1, LAMP2A and LC3B-II were not significantly different with tau knockdown, the other components of the autophagic process may be able to regulate their levels more consistently. The other route for altering p62 levels would be through reduced transcription; however, it is unclear how tau knockdown would affect this.

How could reduced tau facilitate macroautophagy? In chapter 5 I showed how reduction of total *MAPT* transcripts in short-term culture resulted in increased motility of axonal transport cargo. Providing that the level of reduction of tau protein were not deleterious to microtubule stability, cargo would be less hindered in its movement along microtubules. Most evidence, including my own long-term culture knockdown data in chapter 5, suggests that tau impacts primarily on kinesin-mediated anterograde transport (Dixit et al. 2008). However, in neurons, autophagosomes containing damaged proteins/organelles form in the cell periphery and are transported to the soma by dynein-mediated retrograde transport,

fusing with lysosomes early in the process (Maday et al. 2012). Lysosomes are themselves regulated in their location in a manner that alters the rate of autophagosome-lysosome fusion (Korolchuk et al. 2011); in non-neuronal cells fusion is increased when lysosomes are close to the nucleus (Korolchuk et al. 2011), whereas fusion in neurons takes place within axons far from the soma (Maday et al. 2012). Additionally, the macroautophagy machinery proteins, particularly Atg9 that is key to the initial formation of autophagosomes (Legakis et al. 2007), require anterograde transport along axons and could be a link between improved transport and facilitated macroautophagy.

Alternatively, dynein-mediated retrograde transport itself could be altered in conditions of tau knockdown, especially as total tau knockdown affected the velocity of both unidirectional and bidirectional mitochondria in the mature cultures in chapter 5. Tau inhibited dynein-mediated retrograde transport in cell-free studies, although to a lesser degree than for kinesin-mediated anterograde transport (Dixit et al. 2008). Tau also interacts directly with the dynactin complex that functions alongside dynein, although tau was shown to favourably increase interaction of the dynactin complex with microtubules rather than play an inhibitory role (Magnani et al. 2007). Alternatively, kinesin remains attached to autophagosomes during dynein-mediated retrograde transport (Maday et al. 2012) and is necessary for motility of dynein, at least in *Drosophila* (Martin et al. 1999; Pilling et al. 2006). Even if kinesin is not the active motor during the autophagic process, it is possible that improved anterograde transport of kinesin to the distal end of axons could increase the concentration of kinesin to increase initiation of macroautophagy. Additional work would be needed to provide further insight.

Chapter 7: General Discussion

The two broad aims of this thesis were: (1) to investigate the haplotype-specific expression of *MAPT* in iPSC-derived dopaminergic neuronal cultures as an underlying determinant for risk for PD; (2) to investigate the consequent effect of the level of expression of tau and its isoforms on neuronal function in iPSC-derived dopaminergic neuronal cultures.

7.1 Investigation of *MAPT* expression in iPSC-derived dopaminergic neuronal cultures

In Chapter 4 I determined the degree of haplotype-specific control of the expression of *MAPT* in iPSC-derived dopaminergic neuronal cultures and post-mortem human midbrain containing *substantia nigra*. The use of cultures that had been matured for six months enabled clear detection of all six major isoforms of tau protein expressed in the adult CNS and gave confidence that the isoform detection in qRT-PCR assays would be robust and not affected by stochastic differences that could be the case when expression levels are low. Expression assays that did not specify haplotype were used to show the increasing inclusion of adult exons 3 and 10 over the six months' maturation so that by six months the inclusion of exon 3 in iPSC-derived cultures was comparable to that of post-mortem midbrain and the inclusion of exon 10 in iPSC-derived cultures was approximately half that detected in post-mortem midbrain. Through the use of allele-specific qRT-PCR assays developed by myself and Dr M-C.Lai I showed that expression of transcripts encoding 2N tau, 4R tau and total tau were under haplotype-specific control, though differing between iPSC-derived dopaminergic neuronal cultures and post-mortem human midbrain. The strongest effect seen was for exon 3+ transcripts encoding 2N tau, wherein the H2 allele expressed two-fold more than

the H1 allele in all sample sets, corroborating previous findings in other brain regions (Caffrey et al. 2008; Trabzuni et al. 2012). Post-mortem human midbrain only showed haplotype-specific control of exon 10+ transcripts encoding 4R tau and not of total *MAPT* transcripts reflecting promoter strength and/or transcript stability, which data matched those of the globus pallidus and frontal cortex as previously determined in our laboratory (Caffrey et al. 2006); the H1 allele expressed 1.2-fold more exon 10+ transcripts than the H2 allele. However, iPSC-derived dopaminergic neuronal cultures showed no haplotype-specific control of exon 10+ transcripts, but rather a haplotype-specific control of total transcripts, being 1.2-fold more from the H1 allele than the H2 allele. Generally the supporting evidence for haplotype-specific control of total *MAPT* expression has come from cell culture models and promoter-luciferase constructs (Kwok et al. 2004; Caffrey et al. 2006; Myers et al. 2007a) given that the studies of post-mortem human brain have been vulnerable to problems with polymorphisms within microarray probes (Trabzuni et al. 2012; Ramasamy et al. 2013). The haplotype-specific control of total *MAPT* and exon 10+ transcripts could therefore be one aspect in which the chromatin environment, other epigenetic markings, or complement of transcription factors makes a difference between cultured cells and true aged human brain.

Despite the differences in haplotype-specific control of *MAPT* seen between iPSC-derived dopaminergic neuronal cultures and post-mortem human midbrain, the iPSC-derived cultures were well placed to reveal differences in *MAPT* expression as a result of specific variation, namely a newly discovered deletion (ΔCTT) in intron 10. The variant increased overall inclusion of exon 10 by over 40%, which allele-specific analysis revealed was due to a two-fold increase in expression of exon 10+ transcripts from the ΔCTT allele. The variant confirmed the importance of that region of intron 10 in regulating exon 10 inclusion (Kar et al. 2006). When stem cells are not available with a particular variant, both ESCs and iPSCs are amenable to genome editing to generate isogenic lines that include or remove specific

variants to examine their effect in a cell type of interest following differentiation; this has been reported recently with editing of *SNCA* variation in ESCs followed by differentiation to cortical cultures where allele-specific qRT-PCR revealed the effect of variation on allelic expression (Soldner et al. 2016). However, another technique has been used in our laboratory to examine the effect of haplotype-specific variation on expression and splicing. PAC constructs carrying either the H1 or H2 haplotype of the entire *MAPT* locus have been used for transfection of neuroblastoma cell lines and their expression determined by construct-specific qRT-PCR. As described in his DPhil thesis and a forthcoming publication, Dr M-C. Lai detected the haplotype-specific control of exon 3+ transcripts and perturbed this by exchanging the identities of H1/H2 SNPs in the proximity of exon 3 within the two PACs in order to identify which SNPs were functionally active in controlling exon 3 inclusion. Further studies examining expression of total and exon 10+ transcripts are awaited.

Additionally in Chapter 4, I aimed to assess *MAPT* expression in purified dopaminergic neurons following a protocol of intracellular staining and FACS; however, the expression analysis from these samples was not successful and was likely due to the damaged state of the RNA following aldehyde fixation, although such was sufficient previously for unbiased analysis with RNA-seq (Sandor and Robertson et al. 2016, under review). An alternative approach would have been to use a live fluorescent reporter of dopaminergic neurons, such as the one that I attempted to generate in Chapter 3. The reporter was constructed using the entire genomic locus of human *TH*, with the coding portion of exon 1 replaced by a fluorescent protein and antibacterial resistance cassette. Expression of the *TH*-driven fluorescent protein was improved by separating the fluorescent protein and resistance marker with a 3'UTR and polyadenylation signal. Testing of the construct as HSV-1 amplicons delivered to iPSC-derived dopaminergic neuronal cultures found that only a small subset of cells expressed the fluorescent protein from the *TH* promoter, but that these were TH+ by immunocytochemistry. Poor titres of amplicons of this size made further testing and

downstream use impracticable. However, once a reliable means of identifying dopaminergic neurons in live culture is available, sorting of these cells to study a pure population of dopaminergic neurons would be possible. The closest that this has been shown in human neurons is with the protocol by Woodard and colleagues, who claimed enrichment first for midbrain dopaminergic neuronal progenitors using FACS for NCAM+/CD133+ and later for midbrain dopaminergic neurons using FACS for NCAM+/CD24+/CD15-/CD184-, resulting in approximately 80% TH+/Tuj1+ neurons (Woodard et al. 2014). However, these are not actual dopaminergic neuronal markers as a higher percentage purity would be expected if so; notably CD133 is also highly expressed in human ESCs so may not be reliable (Yuan et al. 2011) and the combination of CD24+/CD15^{LOW}/CD184- with CD44- formed a strategy for obtaining a 98% pure neuronal population containing some TH+ neurons in another study (Yuan et al. 2011). Nevertheless, a significant enrichment of TH+/Tuj1+ neurons to a final obtained purity of ~80% would be informative about the true nature of dopaminergic neurons without the need for viral transduction or genetic modification.

In summary, I have shown that the protective H2 haplotype expresses two-fold more exon 3+ transcripts in all samples and that the risk-bearing H1 haplotype can express 1.2-fold more exon 10+ transcripts or total *MAPT* transcripts in a sample-dependent manner. These data strongly support the hypothesis that the association between *MAPT* haplotype and risk for PD is underlined by haplotype-specific control of *MAPT* isoforms, wherein I purport that increased 2N tau offers protection against PD and increased 4R tau brings further susceptibility to PD.

7.2 Investigation of the role of tau and its isoforms in iPSC-derived dopaminergic neuronal cultures

To understand more about the effect of the cellular levels of tau isoforms in dopaminergic neuronal cultures, in Chapter 5 I generated a panel of RNA interference constructs to target individual tau isoforms or total tau. siRNA constructs were effective at knocking down individual isoforms but could not be delivered to iPSC-derived neuronal cultures. Following conversion to shRNA sequences and incorporation into lentiviral particles, successful constructs were identified that knocked down 4R tau or total tau, in addition to a non-targeting/scrambled control construct. In Chapter 5 these constructs were used to knock down tau isoforms with analysis of axonal transport of mitochondria after maturation for four weeks or five months. Cultures matured for four weeks with knockdown of total tau protein by ~60% showed no significant difference in mitochondrial velocity or amount of pausing, but did show a small increase in the number of mitochondria that were motile. In contrast, cultures matured for five months with knockdown of total tau protein or just the 4R tau isoforms showed no difference in mitochondrial motility between treatments. Instead, 4R tau knockdown increased transport velocity, which, when stratified, corresponded to increased velocity of unidirectional transport that is most likely to be mediated by kinesin. Knockdown of total tau at this mature time point increased transport velocity of all mitochondria regardless of directionality but only when the pause times were removed from the average velocity calculations, thus corresponding to an increase in absolute velocity. Therefore total tau and 4R tau have distinct though inter-related effects on axonal transport.

In Chapter 6 the shRNA lentiviral tools were used to investigate potential roles of tau in existing PD-related phenotypes in iPSC-derived dopaminergic neuronal cultures bearing the *GBA* N370S mutation, specifically in the areas of macroautophagy and ER stress. The

baseline phenotypes previously reported by our laboratory (Fernandes et al. 2016) were not observed in the current study, with the exception of reduced β-glucocerebrosidase enzyme activity in *GBA* N370S cultures. Notwithstanding, analysis of the specific effect of knockdown of total tau showed that no protein was significantly affected except the macroautophagy adaptor protein p62, which was mildly reduced in conditions of tau knockdown.

Integrating the findings from Chapters 5 and 6, it is proposed that improved parameters of axonal transport may lead to facilitation of the process of macroautophagy by increasing the availability of autophagic components. In concert with this proposal, increased expression of total or 4R tau from the H1 haplotype could be expected to mildly hinder both axonal transport and macroautophagy, increasing susceptibility of neurons to dysfunction and the disease processes of PD.

Autophagy is a central theme in PD, particularly as disease-related autophagy phenotypes have been reported in iPSC-derived neuronal models bearing mutations in *LRRK2* (Sánchez-Danés et al. 2012b; Orenstein et al. 2013; Su and Qi 2013), *PINK1* (Seibler et al. 2011)*, PARK2* (Imaizumi et al. 2012), *GBA* (Fernandes et al. 2016; Mazzulli et al. 2016), those with increased expression of α-synuclein (Mazzulli et al. 2016), and models of idiopathic PD (Sánchez-Danés et al. 2012b; Mazzulli et al. 2016). Classical Lewy bodies from post-mortem PD brains are comprised of many proteins in addition to the principal component α-synuclein, but notably include some proteins related to autophagy and lysosomal degradation, such as LC3, p62, GABARAP proteins and β-glucocerebrosidase (Wakabayashi et al. 2013). As PD is an α-synucleinopathy, autophagy is particularly relevant with relation to α-synuclein, which has been shown to reduce clearance of proteins from lysosomes (Mazzulli et al. 2016), although α-synuclein enters lysosomes via LAMP2A using the HSC70 chaperone in the process of chaperone-mediated autophagy (Cuervo et al. 2004) rather than by macroautophagy. A small reduction in the efficiency of axonal transport and autophagy in

neurons, amplified over a long period of time and on top of the decline already present in the ageing process, could increase the susceptibility of neurons to accumulation of α-synuclein. As overexpression of A30P α-synuclein reduced levels of kinesin and dynein in rats (Chu et al. 2012), the cellular accumulation of α-synuclein may produce a multi-faceted vicious cycle reducing the efficiency of protein clearance mechanisms.

7.3 Therapeutic reduction of 4R tau

One natural conclusion from the above data is that a treatment that reduces 4R tau expression could be advantageous – a pursuit that is particularly relevant for *MAPT* mutations that cause FTDP-17 by altering exon 10 inclusion. This was first shown in 2001 when antisense oligonucleotides targeting the 3' and 5' splice sites of exon 10 reduced exon inclusion and 4R tau protein levels, which was shown to affect microtubule stability in a non-neuronal cell line (Kalbfuss et al. 2001); reduced exon 10 inclusion was confirmed in later trials with bipartite antisense molecules that target either side of the proposed stem loop at the 5' splice site (Peacey et al. 2012). Delivery of a plasmid that expressed RNA containing a complementary sequence for binding to *MAPT* intron 9, a 3' splice site and *MAPT* exons 11-13 has been used to induce *trans*-splicing, wherein the spliceosome catalyses splicing from the 5' splice site of pre-mRNA transcripts to the 3' splice site of the therapeutic pre-RNA *trans*-splicing molecule, resulting in fewer transcripts that include exon 10 (Rodriguez-Martin et al. 2009). In that particular study, the exon exclusion treatment had only a small effect on wild-type transcripts (Rodriguez-Martin et al. 2009), although this could make it suitable for modulating the subtle increase in expression from the H1 haplotype. However, critically this method would require delivery of the DNA sequence, which, even if achieved by viral means, is not a desirable therapy for modulation of a susceptibility factor; oligonucleotide therapies may eventually be able to use exosomes as a

means of delivering to the brain (Alvarez-Erviti et al. 2011). Finally, screening for small molecule therapeutics identified 5-iodotubercidin as a compound inducing skipping of isolated *MAPT* exon 10 but which produced significant effects on splicing of other genes (Stoilov et al. 2008) and LDN-13978 (mitoxantrone) as a compound that stabilised the proposed stem loop at the 5' splice site predicted to decrease exon 10 inclusion (Donahue et al. 2007; Zheng et al. 2009; Lisowiec et al. 2015). Molecules have also been designed *in silico* to affect only FTDP-17 mutant-specific transcripts (Luo and Disney 2014).

In tauopathies with strong 4R tau-mediated pathology the exon-skipping approaches above may have merit. An alternative approach would be to reduce the levels of splicing factors known to control *MAPT* exon 10 inclusion; however, as these splicing factors will control many other genes, it is possible that this would produce undesired effects (Wood et al. 2007). For PD where *MAPT* haplotype is associated only with a small odds ratio of disease susceptibility, realistically it is unlikely that a safe cheap treatment to reduce 4R tau expression will be found that is advisable for prophylactic use to reduce PD risk. Instead it would be more advantageous to invest in treatments that improve neuronal health, reduce the effects of ageing or that target pathways, such as autophagy, that are commonly perturbed in PD. Further, as altered inclusion and exclusion of exon 10 are both routes to FTDP-17, it appears that a balance of isoforms is key, which would be difficult in practice to measure and achieve with treatment.

7.4 Future directions

Finally I will outline some suggested future directions for this area of study.

First, efforts should continue to identify and isolate human dopaminergic neurons in live culture. As suggested in Chapter 3, a more amenable design for a fluorescent reporter could be using the *PITX3* promoter within a lentiviral construct. Additionally the use of the cold harvest protocol of Goudriaan et al. (2014) would enable the isolation of only the iPSC-derived neurons from within neuron:astrocyte co-cultures. Expression analysis in pure iPSC-derived dopaminergic neurons with and without astrocytes could be used not only to confirm the role of *MAPT* haplotypes on expression and the effect of astrocytes on *MAPT* transcript maturation, but also these samples could be analysed by RNA-seq to detect changes elsewhere in the transcriptome.

Second, functional H1/H2 SNP variants controlling expression of total *MAPT* and exon 10+ transcripts could be identified by exchanging SNP identities on the two backgrounds. This could be achieved either using H1 and H2 *MAPT* BAC constructs with transfection of neuroblastoma cell lines followed by standard qRT-PCR or by the more complex but physiological technique of genome editing followed by allele-specific qRT-PCR (Soldner et al. 2016).

Third, the shRNA tools for knocking down tau and its isoforms should be expanded so that there are two validated shRNA constructs per target (2N tau, 4R tau, total tau, non-targeting construct) and then used to continue work investigating the roles of these isoforms. In particular, little has been done to investigate the role of 2N tau. The use of mature iPSC-derived dopaminergic neuronal cultures allows these isoforms to be investigated in a highly relevant neuronal setting.

Finally, further investigation into the role of tau in axonal transport and autophagy should be undertaken, notably with multiple shRNA constructs. For example, in mature cultures, is the p62 phenotype more enhanced by 4R tau knockdown with its likely major effect on kinesin-mediated transport, or by total tau knockdown with its less pronounced effect on axonal transport? Can a similar effect be achieved by bypassing tau knockdown, such as with compounds that stabilise/destabilise microtubules or by increasing/decreasing expression of motor proteins? Additionally it would be important to perform assays of autophagy flux with/without tau knockdown, using bafilomycin A1 to block fusion of autophagosomes and lysosomes during macroautophagy and measuring the effect on LC3B-II (Mizushima and Yoshimori 2007). Expression analysis of motor proteins, their adaptors and other potential secondary mediators in axonal transport should also be performed with/without tau knockdown to determine the mechanism of how tau knockdown affects axonal transport in human iPSC-derived dopaminergic neuronal cultures. These further studies will provide valuable insight into how alterations in the balance of tau isoforms impacts on human neuronal function and could play a role in the disease aetiology of PD and tauopathies.

References

Aarsland, D., K. Andersen, J. P. Larsen, A. Lolk, and P. Kragh-Sørensen. 2003. 'Prevalence and characteristics of dementia in Parkinson disease: an 8-year prospective study', *Arch Neurol*, 60: 387-92.

Abeliovich, A., Y. Schmitz, I. Fariñas, D. Choi-Lundberg, W. H. Ho, P. E. Castillo, N. Shinsky, J. M. Verdugo, M. Armanini, A. Ryan, M. Hynes, H. Phillips, D. Sulzer, and A. Rosenthal. 2000. 'Mice lacking alpha-synuclein display functional deficits in the nigrostriatal dopamine system', *Neuron*, 25: 239-52.

Aboud, A. A., A. M. Tidball, K. K. Kumar, M. D. Neely, K. C. Ess, K. M. Erikson, and A. B. Bowman. 2012. 'Genetic risk for Parkinson's disease correlates with alterations in neuronal manganese sensitivity between two human subjects', *Neurotoxicology*, 33: 1443-9.

Abraham, R., R. Sims, L. Carroll, P. Hollingworth, M. C. O'Donovan, J. Williams, and M. J. Owen. 2009. 'An association study of common variation at the MAPT locus with late-onset Alzheimer's disease', *Am J Med Genet B Neuropsychiatr Genet*, 150B: 1152-5.

Agholme, L., T. Lindström, K. Kågedal, J. Marcusson, and M. Hallbeck. 2010. 'An in vitro model for neuroscience: differentiation of SH-SY5Y cells into cells with morphological and biochemical characteristics of mature neurons', *J Alzheimers Dis*, 20: 1069-82.

Aharon-Peretz, J., H. Rosenbaum, and R. Gershoni-Baruch. 2004. 'Mutations in the glucocerebrosidase gene and Parkinson's disease in Ashkenazi Jews', *N Engl J Med*, 351: 1972-7.

Ai, H. W., N. C. Shaner, Z. Cheng, R. Y. Tsien, and R. E. Campbell. 2007. 'Exploration of new chromophore structures leads to the identification of improved blue fluorescent proteins', *Biochemistry*, 46: 5904-10.

Albanèse, V., N. F. Biguet, H. Kiefer, E. Bayard, J. Mallet, and R. Meloni. 2001. 'Quantitative effects on gene silencing by allelic variation at a tetranucleotide microsatellite', *Hum Mol Genet*, 10: 1785-92.

Alegre-Abarrategui, J., H. Christian, M. M. Lufino, R. Mutihac, L. L. Venda, O. Ansorge, and R. Wade-Martins. 2009. 'LRRK2 regulates autophagic activity and localizes to specific membrane microdomains in a novel human genomic reporter cellular model', *Hum Mol Genet*, 18: 4022-34.

Allen, M., M. Kachadoorian, Z. Quicksall, F. Zou, H. S. Chai, C. Younkin, J. E. Crook, V. S. Pankratz, M. M. Carrasquillo, S. Krishnan, T. Nguyen, L. Ma, K. Malphrus, S. Lincoln, G. Bisceglio, C. P. Kolbert, J. Jen, S. Mukherjee, J. K. Kauwe, P. K. Crane, J. L. Haines, R. Mayeux, M. A. Pericak-Vance, L. A. Farrer, G. D. Schellenberg, J. E. Parisi, R. C. Petersen, N. R. Graff-Radford, D. W. Dickson, S. G. Younkin, and N. Ertekin-Taner. 2014. 'Association of MAPT haplotypes with Alzheimer's disease risk and MAPT brain gene expression levels', *Alzheimers Res Ther*, 6: 39.

Alvarez-Erviti, L., Y. Seow, H. Yin, C. Betts, S. Lakhal, and M. J. Wood. 2011. 'Delivery of siRNA to the mouse brain by systemic injection of targeted exosomes', *Nat Biotechnol*, 29: 341-5.

Andorfer, C., Y. Kress, M. Espinoza, R. de Silva, K. L. Tucker, Y. A. Barde, K. Duff, and P. Davies. 2003. 'Hyperphosphorylation and aggregation of tau in mice expressing normal human tau isoforms', *J Neurochem*, 86: 582-90.

Andreadis, A. 2005. 'Tau gene alternative splicing: expression patterns, regulation and modulation of function in normal brain and neurodegenerative diseases', *Biochim Biophys Acta*, 1739: 91-103.

Andreadis, A. 2012. 'Tau splicing and the intricacies of dementia', *J Cell Physiol*, 227: 1220-5.
Andreadis, A., W. M. Brown, and K. S. Kosik. 1992. 'Structure and novel exons of the human tau gene', *Biochemistry*, 31: 10626-33.
Arányi, T., B. A. Faucheux, O. Khalfallah, G. Vodjdani, N. F. Biguet, J. Mallet, and R. Meloni. 2005. 'The tissue-specific methylation of the human tyrosine hydroxylase gene reveals new regulatory elements in the first exon', *J Neurochem*, 94: 129-39.
Badger, J. L., O. Cordero-Llana, E. M. Hartfield, and R. Wade-Martins. 2014. 'Parkinson's disease in a dish - Using stem cells as a molecular tool', *Neuropharmacology*, 76 Pt A: 88-96.
Baker, M., I. Litvan, H. Houlden, J. Adamson, D. Dickson, J. Perez-Tur, J. Hardy, T. Lynch, E. Bigio, and M. Hutton. 1999. 'Association of an extended haplotype in the *tau* gene with progressive supranuclear palsy', *Hum Mol Genet*, 8: 711-5.
Baker, M., I. R. Mackenzie, S. M. Pickering-Brown, J. Gass, R. Rademakers, C. Lindholm, J. Snowden, J. Adamson, A. D. Sadovnick, S. Rollinson, A. Cannon, E. Dwosh, D. Neary, S. Melquist, A. Richardson, D. Dickson, Z. Berger, J. Eriksen, T. Robinson, C. Zehr, C. A. Dickey, R. Crook, E. McGowan, D. Mann, B. Boeve, H. Feldman, and M. Hutton. 2006. 'Mutations in progranulin cause tau-negative frontotemporal dementia linked to chromosome 17', *Nature*, 442: 916-9.
Ball, M. J., and K. Nuttall. 1980. 'Neurofibrillary tangles, granulovacuolar degeneration, and neuron loss in Down Syndrome: quantitative comparison with Alzheimer dementia', Ann Neurol, 7: 462-5.
Beevers, J. E., T. M. Caffrey, and R. Wade-Martins. 2013. 'Induced pluripotent stem cell (iPSC)-derived dopaminergic models of Parkinson's disease', *Biochem Soc Trans*, 41: 1503-8.
Benitez, B. A., A. A. Davis, S. C. Jin, L. Ibanez, S. Ortega-Cubero, P. Pastor, J. Choi, B. Cooper, J. S. Perlmutter, and C. Cruchaga. 2016. 'Resequencing analysis of five Mendelian genes and the top genes from genome-wide association studies in Parkinson's Disease', *Mol Neurodegener*, 11: 29.
Benussi, L., R. Ghidoni, A. Paterlini, F. Nicosia, A. C. Alberici, S. Signorini, L. Barbiero, and G. Binetti. 2005. 'Interaction between tau and alpha-synuclein proteins is impaired in the presence of P301L tau mutation', *Exp Cell Res*, 308: 78-84.
Bertram, L., M. B. McQueen, K. Mullin, D. Blacker, and R. E. Tanzi. 2007. 'Systematic meta-analyses of Alzheimer disease genetic association studies: the AlzGene database', *Nat Genet*, 39: 17-23.
Bertram, L., and R. E. Tanzi. 2009. 'Genome-wide association studies in Alzheimer's disease', *Hum Mol Genet*, 18: R137-45.
Bibbiani, F., L. C. Costantini, R. Patel, and T. N. Chase. 2005. 'Continuous dopaminergic stimulation reduces risk of motor complications in parkinsonian primates', *Exp Neurol*, 192: 73-8.
Biernacka, J. M., S. M. Armasu, J. M. Cunningham, J. E. Ahlskog, S. J. Chung, and D. M. Maraganore. 2011. 'Do interactions between SNCA, MAPT, and LRRK2 genes contribute to Parkinson's disease susceptibility?', *Parkinsonism Relat Disord*, 17: 730-6.
Biernat, J., N. Gustke, G. Drewes, E. M. Mandelkow, and E. Mandelkow. 1993. 'Phosphorylation of Ser262 strongly reduces binding of tau to microtubules: distinction between PHF-like immunoreactivity and microtubule binding', *Neuron*, 11: 153-63.
Bjørkøy, G., T. Lamark, A. Brech, H. Outzen, M. Perander, A. Overvatn, H. Stenmark, and T. Johansen. 2005. 'p62/SQSTM1 forms protein aggregates degraded by autophagy and has a protective effect on huntingtin-induced cell death', *J Cell Biol*, 171: 603-14.

Black, M. M., and P. W. Baas. 1989. 'The basis of polarity in neurons', *Trends Neurosci*, 12: 211-4.

Boeve, B. F., M. H. Silber, T. J. Ferman, E. Kokmen, G. E. Smith, R. J. Ivnik, J. E. Parisi, E. J. Olson, and R. C. Petersen. 1998. 'REM sleep behavior disorder and degenerative dementia: an association likely reflecting Lewy body disease', *Neurology*, 51: 363-70.

Borghese, L., D. Dolezalova, T. Opitz, S. Haupt, A. Leinhaas, B. Steinfarz, P. Koch, F. Edenhofer, A. Hampl, and O. Brüstle. 2010. 'Inhibition of notch signaling in human embryonic stem cell-derived neural stem cells delays G1/S phase transition and accelerates neuronal differentiation in vitro and in vivo', *Stem Cells*, 28: 955-64.

Borgohain, R., R. M. Kandadai, A. Jabeen, and M. A. Kannikannan. 2012. 'Nonmotor outcomes in Parkinson's disease: is deep brain stimulation better than dopamine replacement therapy?', *Ther Adv Neurol Disord*, 5: 23-41.

Botta-Orfila, T., M. Ezquerra, J. Ríos, R. Fernández-Santiago, S. Cervantes, L. Samaranch, P. Pastor, M. J. Martí, E. Muñoz, F. Valldeoriola, M. Aguilar, M. Calopa, J. Hernández-Vara, and E. Tolosa. 2011. 'Lack of interaction of SNCA and MAPT genotypes in Parkinson's disease', *Eur J Neurol*, 18: e32.

Boulting, G. L., E. Kiskinis, G. F. Croft, M. W. Amoroso, D. H. Oakley, B. J. Wainger, D. J. Williams, D. J. Kahler, M. Yamaki, L. Davidow, C. T. Rodolfa, J. T. Dimos, S. Mikkilineni, A. B. MacDermott, C. J. Woolf, C. E. Henderson, H. Wichterle, and K. Eggan. 2011. 'A functionally characterized test set of human induced pluripotent stem cells', *Nat Biotechnol*, 29: 279-86.

Boutajangout, A., A. Boom, K. Leroy, and J. P. Brion. 2004. 'Expression of tau mRNA and soluble tau isoforms in affected and non-affected brain areas in Alzheimer's disease', *FEBS Lett*, 576: 183-9.

Braak, H., K. Del Tredici, U. Rüb, R. A. de Vos, E. N. Jansen Steur, and E. Braak. 2003. 'Staging of brain pathology related to sporadic Parkinson's disease', *Neurobiol Aging*, 24: 197-211.

Brady, R. O., J. N. Kanfer, R. M. Bradley, and D. Shapiro. 1966. 'Demonstration of a deficiency of glucocerebroside-cleaving enzyme in Gaucher's disease', *J Clin Invest*, 45: 1112-5.

Brandt, R., J. Léger, and G. Lee. 1995. 'Interaction of tau with the neural plasma membrane mediated by tau's amino-terminal projection domain', *J Cell Biol*, 131: 1327-40.

Bratt-Leal, A. M., R. L. Carpenedo, and T. C. McDevitt. 2009. 'Engineering the embryoid body microenvironment to direct embryonic stem cell differentiation', *Biotechnol Prog*, 25: 43-51.

Bray, N. J., P. R. Buckland, M. J. Owen, and M. C. O'Donovan. 2003a. 'Cis-acting variation in the expression of a high proportion of genes in human brain', *Hum Genet*, 113: 149-53.

Bray, N. J., P. R. Buckland, N. M. Williams, H. J. Williams, N. Norton, M. J. Owen, and M. C. O'Donovan. 2003b. 'A haplotype implicated in schizophrenia susceptibility is associated with reduced COMT expression in human brain.', *Am J Hum Genet*, 73: 152-61.

Bray, N. J., L. Jehu, V. Moskvina, J. D. Buxbaum, S. Dracheva, V. Haroutunian, J. Williams, P. R. Buckland, M. J. Owen, and M. C. O'Donovan. 2004. 'Allelic expression of APOE in human brain: effects of epsilon status and promoter haplotypes', *Hum Mol Genet*, 13: 2885-92.

Brockmann, K., K. Srulijes, A. K. Hauser, C. Schulte, I. Csoti, T. Gasser, and D. Berg. 2011. 'GBA-associated PD presents with nonmotor characteristics', *Neurology*, 77: 276-80.

Buckland, P. R. 2004. 'Allele-specific gene expression differences in humans', *Hum Mol Genet*, 13 Spec No 2: R255-60.

Bye, C. R., M. E. Jönsson, A. Björklund, C. L. Parish, and L. H. Thompson. 2015. 'Transcriptome analysis reveals transmembrane targets on transplantable midbrain dopamine progenitors', *Proc Natl Acad Sci U S A*, 112: E1946-55.

Byers, B., B. Cord, H. N. Nguyen, B. Schüle, L. Fenno, P. C. Lee, K. Deisseroth, J. W. Langston, R. R. Pera, and T. D. Palmer. 2011. 'SNCA triplication Parkinson's patient's iPSC-derived DA neurons accumulate α-synuclein and are susceptible to oxidative stress', *PLoS One*, 6: e26159.

Caceres, A., and K. S. Kosik. 1990. 'Inhibition of neurite polarity by tau antisense oligonucleotides in primary cerebellar neurons', *Nature*, 343: 461-3.

Caffrey, T. M., C. Joachim, S. Paracchini, M. M. Esiri, and R. Wade-Martins. 2006. 'Haplotype-specific expression of exon 10 at the human *MAPT* locus', *Hum Mol Genet*, 15: 3529-37.

Caffrey, T. M., C. Joachim, and R. Wade-Martins. 2008. 'Haplotype-specific expression of the N-terminal exons 2 and 3 at the human *MAPT* locus', *Neurobiol Aging*, 29: 1923-9.

Caffrey, T. M., and R. Wade-Martins. 2012. 'The role of MAPT sequence variation in mechanisms of disease susceptibility', *Biochem Soc Trans*, 40: 687-92.

Cai, Q., C. Gerwin, and Z. H. Sheng. 2005. 'Syntabulin-mediated anterograde transport of mitochondria along neuronal processes', *J Cell Biol*, 170: 959-69.

Cai, Q., L. Lu, J. H. Tian, Y. B. Zhu, H. Qiao, and Z. H. Sheng. 2010. 'Snapin-regulated late endosomal transport is critical for efficient autophagy-lysosomal function in neurons', *Neuron*, 68: 73-86.

Caiazzo, M., M. T. Dell'Anno, E. Dvoretskova, D. Lazarevic, S. Taverna, D. Leo, T. D. Sotnikova, A. Menegon, P. Roncaglia, G. Colciago, G. Russo, P. Carninci, G. Pezzoli, R. R. Gainetdinov, S. Gustincich, A. Dityatev, and V. Broccoli. 2011. 'Direct generation of functional dopaminergic neurons from mouse and human fibroblasts', Nature, 476: 224-7.

Castillo-Carranza, D. L., H. Rodríguez-Rocha, R. Montes-de-Oca-Luna, J. Sepúlveda-Saavedra, H. R. Martínez, Y. López-Vidal, and O. Saucedo-Cárdenas. 2008. 'Pitx3 promoter directs Cre-recombinase specifically in a human neuroblastoma cell line', *Mol Cell Biochem*, 309: 223-7.

Chambers, S. M., C. A. Fasano, E. P. Papapetrou, M. Tomishima, M. Sadelain, and L. Studer. 2009. 'Highly efficient neural conversion of human ES and iPS cells by dual inhibition of SMAD signaling', *Nat Biotechnol*, 27: 275-80.

Chapin, S. J., and J. C. Bulinski. 1992. 'Microtubule stabilization by assembly-promoting microtubule-associated proteins: a repeat performance', *Cell Motil Cytoskeleton*, 23: 236-43.

Charlesworth, G., S. Gandhi, J. M. Bras, R. A. Barker, D. J. Burn, P. F. Chinnery, S. M. Gentleman, R. Guerreiro, J. Hardy, J. L. Holton, A. Lees, K. Morrison, U. M. Sheerin, N. Williams, H. Morris, T. Revesz, and N. W. Wood. 2012. 'Tau acts as an independent genetic risk factor in pathologically proven PD', *Neurobiol Aging*, 33: 838.e7-11.

Charrow, J., H. C. Andersson, P. Kaplan, E. H. Kolodny, P. Mistry, G. Pastores, B. E. Rosenbloom, C. R. Scott, R. S. Wappner, N. J. Weinreb, and A. Zimran. 2000. 'The Gaucher registry: demographics and disease characteristics of 1698 patients with Gaucher disease', *Arch Intern Med*, 160: 2835-43.

Chartier-Harlin, M. C., J. Kachergus, C. Roumier, V. Mouroux, X. Douay, S. Lincoln, C. Levecque, L. Larvor, J. Andrieux, M. Hulihan, N. Waucquier, L. Defebvre, P. Amouyel, M. Farrer, and A. Destée. 2004. 'Alpha-synuclein locus duplication as a cause of familial Parkinson's disease', *Lancet*, 364: 1167-9.

Chen, H., X. Huang, X. Guo, R. B. Mailman, Y. Park, F. Kamel, D. M. Umbach, Q. Xu, A. Hollenbeck, A. Schatzkin, and A. Blair. 2010. 'Smoking duration, intensity, and risk of Parkinson disease', *Neurology*, 74: 878-84.

Chen, J., Y. Kanai, N. J. Cowan, and N. Hirokawa. 1992. 'Projection domains of MAP2 and tau determine spacings between microtubules in dendrites and axons', *Nature*, 360: 674-7.

Chen, X., J. Weaver, B. A. Bove, L. A. Vanderveer, S. C. Weil, A. Miron, M. B. Daly, and A. K. Godwin. 2008. 'Allelic imbalance in BRCA1 and BRCA2 gene expression is associated with an increased breast cancer risk', *Hum Mol Genet*, 17: 1336-48.

Cheng, H. C., C. M. Ulane, and R. E. Burke. 2010. 'Clinical progression in Parkinson disease and the neurobiology of axons', *Ann Neurol*, 67: 715-25.

Chu, Y., G. A. Morfini, L. B. Langhamer, Y. He, S. T. Brady, and J. H. Kordower. 2012. 'Alterations in axonal transport motor proteins in sporadic and experimental Parkinson's disease', *Brain*, 135: 2058-73.

Chung, P. J., C. Song, J. Deek, H. P. Miller, Y. Li, M. C. Choi, L. Wilson, S. C. Feinstein, and C. R. Safinya. 2016. 'Tau mediates microtubule bundle architectures mimicking fascicles of microtubules found in the axon initial segment', *Nat Commun*, 7: 12278.

Chung, S., J. I. Moon, A. Leung, D. Aldrich, S. Lukianov, Y. Kitayama, S. Park, Y. Li, V. Y. Bolshakov, T. Lamonerie, and K. S. Kim. 2011. 'ES cell-derived renewable and functional midbrain dopaminergic progenitors', *Proc Natl Acad Sci U S A*, 108: 9703-8.

Ciasca, G., G. Campi, A. Battisti, G. Rea, M. Rodio, M. Papi, P. Pernot, A. Tenenbaum, and A. Bianconi. 2012. 'Continuous thermal collapse of the intrinsically disordered protein tau is driven by its entropic flexible domain', *Langmuir*, 28: 13405-10.

Clark, L. N., G. Levy, M. X. Tang, H. Mejia-Santana, A. Ciappa, B. Tycko, L. J. Cote, E. D. Louis, R. Mayeux, and K. Marder. 2003. 'The *Saitohin* 'Q7R' polymorphism and tau haplotype in multi-ethnic Alzheimer disease and Parkinson's disease cohorts', *Neurosci Lett*, 347: 17-20.

Cleveland, D. W., S. Y. Hwo, and M. W. Kirschner. 1977. 'Purification of tau, a microtubule-associated protein that induces assembly of microtubules from purified tubulin', *J Mol Biol*, 116: 207-25.

Cohen, T. J., B. H. Constance, A. W. Hwang, M. James, and C. X. Yuan. 2016. 'Intrinsic Tau Acetylation Is Coupled to Auto-Proteolytic Tau Fragmentation', *PLoS One*, 11: e0158470.

Conrad, C., N. Amano, A. Andreadis, Y. Xia, K. Namekataf, F. Oyama, K. Ikeda, K. Wakabayashi, H. Takahashi, L. J. Thal, R. Katzman, D. A. Shackelford, M. Matsushita, E. Masliah, and A. Sawa. 1998. 'Differences in a dinucleotide repeat polymorphism in the tau gene between Caucasian and Japanese populations: implication for progressive supranuclear palsy', *Neurosci Lett*, 250: 135-7.

Conrad, C., A. Andreadis, J. Q. Trojanowski, D. W. Dickson, D. Kang, X. Chen, W. Wiederholt, L. Hansen, E. Masliah, L. J. Thal, R. Katzman, Y. Xia, and T. Saitoh. 1997. 'Genetic evidence for the involvement of tau in progressive supranuclear palsy', *Ann Neurol*, 41: 277-81.

Conway, L., M. W. Gramlich, S. M. Ali Tabei, and J. L. Ross. 2014. 'Microtubule orientation and spacing within bundles is critical for long-range kinesin-1 motility', *Cytoskeleton (Hoboken)*, 71: 595-610.

Cookson, M. R. 2010. 'The role of leucine-rich repeat kinase 2 (LRRK2) in Parkinson's disease', *Nat Rev Neurosci*, 11: 791-7.

Cooper, O., H. Seo, S. Andrabi, C. Guardia-Laguarta, J. Graziotto, M. Sundberg, J. R. McLean, L. Carrillo-Reid, Z. Xie, T. Osborn, G. Hargus, M. Deleidi, T. Lawson, H. Bogetofte, E. Perez-Torres, L. Clark, C. Moskowitz, J. Mazzulli, L. Chen, L. Volpicelli-Daley, N.

Romero, H. Jiang, R. J. Uitti, Z. Huang, G. Opala, L. A. Scarffe, V. L. Dawson, C. Klein, J. Feng, O. A. Ross, J. Q. Trojanowski, V. M. Lee, K. Marder, D. J. Surmeier, Z. K. Wszolek, S. Przedborski, D. Krainc, T. M. Dawson, and O. Isacson. 2012. 'Pharmacological rescue of mitochondrial deficits in iPSC-derived neural cells from patients with familial Parkinson's disease', *Sci Transl Med*, 4: 141ra90.

Crawford, T. Q., and H. Roelink. 2007. 'The notch response inhibitor DAPT enhances neuronal differentiation in embryonic stem cell-derived embryoid bodies independently of sonic hedgehog signaling', *Dev Dyn*, 236: 886-92.

Cruts, M., I. Gijselinck, J. van der Zee, S. Engelborghs, H. Wils, D. Pirici, R. Rademakers, R. Vandenberghe, B. Dermaut, J. J. Martin, C. van Duijn, K. Peeters, R. Sciot, P. Santens, T. De Pooter, M. Mattheijssens, M. Van den Broeck, I. Cuijt, K. Vennekens, P. P. De Deyn, S. Kumar-Singh, and C. Van Broeckhoven. 2006. 'Null mutations in progranulin cause ubiquitin-positive frontotemporal dementia linked to chromosome 17q21', *Nature*, 442: 920-4.

Cruts, M., R. Rademakers, I. Gijselinck, J. van der Zee, B. Dermaut, T. de Pooter, P. de Rijk, J. Del-Favero, and C. van Broeckhoven. 2005. 'Genomic architecture of human 17q21 linked to frontotemporal dementia uncovers a highly homologous family of low-copy repeats in the tau region', *Hum Mol Genet*, 14: 1753-62.

Cuervo, A. M., L. Stefanis, R. Fredenburg, P. T. Lansbury, and D. Sulzer. 2004. 'Impaired degradation of mutant alpha-synuclein by chaperone-mediated autophagy', *Science*, 305: 1292-5.

Das, G., A. K. Misra, S. K. Das, K. Ray, and J. Ray. 2009. 'Microtubule-associated protein tau (*MAPT*) influences the risk of Parkinson's disease among Indians', *Neurosci Lett*, 460: 16-20.

Davis, A. A., K. M. Andruska, B. A. Benitez, B. A. Racette, J. S. Perlmutter, and C. Cruchaga. 2016. 'Variants in GBA, SNCA, and MAPT influence Parkinson disease risk, age at onset, and progression', *Neurobiol Aging*, 37: 209.e1-7.

Dawson, H. N., A. Ferreira, M. V. Eyster, N. Ghoshal, L. I. Binder, and M. P. Vitek. 2001. 'Inhibition of neuronal maturation in primary hippocampal neurons from tau deficient mice', *J Cell Sci*, 114: 1179-87.

de Silva, R., J. Hardy, J. Crook, N. Khan, E. A. Graham, C. M. Morris, N. W. Wood, and A. J. Lees. 2002. 'The tau locus is not significantly associated with pathologically confirmed sporadic Parkinson's disease', *Neurosci Lett*, 330: 201-3.

Dell'Anno, M. T., M. Caiazzo, D. Leo, E. Dvoretskova, L. Medrihan, G. Colasante, S. Giannelli, I. Theka, G. Russo, L. Mus, G. Pezzoli, R. R. Gainetdinov, F. Benfenati, S. Taverna, A. Dityatev, and V. Broccoli. 2014. 'Remote control of induced dopaminergic neurons in parkinsonian rats', J Clin Invest, 124: 3215-29.

Deng, J., P. A. Lewis, E. Greggio, E. Sluch, A. Beilina, and M. R. Cookson. 2008. 'Structure of the ROC domain from the Parkinson's disease-associated leucine-rich repeat kinase 2 reveals a dimeric GTPase', *Proc Natl Acad Sci U S A*, 105: 1499-504.

DeStefano, A. L., L. I. Golbe, M. H. Mark, A. M. Lazzarini, N. E. Maher, M. Saint-Hilaire, R. G. Feldman, M. Guttman, R. L. Watts, O. Suchowersky, A. L. Lafontaine, N. Labelle, M. F. Lew, C. H. Waters, J. H. Growdon, C. Singer, L. J. Currie, G. F. Wooten, P. Vieregge, P. P. Pramstaller, C. Klein, J. P. Hubble, M. Stacy, E. Montgomery, M. E. MacDonald, J. F. Gusella, and R. H. Myers. 2001. 'Genome-wide scan for Parkinson's disease: the GenePD Study', *Neurology*, 57: 1124-6.

Devine, M. J., M. Ryten, P. Vodicka, A. J. Thomson, T. Burdon, H. Houlden, F. Cavaleri, M. Nagano, N. J. Drummond, J. W. Taanman, A. H. Schapira, K. Gwinn, J. Hardy, P. A. Lewis, and T. Kunath. 2011. 'Parkinson's disease induced pluripotent stem cells with triplication of the α-synuclein locus', *Nat Commun*, 2: 440.

DeVos, S. L., D. K. Goncharoff, G. Chen, C. S. Kebodeaux, K. Yamada, F. R. Stewart, D. R. Schuler, S. E. Maloney, D. F. Wozniak, F. Rigo, C. F. Bennett, J. R. Cirrito, D. M. Holtzman, and T. M. Miller. 2013. 'Antisense reduction of tau in adult mice protects against seizures', *J Neurosci*, 33: 12887-97.

Di Maria, E., M. Tabaton, T. Vigo, G. Abbruzzese, E. Bellone, C. Donati, E. Frasson, R. Marchese, P. Montagna, D. G. Munoz, P. P. Pramstaller, G. Zanusso, F. Ajmar, and P. Mandich. 2000. 'Corticobasal degeneration shares a common genetic background with progressive supranuclear palsy', *Ann Neurol*, 47: 374-7.

Dixit, R., J. L. Ross, Y. E. Goldman, and E. L. Holzbaur. 2008. 'Differential regulation of dynein and kinesin motor proteins by tau', *Science*, 319: 1086-9.

Dodson, P. D., J. K. Dreyer, K. A. Jennings, E. C. Syed, R. Wade-Martins, S. J. Cragg, J. P. Bolam, and P. J. Magill. 2016. 'Representation of spontaneous movement by dopaminergic neurons is cell-type selective and disrupted in parkinsonism', *Proc Natl Acad Sci U S A*, 113: E2180-8.

Donahue, C. P., J. Ni, E. Rozners, M. A. Glicksman, and M. S. Wolfe. 2007. 'Identification of tau stem loop RNA stabilizers', *J Biomol Screen*, 12: 789-99.

Doty, R. L., D. A. Deems, and S. Stellar. 1988. 'Olfactory dysfunction in parkinsonism: a general deficit unrelated to neurologic signs, disease stage, or disease duration', *Neurology*, 38: 1237-44.

Drubin, D. G., and M. W. Kirschner. 1986. 'Tau protein function in living cells', *J Cell Biol*, 103: 2739-46.

Dubey, M., P. Chaudhury, H. Kabiru, and T. B. Shea. 2008. 'Tau inhibits anterograde axonal transport and perturbs stability in growing axonal neurites in part by displacing kinesin cargo: neurofilaments attenuate tau-mediated neurite instability', *Cell Motil Cytoskeleton*, 65: 89-99.

Duka, T., M. Rusnak, R. E. Drolet, V. Duka, C. Wersinger, J. L. Goudreau, and A. Sidhu. 2006. 'Alpha-synuclein induces hyperphosphorylation of Tau in the MPTP model of parkinsonism', *FASEB J*, 20: 2302-12.

Dull, T., R. Zufferey, M. Kelly, R. J. Mandel, M. Nguyen, D. Trono, and L. Naldini. 1998. 'A third-generation lentivirus vector with a conditional packaging system', *J Virol*, 72: 8463-71.

Dächsel, J. C., B. Behrouz, M. Yue, J. E. Beevers, H. L. Melrose, and M. J. Farrer. 2010. 'A comparative study of Lrrk2 function in primary neuronal cultures', *Parkinsonism Relat Disord*, 16: 650-5.

Ebneth, A., R. Godemann, K. Stamer, S. Illenberger, B. Trinczek, and E. Mandelkow. 1998. 'Overexpression of tau protein inhibits kinesin-dependent trafficking of vesicles, mitochondria, and endoplasmic reticulum: implications for Alzheimer's disease', *J Cell Biol*, 143: 777-94.

Edwards, L. L., R. F. Pfeiffer, E. M. Quigley, R. Hofman, and M. Balluff. 1991. 'Gastrointestinal symptoms in Parkinson's disease', *Mov Disord*, 6: 151-6.

Edwards, T. L., W. K. Scott, C. Almonte, A. Burt, E. H. Powell, G. W. Beecham, L. Wang, S. Zuchner, I. Konidari, G. Wang, C. Singer, F. Nahab, B. Scott, J. M. Stajich, M. Pericak-Vance, J. Haines, J. M. Vance, and E. R. Martin. 2010. 'Genome-wide association study confirms SNPs in *SNCA* and the *MAPT* region as common risk factors for Parkinson disease', *Ann Hum Genet*, 74: 97-109.

Ehrlich, M., A. L. Hallmann, P. Reinhardt, M. J. Araúzo-Bravo, S. Korr, A. Röpke, O. E. Psathaki, P. Ehling, S. G. Meuth, A. L. Oblak, J. R. Murrell, B. Ghetti, H. Zaehres, H. R. Schöler, J. Sterneckert, T. Kuhlmann, and G. Hargus. 2015. 'Distinct Neurodegenerative Changes in an Induced Pluripotent Stem Cell Model of Frontotemporal Dementia Linked to Mutant TAU Protein', *Stem Cell Reports*, 5: 83-96.

Elbaz, A., O. A. Ross, J. P. Ioannidis, A. I. Soto-Ortolaza, F. Moisan, J. Aasly, G. Annesi, M. Bozi, L. Brighina, M. C. Chartier-Harlin, A. Destee, C. Ferrarese, A. Ferraris, J. M. Gibson, S. Gispert, G. M. Hadjigeorgiou, B. Jasinska-Myga, C. Klein, R. Kruger, J. C. Lambert, K. Lohmann, S. van de Loo, M. A. Loriot, T. Lynch, G. D. Mellick, E. Mutez, C. Nilsson, G. Opala, A. Puschmann, A. Quattrone, M. Sharma, P. A. Silburn, L. Stefanis, R. J. Uitti, E. M. Valente, C. Vilariño-Güell, K. Wirdefeldt, Z. K. Wszolek, G. Xiromerisiou, D. M. Maraganore, and M. J. Farrer. 2011. 'Independent and joint effects of the *MAPT* and *SNCA* genes in Parkinson disease', *Ann Neurol*, 69: 778-92.

Elie, A., E. Prezel, C. Guerin, E. Denarier, S. Ramirez-Rios, L. Serre, A. Andrieux, A. Fourest-Lieuvin, L. Blanchoin, and I. Arnal. 2015. 'Tau co-organizes dynamic microtubule and actin networks', *Sci Rep*, 5: 9964.

Esposito, A., C. P. Dohm, P. Kermer, M. Bähr, and F. S. Wouters. 2007. 'alpha-Synuclein and its disease-related mutants interact differentially with the microtubule protein tau and associate with the actin cytoskeleton', *Neurobiol Dis*, 26: 521-31.

Ezquerra, M., C. Gaig, C. Ascaso, E. Muñoz, and E. Tolosa. 2007. 'Tau and saitohin gene expression pattern in progressive supranuclear palsy', *Brain Res*, 1145: 168-76.

Ezquerra, M., P. Pastor, C. Gaig, J. M. Vidal-Taboada, C. Cruchaga, E. Munoz, M. J. Marti, F. Valldeoriola, M. Aguilar, M. Calopa, J. Hernandez-Vara, and E. Tolosa. 2011. 'Different *MAPT* haplotypes are associated with Parkinson's disease and progressive supranuclear palsy', *Neurobiol Aging*, 32: 547 e11-6.

Farrer, L. A., L. A. Cupples, J. L. Haines, B. Hyman, W. A. Kukull, R. Mayeux, R. H. Myers, M. A. Pericak-Vance, N. Risch, and C. M. van Duijn. 1997. 'Effects of age, sex, and ethnicity on the association between apolipoprotein E genotype and Alzheimer disease. A meta-analysis. APOE and Alzheimer Disease Meta Analysis Consortium', *JAMA*, 278: 1349-56.

Farrer, M., L. Skipper, M. Berg, G. Bisceglio, M. Hanson, J. Hardy, A. Adam, K. Gwinn-Hardy, and J. Aasly. 2002. 'The Tau H1 haplotype is associated with Parkinson's disease in the Norwegian population', *Neurosci Lett*, 322: 83-6.

Fearnley, J. M., and A. J. Lees. 1991. 'Ageing and Parkinson's disease: substantia nigra regional selectivity', *Brain*, 114 (Pt 5): 2283-301.

Fellous, A., J. Francon, A. M. Lennon, and J. Nunez. 1977. 'Microtubule assembly in vitro. Purification of assembly-promoting factors', *Eur J Biochem*, 78: 167-74.

Fernandes, H. J., E. M. Hartfield, H. C. Christian, E. Emmanoulidou, Y. Zheng, H. Booth, H. Bogetofte, C. Lang, B. J. Ryan, S. P. Sardi, J. Badger, J. Vowles, S. Evetts, G. K. Tofaris, K. Vekrellis, K. Talbot, M. T. Hu, W. James, S. A. Cowley, and R. Wade-Martins. 2016. 'ER Stress and Autophagic Perturbations Lead to Elevated Extracellular alpha-Synuclein in GBA-N370S Parkinson's iPSC-Derived Dopamine Neurons', *Stem Cell Reports*, 6: 342-56.

Fernández-Santiago, R., I. Carballo-Carbajal, G. Castellano, R. Torrent, Y. Richaud, A. Sánchez-Danés, R. Vilarrasa-Blasi, A. Sánchez-Pla, J. L. Mosquera, J. Soriano, J. López-Barneo, J. M. Canals, J. Alberch, Á Raya, M. Vila, A. Consiglio, J. I. Martín-Subero, M. Ezquerra, and E. Tolosa. 2015. 'Aberrant epigenome in iPSC-derived dopaminergic neurons from Parkinson's disease patients', *EMBO Mol Med*, 7: 1529-46.

Fidani, L., K. Kalinderi, S. Bostantjopoulou, J. Clarimon, A. Goulas, Z. Katsarou, J. Hardy, and A. Kotsis. 2006. 'Association of the *Tau* haplotype with Parkinson's disease in the Greek population', *Mov Disord*, 21: 1036-9.

Foltynie, T., B. Cheeran, C. H. Williams-Gray, M. J. Edwards, S. A. Schneider, D. Weinberger, J. C. Rothwell, R. A. Barker, and K. P. Bhatia. 2009. 'BDNF val66met influences time to onset of levodopa induced dyskinesia in Parkinson's disease', *J Neurol Neurosurg Psychiatry*, 80: 141-4.

Foster, N. L., K. Wilhelmsen, A. A. Sima, M. Z. Jones, C. J. D'Amato, and S. Gilman. 1997. 'Frontotemporal dementia and parkinsonism linked to chromosome 17: a consensus conference. Conference Participants', *Ann Neurol*, 41: 706-15.

Fowler, J. S., N. D. Volkow, G. J. Wang, N. Pappas, J. Logan, R. MacGregor, D. Alexoff, C. Shea, D. Schlyer, A. P. Wolf, D. Warner, I. Zezulkova, and R. Cilento. 1996. 'Inhibition of monoamine oxidase B in the brains of smokers', *Nature*, 379: 733-6.

Frasier, M., M. Walzer, L. McCarthy, D. Magnuson, J. M. Lee, C. Haas, P. Kahle, and B. Wolozin. 2005. 'Tau phosphorylation increases in symptomatic mice overexpressing A30P alpha-synuclein', *Exp Neurol*, 192: 274-87.

Fung, H. C., S. Scholz, M. Matarin, J. Simon-Sanchez, D. Hernandez, A. Britton, J. R. Gibbs, C. Langefeld, M. L. Stiegert, J. Schymick, M. S. Okun, R. J. Mandel, H. H. Fernandez, K. D. Foote, R. L. Rodriguez, E. Peckham, F. W. De Vrieze, K. Gwinn-Hardy, J. A. Hardy, and A. Singleton. 2006. 'Genome-wide genotyping in Parkinson's disease and neurologically normal controls: first stage analysis and public release of data', *Lancet Neurol*, 5: 911-6.

Fung, H. C., G. Xiromerisiou, J. R. Gibbs, Y. R. Wu, J. Eerola, V. Gourbali, O. Hellstrom, C. M. Chen, J. Duckworth, A. Papadimitriou, P. J. Tienari, G. M. Hadjigeorgiou, J. Hardy, and A. B. Singleton. 2006. 'Association of Tau haplotype-tagging polymorphisms with Parkinson's disease in diverse ethnic Parkinson's disease cohorts', *Neurodegener Dis*, 3: 327-33.

Geller, A. I., K. Keyomarsi, J. Bryan, and A. B. Pardee. 1990. 'An efficient deletion mutant packaging system for defective herpes simplex virus vectors: potential applications to human gene therapy and neuronal physiology', *Proc Natl Acad Sci U S A*, 87: 8950-4.

Gerrish, A., G. Russo, A. Richards, V. Moskvina, D. Ivanov, D. Harold, R. Sims, R. Abraham, P. Hollingworth, J. Chapman, M. Hamshere, J. S. Pahwa, K. Dowzell, A. Williams, N. Jones, C. Thomas, A. Stretton, A. R. Morgan, S. Lovestone, J. Powell, P. Proitsi, M. K. Lupton, C. Brayne, D. C. Rubinsztein, M. Gill, B. Lawlor, A. Lynch, K. Morgan, K. S. Brown, P. A. Passmore, D. Craig, B. McGuinness, S. Todd, J. A. Johnston, C. Holmes, D. Mann, A. D. Smith, S. Love, P. G. Kehoe, J. Hardy, S. Mead, N. Fox, M. Rossor, J. Collinge, W. Maier, F. Jessen, H. Kölsch, R. Heun, B. Schürmann, H. van den Bussche, I. Heuser, J. Kornhuber, J. Wiltfang, M. Dichgans, L. Frölich, H. Hampel, M. Hüll, D. Rujescu, A. M. Goate, J. S. Kauwe, C. Cruchaga, P. Nowotny, J. C. Morris, K. Mayo, G. Livingston, N. J. Bass, H. Gurling, A. McQuillin, R. Gwilliam, P. Deloukas, G. Davies, S. E. Harris, J. M. Starr, I. J. Deary, A. Al-Chalabi, C. E. Shaw, M. Tsolaki, A. B. Singleton, R. Guerreiro, T. W. Mühleisen, M. M. Nöthen, S. Moebus, K. H. Jöckel, N. Klopp, H. E. Wichmann, M. M. Carrasquillo, V. S. Pankratz, S. G. Younkin, L. Jones, P. A. Holmans, M. C. O'Donovan, M. J. Owen, and J. Williams. 2012. 'The role of variation at AβPP, PSEN1, PSEN2, and MAPT in late onset Alzheimer's disease', *J Alzheimers Dis*, 28: 377-87.

Giasson, B. I., M. S. Forman, M. Higuchi, L. I. Golbe, C. L. Graves, P. T. Kotzbauer, J. Q. Trojanowski, and V. M. Lee. 2003. 'Initiation and synergistic fibrillization of tau and alpha-synuclein', *Science*, 300: 636-40.

Gibbs, J. R., M. P. van der Brug, D. G. Hernandez, B. J. Traynor, M. A. Nalls, S. L. Lai, S. Arepalli, A. Dillman, I. P. Rafferty, J. Troncoso, R. Johnson, H. R. Zielke, L. Ferrucci, D. L. Longo, M. R. Cookson, and A. B. Singleton. 2010. 'Abundant quantitative trait loci exist for DNA methylation and gene expression in human brain', *PLoS Genet*, 6: e1000952.

Gibson, D. G., L. Young, R. Y. Chuang, J. C. Venter, C. A. Hutchison, 3rd, and H. O. Smith. 2009. 'Enzymatic assembly of DNA molecules up to several hundred kilobases', *Nat Methods*, 6: 343-5.

Goate, A., M. C. Chartier-Harlin, M. Mullan, J. Brown, F. Crawford, L. Fidani, L. Giuffra, A. Haynes, N. Irving, and L. James. 1991. 'Segregation of a missense mutation in the amyloid precursor protein gene with familial Alzheimer's disease', *Nature*, 349: 704-6.

Goedert, M., and R. Jakes. 1990. 'Expression of separate isoforms of human tau protein: correlation with the tau pattern in brain and effects on tubulin polymerization', *EMBO J*, 9: 4225-30.

Goedert, M., M. G. Spillantini, R. Jakes, D. Rutherford, and R. A. Crowther. 1989b. 'Multiple isoforms of human microtubule-associated protein tau: sequences and localization in neurofibrillary tangles of Alzheimer's disease', *Neuron*, 3: 519-26.

Goedert, M., M. G. Spillantini, M. C. Potier, J. Ulrich, and R. A. Crowther. 1989a. 'Cloning and sequencing of the cDNA encoding an isoform of microtubule-associated protein tau containing four tandem repeats: differential expression of tau protein mRNAs in human brain', *EMBO J*, 8: 393-9.

Goker-Alpan, O., R. Schiffmann, M. E. LaMarca, R. L. Nussbaum, A. McInerney-Leo, and E. Sidransky. 2004. 'Parkinsonism among Gaucher disease carriers', *J Med Genet*, 41: 937-40.

Golbe, L. I., A. M. Lazzarini, J. R. Spychala, W. G. Johnson, E. S. Stenroos, M. H. Mark, and J. I. Sage. 2001. 'The Tau A0 allele in Parkinson's disease', *Mov Disord*, 16: 442-7.

Goode, B. L., and S. C. Feinstein. 1994. 'Identification of a novel microtubule binding and assembly domain in the developmentally regulated inter-repeat region of tau', *J Cell Biol*, 124: 769-82.

Goris, A., C. H. Williams-Gray, G. R. Clark, T. Foltynie, S. J. Lewis, J. Brown, M. Ban, M. G. Spillantini, A. Compston, D. J. Burn, P. F. Chinnery, R. A. Barker, and S. J. Sawcer. 2007. 'Tau and α-synuclein in susceptibility to, and dementia in, Parkinson's disease', *Ann Neurol*, 62: 145-53.

Götz, J., F. Chen, J. van Dorpe, and R. M. Nitsch. 2001. 'Formation of neurofibrillary tangles in P301l tau transgenic mice induced by Abeta 42 fibrils', Science, 293: 1491-5.

Goudriaan, A., N. Camargo, K. E. Carney, S. H. Oliet, A. B. Smit, and M. H. Verheijen. 2014. 'Novel cell separation method for molecular analysis of neuron-astrocyte co-cultures', *Front Cell Neurosci*, 8: 12.

Greggio, E., S. Jain, A. Kingsbury, R. Bandopadhyay, P. Lewis, A. Kaganovich, M. P. van der Brug, A. Beilina, J. Blackinton, K. J. Thomas, R. Ahmad, D. W. Miller, S. Kesavapany, A. Singleton, A. Lees, R. J. Harvey, K. Harvey, and M. R. Cookson. 2006. 'Kinase activity is required for the toxic effects of mutant LRRK2/dardarin', *Neurobiol Dis*, 23: 329-41.

Grenier, K., G. L. McLelland, and E. A. Fon. 2013. 'Parkin- and PINK1-Dependent Mitophagy in Neurons: Will the Real Pathway Please Stand Up?', *Front Neurol*, 4: 100.

Griffith, L. M., and T. D. Pollard. 1978. 'Evidence for actin filament-microtubule interaction mediated by microtubule-associated proteins', *J Cell Biol*, 78: 958-65.

Griffith, L. M., and T. D. Pollard. 1982. 'The interaction of actin filaments with microtubules and microtubule-associated proteins', *J Biol Chem*, 257: 9143-51.

Grover, A., E. England, M. Baker, N. Sahara, J. Adamson, B. Granger, H. Houlden, U. Passant, S. H. Yen, M. DeTure, and M. Hutton. 2003. 'A novel tau mutation in exon 9 (1260V) causes a four-repeat tauopathy', *Exp Neurol*, 184: 131-40.

Gumucio, A., L. Lannfelt, and L. N. Nilsson. 2013. 'Lack of exon 10 in the murine tau gene results in mild sensorimotor defects with aging', *BMC Neurosci*, 14: 148.

Gustke, N., B. Trinczek, J. Biernat, E. M. Mandelkow, and E. Mandelkow. 1994. 'Domains of tau protein and interactions with microtubules', *Biochemistry*, 33: 9511-22.

Hamza, T. H., C. P. Zabetian, A. Tenesa, A. Laederach, J. Montimurro, D. Yearout, D. M. Kay, K. F. Doheny, J. Paschall, E. Pugh, V. I. Kusel, R. Collura, J. Roberts, A. Griffith, A.

Samii, W. K. Scott, J. Nutt, S. A. Factor, and H. Payami. 2010. 'Common genetic variation in the *HLA* region is associated with late-onset sporadic Parkinson's disease', *Nat Genet*, 42: 781-5.

Handel, A. E., S. Chintawar, T. Lalic, E. Whiteley, J. Vowles, A. Giustacchini, K. Argoud, P. Sopp, M. Nakanishi, R. Bowden, S. Cowley, S. Newey, C. Akerman, C. P. Ponting, and M. Z. Cader. 2016. 'Assessing similarity to primary tissue and cortical layer identity in induced pluripotent stem cell-derived cortical neurons through single-cell transcriptomics', Hum Mol Genet, 25: 989-1000.

Hardy, J. A., and G. A. Higgins. 1992. 'Alzheimer's disease: the amyloid cascade hypothesis', Science, 256: 184-5.

Hargus, G., O. Cooper, M. Deleidi, A. Levy, K. Lee, E. Marlow, A. Yow, F. Soldner, D. Hockemeyer, P. J. Hallett, T. Osborn, R. Jaenisch, and O. Isacson. 2010. 'Differentiated Parkinson patient-derived induced pluripotent stem cells grow in the adult rodent brain and reduce motor asymmetry in Parkinsonian rats', *Proc Natl Acad Sci U S A*, 107: 15921-6.

Harper, S. Q., and B. L. Davidson. 2005. 'Plasmid-based RNA interference: construction of small-hairpin RNA expression vectors', *Methods Mol Biol*, 309: 219-35.

Hartfield, E. M., M. Yamasaki-Mann, H. J. Ribeiro Fernandes, J. Vowles, W. S. James, S. A. Cowley, and R. Wade-Martins. 2014. 'Physiological characterisation of human iPS-derived dopaminergic neurons', *PLoS One*, 9: e87388.

Hasegawa, M., M. J. Smith, M. Iijima, T. Tabira, and M. Goedert. 1999. 'FTDP-17 mutations N279K and S305N in tau produce increased splicing of exon 10', *FEBS Lett*, 443: 93-6.

Hayesmoore, J. B., N. J. Bray, W. C. Cross, M. J. Owen, M. C. O'Donovan, and H. R. Morris. 2009. 'The effect of age and the H1c MAPT haplotype on MAPT expression in human brain', *Neurobiol Aging*, 30: 1652-6.

He, H. J., X. S. Wang, R. Pan, D. L. Wang, M. N. Liu, and R. Q. He. 2009. 'The proline-rich domain of tau plays a role in interactions with actin', *BMC Cell Biol*, 10: 81.

Healy, D. G., P. M. Abou-Sleiman, A. J. Lees, J. P. Casas, N. Quinn, K. Bhatia, A. D. Hingorani, and N. W. Wood. 2004. 'Tau gene and Parkinson's disease: a case-control study and meta-analysis', *J Neurol Neurosurg Psychiatry*, 75: 962-5.

Hedlund, E., J. Pruszak, A. Ferree, A. Viñuela, S. Hong, O. Isacson, and K. S. Kim. 2007. 'Selection of embryonic stem cell-derived enhanced green fluorescent protein-positive dopamine neurons using the tyrosine hydroxylase promoter is confounded by reporter gene expression in immature cell populations', *Stem Cells*, 25: 1126-35.

Hedlund, E., J. Pruszak, T. Lardaro, W. Ludwig, A. Viñuela, K. S. Kim, and O. Isacson. 2008. 'Embryonic stem cell-derived Pitx3-enhanced green fluorescent protein midbrain dopamine neurons survive enrichment by fluorescence-activated cell sorting and function in an animal model of Parkinson's disease', *Stem Cells*, 26: 1526-36.

Heikkila, R. E., A. Hess, and R. C. Duvoisin. 1984. 'Dopaminergic neurotoxicity of 1-methyl-4-phenyl-1,2,5,6-tetrahydropyridine in mice', *Science*, 224: 1451-3.

Hirsch, E., A. M. Graybiel, and Y. A. Agid. 1988. 'Melanized dopaminergic neurons are differentially susceptible to degeneration in Parkinson's disease', *Nature*, 334: 345-8.

Hockemeyer, D., H. Wang, S. Kiani, C. S. Lai, Q. Gao, J. P. Cassady, G. J. Cost, L. Zhang, Y. Santiago, J. C. Miller, B. Zeitler, J. M. Cherone, X. Meng, S. J. Hinkley, E. J. Rebar, P. D. Gregory, F. D. Urnov, and R. Jaenisch. 2011. 'Genetic engineering of human pluripotent cells using TALE nucleases', *Nat Biotechnol*, 29: 731-4.

Hoenicka, J., M. Perez, J. Perez-Tur, A. Barabash, M. Godoy, L. Vidal, R. Astarloa, J. Avila, T. Nygaard, and J. G. de Yebenes. 1999. 'The *tau* gene A0 allele and progressive supranuclear palsy', *Neurology*, 53: 1219-25.

Hong, M., V. Zhukareva, V. Vogelsberg-Ragaglia, Z. Wszolek, L. Reed, B. I. Miller, D. H. Geschwind, T. D. Bird, D. McKeel, A. Goate, J. C. Morris, K. C. Wilhelmsen, G. D.

Schellenberg, J. Q. Trojanowski, and V. M. Lee. 1998. 'Mutation-specific functional impairments in distinct tau isoforms of hereditary FTDP-17', *Science*, 282: 1914-7.

Horowitz, P. M., N. LaPointe, A. L. Guillozet-Bongaarts, R. W. Berry, and L. I. Binder. 2006. 'N-terminal fragments of tau inhibit full-length tau polymerization in vitro', *Biochemistry*, 45: 12859-66.

Houlden, H., M. Baker, H. R. Morris, N. MacDonald, S. Pickering-Brown, J. Adamson, A. J. Lees, M. N. Rossor, N. P. Quinn, A. Kertesz, M. N. Khan, J. Hardy, P. L. Lantos, P. St George-Hyslop, D. G. Munoz, D. Mann, A. E. Lang, C. Bergeron, E. H. Bigio, I. Litvan, K. P. Bhatia, D. Dickson, N. W. Wood, and M. Hutton. 2001. 'Corticobasal degeneration and progressive supranuclear palsy share a common tau haplotype', *Neurology*, 56: 1702-6.

Hrvatin, S., F. Deng, C. W. O'Donnell, D. K. Gifford, and D. A. Melton. 2014. 'MARIS: method for analyzing RNA following intracellular sorting', *PLoS One*, 9: e89459.

Hsieh, C. H., A. Shaltouki, A. E. Gonzalez, A. Bettencourt da Cruz, L. F. Burbulla, E. St Lawrence, B. Schüle, D. Krainc, T. D. Palmer, and X. Wang. 2016. 'Functional Impairment in Miro Degradation and Mitophagy Is a Shared Feature in Familial and Sporadic Parkinson's Disease', *Cell Stem Cell*.

Hunn, B. H., S. J. Cragg, J. P. Bolam, M. G. Spillantini, and R. Wade-Martins. 2015. 'Impaired intracellular trafficking defines early Parkinson's disease', *Trends Neurosci*, 38: 178-88.

Huot, P., S. H. Fox, and J. M. Brotchie. 2016. 'Dopamine Reuptake Inhibitors in Parkinson's Disease: A Review of Nonhuman Primate Studies and Clinical Trials', *J Pharmacol Exp Ther*, 357: 562-9.

Hutton, M., C. L. Lendon, P. Rizzu, M. Baker, S. Froelich, H. Houlden, S. Pickering-Brown, S. Chakraverty, A. Isaacs, A. Grover, J. Hackett, J. Adamson, S. Lincoln, D. Dickson, P. Davies, R. C. Petersen, M. Stevens, E. de Graaff, E. Wauters, J. van Baren, M. Hillebrand, M. Joosse, J. M. Kwon, P. Nowotny, L. K. Che, J. Norton, J. C. Morris, L. A. Reed, J. Trojanowski, H. Basun, L. Lannfelt, M. Neystat, S. Fahn, F. Dark, T. Tannenberg, P. R. Dodd, N. Hayward, J. B. Kwok, P. R. Schofield, A. Andreadis, J. Snowden, D. Craufurd, D. Neary, F. Owen, B. A. Oostra, J. Hardy, A. Goate, J. van Swieten, D. Mann, T. Lynch, and P. Heutink. 1998. 'Association of missense and 5'-splice-site mutations in tau with the inherited dementia FTDP-17', *Nature*, 393: 702-5.

Höglinger, G. U., N. M. Melhem, D. W. Dickson, P. M. Sleiman, L. S. Wang, L. Klei, R. Rademakers, R. de Silva, I. Litvan, D. E. Riley, J. C. van Swieten, P. Heutink, Z. K. Wszolek, R. J. Uitti, J. Vandrovcova, H. I. Hurtig, R. G. Gross, W. Maetzler, S. Goldwurm, E. Tolosa, B. Borroni, P. Pastor, L. B. Cantwell, M. R. Han, A. Dillman, M. P. van der Brug, J. R. Gibbs, M. R. Cookson, D. G. Hernandez, A. B. Singleton, M. J. Farrer, C. E. Yu, L. I. Golbe, T. Revesz, J. Hardy, A. J. Lees, B. Devlin, H. Hakonarson, U. Müller, G. D. Schellenberg, and PSP Genetics Study Group. 2011. 'Identification of common variants influencing risk of the tauopathy progressive supranuclear palsy', *Nat Genet*, 43: 699-705.

Iacovitti, L., X. Wei, J. Cai, E. W. Kostuk, R. Lin, A. Gorodinsky, P. Roman, G. Kusek, S. S. Das, A. Dufour, T. N. Martinez, and K. D. Dave. 2014. 'The hTH-GFP reporter rat model for the study of Parkinson's disease', *PLoS One*, 9: e113151.

Ibáñez, P., A. M. Bonnet, B. Débarges, E. Lohmann, F. Tison, P. Pollak, Y. Agid, A. Dürr, and A. Brice. 2004. 'Causal relation between alpha-synuclein gene duplication and familial Parkinson's disease', *Lancet*, 364: 1169-71.

Imaizumi, Y., Y. Okada, W. Akamatsu, M. Koike, N. Kuzumaki, H. Hayakawa, T. Nihira, T. Kobayashi, M. Ohyama, S. Sato, M. Takanashi, M. Funayama, A. Hirayama, T. Soga, T. Hishiki, M. Suematsu, T. Yagi, D. Ito, A. Kosakai, K. Hayashi, M. Shouji, A. Nakanishi,

N. Suzuki, Y. Mizuno, N. Mizushima, M. Amagai, Y. Uchiyama, H. Mochizuki, N. Hattori, and H. Okano. 2012. 'Mitochondrial dysfunction associated with increased oxidative stress and α-synuclein accumulation in PARK2 iPSC-derived neurons and postmortem brain tissue', *Mol Brain*, 5: 35.

Ingelsson, M., K. Ramasamy, C. Russ, S. H. Freeman, J. Orne, S. Raju, T. Matsui, J. H. Growdon, M. P. Frosch, B. Ghetti, R. H. Brown, M. C. Irizarry, and B. T. Hyman. 2007. 'Increase in the relative expression of tau with four microtubule binding repeat regions in frontotemporal lobar degeneration and progressive supranuclear palsy brains', *Acta Neuropathol*, 114: 471-9.

Inoue, R., K. A. Moghaddam, M. Ranasinghe, Y. Saeki, E. A. Chiocca, and R. Wade-Martins. 2004. 'Infectious delivery of the 132 kb CDKN2A/CDKN2B genomic DNA region results in correctly spliced gene expression and growth suppression in glioma cells', *Gene Ther*, 11: 1195-204.

International Parkinson Disease Genomics Consortium (IPDGC), M. A. Nalls, V. Plagnol, D. G. Hernandez, M. Sharma, U. M. Sheerin, M. Saad, J. Simon-Sanchez, C. Schulte, S. Lesage, S. Sveinbjornsdottir, K. Stefansson, M. Martinez, J. Hardy, P. Heutink, A. Brice, T. Gasser, A. B. Singleton, and N. W. Wood. 2011. 'Imputation of sequence variants for identification of genetic risks for Parkinson's disease: a meta-analysis of genome-wide association studies', *Lancet*, 377: 641-9.

International Parkinson's Disease Genomics Consortium (IPDGC) and Wellcome Trust Case Control Consortium 2 (WTCCC2). 2011. 'A two-stage meta-analysis identifies several new loci for Parkinson's disease', *PLoS Genet*, 7: e1002142.

Iovino, M., S. Agathou, A. González-Rueda, M. Del Castillo Velasco-Herrera, B. Borroni, A. Alberici, T. Lynch, S. O'Dowd, I. Geti, D. Gaffney, L. Vallier, O. Paulsen, R. T. Káradóttir, and M. G. Spillantini. 2015. 'Early maturation and distinct tau pathology in induced pluripotent stem cell-derived neurons from patients with MAPT mutations', *Brain*, 138: 3345-59.

Iovino, M., R. Patani, C. Watts, S. Chandran, and M. G. Spillantini. 2010. 'Human stem cell-derived neurons: a system to study human tau function and dysfunction', *PLoS One*, 5: e13947.

Iovino, M., U. Pfisterer, J. L. Holton, T. Lashley, R. J. Swingler, L. Calo, R. Treacy, T. Revesz, M. Parmar, M. Goedert, M. M. Muqit, and M. G. Spillantini. 2014. 'The novel MAPT mutation K298E: mechanisms of mutant tau toxicity, brain pathology and tau expression in induced fibroblast-derived neurons', *Acta Neuropathol*, 127: 283-95.

Ittner, L. M., Y. D. Ke, F. Delerue, M. Bi, A. Gladbach, J. van Eersel, H. Wölfing, B. C. Chieng, M. J. Christie, I. A. Napier, A. Eckert, M. Staufenbiel, E. Hardeman, and J. Götz. 2010. 'Dendritic function of tau mediates amyloid-beta toxicity in Alzheimer's disease mouse models', *Cell*, 142: 387-97.

Janezic, S., S. Threlfell, P. D. Dodson, M. J. Dowie, T. N. Taylor, D. Potgieter, L. Parkkinen, S. L. Senior, S. Anwar, B. Ryan, T. Deltheil, P. Kosillo, M. Cioroch, K. Wagner, O. Ansorge, D. M. Bannerman, J. P. Bolam, P. J. Magill, S. J. Cragg, and R. Wade-Martins. 2013. 'Deficits in dopaminergic transmission precede neuron loss and dysfunction in a new Parkinson model', *Proc Natl Acad Sci U S A*, 110: E4016-25.

Jeganathan, S., M. von Bergen, H. Brutlach, H. J. Steinhoff, and E. Mandelkow. 2006. 'Global hairpin folding of tau in solution', *Biochemistry*, 45: 2283-93.

Jensen, P. H., H. Hager, M. S. Nielsen, P. Hojrup, J. Gliemann, and R. Jakes. 1999. 'alpha-synuclein binds to Tau and stimulates the protein kinase A-catalyzed tau phosphorylation of serine residues 262 and 356', *J Biol Chem*, 274: 25481-9.

Jeong, K. H., J. C. Bakowska, I. O. Song, N. Fu, X. O. Breakefield, and U. B. Kaiser. 2007. 'Improvement in reproductive parameters in hypogonadal female mice by regulated gene replacement therapy in the central nervous system', *Gene Ther*, 14: 1092-101.

Jiang, H., Y. Ren, E. Y. Yuen, P. Zhong, M. Ghaedi, Z. Hu, G. Azabdaftari, K. Nakaso, Z. Yan, and J. Feng. 2012. 'Parkin controls dopamine utilization in human midbrain dopaminergic neurons derived from induced pluripotent stem cells', *Nat Commun*, 3: 668.

Jiang, H., Z. Xu, P. Zhong, Y. Ren, G. Liang, H. A. Schilling, Z. Hu, Y. Zhang, X. Wang, S. Chen, Z. Yan, and J. Feng. 2015. 'Cell cycle and p53 gate the direct conversion of human fibroblasts to dopaminergic neurons', Nat Commun, 6: 10100.

Johansson, A., H. Zetterberg, A. Hakansson, H. Nissbrandt, and K. Blennow. 2005. '*TAU* haplotype and the *Saitohin* Q7R gene polymorphism do not influence CSF Tau in Alzheimer's disease and are not associated with frontotemporal dementia or Parkinson's disease', *Neurodegener Dis*, 2: 28-35.

Jones, E. V., D. Cook, and K. K. Murai. 2012. 'A neuron-astrocyte co-culture system to investigate astrocyte-secreted factors in mouse neuronal development', *Methods Mol Biol*, 814: 341-52.

Jun, G., C. A. Ibrahim-Verbaas, M. Vronskaya, J. C. Lambert, J. Chung, A. C. Naj, B. W. Kunkle, L. S. Wang, J. C. Bis, C. Bellenguez, D. Harold, K. L. Lunetta, A. L. Destefano, B. Grenier-Boley, R. Sims, G. W. Beecham, A. V. Smith, V. Chouraki, K. L. Hamilton-Nelson, M. A. Ikram, N. Fievet, N. Denning, E. R. Martin, H. Schmidt, Y. Kamatani, M. L. Dunstan, O. Valladares, A. R. Laza, D. Zelenika, A. Ramirez, T. M. Foroud, S. H. Choi, A. Boland, T. Becker, W. A. Kukull, S. J. van der Lee, F. Pasquier, C. Cruchaga, D. Beekly, A. L. Fitzpatrick, O. Hanon, M. Gill, R. Barber, V. Gudnason, D. Campion, S. Love, D. A. Bennett, N. Amin, C. Berr, M. Tsolaki, J. D. Buxbaum, O. L. Lopez, V. Deramecourt, N. C. Fox, L. B. Cantwell, L. Tárraga, C. Dufouil, J. Hardy, P. K. Crane, G. Eiriksdottir, D. Hannequin, R. Clarke, D. Evans, T. H. Mosley, L. Letenneur, C. Brayne, W. Maier, P. De Jager, V. Emilsson, J. F. Dartigues, H. Hampel, M. I. Kamboh, R. F. de Bruijn, C. Tzourio, P. Pastor, E. B. Larson, J. I. Rotter, M. C. O'Donovan, T. J. Montine, M. A. Nalls, S. Mead, E. M. Reiman, P. V. Jonsson, C. Holmes, P. H. St George-Hyslop, M. Boada, P. Passmore, J. R. Wendland, R. Schmidt, K. Morgan, A. R. Winslow, J. F. Powell, M. Carasquillo, S. G. Younkin, J. Jakobsdóttir, J. S. Kauwe, K. C. Wilhelmsen, D. Rujescu, M. M. Nöthen, A. Hofman, L. Jones, J. L. Haines, B. M. Psaty, C. Van Broeckhoven, P. Holmans, L. J. Launer, R. Mayeux, M. Lathrop, A. M. Goate, V. Escott-Price, S. Seshadri, M. A. Pericak-Vance, P. Amouyel, J. Williams, C. M. van Duijn, G. D. Schellenberg, L. A. Farrer, and IGAP Consortium. 2016. 'A novel Alzheimer disease locus located near the gene encoding tau protein', *Mol Psychiatry*, 21: 108-17.

Kachergus, J., I. F. Mata, M. Hulihan, J. P. Taylor, S. Lincoln, J. Aasly, J. M. Gibson, O. A. Ross, T. Lynch, J. Wiley, H. Payami, J. Nutt, D. M. Maraganore, K. Czyzewski, M. Styczynska, Z. K. Wszolek, M. J. Farrer, and M. Toft. 2005. 'Identification of a novel LRRK2 mutation linked to autosomal dominant parkinsonism: evidence of a common founder across European populations', *Am J Hum Genet*, 76: 672-80.

Kahle, P. J., M. Neumann, L. Ozmen, V. Muller, H. Jacobsen, A. Schindzielorz, M. Okochi, U. Leimer, H. van Der Putten, A. Probst, E. Kremmer, H. A. Kretzschmar, and C. Haass. 2000. 'Subcellular localization of wild-type and Parkinson's disease-associated mutant alpha -synuclein in human and transgenic mouse brain', *J Neurosci*, 20: 6365-73.

Kalbfuss, B., S. A. Mabon, and T. Misteli. 2001. 'Correction of alternative splicing of tau in frontotemporal dementia and parkinsonism linked to chromosome 17', *J Biol Chem*, 276: 42986-93.

Kaneda, N., T. Sasaoka, K. Kobayashi, K. Kiuchi, I. Nagatsu, Y. Kurosawa, K. Fujita, M. Yokoyama, T. Nomura, and M. Katsuki. 1991. 'Tissue-specific and high-level expression of the human tyrosine hydroxylase gene in transgenic mice', *Neuron*, 6: 583-94.

Kar, A., N. Havlioglu, W. Y. Tarn, and J. Y. Wu. 2006. 'RBM4 interacts with an intronic element and stimulates tau exon 10 inclusion', *J Biol Chem*, 281: 24479-88.

Kelly, B. B., E. Hedlund, C. Kim, H. Ishiguro, O. Isacson, D. M. Chikaraishi, K. S. Kim, and G. Feng. 2006. 'A tyrosine hydroxylase-yellow fluorescent protein knock-in reporter system labeling dopaminergic neurons reveals potential regulatory role for the first intron of the rodent tyrosine hydroxylase gene', *Neuroscience*, 142: 343-54.

Kessler, M. A., M. Yang, K. L. Gollomp, H. Jin, and L. Iacovitti. 2003. 'The human tyrosine hydroxylase gene promoter', *Brain Res Mol Brain Res*, 112: 8-23.

King, M. E., H. M. Kan, P. W. Baas, A. Erisir, C. G. Glabe, and G. S. Bloom. 2006. 'Tau-dependent microtubule disassembly initiated by prefibrillar beta-amyloid', *J Cell Biol*, 175: 541-6.

Kobayashi, H., H. Ujike, J. Hasegawa, M. Yamamoto, A. Kanzaki, and I. Sora. 2006. 'Correlation of tau gene polymorphism with age at onset of Parkinson's disease', *Neurosci Lett*, 405: 202-6.

Koepp, M. J., R. N. Gunn, A. D. Lawrence, V. J. Cunningham, A. Dagher, T. Jones, D. J. Brooks, C. J. Bench, and P. M. Grasby. 1998. 'Evidence for striatal dopamine release during a video game', *Nature*, 393: 266-8.

Koprivica, V., D. L. Stone, J. K. Park, M. Callahan, A. Frisch, I. J. Cohen, N. Tayebi, and E. Sidransky. 2000. 'Analysis and classification of 304 mutant alleles in patients with type 1 and type 3 Gaucher disease', *Am J Hum Genet*, 66: 1777-86.

Kordower, J. H., Y. Chu, R. A. Hauser, T. B. Freeman, and C. W. Olanow. 2008. 'Lewy body-like pathology in long-term embryonic nigral transplants in Parkinson's disease', *Nat Med*, 14: 504-6.

Korolchuk, V. I., S. Saiki, M. Lichtenberg, F. H. Siddiqi, E. A. Roberts, S. Imarisio, L. Jahreiss, S. Sarkar, M. Futter, F. M. Menzies, C. J. O'Kane, V. Deretic, and D. C. Rubinsztein. 2011. 'Lysosomal positioning coordinates cellular nutrient responses', *Nat Cell Biol*, 13: 453-60.

Kouri, N., O. A. Ross, B. Dombroski, C. S. Younkin, D. J. Serie, A. Soto-Ortolaza, M. Baker, N. C. Finch, H. Yoon, J. Kim, S. Fujioka, C. A. McLean, B. Ghetti, S. Spina, L. B. Cantwell, M. R. Farlow, J. Grafman, E. D. Huey, M. Ryung Han, S. Beecher, E. T. Geller, H. A. Kretzschmar, S. Roeber, M. Gearing, J. L. Juncos, J. P. Vonsattel, V. M. Van Deerlin, M. Grossman, H. I. Hurtig, R. G. Gross, S. E. Arnold, J. Q. Trojanowski, V. M. Lee, G. K. Wenning, C. L. White, G. U. Höglinger, U. Müller, B. Devlin, L. I. Golbe, J. Crook, J. E. Parisi, B. F. Boeve, K. A. Josephs, Z. K. Wszolek, R. J. Uitti, N. R. Graff-Radford, I. Litvan, S. G. Younkin, L. S. Wang, N. Ertekin-Taner, R. Rademakers, H. Hakonarsen, G. D. Schellenberg, and D. W. Dickson. 2015. 'Genome-wide association study of corticobasal degeneration identifies risk variants shared with progressive supranuclear palsy', *Nat Commun*, 6: 7247.

Kriks, S., J. W. Shim, J. Piao, Y. M. Ganat, D. R. Wakeman, Z. Xie, L. Carrillo-Reid, G. Auyeung, C. Antonacci, A. Buch, L. Yang, M. F. Beal, D. J. Surmeier, J. H. Kordower, V. Tabar, and L. Studer. 2011. 'Dopamine neurons derived from human ES cells efficiently engraft in animal models of Parkinson's disease', *Nature*, 480: 547-51.

Krüger, R., W. Kuhn, T. Müller, D. Woitalla, M. Graeber, S. Kösel, H. Przuntek, J. T. Epplen, L. Schöls, and O. Riess. 1998. 'Ala30Pro mutation in the gene encoding alpha-synuclein in Parkinson's disease', *Nat Genet*, 18: 106-8.

Kural, C., H. Kim, S. Syed, G. Goshima, V. I. Gelfand, and P. R. Selvin. 2005. 'Kinesin and dynein move a peroxisome in vivo: a tug-of-war or coordinated movement?', *Science*, 308: 1469-72.

Kwok, J. B., E. T. Teber, C. Loy, M. Hallupp, G. Nicholson, G. D. Mellick, D. D. Buchanan, P. A. Silburn, and P. R. Schofield. 2004. 'Tau haplotypes regulate transcription and are associated with Parkinson's disease', *Ann Neurol*, 55: 329-34.

Laemmli, U. K. 1970. 'Cleavage of structural proteins during the assembly of the head of bacteriophage T4', *Nature*, 227: 680-5.

Lamark, T., V. Kirkin, I. Dikic, and T. Johansen. 2009. 'NBR1 and p62 as cargo receptors for selective autophagy of ubiquitinated targets', *Cell Cycle*, 8: 1986-90.

Lambert, J. C., C. A. Ibrahim-Verbaas, D. Harold, A. C. Naj, R. Sims, C. Bellenguez, A. L. DeStafano, J. C. Bis, G. W. Beecham, B. Grenier-Boley, G. Russo, T. A. Thorton-Wells, N. Jones, A. V. Smith, V. Chouraki, C. Thomas, M. A. Ikram, D. Zelenika, B. N. Vardarajan, Y. Kamatani, C. F. Lin, A. Gerrish, H. Schmidt, B. Kunkle, M. L. Dunstan, A. Ruiz, M. T. Bihoreau, S. H. Choi, C. Reitz, F. Pasquier, C. Cruchaga, D. Craig, N. Amin, C. Berr, O. L. Lopez, P. L. De Jager, V. Deramecourt, J. A. Johnston, D. Evans, S. Lovestone, L. Letenneur, F. J. Morón, D. C. Rubinsztein, G. Eiriksdottir, K. Sleegers, A. M. Goate, N. Fiévet, M. W. Huentelman, M. Gill, K. Brown, M. I. Kamboh, L. Keller, P. Barberger-Gateau, B. McGuiness, E. B. Larson, R. Green, A. J. Myers, C. Dufouil, S. Todd, D. Wallon, S. Love, E. Rogaeva, J. Gallacher, P. St George-Hyslop, J. Clarimon, A. Lleo, A. Bayer, D. W. Tsuang, L. Yu, M. Tsolaki, P. Bossù, G. Spalletta, P. Proitsi, J. Collinge, S. Sorbi, F. Sanchez-Garcia, N. C. Fox, J. Hardy, M. C. Deniz Naranjo, P. Bosco, R. Clarke, C. Brayne, D. Galimberti, M. Mancuso, F. Matthews, S. Moebus, P. Mecocci, M. Del Zompo, W. Maier, H. Hampel, A. Pilotto, M. Bullido, F. Panza, P. Caffarra, B. Nacmias, J. R. Gilbert, M. Mayhaus, L. Lannefelt, H. Hakonarson, S. Pichler, M. M. Carrasquillo, M. Ingelsson, D. Beekly, V. Alvarez, F. Zou, O. Valladares, S. G. Younkin, E. Coto, K. L. Hamilton-Nelson, W. Gu, C. Razquin, P. Pastor, I. Mateo, M. J. Owen, K. M. Faber, P. V. Jonsson, O. Combarros, M. C. O'Donovan, L. B. Cantwell, H. Soininen, D. Blacker, S. Mead, T. H. Mosley, D. A. Bennett, T. B. Harris, L. Fratiglioni, C. Holmes, R. F. de Bruijn, P. Passmore, T. J. Montine, K. Bettens, J. I. Rotter, A. Brice, K. Morgan, T. M. Foroud, W. A. Kukull, D. Hannequin, J. F. Powell, M. A. Nalls, K. Ritchie, K. L. Lunetta, J. S. Kauwe, E. Boerwinkle, M. Riemenschneider, M. Boada, M. Hiltuenen, E. R. Martin, R. Schmidt, D. Rujescu, L. S. Wang, J. F. Dartigues, R. Mayeux, C. Tzourio, A. Hofman, M. M. Nöthen, C. Graff, B. M. Psaty, L. Jones, J. L. Haines, P. A. Holmans, M. Lathrop, M. A. Pericak-Vance, L. J. Launer, L. A. Farrer, C. M. van Duijn, C. Van Broeckhoven, V. Moskvina, S. Seshadri, J. Williams, G. D. Schellenberg, P. Amouyel, European Alzheimer's Disease Initiative (EADI), Genetic and Environmental Risk in Alzheimer's Disease, Alzheimer's Disease Genetic Consortium, and Cohorts for Heart and Aging Research in Genomic Epidemiology. 2013. 'Meta-analysis of 74,046 individuals identifies 11 new susceptibility loci for Alzheimer's disease', *Nat Genet*, 45: 1452-8.

LaPointe, N. E., G. Morfini, G. Pigino, I. N. Gaisina, A. P. Kozikowski, L. I. Binder, and S. T. Brady. 2009. 'The amino terminus of tau inhibits kinesin-dependent axonal transport: implications for filament toxicity', *J Neurosci Res*, 87: 440-51.

Larkin, M. A., G. Blackshields, N. P. Brown, R. Chenna, P. A. McGettigan, H. McWilliam, F. Valentin, I. M. Wallace, A. Wilm, R. Lopez, J. D. Thompson, T. J. Gibson, and D. G. Higgins. 2007. 'Clustal W and Clustal X version 2.0', *Bioinformatics*, 23: 2947-8.

Lashuel, H. A., C. R. Overk, A. Oueslati, and E. Masliah. 2013. 'The many faces of α-synuclein: from structure and toxicity to therapeutic target', *Nat Rev Neurosci*, 14: 38-48.

Latourelle, J. C., A. Dumitriu, T. C. Hadzi, T. G. Beach, and R. H. Myers. 2012. 'Evaluation of Parkinson Disease Risk Variants as Expression-QTLs', *PLoS One*, 7: e46199.

Lau, D. H., M. Hogseth, E. C. Phillips, M. J. O'Neill, A. M. Pooler, W. Noble, and D. P. Hanger. 2016. 'Critical residues involved in tau binding to fyn: implications for tau phosphorylation in Alzheimer's disease', *Acta Neuropathol Commun*, 4: 49.

Lazzarini, AM, LI Golbe, DW Dickson, RC Duvoisin, and WG Johnson. 1997. 'Tau intronic polymorphism in Parkinson's disease and progressive supranuclear palsy [*American*

Academy of Neurology 49th Annual Meeting – Poster Abstract P06.088]', *Neurology*, 48: A427.

Lee, G., S. T. Newman, D. L. Gard, H. Band, and G. Panchamoorthy. 1998. 'Tau interacts with src-family non-receptor tyrosine kinases', *J Cell Sci*, 111 (Pt 21): 3167-77.

Lee, G., R. Thangavel, V. M. Sharma, J. M. Litersky, K. Bhaskar, S. M. Fang, L. H. Do, A. Andreadis, G. Van Hoesen, and H. Ksiezak-Reding. 2004. 'Phosphorylation of tau by fyn: implications for Alzheimer's disease', *J Neurosci*, 24: 2304-12.

Lee, J., K. Inoue, R. Ono, N. Ogonuki, T. Kohda, T. Kaneko-Ishino, A. Ogura, and F. Ishino. 2002. 'Erasing genomic imprinting memory in mouse clone embryos produced from day 11.5 primordial germ cells', *Development*, 129: 1807-17.

Lee, S., Y. Sato, and R. A. Nixon. 2011. 'Lysosomal proteolysis inhibition selectively disrupts axonal transport of degradative organelles and causes an Alzheimer's-like axonal dystrophy', *J Neurosci*, 31: 7817-30.

Legakis, J. E., W. L. Yen, and D. J. Klionsky. 2007. 'A cycling protein complex required for selective autophagy', *Autophagy*, 3: 422-32.

Lei, P., S. Ayton, D. I. Finkelstein, L. Spoerri, G. D. Ciccotosto, D. K. Wright, B. X. Wong, P. A. Adlard, R. A. Cherny, L. Q. Lam, B. R. Roberts, I. Volitakis, G. F. Egan, C. A. McLean, R. Cappai, J. A. Duce, and A. I. Bush. 2012. 'Tau deficiency induces parkinsonism with dementia by impairing APP-mediated iron export', *Nat Med*, 18: 291-5.

Lenartowski, R., and A. Goc. 2002. 'Tissue-specific association of the human tyrosine hydroxylase gene with the nuclear matrix', *Neurosci Lett*, 330: 151-4.

Lesage, S., M. Anheim, F. Letournel, L. Bousset, A. Honoré, N. Rozas, L. Pieri, K. Madiona, A. Dürr, R. Melki, C. Verny, A. Brice, and French Parkinson's Disease Genetics Study Group. 2013. 'G51D α-synuclein mutation causes a novel parkinsonian-pyramidal syndrome', *Ann Neurol*, 73: 459-71.

Levecque, C., A. Elbaz, J. Clavel, J. S. Vidal, P. Amouyel, A. Alperovitch, C. Tzourio, and M. C. Chartier-Harlin. 2004. 'Association of polymorphisms in the *Tau* and *Saitohin* genes with Parkinson's disease', *J Neurol Neurosurg Psychiatry*, 75: 478-80.

Levy, S. F., A. C. Leboeuf, M. R. Massie, M. A. Jordan, L. Wilson, and S. C. Feinstein. 2005. 'Three- and four-repeat tau regulate the dynamic instability of two distinct microtubule subpopulations in qualitatively different manners. Implications for neurodegeneration', *J Biol Chem*, 280: 13520-8.

Levy-Lahad, E., W. Wasco, P. Poorkaj, D. M. Romano, J. Oshima, W. H. Pettingell, C. E. Yu, P. D. Jondro, S. D. Schmidt, and K. Wang. 1995. 'Candidate gene for the chromosome 1 familial Alzheimer's disease locus', *Science*, 269: 973-7.

Lewis, J., D. W. Dickson, W. L. Lin, L. Chisholm, A. Corral, G. Jones, S. H. Yen, N. Sahara, L. Skipper, D. Yager, C. Eckman, J. Hardy, M. Hutton, and E. McGowan. 2001. 'Enhanced neurofibrillary degeneration in transgenic mice expressing mutant tau and APP', Science, 293: 1487-91.

Li, J. Y., E. Englund, J. L. Holton, D. Soulet, P. Hagell, A. J. Lees, T. Lashley, N. P. Quinn, S. Rehncrona, A. Björklund, H. Widner, T. Revesz, O. Lindvall, and P. Brundin. 2008. 'Lewy bodies in grafted neurons in subjects with Parkinson's disease suggest host-to-graft disease propagation', *Nat Med*, 14: 501-3.

Liao, H., Y. Li, D. L. Brautigan, and G. G. Gundersen. 1998. 'Protein phosphatase 1 is targeted to microtubules by the microtubule-associated protein Tau', *J Biol Chem*, 273: 21901-8.

Lieu, P. T., A. Fontes, M. C. Vemuri, and C. C. Macarthur. 2013. 'Generation of induced pluripotent stem cells with CytoTune, a non-integrating Sendai virus', *Methods Mol Biol*, 997: 45-56.

Lin, J. C., and W. Y. Tarn. 2005. 'Exon selection in alpha-tropomyosin mRNA is regulated by the antagonistic action of RBM4 and PTB', *Mol Cell Biol*, 25: 10111-21.

Lin, X., X. Ruan, M. G. Anderson, J. A. McDowell, P. E. Kroeger, S. W. Fesik, and Y. Shen. 2005. 'siRNA-mediated off-target gene silencing triggered by a 7 nt complementation', *Nucleic Acids Res*, 33: 4527-35.

Lisowiec, J., D. Magner, E. Kierzek, E. Lenartowicz, and R. Kierzek. 2015. 'Structural determinants for alternative splicing regulation of the MAPT pre-mRNA', *RNA Biol*, 12: 330-42.

Litersky, J. M., G. V. Johnson, R. Jakes, M. Goedert, M. Lee, and P. Seubert. 1996. 'Tau protein is phosphorylated by cyclic AMP-dependent protein kinase and calcium/calmodulin-dependent protein kinase II within its microtubule-binding domains at Ser-262 and Ser-356', *Biochem J*, 316 (Pt 2): 655-60.

Litvan, I., J. J. Hauw, J. J. Bartko, P. L. Lantos, S. E. Daniel, D. S. Horoupian, A. McKee, D. Dickson, C. Bancher, M. Tabaton, K. Jellinger, and D. W. Anderson. 1996. 'Validity and reliability of the preliminary NINDS neuropathologic criteria for progressive supranuclear palsy and related disorders', *J Neuropathol Exp Neurol*, 55: 97-105.

Liu, C., X. Song, R. Nisbet, and J. Götz. 2016. 'Co-immunoprecipitation with Tau Isoform-specific Antibodies Reveals Distinct Protein Interactions and Highlights a Putative Role for 2N Tau in Disease', *J Biol Chem*, 291: 8173-88.

Liu, C. W., G. Lee, and D. G. Jay. 1999. 'Tau is required for neurite outgrowth and growth cone motility of chick sensory neurons', *Cell Motil Cytoskeleton*, 43: 232-42.

Liu, G. H., K. Suzuki, J. Qu, I. Sancho-Martinez, F. Yi, M. Li, S. Kumar, E. Nivet, J. Kim, R. D. Soligalla, I. Dubova, A. Goebl, N. Plongthongkum, H. L. Fung, K. Zhang, J. F. Loring, L. C. Laurent, and J. C. Izpisua Belmonte. 2011. 'Targeted gene correction of laminopathy-associated LMNA mutations in patient-specific iPSCs', *Cell Stem Cell*, 8: 688-94.

Lubarsky, M., and J. L. Juncos. 2008. 'Progressive supranuclear palsy: a current review', *Neurologist*, 14: 79-88.

Lufino, M. M., R. Manservigi, and R. Wade-Martins. 2007. 'An S/MAR-based infectious episomal genomic DNA expression vector provides long-term regulated functional complementation of LDLR deficiency', *Nucleic Acids Res*, 35: e98.

Lufino, M. M., A. R. Popplestone, S. A. Cowley, P. A. Edser, W. S. James, and R. Wade-Martins. 2011. 'Episomal transgene expression in pluripotent stem cells', *Methods Mol Biol*, 767: 369-87.

Luk, C., G. Giovannoni, D. R. Williams, A. J. Lees, and R. de Silva. 2009. 'Development of a sensitive ELISA for quantification of three- and four-repeat tau isoforms in tauopathies', *J Neurosci Methods*, 180: 34-42.

Luo, Y., and M. D. Disney. 2014. 'Bottom-up design of small molecules that stimulate exon 10 skipping in mutant MAPT pre-mRNA', *Chembiochem*, 15: 2041-4.

Lwin, A., E. Orvisky, O. Goker-Alpan, M. E. LaMarca, and E. Sidransky. 2004. 'Glucocerebrosidase mutations in subjects with parkinsonism', *Mol Genet Metab*, 81: 70-3.

Ma, S. Y., M. Röyttä, J. O. Rinne, Y. Collan, and U. K. Rinne. 1997. 'Correlation between neuromorphometry in the substantia nigra and clinical features in Parkinson's disease using disector counts', *J Neurol Sci*, 151: 83-7.

MacAskill, A. F., K. Brickley, F. A. Stephenson, and J. T. Kittler. 2009. 'GTPase dependent recruitment of Grif-1 by Miro1 regulates mitochondrial trafficking in hippocampal neurons', *Mol Cell Neurosci*, 40: 301-12.

MacLeod, D., J. Dowman, R. Hammond, T. Leete, K. Inoue, and A. Abeliovich. 2006. 'The familial Parkinsonism gene LRRK2 regulates neurite process morphology', *Neuron*, 52: 587-93.

Maday, S., K. E. Wallace, and E. L. Holzbaur. 2012. 'Autophagosomes initiate distally and mature during transport toward the cell soma in primary neurons', *J Cell Biol*, 196: 407-17.

Magnani, E., J. Fan, L. Gasparini, M. Golding, M. Williams, G. Schiavo, M. Goedert, L. A. Amos, and M. G. Spillantini. 2007. 'Interaction of tau protein with the dynactin complex', *EMBO J*, 26: 4546-54.

Majounie, E., W. Cross, V. Newsway, A. Dillman, J. Vandrovcova, C. M. Morris, M. A. Nalls, L. Ferrucci, M. J. Owen, M. C. O'Donovan, M. R. Cookson, A. B. Singleton, R. de Silva, and H. R. Morris. 2013. 'Variation in tau isoform expression in different brain regions and disease states', *Neurobiol Aging*, 34: 1922.e7-22.e12.

Mali, P., L. Yang, K. M. Esvelt, J. Aach, M. Guell, J. E. DiCarlo, J. E. Norville, and G. M. Church. 2013. 'RNA-guided human genome engineering via Cas9', *Science*, 339: 823-6.

Mamah, C. E., T. G. Lesnick, S. J. Lincoln, K. J. Strain, M. de Andrade, J. H. Bower, J. E. Ahlskog, W. A. Rocca, M. J. Farrer, and D. M. Maraganore. 2005. 'Interaction of alpha-synuclein and tau genotypes in Parkinson's disease', *Ann Neurol*, 57: 439-43.

Mandelkow, E. M., E. Thies, B. Trinczek, J. Biernat, and E. Mandelkow. 2004. 'MARK/PAR1 kinase is a regulator of microtubule-dependent transport in axons', *J Cell Biol*, 167: 99-110.

Manzoni, C., A. Mamais, S. Dihanich, R. Abeti, M. P. Soutar, H. Plun-Favreau, P. Giunti, S. A. Tooze, R. Bandopadhyay, and P. A. Lewis. 2013. 'Inhibition of LRRK2 kinase activity stimulates macroautophagy', *Biochim Biophys Acta*, 1833: 2900-10.

Manzoni, C., A. Mamais, S. Dihanich, P. McGoldrick, M. J. Devine, J. Zerle, E. Kara, J. W. Taanman, D. G. Healy, J. F. Marti-Masso, A. H. Schapira, H. Plun-Favreau, S. Tooze, J. Hardy, R. Bandopadhyay, and P. A. Lewis. 2013. 'Pathogenic Parkinson's disease mutations across the functional domains of LRRK2 alter the autophagic/lysosomal response to starvation', *Biochem Biophys Res Commun*, 441: 862-6.

Maraganore, D. M., M. de Andrade, A. Elbaz, M. J. Farrer, J. P. Ioannidis, R. Krüger, W. A. Rocca, N. K. Schneider, T. G. Lesnick, S. J. Lincoln, M. M. Hulihan, J. O. Aasly, T. Ashizawa, M. C. Chartier-Harlin, H. Checkoway, C. Ferrarese, G. Hadjigeorgiou, N. Hattori, H. Kawakami, J. C. Lambert, T. Lynch, G. D. Mellick, S. Papapetropoulos, A. Parsian, A. Quattrone, O. Riess, E. K. Tan, C. Van Broeckhoven, and Genetic Epidemiology of Parkinson's Disease (GEO-PD) Consortium. 2006. 'Collaborative analysis of alpha-synuclein gene promoter variability and Parkinson disease', *JAMA*, 296: 661-70.

Maraganore, D. M., M. de Andrade, T. G. Lesnick, K. J. Strain, M. J. Farrer, W. A. Rocca, P. V. Pant, K. A. Frazer, D. R. Cox, and D. G. Ballinger. 2005. 'High-resolution whole-genome association study of Parkinson disease', *Am J Hum Genet*, 77: 685-93.

Maraganore, D. M., D. G. Hernandez, A. B. Singleton, M. J. Farrer, S. K. McDonnell, M. L. Hutton, J. A. Hardy, and W. A. Rocca. 2001. 'Case-Control study of the extended tau gene haplotype in Parkinson's disease', *Ann Neurol*, 50: 658-61.

Martin, E. R., W. K. Scott, M. A. Nance, R. L. Watts, J. P. Hubble, W. C. Koller, K. Lyons, R. Pahwa, M. B. Stern, A. Colcher, B. C. Hiner, J. Jankovic, W. G. Ondo, F. H. Allen, Jr., C. G. Goetz, G. W. Small, D. Masterman, F. Mastaglia, N. G. Laing, J. M. Stajich, R. C. Ribble, M. W. Booze, A. Rogala, M. A. Hauser, F. Zhang, R. A. Gibson, L. T. Middleton, A. D. Roses, J. L. Haines, B. L. Scott, M. A. Pericak-Vance, and J. M. Vance. 2001. 'Association of single-nucleotide polymorphisms of the tau gene with late-onset Parkinson disease', *JAMA*, 286: 2245-50.

Martin, M., S. J. Iyadurai, A. Gassman, J. G. Gindhart, T. S. Hays, and W. M. Saxton. 1999. 'Cytoplasmic dynein, the dynactin complex, and kinesin are interdependent and essential for fast axonal transport', *Mol Biol Cell*, 10: 3717-28.

Marx, A., J. Pless, E. M. Mandelkow, and E. Mandelkow. 2000. 'On the rigidity of the cytoskeleton: are MAPs crosslinkers or spacers of microtubules?', *Cell Mol Biol (Noisy-le-grand)*, 46: 949-65.

Marín, I., W. N. van Egmond, and P. J. van Haastert. 2008. 'The Roco protein family: a functional perspective', *FASEB J*, 22: 3103-10.

Mazzulli, J. R., Y. H. Xu, Y. Sun, A. L. Knight, P. J. McLean, G. A. Caldwell, E. Sidransky, G. A. Grabowski, and D. Krainc. 2011. 'Gaucher disease glucocerebrosidase and α-synuclein form a bidirectional pathogenic loop in synucleinopathies', *Cell*, 146: 37-52.

Mazzulli, J. R., F. Zunke, O. Isacson, L. Studer, and D. Krainc. 2016. 'α-Synuclein-induced lysosomal dysfunction occurs through disruptions in protein trafficking in human midbrain synucleinopathy models', *Proc Natl Acad Sci U S A*, 113: 1931-6.

McMillan, P., E. Korvatska, P. Poorkaj, Z. Evstafjeva, L. Robinson, L. Greenup, J. Leverenz, G. D. Schellenberg, and I. D'Souza. 2008. 'Tau isoform regulation is region- and cell-specific in mouse brain', *J Comp Neurol*, 511: 788-803.

Meloni, R., V. Albanèse, P. Ravassard, F. Treilhou, and J. Mallet. 1998. 'A tetranucleotide polymorphic microsatellite, located in the first intron of the tyrosine hydroxylase gene, acts as a transcription regulatory element in vitro', *Hum Mol Genet*, 7: 423-8.

Mena, M. A., M. J. Casarejos, A. Bonin, J. A. Ramos, and J. García Yébenes. 1995. 'Effects of dibutyryl cyclic AMP and retinoic acid on the differentiation of dopamine neurons: prevention of cell death by dibutyryl cyclic AMP', *J Neurochem*, 65: 2612-20.

Mertens, J., A. C. Paquola, M. Ku, E. Hatch, L. Böhnke, S. Ladjevardi, S. McGrath, B. Campbell, H. Lee, J. R. Herdy, J. T. Gonçalves, T. Toda, Y. Kim, J. Winkler, J. Yao, M. W. Hetzer, and F. H. Gage. 2015. 'Directly Reprogrammed Human Neurons Retain Aging-Associated Transcriptomic Signatures and Reveal Age-Related Nucleocytoplasmic Defects', Cell Stem Cell, 17: 705-18.

Mertens, J., K. Stüber, D. Poppe, J. Doerr, J. Ladewig, O. Brüstle, and P. Koch. 2013. 'Embryonic stem cell-based modeling of tau pathology in human neurons', *Am J Pathol*, 182: 1769-79.

Messmer, K., M. P. Remington, F. Skidmore, and P. S. Fishman. 2007. 'Induction of tyrosine hydroxylase expression by the transcription factor Pitx3', *Int J Dev Neurosci*, 25: 29-37.

Miller, J. D., Y. M. Ganat, S. Kishinevsky, R. L. Bowman, B. Liu, E. Y. Tu, P. K. Mandal, E. Vera, J. W. Shim, S. Kriks, T. Taldone, N. Fusaki, M. J. Tomishima, D. Krainc, T. A. Milner, D. J. Rossi, and L. Studer. 2013. 'Human iPSC-based modeling of late-onset disease via progerin-induced aging', Cell Stem Cell, 13: 691-705.

Mizushima, N., and T. Yoshimori. 2007. 'How to interpret LC3 immunoblotting', *Autophagy*, 3: 542-5.

Morfini, G., G. Pigino, N. Mizuno, M. Kikkawa, and S. T. Brady. 2007. 'Tau binding to microtubules does not directly affect microtubule-based vesicle motility', *J Neurosci Res*, 85: 2620-30.

Morris, H. R., J. C. Janssen, O. Bandmann, S. E. Daniel, M. N. Rossor, A. J. Lees, and N. W. Wood. 1999. 'The *tau* gene A0 polymorphism in progressive supranuclear palsy and related neurodegenerative diseases', *J Neurol Neurosurg Psychiatry*, 66: 665-7.

Morris, M., A. Koyama, E. Masliah, and L. Mucke. 2011. 'Tau reduction does not prevent motor deficits in two mouse models of Parkinson's disease', *PLoS One*, 6: e29257.

Morris, R. L., and P. J. Hollenbeck. 1995. 'Axonal transport of mitochondria along microtubules and F-actin in living vertebrate neurons', *J Cell Biol*, 131: 1315-26.

Mukherjee, O., J. S. Kauwe, K. Mayo, J. C. Morris, and A. M. Goate. 2007. 'Haplotype-based association analysis of the MAPT locus in late onset Alzheimer's disease', *BMC Genet*, 8: 3.

Mukhopadhyay, R., and J. H. Hoh. 2001. 'AFM force measurements on microtubule-associated proteins: the projection domain exerts a long-range repulsive force', *FEBS Lett*, 505: 374-8.

Mukrasch, M. D., S. Bibow, J. Korukottu, S. Jeganathan, J. Biernat, C. Griesinger, E. Mandelkow, and M. Zweckstetter. 2009. 'Structural polymorphism of 441-residue tau at single residue resolution', *PLoS Biol*, 7: e34.

Mukrasch, M. D., M. von Bergen, J. Biernat, D. Fischer, C. Griesinger, E. Mandelkow, and M. Zweckstetter. 2007. 'The "jaws" of the tau-microtubule interaction', *J Biol Chem*, 282: 12230-9.

Muratore, C. R., P. Srikanth, D. G. Callahan, and T. L. Young-Pearse. 2014. 'Comparison and optimization of hiPSC forebrain cortical differentiation protocols', *PLoS One*, 9: e105807.

Muñoz-Montaño, J. R., F. J. Moreno, J. Avila, and J. Diaz-Nido. 1997. 'Lithium inhibits Alzheimer's disease-like tau protein phosphorylation in neurons', *FEBS Lett*, 411: 183-8.

Myers, A. J., J. R. Gibbs, J. A. Webster, K. Rohrer, A. Zhao, L. Marlowe, M. Kaleem, D. Leung, L. Bryden, P. Nath, V. L. Zismann, K. Joshipura, M. J. Huentelman, D. Hu-Lince, K. D. Coon, D. W. Craig, J. V. Pearson, P. Holmans, C. B. Heward, E. M. Reiman, D. Stephan, and J. Hardy. 2007b. 'A survey of genetic human cortical gene expression', *Nat Genet*, 39: 1494-9.

Myers, A. J., M. Kaleem, L. Marlowe, A. M. Pittman, A. J. Lees, H. C. Fung, J. Duckworth, D. Leung, A. Gibson, C. M. Morris, R. de Silva, and J. Hardy. 2005. 'The H1c haplotype at the *MAPT* locus is associated with Alzheimer's disease', *Hum Mol Genet*, 14: 2399-404.

Myers, A. J., A. M. Pittman, A. S. Zhao, K. Rohrer, M. Kaleem, L. Marlowe, A. Lees, D. Leung, I. G. McKeith, R. H. Perry, C. M. Morris, J. Q. Trojanowski, C. Clark, J. Karlawish, S. Arnold, M. S. Forman, V. Van Deerlin, R. de Silva, and J. Hardy. 2007a. 'The *MAPT* H1c risk haplotype is associated with increased expression of tau and especially of 4 repeat containing transcripts', *Neurobiol Dis*, 25: 561-70.

Müller, R., M. Heinrich, S. Heck, D. Blohm, and C. Richter-Landsberg. 1997. 'Expression of microtubule-associated proteins MAP2 and tau in cultured rat brain oligodendrocytes', *Cell Tissue Res*, 288: 239-49.

Nagatsu, I., N. Karasawa, K. Yamada, M. Sakai, T. Fujii, T. Takeuchi, R. Arai, K. Kobayashi, and T. Nagatsu. 1994. 'Expression of human tyrosine hydroxylase-chloramphenicol acetyltransferase (CAT) fusion gene in the brains of transgenic mice as examined by CAT immunocytochemistry', *J Neural Transm Gen Sect*, 96: 85-104.

Nalls, M. A., N. Pankratz, C. M. Lill, C. B. Do, D. G. Hernandez, M. Saad, A. L. DeStefano, E. Kara, J. Bras, M. Sharma, C. Schulte, M. F. Keller, S. Arepalli, C. Letson, C. Edsall, H. Stefansson, X. Liu, H. Pliner, J. H. Lee, R. Cheng, M. A. Ikram, J. P. Ioannidis, G. M. Hadjigeorgiou, J. C. Bis, M. Martinez, J. S. Perlmutter, A. Goate, K. Marder, B. Fiske, M. Sutherland, G. Xiromerisiou, R. H. Myers, L. N. Clark, K. Stefansson, J. A. Hardy, P. Heutink, H. Chen, N. W. Wood, H. Houlden, H. Payami, A. Brice, W. K. Scott, T. Gasser, L. Bertram, N. Eriksson, T. Foroud, A. B. Singleton, International Parkinson's Disease Genomics Consortium (IPDGC), Parkinson's Study Group (PSG) Parkinson's Research: The Organized GENetics Initiative (PROGENI), 23andMe, GenePD, NeuroGenetics Research Consortium (NGRC), Hussman Institute of Human Genomics (HIHG), Ashkenazi Jewish Dataset Investigator, Cohorts for Health and Aging Research in Genetic Epidemiology (CHARGE), North American Brain Expression Consortium (NABEC), United Kingdom Brain Expression Consortium (UKBEC), Greek Parkinson's Disease Consortium, and Alzheimer Genetic Analysis Group. 2014.

'Large-scale meta-analysis of genome-wide association data identifies six new risk loci for Parkinson's disease', *Nat Genet*, 46: 989-93.

Narendra, D. P., S. M. Jin, A. Tanaka, D. F. Suen, C. A. Gautier, J. Shen, M. R. Cookson, and R. J. Youle. 2010. 'PINK1 is selectively stabilized on impaired mitochondria to activate Parkin', *PLoS Biol*, 8: e1000298.

Narendra, D., A. Tanaka, D. F. Suen, and R. J. Youle. 2008. 'Parkin is recruited selectively to impaired mitochondria and promotes their autophagy', *J Cell Biol*, 183: 795-803.

Nguyen, H. N., B. Byers, B. Cord, A. Shcheglovitov, J. Byrne, P. Gujar, K. Kee, B. Schüle, R. E. Dolmetsch, W. Langston, T. D. Palmer, and R. R. Pera. 2011. 'LRRK2 mutant iPSC-derived DA neurons demonstrate increased susceptibility to oxidative stress', *Cell Stem Cell*, 8: 267-80.

Nichols, W. C., N. Pankratz, D. K. Marek, M. W. Pauciulo, V. E. Elsaesser, C. A. Halter, A. Rudolph, J. Wojcieszek, R. F. Pfeiffer, T. Foroud, and Parkinson Study Group-PROGENI Investigators. 2009. 'Mutations in GBA are associated with familial Parkinson disease susceptibility and age at onset', *Neurology*, 72: 310-6.

Nissan, X., S. Blondel, C. Navarro, Y. Maury, C. Denis, M. Girard, C. Martinat, A. De Sandre-Giovannoli, N. Levy, and M. Peschanski. 2012. 'Unique preservation of neural cells in Hutchinson- Gilford progeria syndrome is due to the expression of the neural-specific miR-9 microRNA', Cell Rep, 2: 1-9.

Oliveira, S. A., W. K. Scott, F. Zhang, J. M. Stajich, K. Fujiwara, M. Hauser, B. L. Scott, M. A. Pericak-Vance, J. M. Vance, and E. R. Martin. 2004. 'Linkage disequilibrium and haplotype tagging polymorphisms in the *Tau* H1 haplotype', *Neurogenetics*, 5: 147-55.

Orenstein, S. J., S. H. Kuo, I. Tasset, E. Arias, H. Koga, I. Fernandez-Carasa, E. Cortes, L. S. Honig, W. Dauer, A. Consiglio, A. Raya, D. Sulzer, and A. M. Cuervo. 2013. 'Interplay of LRRK2 with chaperone-mediated autophagy', *Nat Neurosci*, 16: 394-406.

Oyama, G., K. D. Foote, C. E. Jacobson, F. Velez-Lago, C. Go, N. Limotai, P. R. Zeilman, J. Romrell, S. S. Wu, D. Neal, and M. S. Okun. 2012. 'GPi and STN deep brain stimulation can suppress dyskinesia in Parkinson's disease', *Parkinsonism Relat Disord*, 18: 814-8.

Paisán-Ruíz, C., S. Jain, E. W. Evans, W. P. Gilks, J. Simón, M. van der Brug, A. López de Munain, S. Aparicio, A. M. Gil, N. Khan, J. Johnson, J. R. Martinez, D. Nicholl, I. M. Carrera, A. S. Pena, R. de Silva, A. Lees, J. F. Martí-Massó, J. Pérez-Tur, N. W. Wood, and A. B. Singleton. 2004. 'Cloning of the gene containing mutations that cause PARK8-linked Parkinson's disease', *Neuron*, 44: 595-600.

Panda, D., J. C. Samuel, M. Massie, S. C. Feinstein, and L. Wilson. 2003. 'Differential regulation of microtubule dynamics by three- and four-repeat tau: implications for the onset of neurodegenerative disease', *Proc Natl Acad Sci U S A*, 100: 9548-53.

Pang, Z. P., N. Yang, T. Vierbuchen, A. Ostermeier, D. R. Fuentes, T. Q. Yang, A. Citri, V. Sebastiano, S. Marro, T. C. Südhof, and M. Wernig. 2011. 'Induction of human neuronal cells by defined transcription factors', Nature, 476: 220-3.

Pankratz, N., G. W. Beecham, A. L. DeStefano, T. M. Dawson, K. F. Doheny, S. A. Factor, T. H. Hamza, A. Y. Hung, B. T. Hyman, A. J. Ivinson, D. Krainc, J. C. Latourelle, L. N. Clark, K. Marder, E. R. Martin, R. Mayeux, O. A. Ross, C. R. Scherzer, D. K. Simon, C. Tanner, J. M. Vance, Z. K. Wszolek, C. P. Zabetian, R. H. Myers, H. Payami, W. K. Scott, and T. Foroud. 2012. 'Meta-analysis of Parkinson's disease: identification of a novel locus, *RIT2*', *Ann Neurol*, 71: 370-84.

Pankratz, N., J. B. Wilk, J. C. Latourelle, A. L. DeStefano, C. Halter, E. W. Pugh, K. F. Doheny, J. F. Gusella, W. C. Nichols, T. Foroud, and R. H. Myers. 2009. 'Genomewide association study for susceptibility genes contributing to familial Parkinson disease', *Hum Genet*, 124: 593-605.

Papasozomenos, S. C., and L. I. Binder. 1987. 'Phosphorylation determines two distinct species of Tau in the central nervous system', *Cell Motil Cytoskeleton*, 8: 210-26.

Parisiadou, L., C. Xie, H. J. Cho, X. Lin, X. L. Gu, C. X. Long, E. Lobbestael, V. Baekelandt, J. M. Taymans, L. Sun, and H. Cai. 2009. 'Phosphorylation of ezrin/radixin/moesin proteins by LRRK2 promotes the rearrangement of actin cytoskeleton in neuronal morphogenesis', *J Neurosci*, 29: 13971-80.

Parkkinen, L., S. S. O'Sullivan, C. Collins, A. Petrie, J. L. Holton, T. Revesz, and A. J. Lees. 2011. 'Disentangling the relationship between lewy bodies and nigral neuronal loss in Parkinson's disease', *J Parkinsons Dis*, 1: 277-86.

Pastor, P., M. Ezquerra, E. Munoz, M. J. Marti, R. Blesa, E. Tolosa, and R. Oliva. 2000. 'Significant association between the tau gene A0/A0 genotype and Parkinson's disease', *Ann Neurol*, 47: 242-5.

Pastor, P., M. Ezquerra, J. C. Perez, S. Chakraverty, J. Norton, B. A. Racette, D. McKeel, J. S. Perlmutter, E. Tolosa, and A. M. Goate. 2004. 'Novel haplotypes in 17q21 are associated with progressive supranuclear palsy', *Ann Neurol*, 56: 249-58.

Pastor, P., M. Ezquerra, E. Tolosa, E. Munoz, M. J. Marti, F. Valldeoriola, J. L. Molinuevo, M. Calopa, and R. Oliva. 2002. 'Further extension of the H1 haplotype associated with progressive supranuclear palsy', *Mov Disord*, 17: 550-6.

Peacey, E., L. Rodriguez, Y. Liu, and M. S. Wolfe. 2012. 'Targeting a pre-mRNA structure with bipartite antisense molecules modulates tau alternative splicing', *Nucleic Acids Res*, 40: 9836-49.

Pepłońska, B., C. Żekanowski, D. Religa, K. Czyżewski, M. Styczyńska, A. Pfeffer, T. Gabryelewicz, M. Gołębiowski, E. Łuczywek, B. Wasiak, A. Barczak, M. Chodakowska, M. Barcikowska, and J. Kuźnicki. 2003. 'Strong association between *Saitohin* gene polymorphism and *tau* haplotype in the Polish population.' in, *Neurosci Lett* (Ireland).

Perrier, A. L., V. Tabar, T. Barberi, M. E. Rubio, J. Bruses, N. Topf, N. L. Harrison, and L. Studer. 2004. 'Derivation of midbrain dopamine neurons from human embryonic stem cells', *Proc Natl Acad Sci U S A*, 101: 12543-8.

Peruzzi, P. P., S. E. Lawler, S. L. Senior, N. Dmitrieva, P. A. Edser, D. Gianni, E. A. Chiocca, and R. Wade-Martins. 2009. 'Physiological transgene regulation and functional complementation of a neurological disease gene deficiency in neurons', *Mol Ther*, 17: 1517-26.

Pfisterer, U., A. Kirkeby, O. Torper, J. Wood, J. Nelander, A. Dufour, A. Björklund, O. Lindvall, J. Jakobsson, and M. Parmar. 2011. 'Direct conversion of human fibroblasts to dopaminergic neurons', Proc Natl Acad Sci U S A, 108: 10343-8.

Piccoli, C., A. Sardanelli, R. Scrima, M. Ripoli, G. Quarato, A. D'Aprile, F. Bellomo, S. Scacco, G. De Michele, A. Filla, A. Iuso, D. Boffoli, N. Capitanio, and S. Papa. 2008. 'Mitochondrial respiratory dysfunction in familiar parkinsonism associated with PINK1 mutation', *Neurochem Res*, 33: 2565-74.

Picconi, B., D. Centonze, K. Håkansson, G. Bernardi, P. Greengard, G. Fisone, M. A. Cenci, and P. Calabresi. 2003. 'Loss of bidirectional striatal synaptic plasticity in L-DOPA-induced dyskinesia', *Nat Neurosci*, 6: 501-6.

Pilling, A. D., D. Horiuchi, C. M. Lively, and W. M. Saxton. 2006. 'Kinesin-1 and Dynein are the primary motors for fast transport of mitochondria in Drosophila motor axons', *Mol Biol Cell*, 17: 2057-68.

Pissadaki, E. K., and J. P. Bolam. 2013. 'The energy cost of action potential propagation in dopamine neurons: clues to susceptibility in Parkinson's disease', *Front Comput Neurosci*, 7: 13.

Pittman, A. M., A. J. Myers, P. Abou-Sleiman, H. C. Fung, M. Kaleem, L. Marlowe, J. Duckworth, D. Leung, D. Williams, L. Kilford, N. Thomas, C. M. Morris, D. Dickson, N.

W. Wood, J. Hardy, A. J. Lees, and R. de Silva. 2005. 'Linkage disequilibrium fine mapping and haplotype association analysis of the *tau* gene in progressive supranuclear palsy and corticobasal degeneration', *J Med Genet*, 42: 837-46.

Pittman, A. M., A. J. Myers, J. Duckworth, L. Bryden, M. Hanson, P. Abou-Sleiman, N. W. Wood, J. Hardy, A. Lees, and R. de Silva. 2004. 'The structure of the tau haplotype in controls and in progressive supranuclear palsy', *Hum Mol Genet*, 13: 1267-74.

Piva, F., M. Giulietti, A. B. Burini, and G. Principato. 2012. 'SpliceAid 2: a database of human splicing factors expression data and RNA target motifs', *Hum Mutat*, 33: 81-5.

Polymeropoulos, M. H., C. Lavedan, E. Leroy, S. E. Ide, A. Dehejia, A. Dutra, B. Pike, H. Root, J. Rubenstein, R. Boyer, E. S. Stenroos, S. Chandrasekharappa, A. Athanassiadou, T. Papapetropoulos, W. G. Johnson, A. M. Lazzarini, R. C. Duvoisin, G. Di Iorio, L. I. Golbe, and R. L. Nussbaum. 1997. 'Mutation in the alpha-synuclein gene identified in families with Parkinson's disease', *Science*, 276: 2045-7.

Pooler, A. M., and D. P. Hanger. 2010. 'Functional implications of the association of tau with the plasma membrane', *Biochem Soc Trans*, 38: 1012-5.

Pooler, A. M., A. Usardi, C. J. Evans, K. L. Philpott, W. Noble, and D. P. Hanger. 2012. 'Dynamic association of tau with neuronal membranes is regulated by phosphorylation', *Neurobiol Aging*, 33: 431.e27-38.

Poorkaj P., T. D. Bird, E. Wijsman, E. Nemens, R. M. Garruto, L. Anderson, A. Andreadis, W. C. Wiederholt, M. Raskind, and G. D. Schellenberg. 1998. 'Tau is a candidate gene for chromosome 17 frontotemporal dementia', *Ann Neurol*, 43: 815-25.

Preuss, U., J. Biernat, E. M. Mandelkow, and E. Mandelkow. 1997. 'The 'jaws' model of tau-microtubule interaction examined in CHO cells', *J Cell Sci*, 110 (Pt 6): 789-800.

Proudfoot, N. J. 2011. 'Ending the message: poly(A) signals then and now', *Genes Dev*, 25: 1770-82.

Proukakis, C., C. G. Dudzik, T. Brier, D. S. MacKay, J. M. Cooper, G. L. Millhauser, H. Houlden, and A. H. Schapira. 2013. 'A novel α-synuclein missense mutation in Parkinson disease', *Neurology*, 80: 1062-4.

Rademakers, R., B. Dermaut, K. Peeters, M. Cruts, P. Heutink, A. Goate, and C. Van Broeckhoven. 2003. 'Tau (MAPT) mutation Arg406Trp presenting clinically with Alzheimer disease does not share a common founder in Western Europe', Hum Mutat, 22: 409-11.

Rademakers, R., S. Melquist, M. Cruts, J. Theuns, J. Del-Favero, P. Poorkaj, M. Baker, K. Sleegers, R. Crook, T. De Pooter, S. Bel Kacem, J. Adamson, D. Van den Bossche, M. Van den Broeck, J. Gass, E. Corsmit, P. De Rijk, N. Thomas, S. Engelborghs, M. Heckman, I. Litvan, J. Crook, P. P. De Deyn, D. Dickson, G. D. Schellenberg, C. Van Broeckhoven, and M. L. Hutton. 2005. 'High-density SNP haplotyping suggests altered regulation of *tau* gene expression in progressive supranuclear palsy', *Hum Mol Genet*, 14: 3281-92.

Rakovic, A., K. Shurkewitsch, P. Seibler, A. Grünewald, A. Zanon, J. Hagenah, D. Krainc, and C. Klein. 2013. 'Phosphatase and tensin homolog (PTEN)-induced putative kinase 1 (PINK1)-dependent ubiquitination of endogenous Parkin attenuates mitophagy: study in human primary fibroblasts and induced pluripotent stem cell-derived neurons', *J Biol Chem*, 288: 2223-37.

Ramasamy, A., D. Trabzuni, J. R. Gibbs, A. Dillman, D. G. Hernandez, S. Arepalli, R. Walker, C. Smith, G. P. Ilori, A. A. Shabalin, Y. Li, A. B. Singleton, M. R. Cookson, J. Hardy, M. Ryten, M. E. Weale, NABEC, and UKBEC. 2013. 'Resolving the polymorphism-in-probe problem is critical for correct interpretation of expression QTL studies', *Nucleic Acids Res*, 41: e88.

Rao, D. D., J. S. Vorhies, N. Senzer, and J. Nemunaitis. 2009. 'siRNA vs. shRNA: similarities and differences', *Adv Drug Deliv Rev*, 61: 746-59.

Rapoport, M., H. N. Dawson, L. I. Binder, M. P. Vitek, and A. Ferreira. 2002. 'Tau is essential to beta -amyloid-induced neurotoxicity', *Proc Natl Acad Sci U S A*, 99: 6364-9.

Rasmussen, M., L. Kong, G. R. Zhang, M. Liu, X. Wang, G. Szabo, N. P. Curthoys, and A. I. Geller. 2007. 'Glutamatergic or GABAergic neuron-specific, long-term expression in neocortical neurons from helper virus-free HSV-1 vectors containing the phosphate-activated glutaminase, vesicular glutamate transporter-1, or glutamic acid decarboxylase promoter', *Brain Res*, 1144: 19-32.

Reed, L. A., T. J. Grabowski, M. L. Schmidt, J. C. Morris, A. Goate, A. Solodkin, G. W. Van Hoesen, R. L. Schelper, C. J. Talbot, M. A. Wragg, and J. Q. Trojanowski. 1997. 'Autosomal dominant dementia with widespread neurofibrillary tangles', Ann Neurol, 42: 564-72.

Reeve, A., E. Simcox, and D. Turnbull. 2014. 'Ageing and Parkinson's disease: why is advancing age the biggest risk factor?', *Ageing Res Rev*, 14: 19-30.

Reinhardt, P., B. Schmid, L. F. Burbulla, D. C. Schöndorf, L. Wagner, M. Glatza, S. Höing, G. Hargus, S. A. Heck, A. Dhingra, G. Wu, S. Müller, K. Brockmann, T. Kluba, M. Maisel, R. Krüger, D. Berg, Y. Tsytsyura, C. S. Thiel, O. E. Psathaki, J. Klingauf, T. Kuhlmann, M. Klewin, H. Müller, T. Gasser, H. R. Schöler, and J. Sterneckert. 2013. 'Genetic correction of a LRRK2 mutation in human iPSCs links parkinsonian neurodegeneration to ERK-dependent changes in gene expression', *Cell Stem Cell*, 12: 354-67.

Reis, G. F., G. Yang, L. Szpankowski, C. Weaver, S. B. Shah, J. T. Robinson, T. S. Hays, G. Danuser, and L. S. Goldstein. 2012. 'Molecular motor function in axonal transport in vivo probed by genetic and computational analysis in Drosophila', *Mol Biol Cell*, 23: 1700-14.

Rhinn, M., and M. Brand. 2001. 'The midbrain--hindbrain boundary organizer', *Curr Opin Neurobiol*, 11: 34-42.

Rinaldi, F., E. M. Hartfield, L. A. Crompton, J. L. Badger, C. P. Glover, C. M. Kelly, A. E. Rosser, J. B. Uney, and M. A. Caldwell. 2014. 'Cross-regulation of Connexin43 and beta-catenin influences differentiation of human neural progenitor cells', *Cell Death Dis*, 5: e1017.

Roberson, E. D., B. Halabisky, J. W. Yoo, J. Yao, J. Chin, F. Yan, T. Wu, P. Hamto, N. Devidze, G. Q. Yu, J. J. Palop, J. L. Noebels, and L. Mucke. 2011. 'Amyloid-β/Fyn-induced synaptic, network, and cognitive impairments depend on tau levels in multiple mouse models of Alzheimer's disease', *J Neurosci*, 31: 700-11.

Roberson, E. D., K. Scearce-Levie, J. J. Palop, F. Yan, I. H. Cheng, T. Wu, H. Gerstein, G. Q. Yu, and L. Mucke. 2007. 'Reducing endogenous tau ameliorates amyloid beta-induced deficits in an Alzheimer's disease mouse model', *Science*, 316: 750-4.

Rodriguez, P. C., D. B. Pereira, A. Borgkvist, M. Y. Wong, C. Barnard, M. S. Sonders, H. Zhang, D. Sames, and D. Sulzer. 2013. 'Fluorescent dopamine tracer resolves individual dopaminergic synapses and their activity in the brain', *Proc Natl Acad Sci U S A*, 110: 870-5.

Rodriguez-Martin, T., K. Anthony, M. A. Garcia-Blanco, S. G. Mansfield, B. H. Anderton, and J. M. Gallo. 2009. 'Correction of tau mis-splicing caused by FTDP-17 MAPT mutations by spliceosome-mediated RNA trans-splicing', *Hum Mol Genet*, 18: 3266-73.

Roessler, R., S. A. Smallwood, J. V. Veenvliet, P. Pechlivanoglou, S. P. Peng, K. Chakrabarty, M. J. Groot-Koerkamp, R. J. Pasterkamp, E. Wesseling, G. Kelsey, E. Boddeke, M. P. Smidt, and S. Copray. 2014. 'Detailed analysis of the genetic and epigenetic signatures of iPSC-derived mesodiencephalic dopaminergic neurons', *Stem Cell Reports*, 2: 520-33.

Romano, G., M. Macaluso, C. Lucchetti, and L. Iacovitti. 2007. 'Transcription and epigenetic profile of the promoter, first exon and first intron of the human tyrosine hydroxylase gene', *J Cell Physiol*, 211: 431-8.

Romano, G., S. Suon, H. Jin, A. E. Donaldson, and L. Iacovitti. 2005. 'Characterization of five evolutionary conserved regions of the human tyrosine hydroxylase (TH) promoter: implications for the engineering of a human TH minimal promoter assembled in a self-inactivating lentiviral vector system', *J Cell Physiol*, 204: 666-77.

Roussa, E., M. Wiehle, N. Dünker, S. Becker-Katins, O. Oehlke, and K. Krieglstein. 2006. 'Transforming growth factor beta is required for differentiation of mouse mesencephalic progenitors into dopaminergic neurons in vitro and in vivo: ectopic induction in dorsal mesencephalon', *Stem Cells*, 24: 2120-9.

Russo, G. J., K. Louie, A. Wellington, G. T. Macleod, F. Hu, S. Panchumarthi, and K. E. Zinsmaier. 2009. 'Drosophila Miro is required for both anterograde and retrograde axonal mitochondrial transport', *J Neurosci*, 29: 5443-55.

Saad, M., S. Lesage, A. Saint-Pierre, J. C. Corvol, D. Zelenika, J. C. Lambert, M. Vidailhet, G. D. Mellick, E. Lohmann, F. Durif, P. Pollak, P. Damier, F. Tison, P. A. Silburn, C. Tzourio, S. Forlani, M. A. Loriot, M. Giroud, C. Helmer, F. Portet, P. Amouyel, M. Lathrop, A. Elbaz, A. Durr, M. Martinez, and A. Brice. 2011. 'Genome-wide association study confirms BST1 and suggests a locus on 12q24 as the risk loci for Parkinson's disease in the European population', *Hum Mol Genet*, 20: 615-27.

Saeki, Y., C. Fraefel, T. Ichikawa, X. O. Breakefield, and E. A. Chiocca. 2001. 'Improved helper virus-free packaging system for HSV amplicon vectors using an ICP27-deleted, oversized HSV-1 DNA in a bacterial artificial chromosome', *Mol Ther*, 3: 591-601.

Sahani, M. H., E. Itakura, and N. Mizushima. 2014. 'Expression of the autophagy substrate SQSTM1/p62 is restored during prolonged starvation depending on transcriptional upregulation and autophagy-derived amino acids', *Autophagy*, 10: 431-41.

Sanders, L. H., J. Laganière, O. Cooper, S. K. Mak, B. J. Vu, Y. A. Huang, D. E. Paschon, M. Vangipuram, R. Sundararajan, F. D. Urnov, J. W. Langston, P. D. Gregory, H. S. Zhang, J. T. Greenamyre, O. Isacson, and B. Schüle. 2014. 'LRRK2 mutations cause mitochondrial DNA damage in iPSC-derived neural cells from Parkinson's disease patients: reversal by gene correction', *Neurobiol Dis*, 62: 381-6.

Sapir, T., M. Frotscher, T. Levy, E. M. Mandelkow, and O. Reiner. 2012. 'Tau's role in the developing brain: implications for intellectual disability', *Hum Mol Genet*, 21: 1681-92.

Satake, W., Y. Nakabayashi, I. Mizuta, Y. Hirota, C. Ito, M. Kubo, T. Kawaguchi, T. Tsunoda, M. Watanabe, A. Takeda, H. Tomiyama, K. Nakashima, K. Hasegawa, F. Obata, T. Yoshikawa, H. Kawakami, S. Sakoda, M. Yamamoto, N. Hattori, M. Murata, Y. Nakamura, and T. Toda. 2009. 'Genome-wide association study identifies common variants at four loci as genetic risk factors for Parkinson's disease', *Nat Genet*, 41: 1303-7.

Scales, T. M., P. Derkinderen, K. Y. Leung, H. L. Byers, M. A. Ward, C. Price, I. N. Bird, T. Perera, S. Kellie, R. Williamson, B. H. Anderton, and C. H. Reynolds. 2011. 'Tyrosine phosphorylation of tau by the SRC family kinases lck and fyn', *Mol Neurodegener*, 6: 12.

Schenck, C. H., B. F. Boeve, and M. W. Mahowald. 2013. 'Delayed emergence of a parkinsonian disorder or dementia in 81% of older men initially diagnosed with idiopathic rapid eye movement sleep behavior disorder: a 16-year update on a previously reported series', *Sleep Med*, 14: 744-8.

Schenck, C. H., S. R. Bundlie, and M. W. Mahowald. 1996. 'Delayed emergence of a parkinsonian disorder in 38% of 29 older men initially diagnosed with idiopathic rapid eye movement sleep behaviour disorder', *Neurology*, 46: 388-93.

Schneider, A., J. Biernat, M. von Bergen, E. Mandelkow, and E. M. Mandelkow. 1999. 'Phosphorylation that detaches tau protein from microtubules (Ser262, Ser214) also protects it against aggregation into Alzheimer paired helical filaments', *Biochemistry*, 38: 3549-58.

Schultz, W., P. Dayan, and P. R. Montague. 1997. 'A neural substrate of prediction and reward', *Science*, 275: 1593-9.

Schuster, M., S. Kilaru, G. Fink, J. Collemare, Y. Roger, and G. Steinberg. 2011b. 'Kinesin-3 and dynein cooperate in long-range retrograde endosome motility along a nonuniform microtubule array', *Mol Biol Cell*, 22: 3645-57.

Schuster, M., R. Lipowsky, M. A. Assmann, P. Lenz, and G. Steinberg. 2011a. 'Transient binding of dynein controls bidirectional long-range motility of early endosomes', *Proc Natl Acad Sci U S A*, 108: 3618-23.

Scott, W. K., M. A. Nance, R. L. Watts, J. P. Hubble, W. C. Koller, K. Lyons, R. Pahwa, M. B. Stern, A. Colcher, B. C. Hiner, J. Jankovic, W. G. Ondo, F. H. Allen, Jr., C. G. Goetz, G. W. Small, D. Masterman, F. Mastaglia, N. G. Laing, J. M. Stajich, B. Slotterbeck, M. W. Booze, R. C. Ribble, E. Rampersaud, S. G. West, R. A. Gibson, L. T. Middleton, A. D. Roses, J. L. Haines, B. L. Scott, J. M. Vance, and M. A. Pericak-Vance. 2001. 'Complete genomic screen in Parkinson disease: evidence for multiple genes', *JAMA*, 286: 2239-44.

Seibenhener, M. L., J. R. Babu, T. Geetha, H. C. Wong, N. R. Krishna, and M. W. Wooten. 2004. 'Sequestosome 1/p62 is a polyubiquitin chain binding protein involved in ubiquitin proteasome degradation', *Mol Cell Biol*, 24: 8055-68.

Seibler, P., J. Graziotto, H. Jeong, F. Simunovic, C. Klein, and D. Krainc. 2011. 'Mitochondrial Parkin recruitment is impaired in neurons derived from mutant PINK1 induced pluripotent stem cells', *J Neurosci*, 31: 5970-6.

Seitz, A., H. Kojima, K. Oiwa, E. M. Mandelkow, Y. H. Song, and E. Mandelkow. 2002. 'Single-molecule investigation of the interference between kinesin, tau and MAP2c', *EMBO J*, 21: 4896-905.

Sengupta, U., M. J. Guerrero-Muñoz, D. L. Castillo-Carranza, C. A. Lasagna-Reeves, J. E. Gerson, A. A. Paulucci-Holthauzen, S. Krishnamurthy, M. Farhed, G. R. Jackson, and R. Kayed. 2015. 'Pathological interface between oligomeric alpha-synuclein and tau in synucleinopathies', *Biol Psychiatry*, 78: 672-83.

Setó-Salvia, N., J. Pagonabarraga, H. Houlden, B. Pascual-Sedano, O. Dols-Icardo, A. Tucci, C. Paisán-Ruiz, A. Campolongo, S. Antón-Aguirre, I. Martín, L. Muñoz, E. Bufill, L. Vilageliu, D. Grinberg, M. Cozar, R. Blesa, A. Lleó, J. Hardy, J. Kulisevsky, and J. Clarimón. 2012. 'Glucocerebrosidase mutations confer a greater risk of dementia during Parkinson's disease course', *Mov Disord*, 27: 393-9.

Seward, M. E., E. Swanson, A. Norambuena, A. Reimann, J. N. Cochran, R. Li, E. D. Roberson, and G. S. Bloom. 2013. 'Amyloid-β signals through tau to drive ectopic neuronal cell cycle re-entry in Alzheimer's disease', *J Cell Sci*, 126: 1278-86.

Shahpasand, K., I. Uemura, T. Saito, T. Asano, K. Hata, K. Shibata, Y. Toyoshima, M. Hasegawa, and S. Hisanaga. 2012. 'Regulation of mitochondrial transport and inter-microtubule spacing by tau phosphorylation at the sites hyperphosphorylated in Alzheimer's disease', *J Neurosci*, 32: 2430-41.

Shaltouki, A., R. Sivapatham, Y. Pei, A. A. Gerencser, O. Momčilović, M. S. Rao, and X. Zeng. 2015. 'Mitochondrial alterations by PARKIN in dopaminergic neurons using PARK2 patient-specific and PARK2 knockout isogenic iPSC lines', *Stem Cell Reports*, 4: 847-59.

Sheng, Z. H. 2014. 'Mitochondrial trafficking and anchoring in neurons: New insight and implications', *J Cell Biol*, 204: 1087-98.

Sherrington, R., E. I. Rogaev, Y. Liang, E. A. Rogaeva, G. Levesque, M. Ikeda, H. Chi, C. Lin, G. Li, K. Holman, T. Tsuda, L. Mar, J. F. Foncin, A. C. Bruni, M. P. Montesi, S. Sorbi, I. Rainero, L. Pinessi, L. Nee, I. Chumakov, D. Pollen, A. Brookes, P. Sanseau, R. J. Polinsky, W. Wasco, H. A. Da Silva, J. L. Haines, M. A. Perkicak-Vance, R. E. Tanzi, A. D. Roses, P. E. Fraser, J. M. Rommens, and P. H. St George-Hyslop. 1995. 'Cloning of a gene bearing missense mutations in early-onset familial Alzheimer's disease', *Nature*, 375: 754-60.

Shi, Y., P. Kirwan, and F. J. Livesey. 2012. 'Directed differentiation of human pluripotent stem cells to cerebral cortex neurons and neural networks', Nat Protoc, 7: 1836-46.

Shipton, O. A., J. R. Leitz, J. Dworzak, C. E. Acton, E. M. Tunbridge, F. Denk, H. N. Dawson, M. P. Vitek, R. Wade-Martins, O. Paulsen, and M. Vargas-Caballero. 2011. 'Tau protein is required for amyloid {beta}-induced impairment of hippocampal long-term potentiation', *J Neurosci*, 31: 1688-92.

Sidransky, E., A. Bottler, B. Stubblefield, and E. I. Ginns. 1994. 'DNA mutational analysis of type 1 and type 3 Gaucher patients: how well do mutations predict phenotype?', *Hum Mutat*, 3: 25-8.

Sidransky, E., and E. I. Ginns. 1993. 'Clinical heterogeneity among patients with Gaucher's disease', *JAMA*, 269: 1154-7.

Sidransky, E., and G. Lopez. 2012. 'The link between the GBA gene and parkinsonism', *Lancet Neurol*, 11: 986-98.

Sidransky, E., M. A. Nalls, J. O. Aasly, J. Aharon-Peretz, G. Annesi, E. R. Barbosa, A. Bar-Shira, D. Berg, J. Bras, A. Brice, C. M. Chen, L. N. Clark, C. Condroyer, E. V. De Marco, A. Dürr, M. J. Eblan, S. Fahn, M. J. Farrer, H. C. Fung, Z. Gan-Or, T. Gasser, R. Gershoni-Baruch, N. Giladi, A. Griffith, T. Gurevich, C. Januario, P. Kropp, A. E. Lang, G. J. Lee-Chen, S. Lesage, K. Marder, I. F. Mata, A. Mirelman, J. Mitsui, I. Mizuta, G. Nicoletti, C. Oliveira, R. Ottman, A. Orr-Urtreger, L. V. Pereira, A. Quattrone, E. Rogaeva, A. Rolfs, H. Rosenbaum, R. Rozenberg, A. Samii, T. Samaddar, C. Schulte, M. Sharma, A. Singleton, M. Spitz, E. K. Tan, N. Tayebi, T. Toda, A. R. Troiano, S. Tsuji, M. Wittstock, T. G. Wolfsberg, Y. R. Wu, C. P. Zabetian, Y. Zhao, and S. G. Ziegler. 2009. 'Multicenter analysis of glucocerebrosidase mutations in Parkinson's disease', *N Engl J Med*, 361: 1651-61.

Simón-Sánchez, J., C. Schulte, J. M. Bras, M. Sharma, J. R. Gibbs, D. Berg, C. Paisan-Ruiz, P. Lichtner, S. W. Schölz, D. G. Hernandez, R. Kruger, M. Federoff, C. Klein, A. Goate, J. Perlmutter, M. Bonin, M. A. Nalls, T. Illig, C. Gieger, H. Houlden, M. Steffens, M. S. Okun, B. A. Racette, M. R. Cookson, K. D. Foote, H. H. Fernandez, B. J. Traynor, S. Schreiber, S. Arepalli, R. Zonozi, K. Gwinn, M. van der Brug, G. Lopez, S. J. Chanock, A. Schatzkin, Y. Park, A. Hollenbeck, J. Gao, X. Huang, N. W. Wood, D. Lorenz, G. Deuschl, H. Chen, O. Riess, J. A. Hardy, A. B. Singleton, and T. Gasser. 2009. 'Genome-wide association study reveals genetic risk underlying Parkinson's disease', *Nat Genet*, 41: 1308-12.

Singleton, A. B., M. Farrer, J. Johnson, A. Singleton, S. Hague, J. Kachergus, M. Hulihan, T. Peuralinna, A. Dutra, R. Nussbaum, S. Lincoln, A. Crawley, M. Hanson, D. Maraganore, C. Adler, M. R. Cookson, M. Muenter, M. Baptista, D. Miller, J. Blancato, J. Hardy, and K. Gwinn-Hardy. 2003. 'alpha-Synuclein locus triplication causes Parkinson's disease', *Science*, 302: 841.

Skipper, L., K. Wilkes, M. Toft, M. Baker, S. Lincoln, M. Hulihan, O. A. Ross, M. Hutton, J. Aasly, and M. Farrer. 2004. 'Linkage disequilibrium and association of *MAPT* H1 in Parkinson disease', *Am J Hum Genet*, 75: 669-77.

Soldner, F., D. Hockemeyer, C. Beard, Q. Gao, G. W. Bell, E. G. Cook, G. Hargus, A. Blak, O. Cooper, M. Mitalipova, O. Isacson, and R. Jaenisch. 2009. 'Parkinson's disease

patient-derived induced pluripotent stem cells free of viral reprogramming factors', *Cell*, 136: 964-77.

Soldner, F., J. Laganière, A. W. Cheng, D. Hockemeyer, Q. Gao, R. Alagappan, V. Khurana, L. I. Golbe, R. H. Myers, S. Lindquist, L. Zhang, D. Guschin, L. K. Fong, B. J. Vu, X. Meng, F. D. Urnov, E. J. Rebar, P. D. Gregory, H. S. Zhang, and R. Jaenisch. 2011. 'Generation of isogenic pluripotent stem cells differing exclusively at two early onset Parkinson point mutations', *Cell*, 146: 318-31.

Soldner, F., Y. Stelzer, C. S. Shivalila, B. J. Abraham, J. C. Latourelle, M. I. Barrasa, J. Goldmann, R. H. Myers, R. A. Young, and R. Jaenisch. 2016. 'Parkinson-associated risk variant in distal enhancer of α-synuclein modulates target gene expression', *Nature*, 533: 95-9.

Soto, C., and L. D. Estrada. 2008. 'Protein misfolding and neurodegeneration', *Arch Neurol*, 65: 184-9.

Spillantini, M. G., R. A. Crowther, R. Jakes, N. J. Cairns, P. L. Lantos, and M. Goedert. 1998b. 'Filamentous alpha-synuclein inclusions link multiple system atrophy with Parkinson's disease and dementia with Lewy bodies', *Neurosci Lett*, 251: 205-8.

Spillantini, M. G., and M. Goedert. 2013. 'Tau pathology and neurodegeneration', *Lancet Neurol*, 12: 609-22.

Spillantini, M. G., J. R. Murrell, M. Goedert, M. R. Farlow, A. Klug, and B. Ghetti. 1998a. 'Mutation in the tau gene in familial multiple system tauopathy with presenile dementia', *Proc Natl Acad Sci U S A*, 95: 7737-41.

Spillantini, M. G., M. L. Schmidt, V. M. Lee, J. Q. Trojanowski, R. Jakes, and M. Goedert. 1997. 'Alpha-synuclein in Lewy bodies', *Nature*, 388: 839-40.

Sposito, T., E. Preza, C. J. Mahoney, N. Setó-Salvia, N. S. Ryan, H. R. Morris, C. Arber, M. J. Devine, H. Houlden, T. T. Warner, T. J. Bushell, M. Zagnoni, T. Kunath, F. J. Livesey, N. C. Fox, M. N. Rossor, J. Hardy, and S. Wray. 2015. 'Developmental regulation of tau splicing is disrupted in stem cell-derived neurons from frontotemporal dementia patients with the 10 + 16 splice-site mutation in MAPT', *Hum Mol Genet*, 24: 5260-9.

Stamer, K., R. Vogel, E. Thies, E. Mandelkow, and E. M. Mandelkow. 2002. 'Tau blocks traffic of organelles, neurofilaments, and APP vesicles in neurons and enhances oxidative stress', *J Cell Biol*, 156: 1051-63.

Stanford, P. M., C. E. Shepherd, G. M. Halliday, W. S. Brooks, P. W. Schofield, H. Brodaty, R. N. Martins, J. B. Kwok, and P. R. Schofield. 2003. 'Mutations in the tau gene that cause an increase in three repeat tau and frontotemporal dementia', *Brain*, 126: 814-26.

Stefansson, H., A. Helgason, G. Thorleifsson, V. Steinthorsdottir, G. Masson, J. Barnard, A. Baker, A. Jonasdottir, A. Ingason, V. G. Gudnadottir, N. Desnica, A. Hicks, A. Gylfason, D. F. Gudbjartsson, G. M. Jonsdottir, J. Sainz, K. Agnarsson, B. Birgisdottir, S. Ghosh, A. Olafsdottir, J. B. Cazier, K. Kristjansson, M. L. Frigge, T. E. Thorgeirsson, J. R. Gulcher, A. Kong, and K. Stefansson. 2005. 'A common inversion under selection in Europeans', *Nat Genet*, 37: 129-37.

Stein, P., H. Yu, D. Jain, and P. K. Mistry. 2010. 'Hyperferritinemia and iron overload in type 1 Gaucher disease', *Am J Hematol*, 85: 472-6.

Stoilov, P., C. H. Lin, R. Damoiseaux, J. Nikolic, and D. L. Black. 2008. 'A high-throughput screening strategy identifies cardiotonic steroids as alternative splicing modulators', *Proc Natl Acad Sci U S A*, 105: 11218-23.

Stoothoff, W., P. B. Jones, T. L. Spires-Jones, D. Joyner, E. Chhabra, K. Bercury, Z. Fan, H. Xie, B. Bacskai, J. Edd, D. Irimia, and B. T. Hyman. 2009. 'Differential effect of three-repeat and four-repeat tau on mitochondrial axonal transport', *J Neurochem*, 111: 417-27.

Su, Y. C., and X. Qi. 2013. 'Inhibition of excessive mitochondrial fission reduced aberrant autophagy and neuronal damage caused by LRRK2 G2019S mutation', *Hum Mol Genet*.

Suberbielle, E., P. E. Sanchez, A. V. Kravitz, X. Wang, K. Ho, K. Eilertson, N. Devidze, A. C. Kreitzer, and L. Mucke. 2013. 'Physiologic brain activity causes DNA double-strand breaks in neurons, with exacerbation by amyloid-β', *Nat Neurosci*, 16: 613-21.

Sánchez-Danés, A., A. Consiglio, Y. Richaud, I. Rodríguez-Pizà, B. Dehay, M. Edel, J. Bové, M. Memo, M. Vila, A. Raya, and J. C. Izpisua Belmonte. 2012a. 'Efficient generation of A9 midbrain dopaminergic neurons by lentiviral delivery of LMX1A in human embryonic stem cells and induced pluripotent stem cells', *Hum Gene Ther*, 23: 56-69.

Sánchez-Danés, A., Y. Richaud-Patin, I. Carballo-Carbajal, S. Jiménez-Delgado, C. Caig, S. Mora, C. Di Guglielmo, M. Ezquerra, B. Patel, A. Giralt, J. M. Canals, M. Memo, J. Alberch, J. López-Barneo, M. Vila, A. M. Cuervo, E. Tolosa, A. Consiglio, and A. Raya. 2012b. 'Disease-specific phenotypes in dopamine neurons from human iPS-based models of genetic and sporadic Parkinson's disease', *EMBO Mol Med*, 4: 380-95.

Takahashi, K., K. Tanabe, M. Ohnuki, M. Narita, T. Ichisaka, K. Tomoda, and S. Yamanaka. 2007. 'Induction of pluripotent stem cells from adult human fibroblasts by defined factors', *Cell*, 131: 861-72.

Takahashi, K., and S. Yamanaka. 2006. 'Induction of pluripotent stem cells from mouse embryonic and adult fibroblast cultures by defined factors', *Cell*, 126: 663-76.

Tanner, C. M., F. Kamel, G. W. Ross, J. A. Hoppin, S. M. Goldman, M. Korell, C. Marras, G. S. Bhudhikanok, M. Kasten, A. R. Chade, K. Comyns, M. B. Richards, C. Meng, B. Priestley, H. H. Fernandez, F. Cambi, D. M. Umbach, A. Blair, D. P. Sandler, and J. W. Langston. 2011. 'Rotenone, paraquat, and Parkinson's disease', *Environ Health Perspect*, 119: 866-72.

Tayebi, N., J. Walker, B. Stubblefield, E. Orvisky, M. E. LaMarca, K. Wong, H. Rosenbaum, R. Schiffmann, B. Bembi, and E. Sidransky. 2003. 'Gaucher disease with parkinsonian manifestations: does glucocerebrosidase deficiency contribute to a vulnerability to parkinsonism?', *Mol Genet Metab*, 79: 104-9.

Theka, I., M. Caiazzo, E. Dvoretskova, D. Leo, F. Ungaro, S. Curreli, F. Managò, M. T. Dell'Anno, G. Pezzoli, R. R. Gainetdinov, A. Dityatev, and V. Broccoli. 2013. 'Rapid generation of functional dopaminergic neurons from human induced pluripotent stem cells through a single-step procedure using cell lineage transcription factors', Stem Cells Transl Med, 2: 473-9.

Thomsen, E. R., J. K. Mich, Z. Yao, R. D. Hodge, A. M. Doyle, S. Jang, S. I. Shehata, A. M. Nelson, N. V. Shapovalova, B. P. Levi, and S. Ramanathan. 2016. 'Fixed single-cell transcriptomic characterization of human radial glial diversity', *Nat Methods*, 13: 87-93.

Thomson, J. A., J. Itskovitz-Eldor, S. S. Shapiro, M. A. Waknitz, J. J. Swiergiel, V. S. Marshall, and J. M. Jones. 1998. 'Embryonic stem cell lines derived from human blastocysts', *Science*, 282: 1145-7.

Tobin, J. E., J. C. Latourelle, M. F. Lew, C. Klein, O. Suchowersky, H. A. Shill, L. I. Golbe, M. H. Mark, J. H. Growdon, G. F. Wooten, B. A. Racette, J. S. Perlmutter, R. Watts, M. Guttman, K. B. Baker, S. Goldwurm, G. Pezzoli, C. Singer, M. H. Saint-Hilaire, A. E. Hendricks, S. Williamson, M. W. Nagle, J. B. Wilk, T. Massood, J. M. Laramie, A. L. DeStefano, I. Litvan, G. Nicholson, A. Corbett, S. Isaacson, D. J. Burn, P. F. Chinnery, P. P. Pramstaller, S. Sherman, J. Al-hinti, E. Drasby, M. Nance, A. T. Moller, K. Ostergaard, R. Roxburgh, B. Snow, J. T. Slevin, F. Cambi, J. F. Gusella, and R. H. Myers. 2008. 'Haplotypes and gene expression implicate the *MAPT* region for Parkinson disease: the GenePD Study', *Neurology*, 71: 28-34.

Togo, T., N. Sahara, S. H. Yen, N. Cookson, T. Ishizawa, M. Hutton, R. de Silva, A. Lees, and D. W. Dickson. 2002. 'Argyrophilic grain disease is a sporadic 4-repeat tauopathy', *J Neuropathol Exp Neurol*, 61: 547-56.

Trabzuni, D., S. Wray, J. Vandrovcova, A. Ramasamy, R. Walker, C. Smith, C. Luk, J. R. Gibbs, A. Dillman, D. G. Hernandez, S. Arepalli, A. B. Singleton, M. R. Cookson, A. M. Pittman, R. de Silva, M. E. Weale, J. Hardy, and M. Ryten. 2012. 'MAPT expression and splicing is differentially regulated by brain region: relation to genotype and implication for tauopathies', *Hum Mol Genet*, 21: 4094-103.

Trinczek, B., A. Ebneth, E. M. Mandelkow, and E. Mandelkow. 1999. 'Tau regulates the attachment/detachment but not the speed of motors in microtubule-dependent transport of single vesicles and organelles', *J Cell Sci*, 112 (Pt 14): 2355-67.

Trinh, J., and M. Farrer. 2013. 'Advances in the genetics of Parkinson disease', *Nat Rev Neurol*.

Tritsch, N. X., J. B. Ding, and B. L. Sabatini. 2012. 'Dopaminergic neurons inhibit striatal output through non-canonical release of GABA', *Nature*, 490: 262-6.

Trotta, L., I. Guella, G. Soldà, F. Sironi, S. Tesei, M. Canesi, G. Pezzoli, S. Goldwurm, S. Duga, and R. Asselta. 2012. 'SNCA and MAPT genes: Independent and joint effects in Parkinson disease in the Italian population', *Parkinsonism Relat Disord*, 18: 257-62.

Tsuji, S., P. V. Choudary, B. M. Martin, B. K. Stubblefield, J. A. Mayor, J. A. Barranger, and E. I. Ginns. 1987. 'A mutation in the human glucocerebrosidase gene in neuronopathic Gaucher's disease', *N Engl J Med*, 316: 570-5.

Tsuji, S., B. M. Martin, J. A. Barranger, B. K. Stubblefield, M. E. LaMarca, and E. I. Ginns. 1988. 'Genetic heterogeneity in type 1 Gaucher disease: multiple genotypes in Ashkenazic and non-Ashkenazic individuals', *Proc Natl Acad Sci U S A*, 85: 2349-52.

UK Parkinson's Disease Consortium (UKPDC), Welcome Trust Case-Control Consortium 2 (WTCCC2), C. C. Spencer, V. Plagnol, A. Strange, M. Gardner, C. Paisan-Ruiz, G. Band, R. A. Barker, C. Bellenguez, K. Bhatia, H. Blackburn, J. M. Blackwell, E. Bramon, M. A. Brown, D. Burn, J. P. Casas, P. F. Chinnery, C. E. Clarke, A. Corvin, N. Craddock, P. Deloukas, S. Edkins, J. Evans, C. Freeman, E. Gray, J. Hardy, G. Hudson, S. Hunt, J. Jankowski, C. Langford, A. J. Lees, H. S. Markus, C. G. Mathew, M. I. McCarthy, K. E. Morrison, C. N. Palmer, J. P. Pearson, L. Peltonen, M. Pirinen, R. Plomin, S. Potter, A. Rautanen, S. J. Sawcer, Z. Su, R. C. Trembath, A. C. Viswanathan, N. W. Williams, H. R. Morris, P. Donnelly, and N. W. Wood. 2011. 'Dissection of the genetics of Parkinson's disease identifies an additional association 5' of *SNCA* and multiple associated haplotypes at 17q21', *Hum Mol Genet*, 20: 345-53.

Valenca, G. T., G. P. Srivastava, J. Oliveira-Filho, C. C. White, L. Yu, J. A. Schneider, A. S. Buchman, J. M. Shulman, D. A. Bennett, and P. L. De Jager. 2016. 'The Role of MAPT Haplotype H2 and Isoform 1N/4R in Parkinsonism of Older Adults', *PLoS One*, 11: e0157452.

Vallee, R. 1980. 'Structure and phosphorylation of microtubule-associated protein 2 (MAP 2)', *Proc Natl Acad Sci U S A*, 77: 3206-10.

Vallee, R. B., and G. G. Borisy. 1977. 'Removal of the projections from cytoplasmic microtubules in vitro by digestion with trypsin', *J Biol Chem*, 252: 377-82.

van Swieten, J. C., M. Stevens, S. M. Rosso, P. Rizzu, M. Joosse, I. de Koning, W. Kamphorst, R. Ravid, M. G. Spillantini, Niermeijer, and P. Heutink. 1999. 'Phenotypic variation in hereditary frontotemporal dementia with tau mutations', Ann Neurol, 46: 617-26.

van Wilgenburg, B., C. Browne, J. Vowles, and S. A. Cowley. 2013. 'Efficient, long term production of monocyte-derived macrophages from human pluripotent stem cells under partly-defined and fully-defined conditions', *PLoS One*, 8: e71098.

Vandrovcova, J., A. M. Pittman, E. Malzer, P. M. Abou-Sleiman, A. J. Lees, N. W. Wood, and R. de Silva. 2009. 'Association of *MAPT* haplotype-tagging SNPs with sporadic Parkinson's disease', *Neurobiol Aging*, 30: 1477-82.

Vierbuchen, T., A. Ostermeier, Z. P. Pang, Y. Kokubu, T. C. Südhof, and M. Wernig. 2010. 'Direct conversion of fibroblasts to functional neurons by defined factors', Nature, 463: 1035-41.

Vogel, G. 2010. 'Stem cells. Diseases in a dish take off', *Science*, 330: 1172-3.

Vossel, K. A., J. C. Xu, V. Fomenko, T. Miyamoto, E. Suberbielle, J. A. Knox, K. Ho, D. H. Kim, G. Q. Yu, and L. Mucke. 2015. 'Tau reduction prevents Abeta-induced axonal transport deficits by blocking activation of GSK3beta', *J Cell Biol*, 209: 419-33.

Vossel, K. A., K. Zhang, J. Brodbeck, A. C. Daub, P. Sharma, S. Finkbeiner, B. Cui, and L. Mucke. 2010. 'Tau reduction prevents Abeta-induced defects in axonal transport', *Science*, 330: 198.

Wade-Martins, R., E. R. Smith, E. Tyminski, E. A. Chiocca, and Y. Saeki. 2001. 'An infectious transfer and expression system for genomic DNA loci in human and mouse cells', *Nat Biotechnol*, 19: 1067-70.

Wakabayashi, K., K. Tanji, S. Odagiri, Y. Miki, F. Mori, and H. Takahashi. 2013. 'The Lewy body in Parkinson's disease and related neurodegenerative disorders', *Mol Neurobiol*, 47: 495-508.

Wang, J., Q. S. Gao, Y. Wang, R. Lafyatis, S. Stamm, and A. Andreadis. 2004. 'Tau exon 10, whose missplicing causes frontotemporal dementia, is regulated by an intricate interplay of cis elements and trans factors', *J Neurochem*, 88: 1078-90.

Watmuff, B., B. J. Hartley, C. P. Hunt, S. A. Fabb, C. W. Pouton, and J. M. Haynes. 2015. 'Human pluripotent stem cell derived midbrain PITX3(eGFP/w) neurons: a versatile tool for pharmacological screening and neurodegenerative modeling', *Front Cell Neurosci*, 9: 104.

Weggen, S., and D. Beher. 2012. 'Molecular consequences of amyloid precursor protein and presenilin mutations causing autosomal-dominant Alzheimer's disease', *Alzheimers Res Ther*, 4: 9.

West, A. B., D. J. Moore, S. Biskup, A. Bugayenko, W. W. Smith, C. A. Ross, V. L. Dawson, and T. M. Dawson. 2005. 'Parkinson's disease-associated mutations in leucine-rich repeat kinase 2 augment kinase activity', *Proc Natl Acad Sci U S A*, 102: 16842-7.

Wider, C., C. Vilariño-Güell, M. G. Heckman, B. Jasinska-Myga, A. I. Ortolaza-Soto, N. N. Diehl, J. E. Crook, S. A. Cobb, J. A. Bacon, J. O. Aasly, J. M. Gibson, T. Lynch, R. J. Uitti, Z. K. Wszolek, M. J. Farrer, and O. A. Ross. 2011. 'SNCA, MAPT, and GSK3B in Parkinson disease: a gene-gene interaction study', *Eur J Neurol*, 18: 876-81.

Wider, C., C. Vilariño-Güell, B. Jasinska-Myga, M. G. Heckman, A. I. Soto-Ortolaza, S. A. Cobb, J. O. Aasly, J. M. Gibson, T. Lynch, R. J. Uitti, Z. K. Wszolek, M. J. Farrer, and O. A. Ross. 2010. 'Association of the *MAPT* locus with Parkinson's disease', *Eur J Neurol*, 17: 483-6.

Williams, D. R. 2006. 'Tauopathies: classification and clinical update on neurodegenerative diseases associated with microtubule-associated protein tau', *Intern Med J*, 36: 652-60.

Williams-Gray, C. H., J. R. Evans, A. Goris, T. Foltynie, M. Ban, T. W. Robbins, C. Brayne, B. S. Kolachana, D. R. Weinberger, S. J. Sawcer, and R. A. Barker. 2009. 'The distinct cognitive syndromes of Parkinson's disease: 5 year follow-up of the CamPaIGN cohort', *Brain*, 132: 2958-69.

Winkler, S., I. R. Konig, K. Lohmann-Hedrich, P. Vieregge, V. Kostic, and C. Klein. 2007. 'Role of ethnicity on the association of *MAPT* H1 haplotypes and subhaplotypes in Parkinson's disease', *Eur J Hum Genet*, 15: 1163-8.

Winner, B., R. Jappelli, S. K. Maji, P. A. Desplats, L. Boyer, S. Aigner, C. Hetzer, T. Loher, M. Vilar, S. Campioni, C. Tzitzilonis, A. Soragni, S. Jessberger, H. Mira, A. Consiglio, E. Pham, E. Masliah, F. H. Gage, and R. Riek. 2011. 'In vivo demonstration that alpha-synuclein oligomers are toxic', *Proc Natl Acad Sci U S A*, 108: 4194-9.

Wood, M., H. Yin, and G. McClorey. 2007. 'Modulating the expression of disease genes with RNA-based therapy', *PLoS Genet*, 3: e109.

Woodard, C. M., B. A. Campos, S. H. Kuo, M. J. Nirenberg, M. W. Nestor, M. Zimmer, E. V. Mosharov, D. Sulzer, H. Zhou, D. Paull, L. Clark, E. E. Schadt, S. P. Sardi, L. Rubin, K. Eggan, M. Brock, S. Lipnick, M. Rao, S. Chang, A. Li, and S. A. Noggle. 2014. 'iPSC-derived dopamine neurons reveal differences between monozygotic twins discordant for Parkinson's disease', *Cell Rep*, 9: 1173-82.

Xia, N., P. Zhang, F. Fang, Z. Wang, M. Rothstein, B. Angulo, R. Chiang, J. Taylor, and R. A. Reijo Pera. 2016. 'Transcriptional comparison of human induced and primary midbrain dopaminergic neurons', Sci Rep, 6: 20270.

Xie, Z., and D. J. Klionsky. 2007. 'Autophagosome formation: core machinery and adaptations', *Nat Cell Biol*, 9: 1102-9.

Yan, J., L. Studer, and R. D. McKay. 2001. 'Ascorbic acid increases the yield of dopaminergic neurons derived from basic fibroblast growth factor expanded mesencephalic precursors', *J Neurochem*, 76: 307-11.

Yoo, A. S., A. X. Sun, L. Li, A. Shcheglovitov, T. Portmann, Y. Li, C. Lee-Messer, R. E. Dolmetsch, R. W. Tsien, and G. R. Crabtree. 2011. 'MicroRNA-mediated conversion of human fibroblasts to neurons', Nature, 476: 228-31.

Yuan, A., A. Kumar, C. Peterhoff, K. Duff, and R. A. Nixon. 2008. 'Axonal transport rates in vivo are unaffected by tau deletion or overexpression in mice', *J Neurosci*, 28: 1682-7.

Yuan, A., A. Kumar, T. Sasaki, K. Duff, and R. A. Nixon. 2013. 'Global axonal transport rates are unaltered in htau mice in vivo', *J Alzheimers Dis*, 37: 579-86.

Yuan, S. H., J. Martin, J. Elia, J. Flippin, R. I. Paramban, M. P. Hefferan, J. G. Vidal, Y. Mu, R. L. Killian, M. A. Israel, N. Emre, S. Marsala, M. Marsala, F. H. Gage, L. S. Goldstein, and C. T. Carson. 2011. 'Cell-surface marker signatures for the isolation of neural stem cells, glia and neurons derived from human pluripotent stem cells', *PLoS One*, 6: e17540.

Zabetian, C. P., C. M. Hutter, S. A. Factor, J. G. Nutt, D. S. Higgins, A. Griffith, J. W. Roberts, B. C. Leis, D. M. Kay, D. Yearout, J. S. Montimurro, K. L. Edwards, A. Samii, and H. Payami. 2007. 'Association analysis of *MAPT* H1 haplotype and subhaplotypes in Parkinson's disease', *Ann Neurol*, 62: 137-44.

Zappia, M., G. Annesi, G. Nicoletti, P. Serra, G. Arabia, P. Pugliese, D. Messina, M. Caracciolo, N. Romeo, F. Annesi, A. A. Pasqua, P. Spadafora, D. Civitelli, A. Epifanio, L. Morgante, and A. Quattrone. 2003. 'Association of *tau* gene polymorphism with Parkinson's disease', *Neurol Sci*, 24: 223-4.

Zarranz, J. J., J. Alegre, J. C. Gómez-Esteban, E. Lezcano, R. Ros, I. Ampuero, L. Vidal, J. Hoenicka, O. Rodriguez, B. Atarés, V. Llorens, E. Gomez Tortosa, T. del Ser, D. G. Muñoz, and J. G. de Yebenes. 2004. 'The new mutation, E46K, of alpha-synuclein causes Parkinson and Lewy body dementia', *Ann Neurol*, 55: 164-73.

Zetusky, W. J., J. Jankovic, and F. J. Pirozzolo. 1985. 'The heterogeneity of Parkinson's disease: clinical and prognostic implications', *Neurology*, 35: 522-6.

Zhang, B., A. Maiti, S. Shively, F. Lakhani, G. McDonald-Jones, J. Bruce, E. B. Lee, S. X. Xie, S. Joyce, C. Li, P. M. Toleikis, V. M. Lee, and J. Q. Trojanowski. 2005a. 'Microtubule-binding drugs offset tau sequestration by stabilizing microtubules and reversing fast axonal transport deficits in a tauopathy model', *Proc Natl Acad Sci U S A*, 102: 227-31.

Zhang, J., Y. Song, H. Chen, and D. Fan. 2005b. 'The *Tau* gene haplotype h1 confers a susceptibility to Parkinson's disease', *Eur Neurol*, 53: 15-21.

Zhang, Y., J. P. Muyrers, G. Testa, and A. F. Stewart. 2000. 'DNA cloning by homologous recombination in Escherichia coli', *Nat Biotechnol*, 18: 1314-7.

Zhao, S., S. Maxwell, A. Jimenez-Beristain, J. Vives, E. Kuehner, J. Zhao, C. O'Brien, C. de Felipe, E. Semina, and M. Li. 2004. 'Generation of embryonic stem cells and transgenic mice expressing green fluorescence protein in midbrain dopaminergic neurons', *Eur J Neurosci*, 19: 1133-40.

Zheng, S., Y. Chen, C. P. Donahue, M. S. Wolfe, and G. Varani. 2009. 'Structural basis for stabilization of the tau pre-mRNA splicing regulatory element by novantrone (mitoxantrone)', *Chem Biol*, 16: 557-66.

Zhong, Q., E. E. Congdon, H. N. Nagaraja, and J. Kuret. 2012. 'Tau isoform composition influences rate and extent of filament formation', *J Biol Chem*, 287: 20711-9.

Zimprich, A., S. Biskup, P. Leitner, P. Lichtner, M. Farrer, S. Lincoln, J. Kachergus, M. Hulihan, R. J. Uitti, D. B. Calne, A. J. Stoessl, R. F. Pfeiffer, N. Patenge, I. C. Carbajal, P. Vieregge, F. Asmus, B. Müller-Myhsok, D. W. Dickson, T. Meitinger, T. M. Strom, Z. K. Wszolek, and T. Gasser. 2004. 'Mutations in LRRK2 cause autosomal-dominant parkinsonism with pleomorphic pathology', *Neuron*, 44: 601-7.

Zody, M. C., Z. Jiang, H. C. Fung, F. Antonacci, L. W. Hillier, M. F. Cardone, T. A. Graves, J. M. Kidd, Z. Cheng, A. Abouelleil, L. Chen, J. Wallis, J. Glasscock, R. K. Wilson, A. D. Reily, J. Duckworth, M. Ventura, J. Hardy, W. C. Warren, and E. E. Eichler. 2008. 'Evolutionary toggling of the *MAPT* 17q21.31 inversion region', *Nat Genet*, 40: 1076-83.

Zufferey, R., T. Dull, R. J. Mandel, A. Bukovsky, D. Quiroz, L. Naldini, and D. Trono. 1998. 'Self-inactivating lentivirus vector for safe and efficient in vivo gene delivery', *J Virol*, 72: 9873-80.

Appendix

Appendix Table A: Plasmids used in the construction of the *TH*-PAC reporter constructs.

Plasmid Name	Use	Source
RP11-542J6 BAC	Human *TH* gene locus; Amplification of full Chl^R (CAT) sequence	Children's Hospital Oakland Research Institute
TH-PAC subcloned from RP11-542J6 BAC	Human *TH* gene locus	S.P. Shorkey
pGEM-T (Chl)/PolyAx3	Cassette backbone	S.P. Shorkey (note that the Chl^R sequence lacked the promoter)
mCherry bacterial expression plasmid	Amplification of mCherry sequence	Gift of Roger Tsien laboratory, University of California San Diego
pRed/ET (pSC101-BAD-gbaA)	Bacterial induction of homologous recombination	Gene Bridges
pEHHG	Retrofitting Amplification of EGFP sequence	R. Wade-Martins
pH-FRT-Hy	Retrofitting	J. Alegre-Abarrategui, Wade-Martins laboratory
pDsRed2-C1 p62	Amplification of 3' UTR-PolyA sequence	Addgene (note that this is no longer available)
fHSVΔpacΔ27 0++	Expression of HSV-1 genes for HSV-1 amplicon production	E.A. Chiocca laboratory, Harvard University
pEBHICP27	Expression of HSV-1 ICP27 gene for amplicon production	E.A. Chiocca laboratory, Harvard University

Appendix Table B: Cloning primers used in the construction of *TH*-PAC reporter constructs.

Cloning Primers	
Primer Name	**Primer Sequence (5'→3')**
CAT_F (*Sac*II site)	ACTGATCCGCGGCGCGAATAAATACCTGTGACG
CAT_R (*Spe*I site)	TAGATTACTAGTCATCGAATTTCTGCCATTCA
mCherry_F (ApaI site)	ACTGATGGGCCCTCAATGGTGAGCAAGGGCGAGGA
mCherry_R2 (SacII site)	TAGATTCCGCGGTTACTTGTACAGCTCGTCCATGC
mCherry_longF (homology arm)	GGGCTTTGACGTCAGCTCAGCTTATAAGAGGCTGCTGGGCCAGGGCTGTGG AGACGGAGCCCGGACCTCCACACTGAGCCATGGTGAGCAAGGGCGAGGA
mCherry_longR (homology arm)	CTGCCAGCCAGGCTGGGGAGTAGCAGAGGCAGCTGGCACCAGCCCTGGGC TCCGGTCCACTGCGGCCGCCGGGCACCTACTATGAGAGAATAGGAACTTC
3'UTR-PolyA_F (*Sac*II site)	ACTGATCCGCGGGATCATAATCAGCCATACCA
3'UTR-PolyA_R (*Sac*II site) (*Swa*I site)	TAGATTCCGCGGATTTAAATCGCGTTAAGATACATTGATG

mCherry and EGFP share the same sequence at either end so mCherry primers were used for EGFP cloning as well.

Appendix Table C: Sequencing and analytical primers used to verify the construction of *TH*-PAC reporter constructs.

Primer Name	Primer Sequence (5'→3')
mCherry_seq1F	GATCGGTGCGGGCCTCTTCG
mCherry_seq1R	CCCTCGGCGCGTTCGTACTG
mCherry_seq2F	AAGGACGGCGGCCACTACGA
mCherry_seq2R	AGCACCTTGTCGCCTTGCGT
PolyA_seq3F	GCGTGTTACGGTGAAAACCT
PolyA_seq3R	GACCATGATTACGCCAAGCTA
mCherry_seq4F	TAAAACGACGGCCAGTGAAT
mCherry_seq4R	GTGGGAGGTGATGTCCAACT
EGFP_seq1F	CGATCGGTGCGGGCCTCTTC
EGFP_seq1R	CGTCGCCGATGGGGGTGTTC
EGFP_seq2F	CAACTACAACAGCCACAACG
EGFP_seq2R	GGGCGAAGAAGTTGTCCATA
TH_mCherry_F	CTCCCTGTGTGCTCTCTTGA
TH_mCherry_R	CCGTCCTCGAAGTTCATCAC
TH_ChlPolyA_F	TGTCGGCAGAATGCTTAATG
TH_ChlPolyA_R	CCAACAGGGACTCAAACACC
TH_EGFP_F	TTAGATTCCACGGACGAGCC
TH_EGFP_R	GGTATGGCTGATTATGATCCCG
CAT_seqMidR	GCCGGATAAAACTTGTGCTT
CAT_seqEndF	TCGCCTTCTTGACGAGTTCT
PolyA_seqEndF	GCGGAAGTTCCTATTCTCTC
TH_ex2_F	CATTTCCAGGTACCTTCTCAGG
TH_ex3_F	GACCAGCTGTGGGTGGAG
TH_ex4_F	TTCCTGCTTTTGCTCCCTAA
TH_ex5_F	TCACCAAGATCTCTTCCTCCAT
TH_ex6_F	CAGCACAGCCTCCTGACC
TH_ex7_F	CCTCCTGCCCTTCTCACTC
TH_ex8_F	ACTGGGGTGGGGCATTAG
TH_ex9_F	CGCTTCCTGAAGGGTGTG
TH_ex10_F	CCCTTCTCCCTCCTACGC
TH_ex11_F	AGGGAAGTGTCCCAGAGACC
TH_ex12_F	CTGTCTCTGGGCTGATGCT
TH_ex13_F	GGGTGACTCTACCCAAGGAA
TH_ex14_F	AGCCACTGTGAAGGTGGAAA
TH_ex2_R	AGGGTTGTGGAACATGAAGG
TH_ex3_R	CGGGGAGAAGAGCAGGTTTA
TH_ex4_R	GCACGTCCTCTGACACCTG
TH_ex5_R	GGCTAAGGGTAGGGGATGTG
TH_ex6_R	CCTGTACTGGAAGGCGATCT
TH_ex7_R	CCTCACACGCCAGGATTC
TH_ex8_R	CCTTCAGGAAGCGGGAGAC
TH_ex9_R	CGCGTAGGAGGGAGAAGG
TH_ex10_R	AGCAGGCAGCACACTTCAC
TH_ex11_R	ACCGTGGACAGCTTCTCAAT
TH_ex12_R	GTCCAGGCCTCAGTTTCCTC
TH_ex13_R	CTAGCCCACCTGAGCTTGTC
TH_ex14_R	AAGGGTGTCCAGCTCATCC

Appendix Table D: Primers used for end-point RT-PCR.

Primer Name	Primer Sequence (5'→3')
endoTH_RT_F	GCAGGCAGAGGCCATCAT
endoTH_RT_R	CTTCTCCTCAAAGGCCACAG
GAPDH_F	GTGGACCTGACCTGCCGTCTCG
GAPDH_R	GGAGGAGTGGGTGTCGCTGT
MAPT_ex9-10 F2	GTCCCTTCCAACCCCACC
MAPT_ex9-10 R2	ACTTGGACTGGACGTTGCTA
MAPT_ex0 F	CTTCTCCTCCTCCGCTGTC
MAPT_ex1/4 R (0N)	CTGCTTCTTCAGCTTTCAGG
MAPT_ex2/4 R (1N)	ATGCCTGCTTCTTCAGCTTC
MAPT_ex3 R (2N)	GAGCTCCCTCATCCACTAAGG

Appendix Table E: Primers used for *MAPT* haplotype analysis and *GBA* genotyping.

Primer Name	Primer Sequence (5'-3')	Primer Purpose
tau_indel_F	GGAAGACGTTCTCACTGATCTG	Genotyping H1/H2 (±238 bp), Baker et al. (1999)
tau_indel_R	AAGAGTCTGGCTTCAGTCTCTC	
MAPT_Int9seqF	TGTGAAGTGAGGACCTGCAA	Sequencing upstream of *MAPT* exon 10
MAPT_Int9seqR	AAAAGGATGAGTGACACGCC	
MAPTEx10seqF	CTCTGCCAAGTCCGAAAGTG	Sequencing *MAPT* exon 10 and environs
MAPTEx10seqR	GGTCCGTCATCTGCCCTATT	
MAPT_int9_H1F	GAAATGCAGTCGTGGGAGAC	Generation of H1 sub-clone (with MAPTEx10seqR)
MAPT_int9_H2F	TGGTTTTCTATTTCACAGCCCC	Generation of H2 sub-clone (with MAPTEx10seqR)
M13_F	GTAAAACGACGGCCAGT	Sequencing of sub-clones in pGEM-T Easy
M13_R	CAGGAAACAGCTATGAC	
GBA_N370S_F	GCCTTTGTCCTTACCCTCG	Genotyping *GBA* N370S mutation (Aharon-Peretz et al. 2004)
GBA_N370S_R	GACAAAGTTACGCACCCAA	

Appendix Table F: iPSC clones used in this study.

H1/H2 Controls					
Thesis ID	**OPDC (StemBANCC) codes**	**Age at biopsy**	**Gender**	**Clones used**	**Other information**
Individual 1	NHDF	44	F	NHDF-1 NHDF-2	Normal human dermal fibroblasts (Lonza) Hartfield et al. (2014)
Individual 2	AH016	80	M	AH016-3 AH016-6 AH016-10	
Individual 3	OX1 (SFC841)	36	M	OX1-19 SFC841-03-01 SFC841-03-02	van Wilgenburg et al. (2013) Fernandes et al. (2016)
H1/H1 Controls vs H1/H1 *GBA* N370S					
Thesis ID	**OPDC (StemBANCC) codes**	**Age at biopsy**	**Gender**	**Clones used**	**Other information**
Con1	JR053	68	M	JR053-1	
Con2	JR053	68	M	JR053-6	
Con3	AH017 (SFC840)	67	F	SFC840-03-06	
Con4	OX2	43	M	OX2-28	
GBA1	MK071	81	F	MK071-3	N370S/wt Fernandes et al. (2016)
GBA2	MK088	46	M	MK088-7	N370S/wt
GBA3	MK088	46	M	MK088-1	N370S/wt Fernandes et al. (2016)
GBA4	RH058 (SFC834)	72	M	SFC834-03-01	N370S/wt Fernandes et al. (2016)

Appendix Table G: Single nucleotide polymorphisms genotyped in the three H1/H2 control individuals used in this study.

Primer Name	Primer Sequence 5' --> 3'	AmpliTaq PCR		SNP	Individual		
		Length	Temp		1	2	3
MAPT_gen_Ex0F MAPT_gen_Ex0R	GAGGAACGAGCCGGGAGA GACGGCGAGGCAGATTTC	362 or 361 bp	GC 60º	rs11575895 rs62056779 rs144722105	A/G C/A C/Δ	A/G C/A C/Δ	A/G C/A C/Δ
tau_exon1_F tau_exon1_R	TGAGATCTGCCTGCCATGAA CATGGCTGTCCACTAACCTT	273 bp	60º	rs17650901 (rs6370529)	A/G G/G	A/G G/G	A/G G/G
tau_exon7_F tau_exon7_R	GACTCTTGGTGGCAGTAACT ACCTCTGAGAGCTTCAGCTT	241 bp	60º	rs1052551 (rs63750612)	G/A G/G	G/A G/G	G/A G/G
tau_exon9_F tau_exon9_R	CTGCTGTAGCTGCGCTTCCA CTCCATGCACAGTCCCACGA	540 bp	60º	rs1052553 rs1765121	A/G T/C	A/G T/C	A/G T/C
MAPT_gen_Ex13F MAPT_gen_Ex13R	ATCGACATGGTAGACTCGCC AAGCCGAGTGACAAAAGCAG	234 bp	60º	rs9468	T/C	T/C	T/C
MAPT_gen_Ex13F2 MAPT_gen_Ex13R2	TGGTTGGTTGCAGGAGGTAC AGGGCTCTCTCCATGTCAAC	242 bp	60º	rs17574040 rs16940799	A/C T/C	A/C T/C	A/C T/C
MAPT_gen_Ex13F3 MAPT_gen_Ex13R3	AGATCACTCGCTTCACCCTC TCCTGCTCAACATGGCAAAC	217 bp	60º	rs7521 (rs114213384)	G/A A/A	G/A A/A	G/A A/A
tau_STH_F tau_STH_R	CCCTGTAAACTCTGACCACAC ACAGGGAAGCTACTTCCCATG	226 bp	60º	rs62063857 (rs73317018)	A/G G/G	A/G G/G	A/G G/G
SNCA_gen_Ex6F SNCA_gen_Ex6R	CTGGTTCCTTAAGTGGCTGTG TGTCAGAAAGGTACAGCATTCAC	272 bp	60º	rs356165	C/T	C/T	C/T
SNCA_gen_Ex6F2 SNCA_gen_Ex6R2	GCAGTGACCTAGAACAATTTGAG AGGTGAATGTCTCGGGAGTG	246 bp	60º	rs3857053 rs1045722	G/G A/A	G/G A/A	G/G A/A
hLRRK2_x42s hLRRK2_x42a	GGTTTCGTGCACCTGAAG CCAAATGTGGAGTTCTAACAGC	446 bp	60º	rs33995883	A/A	A/A	A/A
LRRK2_gen_Ex51F LRRK2_gen_Ex51R	ACAATCTTGCTTGACCGTTTG GCAACAGCAACAAAGAGAATTC	675 bp	60º	rs66737902 (rs17520676) (rs10878441) (rs3886747)	T/T A/A C/A T/C	T/T A/A C/C T/C	C/C* A/A C/C T/T
CRHR1_gen_Ex7F CRHR1_gen_Ex7R	GTGACAGCCGCCTACAAC AGTCTGGAGGAGAGGGCAG	206 bp	GC 60º	rs16940665	T/C	T/C	T/C
CRHR1_gen_Ex9F CRHR1_gen_Ex9R	ACAATTGAGGCATGGCAGTG GATTGCCCCTCCCCACTG	299 bp	GC 60º	rs16940674 (rs79608615)	C/T G/G	C/T C/C	C/T G/G
KANSL1_gen_Ex11F KANSL1_gen_Ex11R	CCCAAGGACCCAGATGCTTG TTCTGAGCTTCTACCTGGGC	249 bp	60º	rs17574604	T/C	T/C	T/C
KANSL1_gen_Ex13F KANSL1_gen_Ex13R	CTAGAATGGGGTGGGACTGG CAAACTCCCTGTCCACCCTC	241 bp	GC 60º	rs36076725 (rs35833914)	C/T C/T	C/T C/T	C/T C/T
KANSL1_gen_Ex15F KANSL1_gen_Ex15R	GGAGTGTGAGGACCAGCTG ACTGTGAAAATTTCCGGCATATG	278 bp	60º	rs34579536	T/C	T/C	T/C

*C allele vs T allele carries odds ratio of 1.10 (95% confidence interval: 1.05, 1.15) for risk of Parkinson's disease in PDGene meta-analysis (Nalls et al. 2014). GC, addition of GC buffer.

Appendix Table H: TaqMan Gene Expression Assays from Applied Biosystems.

Gene/Assay Description	Assay ID
MAPT exon3+ transcripts (exon3-4)	Hs00902315_m1 FAM/MGB/NFQ
MAPT exon 10+ transcripts (exon9-10)	Hs00902312_m1 FAM/MGB/NFQ
MAPT all transcripts (exon12-13)	Hs00902194_m1 FAM/MGB/NFQ
GAPDH	Hs02758991_g1 VIC/MGB/NFQ
HPRT1	Hs02800695_m1 VIC/MGB/NFQ
ACTB	Hs01060665_g1 VIC/MGB/NFQ

Appendix Table J: Primers and probes for allele-specific TaqMan qRT-PCR expression assays.

Primer/Probe Name	Primer/Probe Sequence (5'-3')	Primer/Probe Purpose
MAPT exon 0 F	CCTCGCCTCTGTCGACTATC	MAPT all transcripts allele-specific (exon 0-1)
MAPT exon 1 R	TACGTCCCAGCGTGATCTTC	
MAPT exon 0 F	CCTCGCCTCTGTCGACTATC	MAPT exon 3+ transcripts allele-specific (exon 0-3)
MAPT exon 3 R	GTCACATCTTCCGCTGTTGG	
MAPT intron 0 F	CCCCAACACTCCTCAGAACT	MAPT allele-specific exon 1 genomic
MAPT exon 1 R	TACGTCCCAGCGTGATCTTC	
MAPT exon 9 F	AAGAGCCGCCTGCAGACA	MAPT exon 10+ transcripts allele-specific (exon 9-10)
MAPT exon 10 R	GGACGTTGCTAAGATCCAGCTT	
MAPT exon 9 F	AAGAGCCGCCTGCAGACA	MAPT allele-specific exon 9 genomic
MAPT intron 9 R	ACCTCCATGCACAGTCCCA	
SNP1 H1 Probe (FAM/MGB/NFQ)	CTGGTTCAAAG**T**TC	Assay developed by M-C Lai.
SNP1 H2 Probe (VIC/MGB/NFQ)	TGGTTCAAAG**C**TCAC	
SNP9 H1 Probe (FAM/MGB/NFQ)	AGACCTGAAGAA**T**GTCAA	First pair.
SNP9 H2 Probe (VIC/MGB/NFQ)	AGACCTGAAGAA**C**GTCAA	
SNP9ii H1 Probe (FAM/MGB/NFQ)	TTGGACTTGAC**A**TTCT	Second pair. Sequences from Myers et al. (2007a)
SNP9ii H2 Probe (VIC/MGB/NFQ)	CTTGGACTTGAC**G**TTCT	

Appendix Table K: Primers for SYBR Green qRT-PCR.

Primer Name	Primer Sequence (5'-3')	Primer Purpose and Amplicon size
GAPDH_F2	GGTCTCCTCTGACTTCAACA	Housekeeping gene (116 bp)
GAPDH_R2	AGCCAAATTCGTTGTCATAC	
HPRT_F	GCCAGACTTTGTTGGATTTG	Housekeeping gene (141 bp)
HPRT_R	CTCTCATCTTAGGCTTTGTATTTTG	
SDHA_F1	TGGGAACAAGAGGGCATCTG	Housekeeping gene (86 bp)
SDHA_R1	CCACCACTGCATCAAATTCATG	
RBM4_F	GCCGCCATTTTAGCGTTTTG	*RBM4* splicing factor (175 bp)
RBM4_R	CACATTCCAGCACCTTCCCA	
PTBP1_F	TTGGGTCGGTTCCTGCTATT	*PTBP1* splicing factor (115 bp)
PTBP1_R	CGTCAGATCCCCGCTTTGT	

Appendix Table L: Primers for construction of lentiviral shRNA plasmids by Gibson Assembly.

Bold signifies unique shRNA sequence; underline signifies overlapping sequences for Gibson Assembly.

Primer Name	Primer Sequence (5'-3')	Primer Position
LenGib_1F	TTCGCCCTTACGCTCTAGAAC	Before *Spe*I and pU6
LenGib_x3.1R	TGTCCCTCCTCGAGAAAAAA**GATGTGACAGCACCCTTAGTTCGCTAAGGG TGCTGTCACATCTTC**GCAAACAAGGCTTTTCTCCAAG	To add MAPTx3_1 shRNA sequence
LenGib_x3.3R	TGTCCCTCCTCGAGAAAAAA**CCACAGCTGAAGAAGCAGGTTCGCCTGCTTC TTCAGCTGTGGTTC**GCAAACAAGGCTTTTCTCCAAG	To add MAPTx3_3 shRNA sequence
LenGib_x10.1R	TGTCCCTCCTCGAGAAAAAA**TTAATAAGAAGCTGGATCTTTCGAGATCCAG CTTCTTATTAATTC**GCAAACAAGGCTTTTCTCCAAG	To add MAPT10_1 shRNA sequence
LenGib_x10.3R	TGTCCCTCCTCGAGAAAAAA**GGTGCAGATAATTAATAAGTTCGCTTATTAA TTATCTGCACCTTC**GCAAACAAGGCTTTTCTCCAAG	To add MAPT10_3 shRNA sequence
LenGib_T08R	TGTCCCTCCTCGAGAAAAAA**CATCCATCATAAACCAGGATTCGTCCTGGTT TATGATGGATGTTC**GCAAACAAGGCTTTTCTCCAAG	To add s8508 shRNA sequence
LenGib_T09R	TGTCCCTCCTCGAGAAAAAA**CCAGGTGGAAGTAAAATCTGATTCGTCAGA TTTTACTTCCACCTGGC**GCAAACAAGGCTTTTCTCCAAG	To add s8509 shRNA sequence
LenGib_T10R	TGTCCCTCCTCGAGAAAAAA**GCATGGTCAGTAAAAGCAAAGTTCGCTTTG CTTTTACTGACCATGC**GCAAACAAGGCTTTTCTCCAAG	To add s8510 shRNA sequence
LenGib_ScrR	TGTCCCTCCTCGAGAAAAAA**GAAGGCTCGTCGCACTAATTTCGATTAGTGC GACGAGCCTTCTTC**GCAAACAAGGCTTTTCTCCAAG	To add Scrambled MAPTx3_1 shRNA sequence
LenGib_2F	TTTTTTCTCGAGGAGGGACAATTGGAGAAGTG	Before RRE
LenGib_2R	CTGCAGAATTCTCGAGACCG	After pEF1α
LenGib_3F	CGGTCTCGAGAATTCTGCAGGCCACCATGGTGAGCAAGGGCGAGG	Start of EBFP2
LenGib_3R	TGTAATCCAGAGGTTGATTGTCGACTTACTTGTACAGCTCGTCCATG	End of EBFP2

Appendix Table M: Sequencing primers used to verify the construction of lentiviral shRNA plasmids.

Primer Name	Primer Sequence (5'→3')
shseq_1F	AAAGTAAGACCACCGCACAG
shseq_1R	GCTCCTATTCCCACTGCTCT
shseq_2F	CGAGGAGGGACAATTGGAGA
shseq_2R	CCAATTCCACAAACTTGCCC
shseq_3F	TGAAGAATCGCAAAACCAGCA
shseq_3R	GTTCAATTGCCGACCCCTC
shseq_4F	CGGGTTTATTACAGGGACAGC
shseq_4R	GTCGCAGCAGGTCATCAAAA
shseq_5F	GCCTGTCTCGCTGCTTTC
shseq_5R	CATCGCATAAAACCCCTCCC
shseq_6F	GTCCAGGCACCTCGATTAGT
shseq_6R	TTGAAGAAGATGGTGCGCTC
shseq_7F	CACATGAAGCAGCACGACTT
shseq_7R	AAGCAGCGTATCCACATAGC